PHYSICOCHEMICAL, BIOLOGICAL AND β-HAEMATIN INHIBITING ACTIVITY OF PYRIDO-DIBEMEQUINES, PYRIDO[1,2-*a*]BENZIMIDAZOLES AND THEIR DERIVATIVES

University of Cape Town

OJWANG' JOHN OKOMBO

Thesis Presented for the Degree of

DOCTOR OF PHILOSOPHY

in the Department of Chemistry

UNIVERSITY OF CAPE TOWN

September 2017

Supervisors: Professor Timothy J. Egan and Professor Kelly Chibale

The copyright of this thesis vests in the author. No quotation from it or information derived from it is to be published without full acknowledgement of the source. The thesis is to be used for private study or non-commercial research purposes only.

Published by the University of Cape Town (UCT) in terms of the non-exclusive license granted to UCT by the author.

University of Cape Town

PLAGIARISM DECLARATION

"This thesis has been submitted to the Turnitin module and I confirm that my supervisor has seen my report and any concerns revealed by such have been resolved with my supervisor."

Name: Ojwang' John Okombo

Student number: OKMJOH002

Signature:

Date: 6th September 2017

ABSTRACT

There is an urgent need for new antimalarials following the emergence of *Plasmodium falciparum* strains with reduced sensitivity to the currently used artemisinin combination therapies. Classical aminoquinoline-based drugs inhibit the formation of haemozoin (HZ) thereby causing parasite death from the cellular accumulation of toxic 'free' haem. Coincidentally, this immutable pathway also exists in *Schistosoma mansoni*, and presents a vulnerable target for drug design in these haematophagus organisms. Therefore, it would be of interest to explore novel scaffolds that can inhibit HZ formation as well as exploit the merits of established drugs via structural modifications that would harness their pharmacological and pharmacokinetic advantages while circumventing their therapeutic shortcomings.

This project investigated the physicochemical, biological and mechanistic profiles of pyrido-dibemequine (pDBQ) and pyrido[1,2-*a*]benzimidazole (PBI) derivatives whose structural motifs were informed by previously synthesised prototype molecules. Specifically, the aqueous solubility, membrane permeability, lipophilicity, metabolic stability and potential for cardiotoxicity of seven pDBQs, their metabolites and ten PBIs were tested through computational and experimental methods. In addition, their antiplasmodial and antischistosomal activities were determined and correlated with their respective physicochemical properties. As regards mechanistic evaluation, their ability to inhibit formation of abiotic HZ, β-haematin (βH), was assessed and intracellular inhibition of HZ formation probed.

The pDBQs constitute reversed chloroquines with a 4-aminoquinoline nucleus hybridised to a dibenzylmethylamine side group that serves as a chemosensitising moiety. The pDBQ derivatives showed moderate to high solubility (52 – 197 μM) and permeability ($LogP_{app}$: -4.6 – -3.6) at pH 6.5. Their lipophilicity, indexed by cLogP, ranged between 3.7 and 5.6 while the mean LogD at both cytosolic (7.4) and vacuolar (5.0) pH was 3.15 and 0.93, respectively. The compounds also showed low-nanomolar range antiplasmodial activity against both chloroquine (CQ)-sensitive (CQS) and resistant (CQR) strains (IC_{50} range CQS: 14.4 – 126.6 nM, CQR^{Dd2}: 44.5 – 162 nM and CQR^{7G8}: 69.6 – 307.1 nM), with no discernible cross-resistance with CQ and the antiplasmodial activity directly correlated with lipophilicity. Mechanistically, all the pDBQs inhibited βH formation (IC_{50}: 13 – 25 μM) and haem-pyridine fractionation profiles revealed they produced a CQ-like dose-dependent increase in toxic

'free' haem with corresponding decrease in HZ levels. Predicted human-*Ether-a-Go-Go*-Related Gene (hERG) channel inhibition pIC_{50} ranged between 6.2 and 6.6, and correlated strongly with the cLogP and molecular weight. The derivatives were also highly susceptibility to microsomal metabolism, with *N*-dealkylation identified as the main biotransformation route.

The pDBQ metabolites exhibited solubility and membrane permeability profiles similar to the parent compounds at pH 6.5, albeit with reduced lipophilicity (cLogP range: 2.3 – 3.5). Their βH inhibition activity (IC_{50}: 15 – 24 μM) was also comparable to the parent compounds as were the haem-pyridine fractionation profiles. However, they showed greater antiplasmodial activity, with 4/7 derivatives exhibiting IC_{50} < 80 nM against *Pf*Dd2 (CQR strain). The metabolites had reduced hERG channel inhibition potential (pIC_{50}: 5.0 – 5.7) and significantly improved metabolic stability upon incubation with mouse and human liver microsomes.

The PBIs comprise molecules with structural likeness to CQ, including a planar heterocyclic moiety and a basic amine side group. PBI analogues showed low to moderate solubility (<5 – 80 μM) and were moderately lipophilic (mean $LogD_{7.4}$: 3.04). Although most of the derivatives were stable in liver microsomes, their predicted hERG channel inhibition potential was higher (pIC_{50}: 6.11 – 7.50), presumably due to their high molecular weights. All but one derivative had submicromolar activity against CQS and CQR strains, with analogues bearing halo-substituents on the left of the PBI core showing the best antiplasmodial activity (mean IC_{50}: CQS = 26.7 nM and CQR = 30.0 nM), highest selectivity (188 – 341) as well as complete cures in *P. berghei*-infected mice. The PBIs also inhibited βH formation (IC_{50}: 6.8 – 120 μM) but did not all display intracellular inhibition of HZ formation. All derivatives were active against juvenile (mean IC_{50}: 1.97 μM) and adult (mean IC_{50}: 4.38 μM) schistosomes, with the 3, 4-dichloro-substituted analogue exhibiting 48% reduction of worm burden *in vivo*.

In summary, the pDBQs evaluated in this project constitute potent antiplasmodial inhibitors of HZ formation but whose activity is compromised by metabolic and hERG liability while their metabolites seem to possess improved biological and physicochemical features. The observed activity of the PBIs against *P. falciparum* and *S. mansoni* complements the already-established broad antimicrobial potency of this chemotype.

PUBLICATIONS AND CONFERENCE PROCEEDINGS

***Publications*:**

1. Joshi MC, **Okombo J**, Nsumiwa S, Ndove J, Taylor D, Wiesner L, Hunter R, Chibale K, Egan TJ.; *4-Aminoquinoline Antimalarials Containing a Benzylmethylpyridylmethylamine Group Are Active against Drug Resistant Plasmodium falciparum and Exhibit Oral Activity in Mice.* J Med Chem. 2017 Dec 7. doi:10.1021/acs.jmedchem.7b01537.

2. **Okombo J**, Chibale K.; *Insights into Integrated Lead Generation and Target Identification in Malaria and Tuberculosis Drug Discovery*. Acc Chem Res. 2017 Jul 18; 50(7):1606-1616. doi: 10.1021/acs.accounts.6b00631

3. **Okombo J**, Singh K, Mayoka G, Ndubi F, Barnard L, Njogu PM, Njoroge M, Gibhard L, Brunschwig C, Vargas M, Keiser J, Egan TJ, Chibale K.; *Antischistosomal Activity of Pyrido[1,2-a]benzimidazole Derivatives and Correlation with Inhibition of β-Hematin Formation.* ACS Infect Dis. 2017 Jun 9; 3(6):411-420. doi:10.1021/acsinfecdis.6b00205.

4. Singh K, **Okombo J**, Brunschwig C, Ndubi F, Barnard L, Wilkinson C, Njogu PM, Njoroge M, Laing L, Machado M, Prudêncio M, Reader J, Botha M, Nondaba S, Birkholtz LM, Lauterbach S, Churchyard A, Coetzer TL, Burrows JN, Yeates C, Denti P, Wiesner L, Egan TJ, Wittlin S, Chibale K.; *Antimalarial Pyrido[1,2-a]benzimidazoles: Lead Optimization, Parasite Life Cycle Stage Profile, Mechanistic Evaluation, Killing Kinetics, and in Vivo Oral Efficacy in a Mouse Model.* J Med Chem. 2017 Feb 23; 60(4):1432-1448. doi: 10.1021/acs.jmedchem.6b01641.

5. **Okombo J**, Chibale K.; *Antiplasmodial drug targets: a patent review (2000 - 2013).* Expert Opin Ther Pat. 2016; 26(1):107-30. doi: 10.1517/13543776.2016.1113258

6. Njaria PM, **Okombo J**, Njuguna NM, Chibale K.; *Chloroquine-containing compounds: a patent review (2010 - 2014).* Expert Opin Ther Pat. 2015; 25(9):1003-24. doi: 10.1517/13543776.2015.1050791

Conferences/Symposia

1. **2017**: The 66th Annual Meeting of The American Society of Tropical Medicine and Hygiene held at the Baltimore Convention Centre, Baltimore, Maryland, USA on 5 – 9th November 2017.
   Poster Title: Pyrido[1,2-a]benzimidazoles: A Novel Non-quinoline β-Haematin Inhibiting Chemotype.

2. **2017**: The 18th SACI National Inorganic Chemistry Conference and Carman Physical Chemistry Symposium (Inorganic 2017) held at the Arabella Hotel and Spa, Hermanus, Cape Town, South Africa on 25 – 29th June 2017.
   Poster Title: Mechanistic and Physicochemical Profiling of Dibemequine Metabolites.

3. **2016:** H3D Symposium on malaria, TB and Neglected Tropical Diseases: Progress in Drug Discovery and Development held at the Goudini Spa in Cape Town, South Africa on 15 – 18th November 2016.
   Poster Title: Mechanistic Profiling of Pyrido-dibemequines and their Derivatives.

4. **2016**: Keystone Symposia on Molecular and Cellular Biology: Drug Discovery for Parasitic Diseases held at Granlibakken Tahoe, Tahoe City, California, USA on 24 – 28th January 2016.
   Poster Title: Dual-functioning Antimalarials: Mechanistic Profiling of Reversed Chloroquines (rCQs) Containing a Dibenzylmethylamine Side Chain.

ACKNOWLEDGEMENTS

I would like to sincerely thank the following people for their support and without whom this body of work would not have been assembled.

Prof. Timothy J. Egan for giving me the opportunity to be a student in his laboratory as well as for the guidance and support throughout the project. More importantly, I am sincerely grateful that his door was always open. It has been a great honour to learn from you, Prof.

Prof. Kelly Chibale for the chance to come to Cape Town and as co-supervisor was always available to provide support, good banter and a challenge to aim higher. Thank you for everything, Kelly.

All the members of **Egan Haem Team**: **Nikki Dare**, **Roxanne Openshaw**, **Devasha Redhi**, **Fabrizio L'Abatte, Anna de Souza, Dr Jill Combrinck** and especially **Roxanne Mohunlal** whose friendship and support has been invaluable. Sincere gratitude also to past members of the Egan Group, **Dr David Kuter, Dr Aneesa Omar** and **Dr Kathryn Wicht,** from whom I learnt a lot in the brief period we interacted. I also thank every member of **Chibale Academic Group,** all of who space cannot allow me to name.

Many thanks to colleagues at the Division of Pharmacology who afforded me space to learn and conduct tissue culture and ADME assays. **Sumaya Salie, Virgil Verhoog, Dr Carmen de Kock, Dr Dale Taylor** and **Prof. Pete Smith** for their support in the tissue culture lab and **Warren Olifant**, **Dr Liezl Gibhard, Dr Mathew Njoroge, Dr Christel Brunschwig** and **Nina Lawrence** who were always available when I needed assistance with ADME assays and data analysis**.** I also extend my gratitude to **Dr Jennifer Keiser** and **Dr Sergio Wittlin** at the Swiss Tropical and Public Health Institute, in whose laboratories the antischistosomal and *in vivo* antimalarial efficacy testings were conducted. I acknowledge the assistance offered by **Dr Malkeet Kumar**, **Dr Kawaljit Singh** and **Dr Mukesh Joshi** in synthesising the compounds I needed for my experiments

A special applause to the following people who, in their own ways, made this journey worthwhile and who became dependable friends: **Prof. Alexis Nzila** who mentored me into scientific research and challenged me to go further**, Dr Lynnete Isabella Ochola** of the University of Nairobi for taking me under her wings and encouraging me, **Prof. David**

Fidock for the emails of encouragement, support and for providing the next chapter to look forward to, **Dr Moratoa Joale** for being true family to me when Cape Town made little sense, **Dr Tameryn Stringer** for her constant support and **Dr Mpati Ramatsoku** for being an amazing confidant in the same journey and encouraging me to push on when I was stagnating with the write up. I also thank my Kenyan colleagues in the department, **Paul**, **Mathew**, **Antonina**, **Godfrey**, **Charles**, **Nicholas** and **Ferdinand**, with whom it was always nice to share warm meals and remind ourselves of home. Special thanks to **Elaine Rutherfoord-Jones** and **Deidre Brooks** for making my administrative life smooth

Most importantly, I thank my brothers **Joel** and **Patrice Okombo** for always being there for me. The most special mention goes to my mother **Agnes Okombo** who sacrificed everything so I could have a different and better life. Thank you, *mama*!

Lastly, this project would not have been possible without the financial support received from **Novartis Research Foundation** and the **University of Cape Town Postgraduate Funding**, for which I am immensely grateful.

ABBREVIATIONS AND ACRONYMS

ACT:	Artemisinin combination therpay
AQ:	Amodiaquine
AS:	Artesunate
βH:	β-haematin
βHIA:	β-haematin inhibitory activity
CQ:	Chloroquine
CQS:	Chloroquine-sensitive
CQR:	Chloroquine-resistant
DARTS:	Drug Affinity Responsive Target Stability
dbHLF:	desbutyl-Halofantrine
DBQ:	Dibemequine
DHA:	Dihydroartemisinin
DMSO:	Dimethyl sulphoxide
DNA:	Deoxyribonucleic acid
DV:	Digestive vacuole
FACS:	Flow assisted cell sorting
FDA:	Food and Drug Administration
Fe(II)PPIX:	Iron(II) protoporphyrin IX
Fe(III)PPIX:	Iron(III) protoporphyrin IX
FSC:	Forward scatter
FWR:	Female worm reduction
Hb:	Haemoglobin
HDP:	Haem detoxification protein
HEPES:	4-(2-Hydroxyethyl)-1-piperazineethanesulfonic acid
hERG:	Human *Ether-a-Go-Go*-Related Gene
HLF:	Halofantrine

HTS:	High throughput screening
HZ:	Haemozoin
IC_{50}:	50% Inhibitory concentration
MoA:	Mechanism of Action
MFQ:	Mefloquine
MW:	Molecular weight
NBT:	Nitro blue tetrazolium
NP-40:	Nonidet P-40
NTS:	Newly transformed schistomula
PBI:	Pyrido[1,2-a]benzimidazole
PBS:	Phosphate buffered saline
pDBQ:	Pyrido-dibemequine
*Pf*CRT:	*Plasmodium falciparum* chloroquine resistance transporter
*Pf*MDR1:	*Plasmodium falciparum* multidrug resistance protein 1
pLDH:	Parasite lactate dehydrogenase
PZQ:	Praziquantel
QD:	Quinidine
QN:	Quinine
RBC:	Red Blood Cell
rCQ:	Reversed chloroquine
SAR:	Structure Activity Relationship
SDS:	Sodium dodecyl sulphate
SSC:	Side scatter
TWR:	Total worm reduction
VAR:	Vacuolar accumulation ratio
VPL:	Verapamil
WHO:	World Health Organisation

TABLE OF CONTENT

LIST OF FIGURES

LIST OF TABLES

Chapter 1

INTRODUCTION AND LITERATURE REVIEW

1.1 Chapter Overview

This *Chapter* starts with a review of aspects of the epidemiology, pathophysiology and chemotherapy of human malaria. Within the life cycle, the blood stage of the causative agent *Plasmodium falciparum* is discussed, with particular focus on the processes of haemoglobin degradation and haemozoin formation in this human malaria parasite and another hematophagous organism, *Schistosoma mansoni,* the causative agent of human schistosomiasis. A recap of haemozoin-inhibiting antimalarials is provided as well as justification for drug designs that target this pathway. Within this context, literature is reviewed on dual-functioning reversed chloroquines and non-quinoline based chemotypes as potential antimalarial agents. The relevance of physicochemical features required for improved drug-likeness for these compounds is also highlighted. Justification, the research question and specific objectives are provided at the end of the chapter.

1.2. Global Burden of Malaria in 2017

Malaria is an infectious disease that poses a major public health challenge, mainly in tropical and sub-tropical regions of the world. Malaria is caused by protozoan parasites of the genus *Plasmodium*,[1] under which there are five recognised species of the parasite that cause the disease in humans, namely *P. falciparum*, *P. vivax, P. ovale, P. malariae,* and *P. knowlesi*. Despite concerted efforts aimed at reducing incidence and case-related deaths, the disease still remains one of the leading causes of death especially among poor populations.[2] According to the World Health Organisation (WHO) 2016 World Malaria Report, there were an estimated 212 million new cases of malaria (range 148 – 304 million) worldwide in 2015, with 90% of these in Africa, 7% in south East (S.E.) Asia and 2% in the eastern Mediterranean region.[3] In the same year, there were an estimated 429, 000 malaria deaths (range 235, 000 – 639, 000) worldwide, 92% of which occurred in Africa while 6% and 2%

occurred in S.E. Asia and the eastern Mediterranean region, respectively. Children under the age of 5 are particularly susceptible to malaria infection and death, with an estimated 303, 000 deaths in 2015.[3] Encouragingly, these figures nonetheless represent improvements from 2014, when there were 214 million new malaria cases (range 149 – 303 million) and an estimated 438, 000 malaria deaths (range 236 000 – 635 000) worldwide.[4] Furthermore, they corroborate a trend of decreasing global malaria incidence and child mortality in the last 15 years (**Figure 1.1**). However, though the overall burden of *P. falciparum* malaria is gradually declining, it is characterised by spatio-temporal variability that presents new and evolving challenges for control programs. Moreover, the consistent threat of asymptomatic (chronic) infections, which serve as sub-microscopic parasite pools in endemic populations,[5] necessitates the need for sustained efforts aimed at comprehensive malaria control.

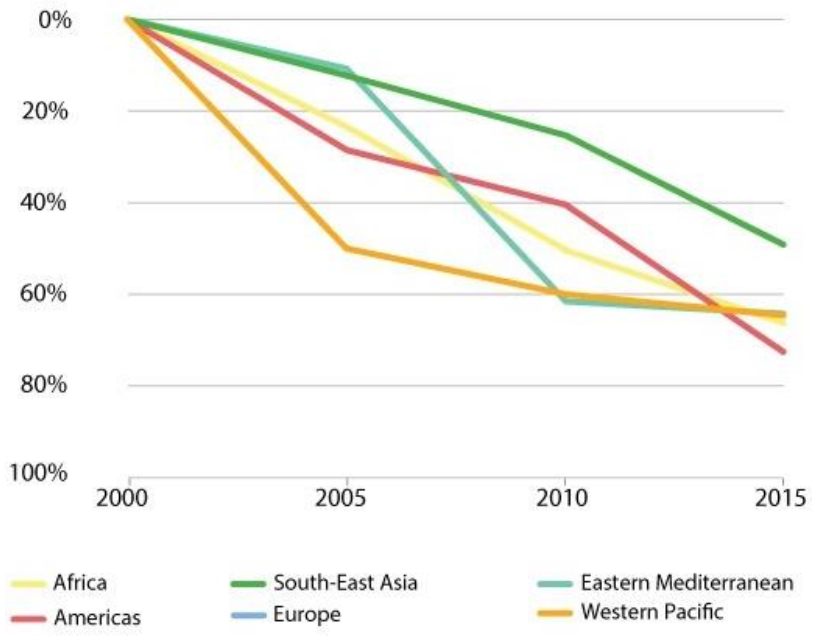

Figure 1.1: Percent decrease in malaria deaths between 2000 and 2015 by World Health Organisation (WHO)-classified regions. Image reproduced from the WHO World Malaria Report 2015.[4]

1.3 The Malaria Parasite Lifecycle

Of the five aforementioned species, *P. falciparum* is considered the most virulent due to the clinical outcomes of its infection. This species has a complicated lifecycle, which can be divided into two parts – the sexual lifecycle within the female *Anopheles* mosquito and the asexual lifecycle within the vertebrate host (**Figure 1.2**). The asexual lifecycle is further divided into a liver stage during which the parasites reside in hepatocytes and an erythrocytic stage when they grow, divide and differentiate within the host red blood cells (RBCs).

During a blood meal, male and female gametocytes may be ingested by a female *Anopheles* mosquito, marking the beginning of the vector-host stage of the lifecycle. In the stomach of the mosquito, these gametocytes fuse to form zygotes, which morph into elongated and motile ookinetes. The ookinetes invade the walls of the mosquito mid-gut where they develop into oocysts, which grow, rupture, and release sporozoites, which travel to the mosquito's salivary glands where they can be passed on to a human host in a subsequent blood meal via dermal tissue.[6, 7] The motile sporozoites enter the host bloodstream and access the liver where they invade hepatocytes to initiate an asymptomatic infection during which the parasites grow, and each sporozoite multiplies into thousands of merozoites that are again released into the bloodstream. This marks the onset of the asexual cycle which is responsible for most of the clinical manifestations associated with malaria, and is characterised by the adhesion of infected RBCs to endothelial cells, reducing the clearance of infected cells by the spleen, thus resulting in potentially fatal placental and cerebral malaria.[8, 9] Though each point in the parasite's lifecycle is potentially exploitable as a drug target, the scope of this literature review and subsequent body of work described herein is limited to the intraerythrocytic asexual stage, and the designing of drugs that target processes and events within this phase.

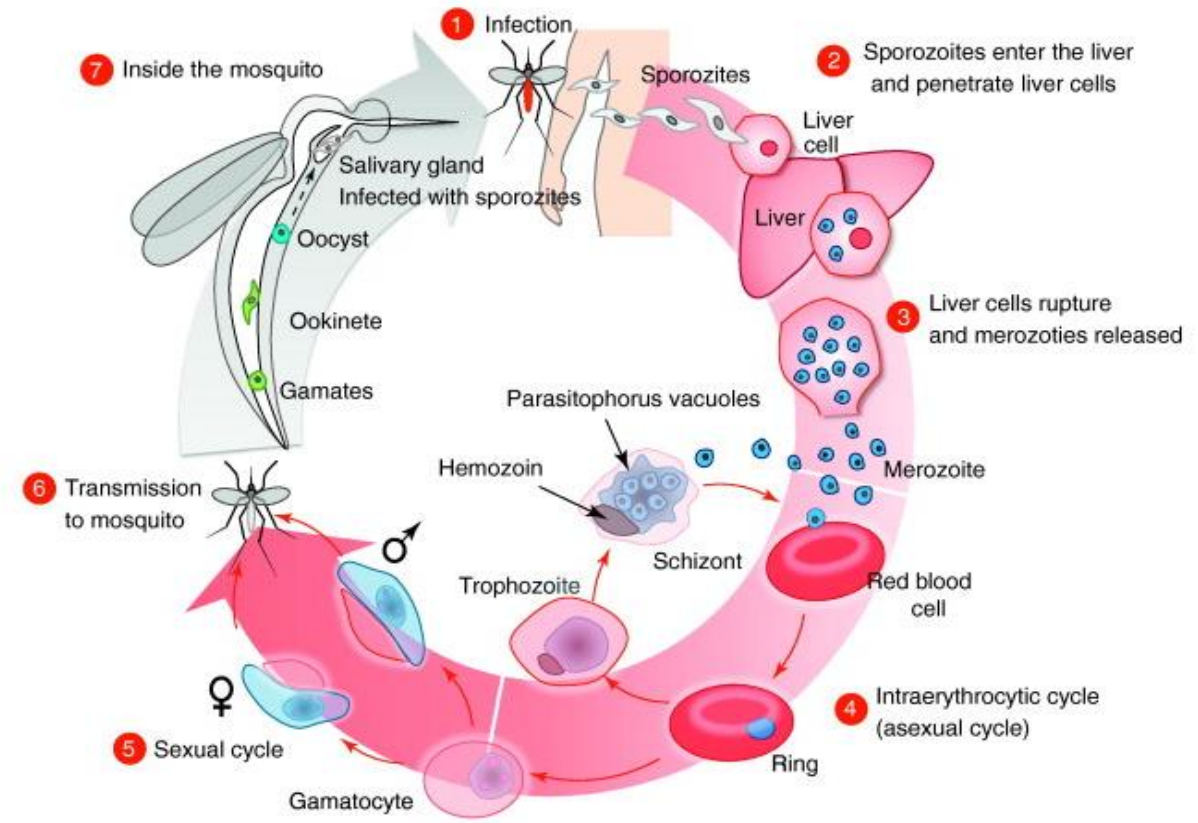

Figure 1.2: The malaria lifecycle showing the vector and mammalian host stages. 1) Infection begins when sporozoites, deposited by an *Anopheles* mosquito during its blood meal, 2) invade the liver and mature over 6 days before rapturing the liver cells to 3) release merozoites which invade RBCs. During the intraerythrocytic stage, 4) parasites grow through the trophozoite (immature and mature) and schizont stages, rapturing in the latter stage to release more merozoites. 5) Some trophozoites differentiate into gametocytes which may be 6) taken up in a blood meal by a female *Anopheles* mosquito to 7) develop through the gamete, ookinete, oocyst and ultimately sporozoite stages. This image was reproduced from *Cho et al., (2012) Trends in Biotechnology Feb; 30(2):71-79* with the permission of Elsevier and Copyright Clearance Centre under licence number 4171300556381.

1.3.1. Asexual Erythrocytic Stage

Upon release from the liver cells into the bloodstream, the merozoites invade the host RBCs where they undergo an asexual erythrocytic cycle (**Figure 1.3**). This invasion process is characterised by adhesion of the merozoites to the RBC surface using a cluster of secretory organelles, micronemes, rhoptry and surface membrane proteins.[10] The merozoites first develop into an immature stage aptly named *rings*, owing to appearance of the parasites at this stage as a signet ring when viewed as a Giemsa-stained slide under a light microscope. The rings develop into mature *trophozoites* which represent a stage marked by high metabolic activity, and during which large volumes of host RBC cytosol are enzymatically digested within the acidic digestive vacuole (DV) to release essential amino acids and toxic by-products.[11] This process of haemoglobin (Hb) degradation is discussed in greater detail in the next section.

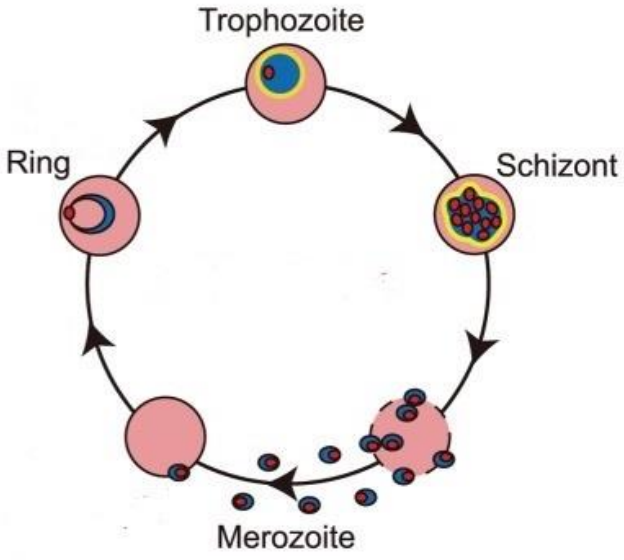

Figure 1.3: Schematic illustration of *P. falciparum* asexual erythrocytic cycle showing the invasion of RBCs by merozoites and the development and maturation of *ring*, *trophozoite* and *schizont* stages of the parasite.

The mature trophozoites progress into a *schizont* stage where the ingestion of host cell cytoplasm and consequent elimination of toxic waste products proceeds and almost expends the Hb content of the RBC. The schizont stage is characterised by nuclear division, resulting in 16 - 24 nuclei each of which moves towards the surface of the parasite and assembles as daughter merozoites for exit. This ultimate egress from the erythrocyte is preceded by the rupture of the parasite membrane and RBC membrane, and is presumably triggered by secretions from the merozoite apical organelles.[12] At this stage, merozoites can either infect new RBCs to begin the erythrocytic cycle again, or, develop into gametocytes which are the hallmark of the sexual stage.

1.3.1.1. Haemoglobin Degradation

During this asexual stage, the parasite ingests and degrades ~75% of host Hb for nourishment and to gain physical space for growth and division so that the lytic volume of the host RBC is not exceeded.[13-15] This proteolytic process by acidic and alkaline enzymes leads to the release of essential amino acids and toxic haem or iron(II)protoporphyrin IX (Fe(II)PPIX) [16] (**Figure 1.4**). Due to the absence of a functional haem oxygenase that oxidatively cleaves haem, the parasite consequently faces a unique waste disposal dilemma since it cannot enzymatically degrade Fe(II)PPIX. Instead, Fe(II)PPIX undergoes auto-oxidation in the parasite to Fe(III)PPIX which, in its solubilised form, is equally toxic.[17] Since unhindered degradation of Hb leads to subsequent generation of vast amounts of Fe(III)PPIX, the parasite converts this toxic product into inert and highly insoluble crystals called haemozoin (HZ).[18] Inhibition of this process in *P. falciparum* and other haematophagous organisms is discussed later in detail as it constitutes an established target for some antimalarials and an attractive one for drug design based on novel scaffolds.

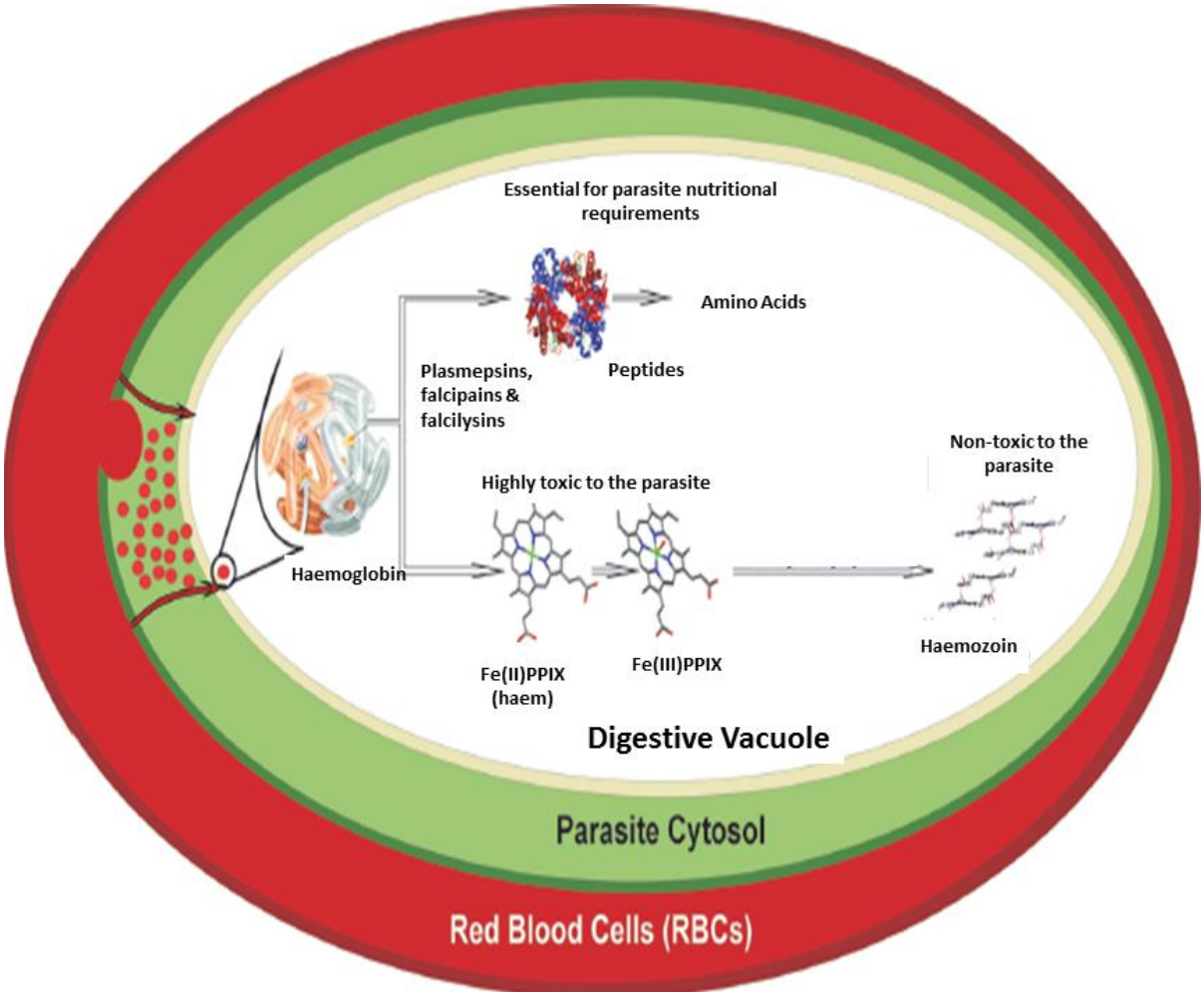

Figure 1.4: An illustration of the process of haemoglobin (Hb) degradation within a host red blood cell (RBC) infected with *P. falciparum*. Also indicated are the resultant formation of peptides and essential amino acids as well as the cytotoxic Fe(III)PPIX and its conversion to the non-toxic haemozoin (HZ).

1.3.1.2. Haemozoin Formation in *P. falciparum* and other Hematophagous Organisms

In higher eukaryotes and eubacteria, Fe(III)PPIX is degraded through the haem-oxygenase/biliverdin reductase pathway.[19, 20] The malaria parasite and other blood-feeding parasites like the bilharzia-causing trematode *Schistosoma mansoni* have, however, evolved a unique detoxification mechanism, which involves converting haematin into dimerised, non-toxic, insoluble HZ crystals. In *P. falciparum*, HZ formation occurs in the DV where the

negatively charged propionate group of one haematin moiety is thought to associate with the positively charged Fe(III) centre of an adjacent haematin molecule via the carboxylate group, consequently initiating the assembly of HZ crystals by the repetitive association of haematin molecules in this fashion.[21] Slater and Cerami suggested an enzyme-catalysed model of HZ formation and showed that *P. falciparum* trophozoite extracts promoted formation of β-haematin (βH), abiotic HZ .[22] This was, however, challenged by Dorn *et al*. who noted that heat treatment of the extracts had little effect on the reaction and suggested the likely involvement of a reaction-promoting haem-derived material associated with HZ [17] which Bendrat *et al*. suggested is a lipid.[23] Though Sullivan *et al*. managed to identify and clone two histidine-rich proteins (HRP-2 and HRP-3) in purified DVs [24] and Choi *et al*. demonstrated the role of HRP-2 in complex formation with Fe(III)PPIX,[25] later findings suggested that parasite clones lacking the genes encoding HRP-2 or 3 can still competently form HZ. Further, orthologs of HRP-2 are absent in *P. vivax* as well as in rodent malaria parasites, which also form HZ,[26] ruling out a role for this protein. The current hypothesis on HZ formation in *P. falciparum* centers around lipid initiation originally proposed by Bendrat *et al*. [23] and later corroborated by Dorn *et al*. [17, 27] and lately by many other researchers.[21, 28, 29] Recent work in *Plasmodium* linked neutral lipid bodies on both the interior and the exterior of the DV with haem crystallisation [30-32] and more recently Pisciotta and co-workers identified neutral lipids closely associated with HZ.[33] Growth of βH under biomimetic conditions have confirmed its efficient formation in a lipid environment,[21, 33, 34] particularly when Fe(III)PPIX is directly introduced at or near the interface between the lipid and aqueous solution.[21] This efficient formation of βH suggests that the lipid-water interface itself probably suffices in bringing about HZ formation within the parasite.[35] In 2008, Jani *et al.* described the identification and characterisation of a haem detoxification protein (HDP) that is extremely potent in converting haem into HZ.[36] This protein is refractory to disruption and is conserved across all *Plasmodium* genus. To illustrate that HDP is indeed

involved in crystallisation of haem into HZ, the authors demonstrated HDP-mediated dose-dependent conversion of toxic haem into inactive HZ. This activity that was lost when HDP was protease-treated, suggesting intact protein is required for this activity. Exploring this hypothesis further, Chugh *et al.* more recently showed that HDP functions in concert with falcipain 2 (a major haemoglobinase) to efficiently convert Hb to HZ.[37] Thus, the jury is still out as to whether HZ formation in *P. falciparum* is protein or lipid mediated.

Using methods previously described for malarial HZ extraction, Oliveira *et al.* described what they observed as a dark-brown insoluble pelleted pigment from homogenised adult females of *S. mansoni*.[38] Polarised light microscopy revealed that this pellet had a crystalline structure and was readily solubilised in 0.1 M NaOH to give an absorption spectrum identical to that of monomeric haem. Fourier transform infrared spectroscopy (FTIR) of this schistosomal pigment in potassium bromide pellets revealed a pattern identical to HZ from *Plasmodium.* Comparing the solubility of haem and this pigment showed ready dissolution of haem in sodium bicarbonate buffer, pH 9.1, whereas this pellet was virtually insoluble. Taken together with powder XRD measurements, these findings unequivocally identified the pigment isolated from *S. mansoni* as HZ. In female adult *S. mansoni* worms, HZ formation has been demonstrated to occur within the gut,[38] in a process presumably catalysed by the extracellular lipid droplets present in the gut lumen,[39, 40] which provide the requisite hydrophilic-hydrophobic interface for the crystallisation process.

1.4. An Update on Current Malaria Treatment and Prevention Strategies

The reduction in malaria burden mentioned in **section 1.2** has largely been attributed to a scale-up of combinations of control strategies. In the main, these comprise long-lasting insecticide-treated nets (LLINs), indoor residual spraying (IRS) and intermittent preventive therapy for pregnant women (IPTp) for prevention, better diagnostics for case

ascertainment, and effective treatments using artemisinin-based combination therapies (ACTs). Admittedly, significant progress has also been made in malaria vaccine development, with the imminent roll-out of the pre-erythrocytic vaccine RTS, S/AS01 in large-scale, pilot projects following a large Phase III clinical trial in seven African countries.[41] In addition, the irradiated sporozoite vaccine, *Pf*SPZ, is closer to pivotal Phase III trials [42] while a number of other pre-erythrocytic and blood stage vaccines have shown efficacy in challenge experiments in volunteers and in endemic populations. However, efficacy has only been limited hence highlighting the significance of chemotherapy and vector control.

The sophistication of the lifecycle of *P. falciparum* (**Figure 1.2** and **1.3**) presents different stages of the parasite's development that can be targeted using drugs or drug combinations to treat malaria. Current antimalarial drugs (**Figure 1.5**) can be grouped into multiple classes namely: 4-aminoquinolines, 8-aminoquinolines, arylaminoalcohols, antifolates, artemisinins, antibiotics and inhibitors of the cytochrome bc1 complex in the parasitic electron transport chain. Several antibiotics that are prokaryotic protein synthesis inhibitors have antimalarial activity because of their action against the protein synthesis machinery of the apicoplast organelle.[43] Antibiotic antimalarials, like doxycycline (DOX) or clindamycin, usually constitute partner drugs to faster-acting antimalarials such as artemisinins or quinine because they are slow-acting. Antifolates include sulfadoxine (SDX) and pyrimethamine (PYR) which respectively inhibit dihydropteroate synthase (*Pf*DHPS) and dihydrofolate reductase (*Pf*DHFR) in the folate pathway.[44] Halofantrine (HLF) and mefloquine (MFQ) are examples of arylaminoalcohols. HLF is not widely used due to severe cardiotoxic effects while MFQ is generally combined with artesunate (AS) since, alone, it is associated with neurotoxicity.[45] Atovaquone (ATQ) represents inhibitors of the respiratory chain, mostly used for chemoprevention and the treatment of uncomplicated *P. falciparum* malaria as exemplified by the ATQ-proguanil combination, Malarone.[46]

The 8-aminoquinoline class of antimalarials is unique due to the efficacy against relapsing forms of malaria.[47, 48] These drugs act against the sexual as well as the pre-erythrocytic stage of the *Plasmodium* parasites. Primaquine (PMQ) is currently the only 8-aminoquinoline drug available, and is the drug of choice against *P. vivax.* Tafenoquine (TFQ) is a more potent and less toxic analogue of PMQ [49] originally synthesised by the Walter Reed Army Institute of Research in the USA and has since been tested in Phase II and III clinical studies.[50-52] In addition, it is longer-acting and therefore, unlike PMQ, does not need to be taken frequently. This class of antimalarials forms part of the quinoline-based drugs, the most-widely known of which is the 4-aminoquinoline, chloroquine (CQ).

ACTs constitute the current WHO-recommended treatment option for uncomplicated malaria. Artemisinins, exemplified by AS and artemether (ART) act on both the early and late stages of the malaria parasite's lifecycle in the human host.[53] They are fast-acting, efficacious and safe, and are commonly combined with other longer-acting antimalarials in a strategy aimed at delaying the onset of resistance. Though still effective in most endemic regions, there is growing evidence of delayed parasite clearance following treatment with ACTs in S.E. Asia,[54, 55] and a recent case report of indigenous artemisinin-tolerant strain from Africa,[56] thus highlighting the potential for full-blown resistance.

i) 4-Aminoquinolines

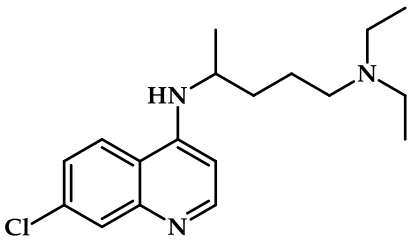

Chloroquine

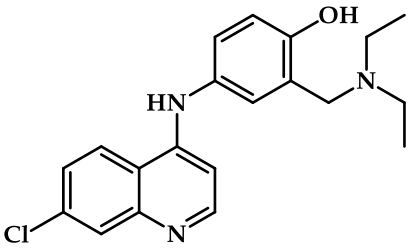

Amodiaquine

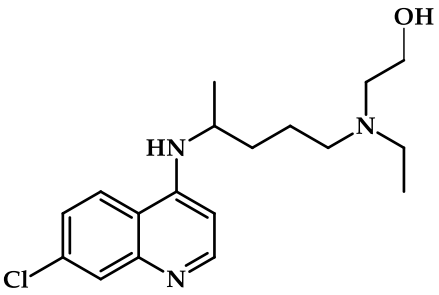

Hydroxychloroquine

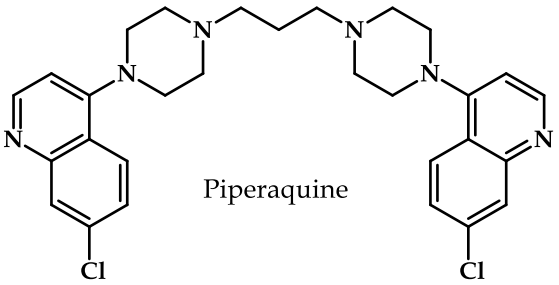

Piperaquine

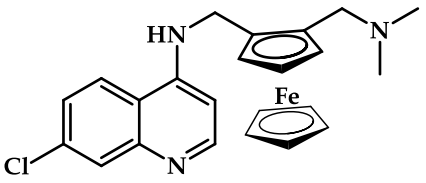

Ferroquine

ii) 8-Aminoquinolines

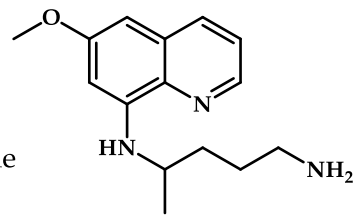

Primaquine

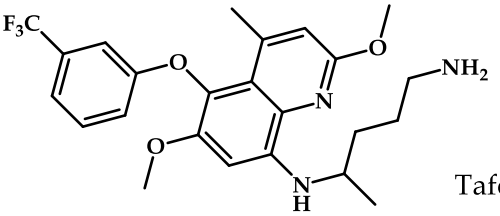

Tafenoquine

iii) Antibiotics

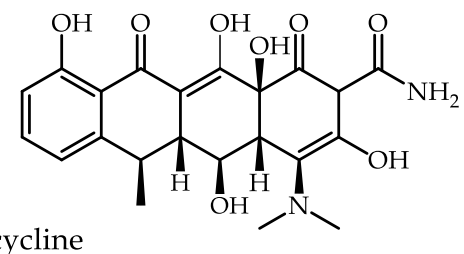

Doxycycline

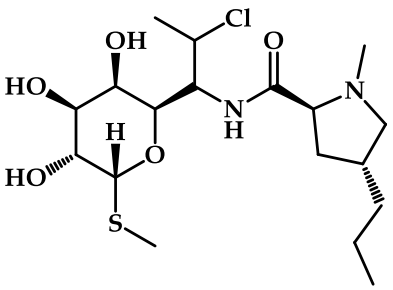

Clindamycin

iv) Antifolates

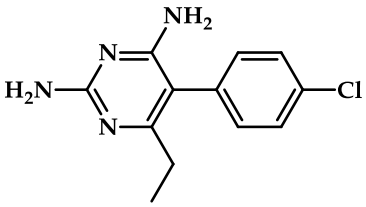

Pyrimethamine

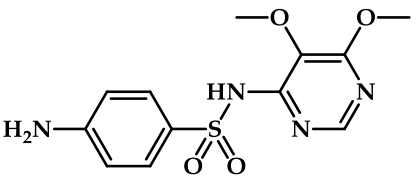

Sulfadoxine

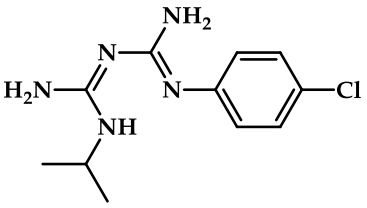

Proguanil

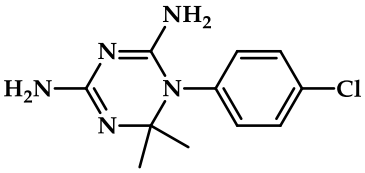

Cycloguanil

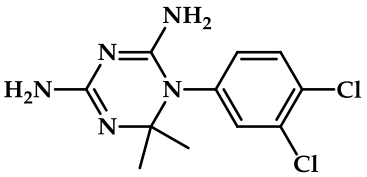

Chlorcycloguanil

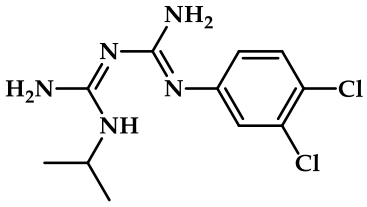

Chlorproguanil

v) Arylaminoalcohols

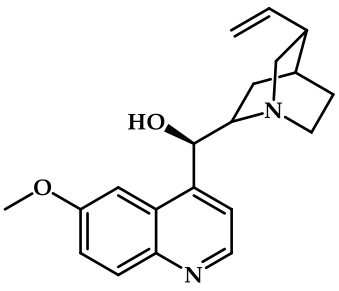

Quinine

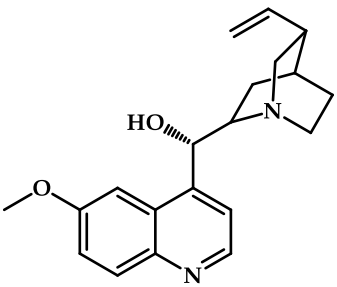

Quinidine

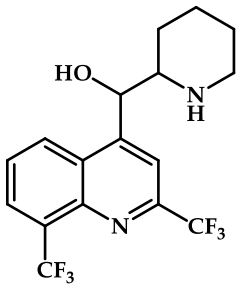

Mefloquine

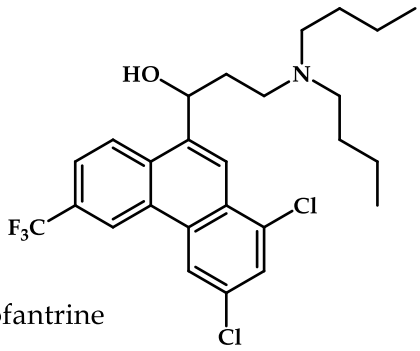

Halofantrine

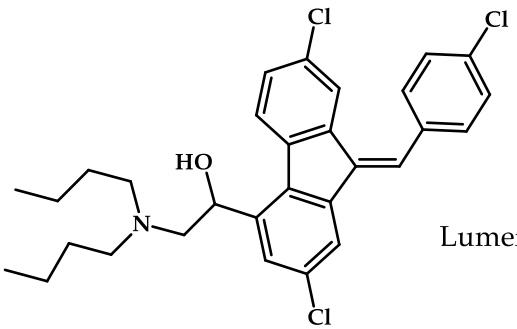

Lumefantrine

vi) Inhibitor of cytochrome bc1 complex

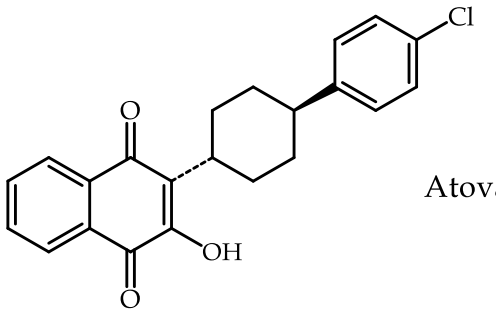

Atovaquone

vii) Artemisinins

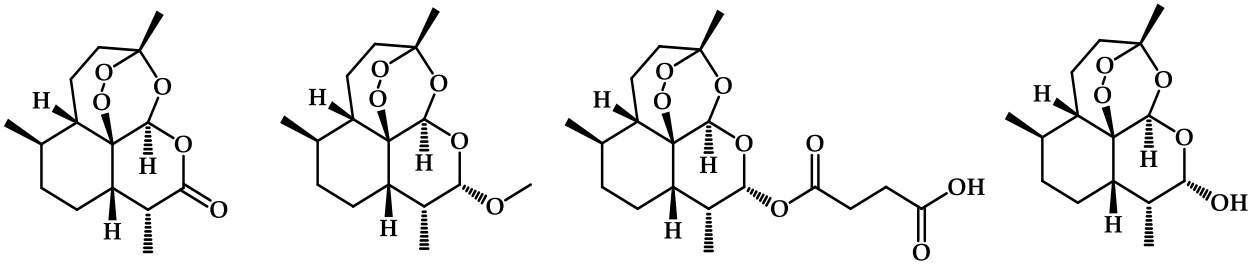

Artemisinin Artemether Artesunate Dihydroartemisinin

Figure 1.5: Chemical structures of current antimalarials grouped according to their classes

1.5. Quinolines and related antimalarial compounds

Quinine (QN) was the first quinoline to be isolated from extracts of the bark of the *Cinchona* tree in 1820 by Pelletier and Caventou. However, extensive use during World War I led to exceedingly high demand, and its severe undesirable side effects further precipitated the need for research into the production of synthetic alternatives. This led to the development of CQ,[57] which, in 1943, was taken into clinical trials and subsequently used widely due to its effectiveness and low risk side effect profile. Since then, many quinoline-based drugs

(**Figure 1.5**) have been important antimalarials. In fact, the quinoline nucleus is an important motif in heterocyclic compounds found in many natural and synthetic products with pharmacological activities such as anti-inflammatory,[58] anticancer,[59] antimycobacterial [60] and antiviral.[61]

CQ has numerous pharmacokinetic (PK) and pharmacological advantages over all other antimalarial drugs. These comprise fast action, low toxicity, water solubility of its salt form and good oral bioavailability.[62] However, CQ causes gastrointestinal disturbances due to its rapid absorption.[63] Following the emergence and spread of CQ resistance, amodiaquine (AQ) was designed as an alternative against low CQ-resistant (CQR) parasites. However, prolonged use of this drug has been shown to possess an unacceptably high risk of agranulocytosis and hepatitis, with fatal outcomes in some cases.[64, 65] Further development led to the discovery of piperaquine (PQ), a bis-4-aminoquinoline with two 4-aminoquinoline moieties attached by a linker and proven potency against both CQ-sensitive (CQS) and CQR parasite strains. Its activity against CQR parasites is thought to be due to its steric bulk which presumably prevents it from being expelled out of its site of action by transporter proteins.[66] PQ is currently used as part of an ACT treatment regimen with dihydroartemisinin (DHA) in a fixed dose combination, which has shown excellent tolerability and high cure rates in malaria endemic settings.[67-69] Discovered more recently is ferroquine (**FQ**), which has completed Phase IIA clinical trials,[70] and has exhibited low toxicity as well as no cross-resistance with CQ.[71]

1.5.1. Mechanism of Action of CQ and related 4-Aminoquinolines

CQ and AQ have been shown to be mostly active only against the early to mid-intraerythrocytic stage of the parasite lifecycle when Hb degradation is optimal.[53] Similarly, treatment of parasites with pharmacologically-relevant concentrations of CQ was shown to

cause swelling of the DV. These two aforementioned phenomena provide the clearest hint that the mechanism of action (MoA) of CQ and related 4-aminoquinolines involves halting events linked to Hb degradation and accumulation within the DV. Nonetheless, a number of theories on the MoA of CQ and related aminoquinolines have been put forward.

1.5.1.1. Inhibition of phospholipase

Phospholipases play central roles in regulating signalling during numerous cellular events including proliferation, G protein-coupled receptor signalling and neuronal activation by catalysing the lysis of phosphorylated lipids. In *P. falciparum*, phospholipase enzymes have been identified within the DV and are thought to be responsible for degrading endocytic vesicle membranes in order to facilitate release of their Hb content into the DV. Ginsburg and Krugliak, (1992) showed that CQ inhibits the activity of phospholipase *in vitro*, albeit at substantially higher concentrations than those likely to occur within the parasite's DV.[72]

1.5.1.2. Inhibition of protease enzymes

All parasitic protozoa contain multiple proteases, some of which are attractive drug targets. CQ has also been shown to inhibit partially purified aspartic protease activity from *P. falciparum* extracts.[73] However, this too was only at concentrations above the therapeutic range. Moreover, haem itself is a competent low-dose inhibitor of acid proteases and this activity is unaltered even in the presence of CQ, thus making the evidence for this MoA less compelling.

1.5.1.3. Binding to Nucleic Acid

CQ, presumably due to its planar structure, was originally thought to exert its antimalarial activity through intercalation into planar bases of deoxyribonucleic acid (DNA) leading to inhibition of DNA replication and ribonucleic acid (RNA) synthesis, hence leading to cell

death.[74] However, this hypothesis has since been refuted on grounds that though *in vitro* binding to DNA has been observed, this has been at markedly higher concentrations (100 μM) than the pharmacological concentration, typically 10 nM.[75] Using super-resolution analysis of fluorescent derivatives of QN and QD attached to 7-nitrobenz-2-oxa-1,3-diazole, Woodland *et al.* recently showed no co-localisation of these drugs with the nucleus, thus further rejecting disruption of DNA replication as a possible MoA of these quinoline-based drugs.[76] Moreover, this theory fails to explain why MFQ, with no binding affinity to DNA,[77] is a potent antimalarial or the non-selective CQ-DNA binding between parasite and host nucleic acids.

1.5.1.4. Inhibition of Polyamine Synthesis

In *P. falciparum,* polyamines are synthesised by the bifunctional ornithine decarboxylase/*S*-adenosylmethionine decarboxylase enzyme.[78] Konigk *et al.* reported inhibition of ornithine decarboxylase activity in trophozoite extracts of infected RBCs by quinoline antimalarials.[79] However, this hypothesis is hazy as no follow-up studies have been conducted and it also fails to convincingly account for the specific activity of CQ on the blood stage but not liver stage parasites, which presumably also harbour this enzyme.

1.5.1.5. Inhibition of Haem Detoxification

Due to their ability to adopt planar conformations, CQ and related 4-aminoquinolines are thought to impede haem crystallisation and consequent HZ formation by docking onto the fastest growing face of haem or haem-drug complex thus blocking attachment of the next haem dimer (**Figure 1.6**). This inevitably leads to accumulation of toxic haem which, in its 'free' form, can inhibit parasite growth and lead to death by inducing formation of oxygen-derived free radicals,[80] lipid peroxidation,[81] and DNA oxidation.[82, 83] First indications of haem-drug complex formation were reported by Cohen and colleagues,[84] with later evidence

provided by other researchers.[17, 27, 85, 86] Dorn *et al*., (1995) demonstrated that HZ formation is autocatalytic,[17] and further confirmed previous observations by Egan *et al*., (1994) that this process could be directly inhibited by CQ. Ginsburg *et al*., (1998) also put forward the hypothesis that CQ acts as a competitive inhibitor of haem degradation by glutathione, thus allowing haem to partition into membranes [87] while Loria and colleagues demonstrated the decomposition of haem in the presence of hydrogen peroxide, hence suggesting that CQ is an efficient inhibitor of the peroxidative degradation of haem by complex formation.[88] However, total iron measurement following cell fractionation, Mössbauer spectroscopy and electron spectroscopic imaging showed that haem is not decomposed in the parasite.[18] The latest and more compelling evidence of inhibition of HZ formation by CQ was provided by Combrinck *et al.* who showed that CQ led to a significant dose-dependent increase in the levels of haem in the parasite and this correlated with a corresponding decrease in the levels of HZ.[89] Further analyses revealed that this increase in haem, measured as the amount of total haem Fe in the cell, directly correlated with decreasing parasite survival. The crystal structure of the Fe(III)PPIX−HLF complex has revealed that coordination to the iron(III) center of the haem monomer, π-π interaction, and hydrogen bonding constitute the key interactions between arylmethanol HZ inhibitors and Fe(III)-PPIX.[90]

Additionally, as a weak diprotic base, CQ in its unprotonated form has been shown to move down the pH gradient into the acidic DV where once protonated, becomes trapped due to membrane impermeability[91, 92] thereby accumulating several thousand-fold.[93, 94] Aside from this pH trapping phenomenon, CQ has also been shown to accumulate in the DV as a result of interaction with 'free' haem in the DV, which acts as a CQ receptor.[95] This body of evidence of CQ accumulation in the DV corroborates the theory that the MoA of CQ and

related 4-aminoquinolines is linked to the DV-localised process of Hb degradation and inhibition of the subsequent detoxification of haem.

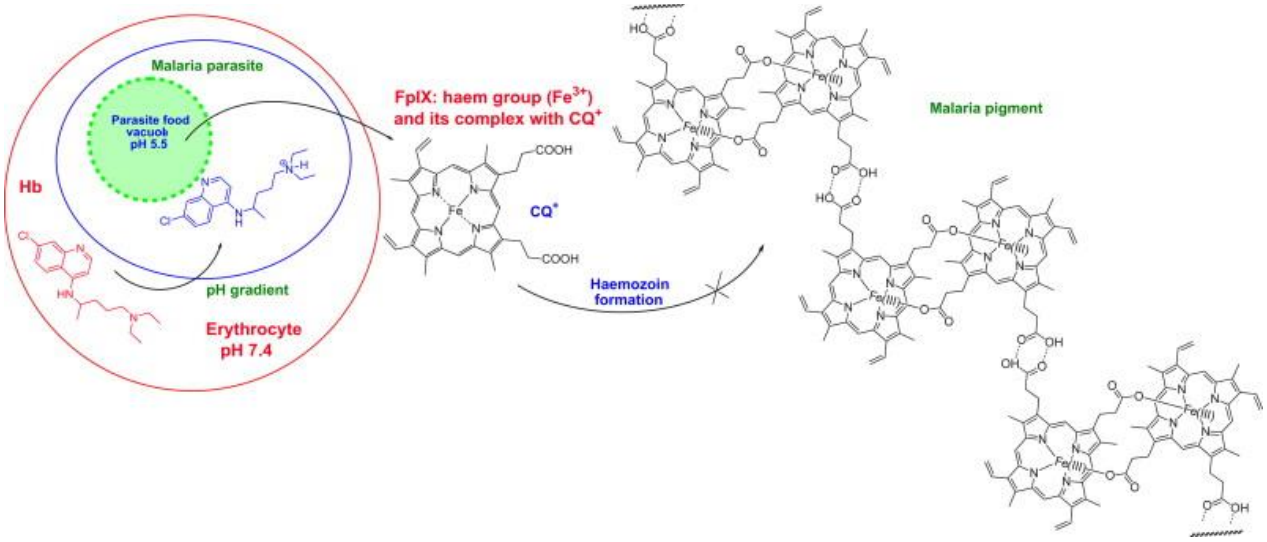

Figure 1.6: Proposed mechanism of action of chloroquine and related 4-aminoquinolines. This image was reproduced from *Kouznetsov V and Gomez-Barrio A., Recent Developments in the Design and Synthesis of Hybrid Molecules Based on Aminoquinoline Ring and Their Antiplasmodial Evaluation. Eur J Med Chem ; 2009;, Aug; 44(8): 3091-113*. Copyright© (2009) Elsevier Masson SAS. All rights reserved

1.5.1.5.1. Measuring Inhibition of Haem Detoxification as a Mechanism of Action of CQ

This inhibition of HZ formation can be quantified *in vitro*, by measuring the formation of βH within a cell-free environment under abiotic conditions that mimic the lipid-mediated process of HZ formation in the DV. This determination relies on UV-vis absorbance measurements for detection of a *bis*-pyridyl-haem complex,[96] with optimum results demonstrated when the detergent Nonidet P-40 (NP-40) is used as the imitator of the neutral lipids involved in this process.[97] In addition, this NP-40 assay is amenable to high throughput screening (HTS) due to its incorporation of the non-interfering aqueous acetone at pH 7.4 to handle poorly-soluble compounds.

This mechanistic hypothesis can be validated using a pyridine-haem cellular fractionation assay to convincingly confirm true inhibitors of HZ formation.[98] In this assay, it was demonstrated that true inhibitors of HZ formation cause a significant concentration-dependent increase in 'free' haem and corresponding decrease in HZ in treated whole cell parasite cultures relative to untreated controls.[89, 98] Crucially, using CQ as an example, Combrinck *et al.* showed that this increase in the proportion and amount of toxic 'free' haem corresponded to a decrease in parasite growth. This trend was, however, not observed in non-βH inhibitors exemplified by PYR and sulfadoxine/pyrimethamine.[89] At this juncture, it is noteworthy that there are several key elements in the structure of CQ that are requisite for its antiplasmodial potency.

1.5.2. Structure Activity Relationship (SAR) Profile of CQ

The 4-aminoquinoline pharmacophore of CQ plays a critical role with respect to accumulation of the drug in the DV, formation of a drug-haem complex and exertion of cytotoxic effects by the complex. The structure activity relationship (SAR) profile of CQ (**Figure 1.7**) identifies and maps out the individual moieties responsible for these activities. The basic amino group in the lateral side chain has been demonstrated to be crucial for the accumulation of the drug in the DV where, upon protonation, CQ becomes membrane impermeable and subsequently trapped, a process referred to as pH trapping.[99, 100] Indeed, replacement of the 4-quinolinyl amino moiety with an ether [101] and sulphur or oxygen atom [102] led to reduction of the basicity of the quinolinyl nitrogen and diminished the antiplasmodial activity of the compound.

Kaschula *et al.,* using different substituents at carbon 7 (C7), investigated the effect of replacing the chloro (-Cl) group at this position on the inhibition of βH formation and

antiplasmodial activity.[100] The antiplasmodial activity of 4-aminoquinoline derivatives with short diaminoalkane side chains ranged from low when -Cl was replaced at this position with 7-OMe to moderate in the 7–F and 7–CF_3 derivatives tested against Haiti 135 (CQS) and Indochina I (CQR) strains of *P. falciparum*.[103] Different studies have established that the group at C7 is also critical for βH inhibition, with compounds bearing a -Cl atom at this position exhibiting the most potent inhibition.[99, 100, 103] An ideal group at C7 was previously proposed to be (*i*) moderately electron withdrawing, which will cause only a moderate decrease in the acid dissociation constant (pKa) of the molecule, thus enabling compound accumulation at the site of action while ensuring inhibition of βH formation and (*ii*) be strongly lipophilic. A strongly lipophilic group will enable a stronger association of the compound with haematin, which would presumably translate to stronger inhibition of βH formation.[100] It is noteworthy, however, that in the Kaschula *et al.* study, the 7–NO_2 substituent showed strong inhibition of βH formation, without being very lipophilic.[100]

The 4-aminoquinoline nucleus was identified to be the haematin-associating nucleus as the introduction of an alkyl side chain to the amino group of the 4-aminoquinoline has been shown to have no significant effect on the association strength.[99, 100, 104] In addition, formation of the CQ-haematin μ-oxo dimer was found to be dominantly a function of the 4-aminoquinoline core with the lateral side chain only contributing minimally to the binding.[105]. Alongside the terminal nitrogen, the quinoline nitrogen was also identified as essential for pH trapping.[100] In summary, Egan and colleagues concluded from these studies that the 4-aminoquinoline nucleus of CQ, the chloro (-Cl) group at C7 and basic nitrogen attached to the aminoalkyl side chain are essential for antiplasmodial activity.[100] These studies lay a platform to further investigate and map possible modifications to the SAR that can enhance or retain activity while improving physicochemical properties.

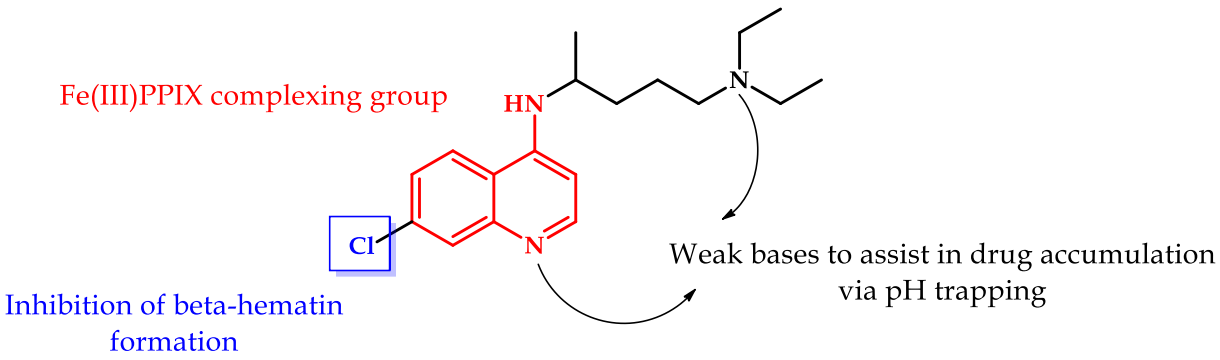

Chloroquine

Figure 1.7: Chloroquine structure-activity relationship (SAR) profile as proposed by Egan and colleagues.[99]

1.5.3. Resistance to CQ and related 4-aminoquinolines

Resistance to CQ emerged in the 1960s in S.E. Asia and South America and by the 1980s, had spread across Africa [106] and in effect, significantly increased the global cost of controlling malaria since new drugs have had to be continually developed to replace those that had lost efficacy. CQ resistance is attributed to polymorphisms in the '*Plasmodium falciparum* CQ resistance transporter' (*Pf*CRT) and other DV membrane proteins, resulting in reduced CQ accumulation.[107-109] Compared to CQS strains, CQR parasites have been shown to accumulate up to 10-fold less CQ in the DV, falling outside the effective therapeutic range of the drug.[110] Though several mutations in *Pf*CRT have been reported in CQR strains, substitution of the positively charged lysine for the neutral hydrophobic threonine in codon 76 (K76T) has been shown to be most essential in conferring CQ resistance.[107, 111] While protonated CQ is unable to interact with wildtype K76 *Pf*CRT, it can interact with 76T *Pf*CRT allowing transport of previously trapped CQ down the electrochemical gradient and out of

the DV, with resistance consequently arising from the reduction in the concentration of accumulated CQ in the DV.[112]

The existence of CQS strains associated with the 76T mutation suggests existence of other loci involved in CQ resistance in *P. falciparum*. Indeed, mutations in proteins other than *Pf*CRT have also been identified as contributors to CQ resistance. For instance, a homologue of the eukaryotic ATP-binding cassette (ABC) protein, the *Plasmodium falciparum* multidrug resistance transporter 1 (*Pf*MDR1) has been linked to reduced CQ sensitivity where allelic exchange experiments have demonstrated that mutations on this DV membrane transporter modulate the degree of sensitivity to CQ.[113] Furthermore, variant parasites bearing *pfmdr1* 86Y, 1034C, 1042D and 1246Y alleles have been shown to exhibit impaired transportation and accumulation of CQ into the DV, hence reduced sensitivity of the drug.[114]

Based on their ability to inhibit βH formation, compounds which share structural similarity to CQ are postulated to share a similar mode of resistance, though this is not always a given. For instance, resistance to the more hydrophobic MFQ has been associated with increased copy number of the *pfmdr1* gene, resulting in increased expression of its cognate *Pf*MDR1 protein.[115-117] Similarly, while resistance to AQ is also linked to polymorphisms in both *Pf*CRT and *Pf*MDR1,[118] the drug retains activity against most CQR parasites. This phenomenon could be attributable, on one hand, to its retention in the hydrophobic lining of the *Pf*CRT^{CQR} channel [119] and on the other, to the observation that the *Pf*CRT haplotypes that mediate AQ and CQ resistance are in fact different.[120] These studies highlight the fact that structurally similar compounds, which share common putative MoAs may exhibit markedly dissimilar modes of interactions with the resistance mechanisms at play within the parasite.

1.6. Strategies to Counter Resistance to Quinoline-based Drugs

Though alternative therapies for treating CQR malaria parasites have been developed, including ACTs, most do not match CQ's ease of use and low cost or are reportedly losing efficacy. Crucially, the MoA of CQ involves inhibition of a critical, parasite-specific event that is amenable to inhibition by small molecules, not under genomic control (hence immutable) and leads to cidality at low-concentration. Strategies to reverse resistance to CQ or design new inhibitors with favourable physicochemical properties that target the same pathway have potential to contain drug-resistant malaria. One approach involves exploring the antimalarial potential of 'reversed chloroquines' (rCQs) which exploit reversal agents (RA) to restore sensitivity to CQ.[121] The RAs are chemosensitising agents that generally work as efflux pump inhibitors, and have previously been shown to restore susceptibility of CQR parasites to a CQS-like phenotype,[122, 123] and in whose presence the *in vivo* antimalarial activity of CQ against CQR strains can be reinstated.[124, 125] These compounds, examples of which are shown in **Figure 1.8**, prevent the expulsion of CQ from the DV leading to local drug accumulation and attendant antiplasmodial effect in CQR strains. Using 3D quantitative SAR and quantum chemical structure-activity analysis, Bhattacharjee *et al.* proposed a pharmacophore model for these RAs which comprised the requirement of two aromatic hydrophobic interaction sites linked by an aliphatic chain to a hydrogen bond acceptor site (generally nitrogen) for activity.[126]

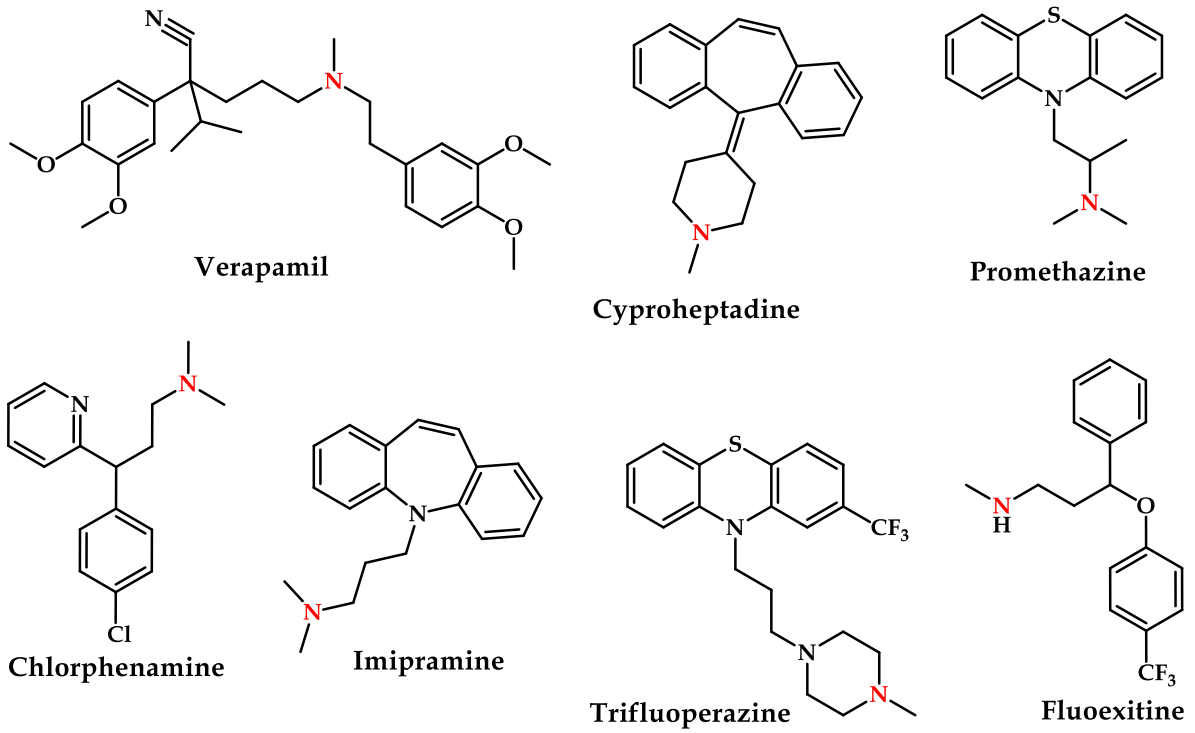

Figure 1.8: Chemical structures of examples of different reversal agents, highlighting their pharmacophore comprising two phenyl head groups linked to a hydrogen bond acceptor (nitrogen shown in red) via an aliphatic chain of variable length.

1.6.1. Reversed Chloroquines: SAR and Antimalarial Potential

Peyton and colleagues postulated that linking a RA-like moiety to a CQ-like moiety can create a class of hybrid molecules with both antimalarial and resistance-reversing properties (**Figure 1.9**).[121] The basis of this concept is the preservation of the fundamental pharmacophore for haem-binding (4-aminoquinoline), inhibition of HZ formation (4-amino-7-chloroquinoline) and drug accumulation by pH trapping (a tertiary amino group in the side-chain) [99] as well as the resistance-reversal pharmacophore, namely two suitably positioned aromatic groups with an amino group separated by a short chain.[126] As a single hybridised unit, the rCQs could directly inhibit the ability of *Pf*CRT to transport the CQ-like

moiety out of the DV [127] or completely fail to be recognised by the efflux machinery, thus rendering the drug active in the DV. As suggested by Warhurst using verapamil as a model, the RAs (in their protonated form) could alternatively reduce the transport of CQ via *Pf*CRT^{Dd2} by restoring the positive charge that was removed by the 76T mutation.[128]

Various groups have subsequently explored the concept of rCQ to design compounds with improved *in vitro* and *in vivo* activity against CQS and CQR parasites. For instance, October *et al.* used the chemistry of 3,4-Dihydropyrimidin-2(1H)-ones to construct rCQ molecules.[129] Although the molecules lacked the protonatable nitrogen of the classical RA pharmacophore, these structures exhibited excellent potency against CQS and CQR strains. Musonda *et al.* designed another set of molecules, linking an astemizole-derived moiety to the CQ quinoline end and likewise proving active.[130] Substitution of adamantyl groups for the phenyls in the RA pharmacophore has also resulted in compounds showing potency.[131] The acridine skeleton has been also been hybridised to the chloroquinoline moiety to generate related rCQ structures,[132] while the dibenzylmethylamine group was also appended to quinolines to generate hybrids, which further showed an ability to inhibit *Pf*CRT-mediated efflux of CQ.[127] A recent *ex vivo* evaluation of two rCQs against multidrug-resistant *P. falciparum* and *P. vivax* clinical isolates in Indonesia revealed high efficacy against CQR isolates of both species.[133] Even more recently, a series of simplified rCQs exhibited oral efficacy when tested *in vivo* against *P. yoelii* in a murine malaria model.[134] The study further evaluated single-dose toxicity and showed a favourable safety margin at doses as high as 150-fold the ED_{50}, suggesting their potential for antimalarial drug development. Indeed, one advantage of a rCQ is that it could be administered at a lower dose than the RA component of a cocktail, since the strong accumulation of CQ in the DV would lead to equally improved accumulation of the linked RA (compared to unlinked) due to a 1:1 drug:RA ratio. Low-dose administration could thus potentially make the hybrid cheaper

and reduce the side effects, including toxicity, often associated with administering two separate drugs.

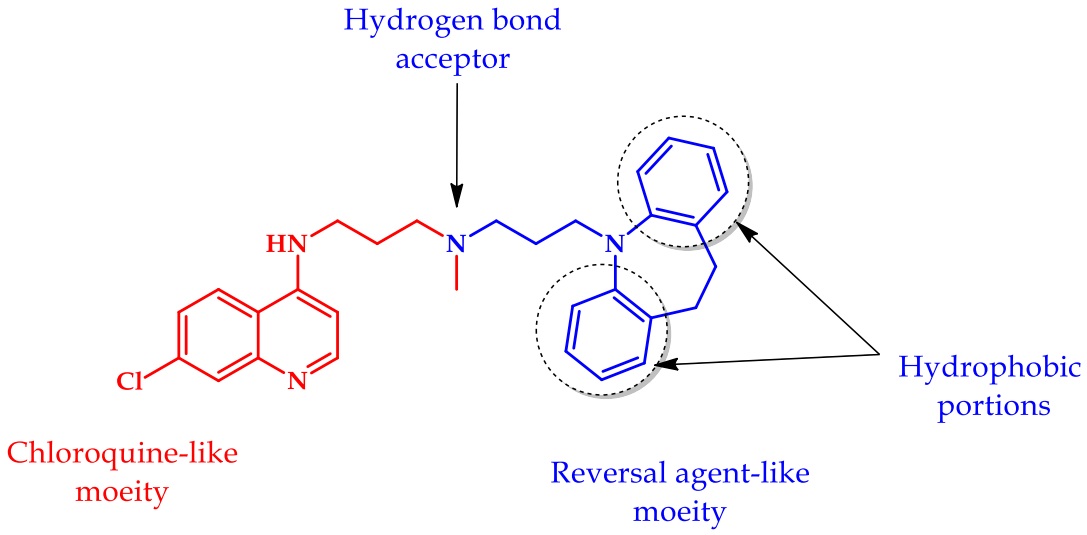

Figure 1.9: Structure activity relationship profile of a simple reversed CQ molecule: PL01 - the first hybrid molecule synthesised by Peyton and colleagues that combines the CQ-like portion and a RA-like moiety (i.e. an imipramine-like portion).[121]

1.6.2. Exploring Non-quinoline βH-Inhibiting Scaffolds

It has previously been shown that the efflux mechanism, described in **section 1.5.3**, is specific to quinoline-based antimalarials.[135] Inhibition of HZ formation, therefore, remains an important drug target for potential development of new non-quinoline antimalarials. In 2010, a pilot HTS using the NP-40 assay was carried out at Vanderbilt University Institute of Chemical Biology (VUICB) where 38, 400 compounds were tested at a concentration of 19.3 μM for their βH inhibition potential.[136] From this screening effort, 161 hits (compounds with UV-vis absorbance at 405 nm above 3 standard deviations of the negative DMSO control) were identified. These were further tested for antiplasmodial activity using the SYBR Green I fluorescence assay where 48 of the 161 hits exhibited ⩾90%inhibition of parasite growth at 23 μM. The success of this pilot study led to evaluation of the 144, 330 commercially

available compounds in the VUICB library using a similar approach.[137] From this set, 729 βH inhibitors were identified as hits (0.5% hit rate), with dose-response analysis showing 530 hits had IC_{50}s ⩽27 μM. Further evaluation revealed that 171 of these βH inhibitors identified in the primary screen were also active against the parasite cultures (32.2% hit rate), with 25 in fact showing activity in the nanomolar range. While the initial pilot screen of this VUICB library identified 6 unique βH-inhibiting scaffolds,[136] the subsequent larger and more refined analysis discovered 14 predominant scaffolds representing 246 of the 530 βH inhibitors identified (**Figure 1.10**).[137]

Of the 530 βH inhibitors, 129 were noted to have a quinoline-based scaffold, with approximately one-third of these active against the parasite. Importantly, however, several non-quinoline scaffolds which had not previously been reported as inhibitors of βH formation were also discovered. For instance, 33 βH-inhibiting phenyl benzamides were also identified from this screen. Though benzamides have previously been reported as inhibitors of the *P. falciparum* pyrimidine biosynthetic enzyme dihydroorotate dehydrogenase (*Pf*DHODH),[136, 138, 139] their activity in this study resulted in drastic increases in intracellular 'free' haem levels corresponding to parasite death. These observations could be due to the specific interactions of the compounds with 'free' haem or HZ crystal. The benzylethene group comprised 12 compounds that grouped into scaffolds with an ethene-bridged phenyl group to either a quinoline or benzimidazole scaffold. Some compounds within this category have been reported to have *in vitro* antiplasmodial activity through inhibition of the M1 alanyl aminopeptidase and the M17 leucine aminopeptidase targets.[138] The screening also yielded 7 triaryl imidazoles with IC_{50} values ranging from 2.4 to 22.9 μM, six of these possessing *in vitro* antiplasmodial activities with IC_{50}s between 0.61 and 11.7 μM.

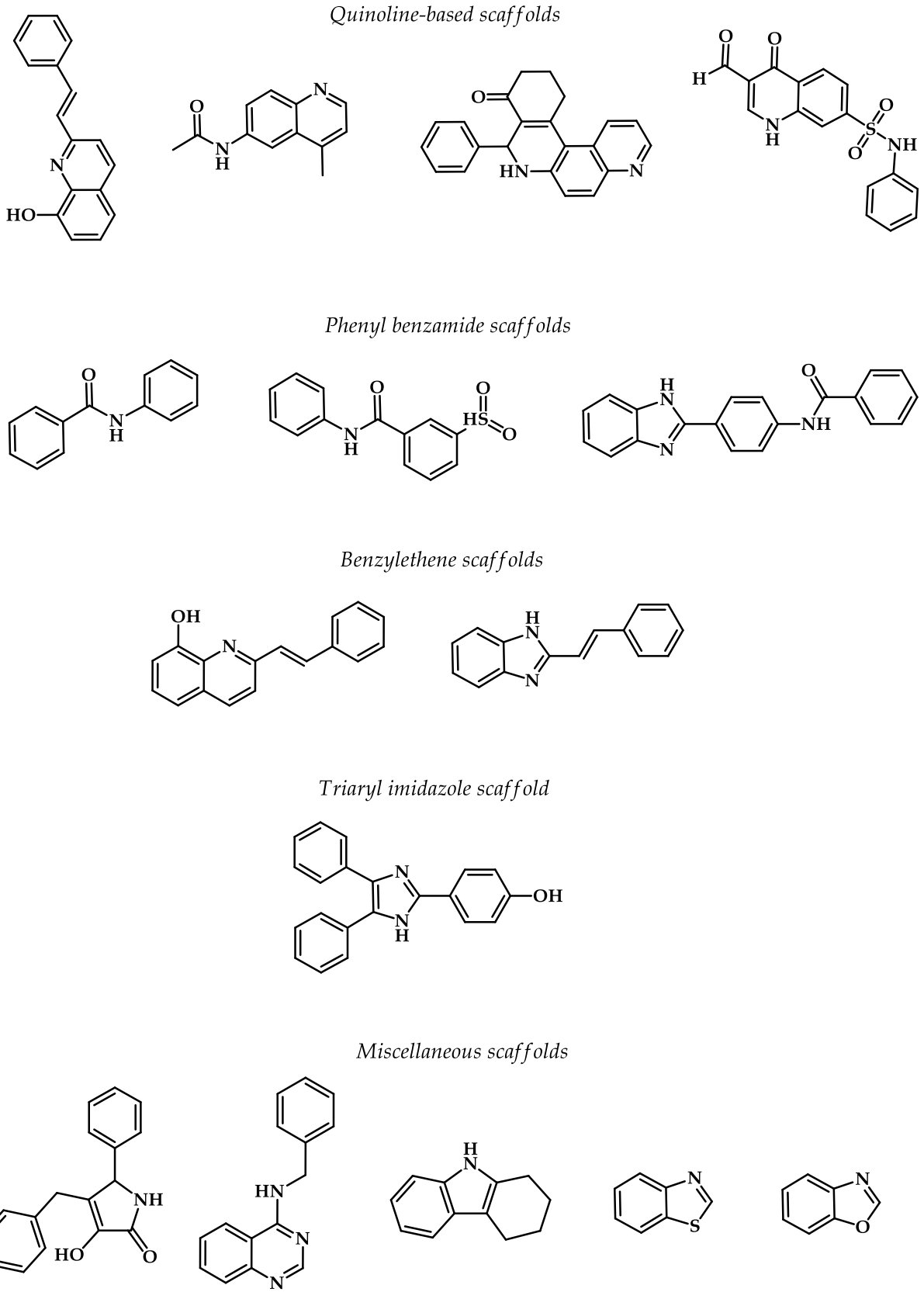

Figure 1.10: The primary scaffolds identified in the high throughput β-haematin inhibitory screen using the Vanderbilt University Institute of Chemical Biology compound library.

In addition to the 14 scaffolds, several other interesting compounds were not associated with a specific scaffold type, or only accounted for a very small proportion of the overall hit rate. In particular, 284 βH inhibitors that did not cluster into a specific scaffold were identified including 92 with antiplasmodial activity. The structural diversity of these miscellaneous compounds includes pyridines, amides, indoles, acridinediones, amides, ethers and thiols, among others.

In addition, Fong *et al.* recently evaluated 400 compounds from the MMV Malaria Box using the same βH formation assay to detect inhibitors of this crystallisation process.[140] Of the 400 compounds, 9 compounds (**Figure 1.11**) were identified to have dose–response βH inhibitory activity more potent than that of CQ, with activities from 8.7 to 22.7 μM. Indeed, the Malaria Box compounds identified as βH inhibitors in this study were reflective of the previously described scaffolds. For instance, consistent with the findings of Sandlin *et al.*, three benzimidazole, one quinoline, two benzamide and three triaryl imidazole scaffolds constituted the 9 hits. Furthermore, this analysis validated inhibition of HZ formation in the parasite as the target of seven of the nine *in vitro* βH-inhibiting hits by demonstrating significant ($p < 0.05$) increases in 'free' haem levels from baseline, corresponding to decreases in HZ and parasite survival.[140]

That some of these scaffolds have been reported elsewhere to afford compounds which target other proteins and pathways within *P. falciparum* presents an added incentive to explore these chemotypes for multi-target inhibition in the parasite. Moreover, the non-quinoline scaffolds provide a basis for designing new drugs which can circumvent the liabilities commonly associated with quinolines namely; the notoriety of cross-resistance to structurally-related scaffolds and toxicity to the human *Ether-ã-go-go* Related Gene (hERG) protein.[141]

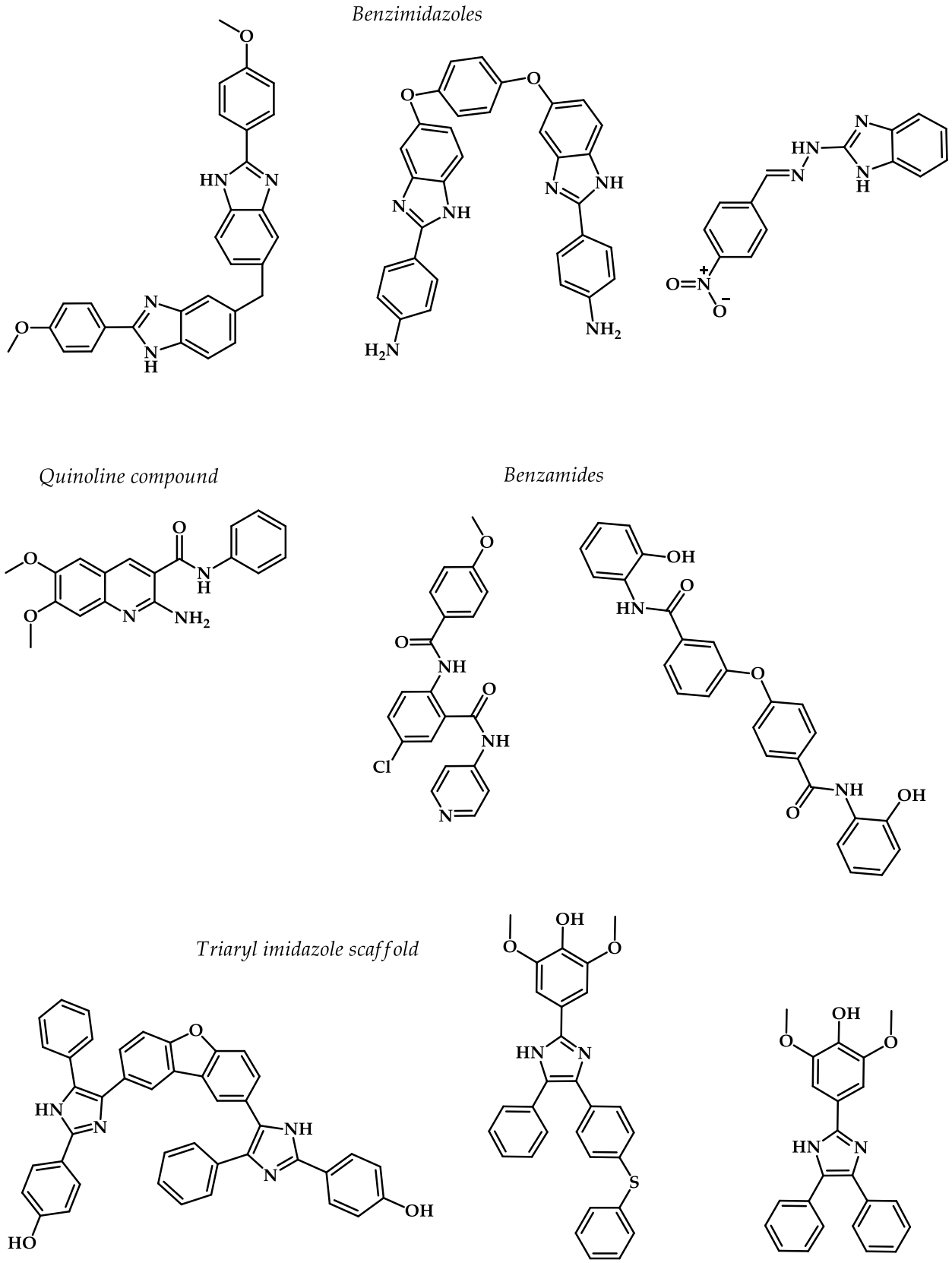

Figure 1.11: Chemical structures of 9 βH inhibitors representing the 4 main scaffolds identified by Fong *et al.,* (2015) through screening the MMV Malaria Box library.[140]

1.7. Medicinal Chemistry Outlook of 4-aminoquinoline and Non-quinoline βH Inhibitors

1.7.1. Absorption-related physicochemical properties

In drug discovery and development, absorption-related physicochemical properties of a compound constitute some of the most significant features of a drug entity.[142] Physicochemical properties like aqueous solubility and lipophilicity are critical in drug discovery because they influence the rate and extent of absorption through biological membranes, an important determinant of bioavailability (and ultimately efficacy) of a compound. On the other hand, this permeation-enhancing lipophilicity has the potential to predispose a drug to rapid metabolic clearance hence the need for a trade-off between these properties. In the example of CQ and other 4-aminoquinolines, the nitrogen in the quinoline core and in the lateral side chain are crucial in the pH trapping process due to their basicity. Indeed, the degree of association with Fe(III)PP1X, acid dissociation constant , and lipophilicity (indexed by distribution and partitioning coefficients) of the drugs are some of the physicochemical properties known to play an important role in their antiplasmodial activity and βH inhibition.[99, 143] Using a principal component analysis and orthogonal molecular descriptors of ~30, 000 diverse GlaxoSmithKline (GSK) compounds, Gleeson reported qualitative predictions of absorption, distribution, metabolism, and excretion (ADME) properties likely to be exhibited by a molecule based its ionisation state, molecular weight (MW) and logarithm of the partitioning coefficient (cLogP).[144] For basic molecules, like most quinolines, increased MW > 400 and cLogP > 4 were predicted to lower solubility and bioavailability while significantly raising *in vivo* clearance and potential for hERG inhibition (**Table 1.1**).

Table 1.1: The influence of molecular weight and cLogP on absorption-related parameters in basic compounds. Green colour code denotes favourable effects, yellow denotes tolerable effects while red highlights undesirable outcome. Reprinted (adapted) with permission from *Gleeson P, (2008); J. Med. Chem. 51: 817 – 834*. Copyright (2008) American Chemical Society

ADME features of basic molecules	Mol. Weight < 400 and cLogP < 4	Mol. Weight > 400 and cLogP >4
Solubility	Higher/average	Lower/average
Permeability	Higher/average	Average
Bioavailability	Average	Lower
Volume of distribution	Higher/average	Higher
Plasma protein binding	Lower	Average
In vivo clearance	Average	Higher/average
hERG inhibition	Average/higher	Higher
P-gp efflux	Average	Higher/average
Brain tissue binding	Lower	Higher

1.7.2. Potential for Cardiotoxicity

Owing to their lipophilicity and basic nature, quinoline antimalarials are thought to possess hERG channel inhibition liabilities. The *hERG* gene encodes a potassium (K^+) channel that creates the rapidly activating delayed rectifier K^+ current called IKr, an important component that regulates the duration of the cardiac action potential.[145] Inhibition of the hERG K^+ channel by pharmaceutical agents or as a result of inherited dysfunction results in the obstruction of the flow of K^+ thus lengthening the time required to repolarise the cell,[146]

which is manifested as an elongation of the QT interval in electrocardiograms. A life threatening ventricular arrhythmia, torsades de pointes, is implicated in the blockade of the hERG K^+ channel,[147] and as a result, several commercial drugs have been withdrawn prior to marketing or have had to contend with major labelling changes that have restricted their use.[148] Computational predictions of hERG liability are in agreement that basic and/or lipophilic compounds are strongly implicated in hERG channel inhibition.[147] Predictive analysis through comparative field molecular analysis and comparative field similarity analysis using 31 and 28 molecules, respectively, identified aromatic (hydrophobic) and central nitrogen as well as ionisable centres as key features for potential binding to hERG.[149, 150] These features are intrinsic to CQ and other 4-aminoquinoline substructures, which have been shown to exert toxic effects by interacting with the hERG K^+ channel causing the elongation of the QT interval resulting in potentially fatal outcomes.[151] The high lipophilicity of some of the quinoline derivatives (cLogP > 3.0) that are extensively distributed in tissues, likely ensures that drug levels in the heart are sufficient to interact with the K^+ channels.[152]

As a result of its notorious ligand promiscuity, the hERG channel has emerged as an important anti-target in early drug discovery and development as preclinical drug candidates are routinely screened against it very early in the drug discovery process. Crucially, the rational design of 4-aminoquinoline related antimalarials bearing modifications that would reduce lipophilicity, basicity and/or electron releasing properties is a strategy to be vigorously pursued in drug discovery and development to rid drug candidates of the physicochemical properties likely to make them prone to undesirable side effects. Finally, it is instructive to consider all the results from *in vitro* determination of hERG channel inhibition in the context of cardiac safety indices which use the ratio of IC_{50} values of hERG inhibition to the compound's free therapeutic plasma concentration to assess the likelihood of inducing cardiac toxicity.[153, 154] To illustrate this point, Traebert and colleagues observed that

differential inhibition of HEK293 cells stably transfected with hERG complimentary DNA (cDNA) by MFQ (IC_{50} = 2.63 μM) and LM (IC_{50} = 8.13 μM) yielded comparable cardiac safety indices of 53 and 48, respectively.[155] This finding demonstrated that, though informative, hERG inhibition IC_{50} on its own cannot sufficiently predict a compound's potential for cardiac toxicity.

1.8. Background to Current Research Question and Hypothesis

1.8.1 Reversed Chloroquines with Improved Physicochemical and Drug-Like Properties.

There is a need to advance the understanding of structural specificity of rCQs based on the 4-aminoquinoline scaffold with regard to the inhibition of βH formation, antiplasmodial activity and physicochemical ADME descriptors. A major limitation of the first prototype compound synthesised by Burgess *et al.* (**Figure 1.9**) was its high lipophilicity (cLogP ~9.0).[121] Further exploration of the SAR gave rise to molecules with improved water solubility, activity against CQS and CQR parasites, which were shown to be orally curative in mice.[156, 157] These compounds, however, still lacked modifications in the quinoline ring system that would reduce hERG channel inhibition. Among the series of compounds that have been designed from this model were the recently reported dibemequines (DBQs), which contain the 7-chloroquinoline nucleus attached to dibemethin-type side chain via a shortened linker, instead of a three carbon aminoalkyl chain positioned between the two aromatic rings (**Figure 1.12a**).[127, 158] These compounds were reported to enhance biological activity through accumulation in the DV via pH trapping. Further modifications were suggested for these molecules to enhance basicity and improve vacuolar accumulation, reduce lipophilicity and lower the MW of the resultant molecules while retaining antiplasmodial and βH-inhibiting activities. These changes included replacing one of the

aromatic rings in the side chain of aminomethyl dibemethin with a pyridine ring (**Figure 1.12b**) to improve accumulation within the DV and further enhance aqueous solubility. The new series of compounds, pyrido-dibemequines (pDBQs), were envisaged as potential rCQs which would be active against both CQS and CQR strains. Additionally, proposals were made for structural alterations that would potentially mitigate the hERG liability in the resultant compounds without compromising their potency. Among the changes for this effect involved replacement of the –Cl group at C7 with a cyano (-CN) group to afford analogues with lower MW and lipophilicity while still retaining βH inhibiting potential. By using different substituents with diverse steric and electronic properties, Kaschula *et al*. had previously defined the characteristics of the groups at C7.[100] However, while it is known that a 4-aminoquinoline compound with the chloro group at C7 will inhibit the formation of βH, the influence of a nitrile group has not been tested.

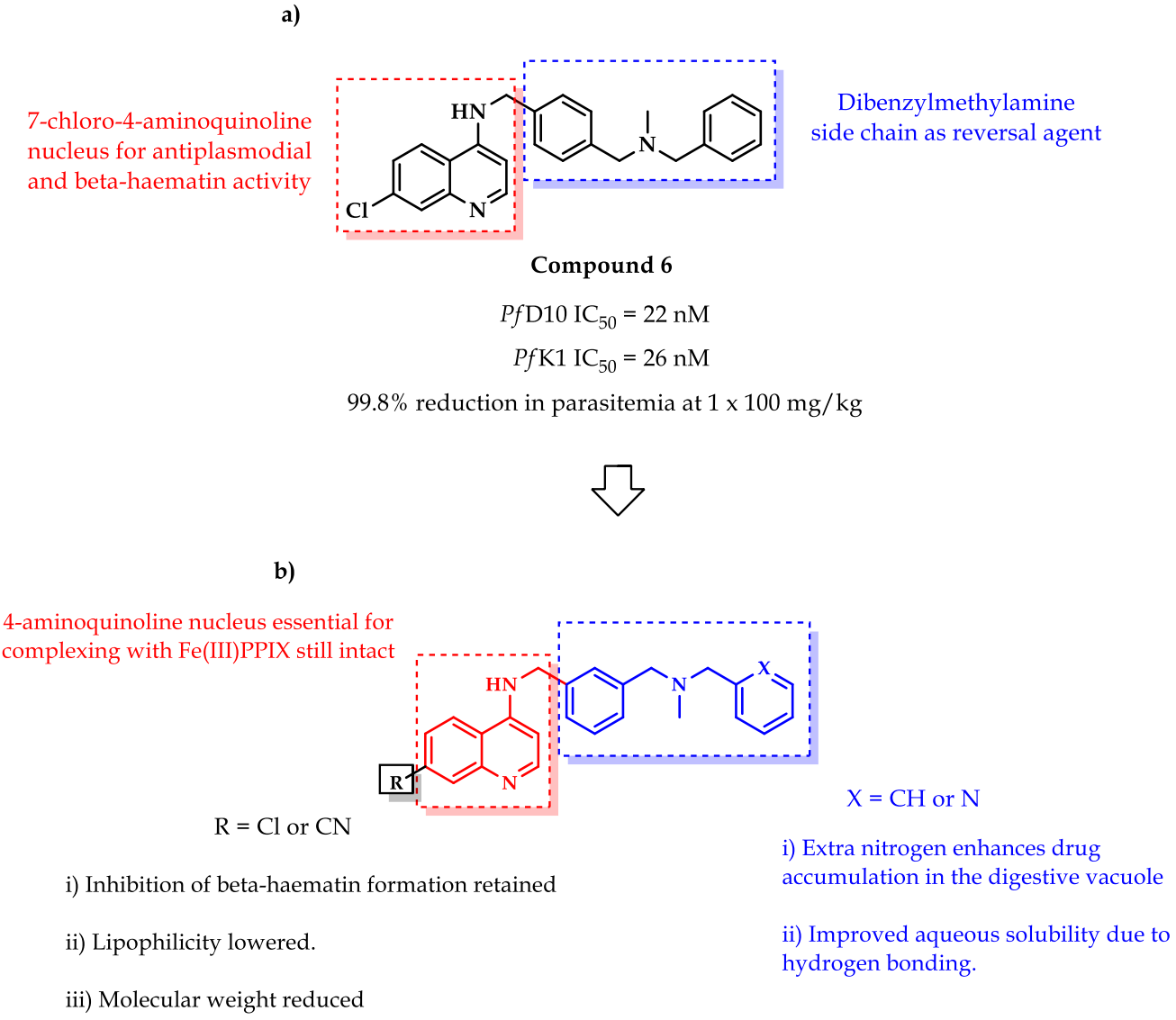

Figure 1.12: Chemical structure of **a**) compound **6** from Zishiri *et al.*, (2011b) showing its SAR[127] and **b**) alterations on the compound to lower MW and lipophilicity, and improve DV accumulation

1.8.2. Pyrido[1,2-a]benzimidazoles a βH-Inhibiting Antimalarial Chemotype

The studies by Sandlin *et al.* using 144, 330 compounds in the VUICB library and Fong *et al.* using compounds in the MMV Malaria Box recognised the benzimidazole scaffold as a potent inhibitor of βH formation.[136, 137, 140] The benzimidazole nucleus is a structural unit of

naturally occurring purine nucleotides [159] and as such, possesses the capacity to interact with many biological systems, leading to a variety of biological activities. The benzimidazole motif is therefore a recognised privileged scaffold in medicinal chemistry due to its capacity to interact with numerous biological systems. Indeed, research and optimisation of substituents around the benzimidazole core has led to compounds with antifungal,[160] antiviral,[161] antitubercular,[162, 163] and anxiolytic activity.[164]

Recently, benzimidazole analogues with potent *in vitro* antiplasmodial activity have been reported.[165] In 2015, Keurulainen *et al.*, illustrated the synthesis and potent antiplasmodial activities of benzimidazole aminopropylamides,[166] while highly potent benzimidazole-2-pyridinyl analogues with *in vitro* antiplasmodial IC_{50} values of 0.16 – 3.0 µM against *P. falciparum* were synthesised and evaluated by Saify *et al.* in 2012.[167] Camacho and colleagues, in 2011, investigated potent benzimidazole-5-carbohydrazide derivatives.[168] On the other hand, pyrido[1,2-*a*]benzimidazoles (PBIs) represent a novel antimalarial chemotype that has previously been investigated for antibacterial, antifungal, antiviral and antitumor activities.[169] In 2011, Ndakala *et al.* reported on the synthesis and antimalarial activity of PBIs from a collaborative screening of a library of 1,440 chemically diverse non-proprietary chemicals against a protozoa panel.[170] From this, the PBI compound **TDR15087** with moderate activity against *P. falciparum* GHA (CQS) and W2 (CQR) strains (IC_{50}: 0.17 and 0.37 µM respectively) was identified. Further SAR exploration on this core on an additional 535 PBI analogues in a medium throughput screen against the K1 (CQR) strain yielded 49 compounds with IC_{50} below 0.1 µg/ml, notably analogues **TDR35885** and **TDR44047** (**Figure 1.13**). All three were, however, inactive in the *P. berghei* mouse model up to high doses of 4 × 100 mg/kg ip, presumably due to poor solubility and metabolic stability.

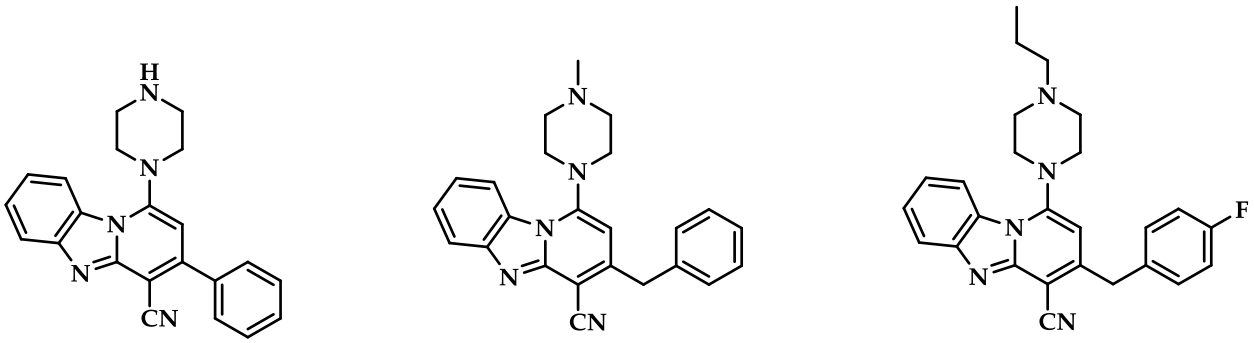

Figure 1.13: Chemical structures of PBI screening hits with potent antiplasmodial activity

In an attempt to identify compounds that would retain activity in the *P. berghei* model, Ndakala *et al.*, embarked on SAR optimisation around the PBI core focusing on 3-aryl derivatives with alkylamino side chains possessing submicromolar activity against K1 (CQR). The most active was compound **4c (**IC_{50} = 0.047 µM). Compound **4c** was, however, metabolically unstable in liver microsomes, rapidly forming the mono-desethyl metabolite, **4h** through *N*-dealkylation (**Figure 1.14**). Although compound **4h** retained activity and stability in murine microsomes, pharmacokinetic pitfalls curtailed *in vivo* activity, most notably low bioavailability presumably resulting from solubility-limited absorption. Single- and multi-dose *in vivo* efficacy studies of the orally administered salt of **4h** against *P. berghei* also indicated that the activity plateaus with doses above 25 mg/kg (50.2%, 71.2% and 79.8% reduction in parasitemia on days 3, 4 and 5, respectively, at 50 mg/kg dose), and the scenario is replicated following subcutaneous administration.

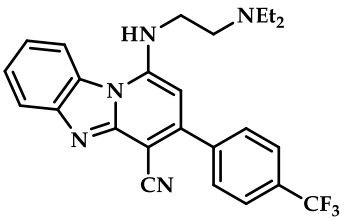

4c

*Pf*K1 = 0.047 μM

Selective Index = 612

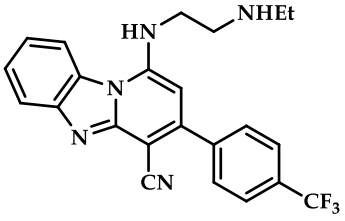

4h

*Pf*K1 = 0.12 μM

Selective Index = 20.5

Figure1. 14: Chemical structures of the lead PBI compound **4c** and its metabolite **4h** identified by Ndakala and colleagues in 2011.[170]

The findings by Ndakala *et al.*, as illustrated above, were crucial because they constituted the seminal published literature related to the antimalarial activity of PBIs, and therefore laid the foundation for further optimisation of the lead PBI to identify analogues with improved pharmacokinetic profiles. SAR investigations on the core structure of compound **4h** (**Figure 1.15**) aimed at exploring effects of modifications around parts of the scaffold not previously investigated for effects on the biological and physicochemical properties. SAR_1 comprised replacement of the alkylamino side chain in **4h** with various moieties containing water-solubilising H-bonding groups, encompassing imidazole, hydroxypyrrolidine or piperidinyl moieties. SAR_2 involved distortion of molecular planarity through introduction of a small hydrophobic substituent at C2 thus lowering the crystal packing energies, and consequently improving aqueous solubility.[171] In this regard, fluorine was preferred since, due to the small size, it is less likely to interfere with protein-drug interactions and hence more likely to increase the dihedral angle without loss of biological activity.[171] SAR_3 comprised two derivatives bearing replacement of the 4-trifluoromethylphenyl (4-CF_3Ph) group at C3 with *meta*- and di-substituted phenyl rings. Finally, SAR_4 involved introduction of substituents on the previously unexplored left hand side (LHS) aromatic ring, including mono- and di-chloro substitutions at C7, C8 and C9.

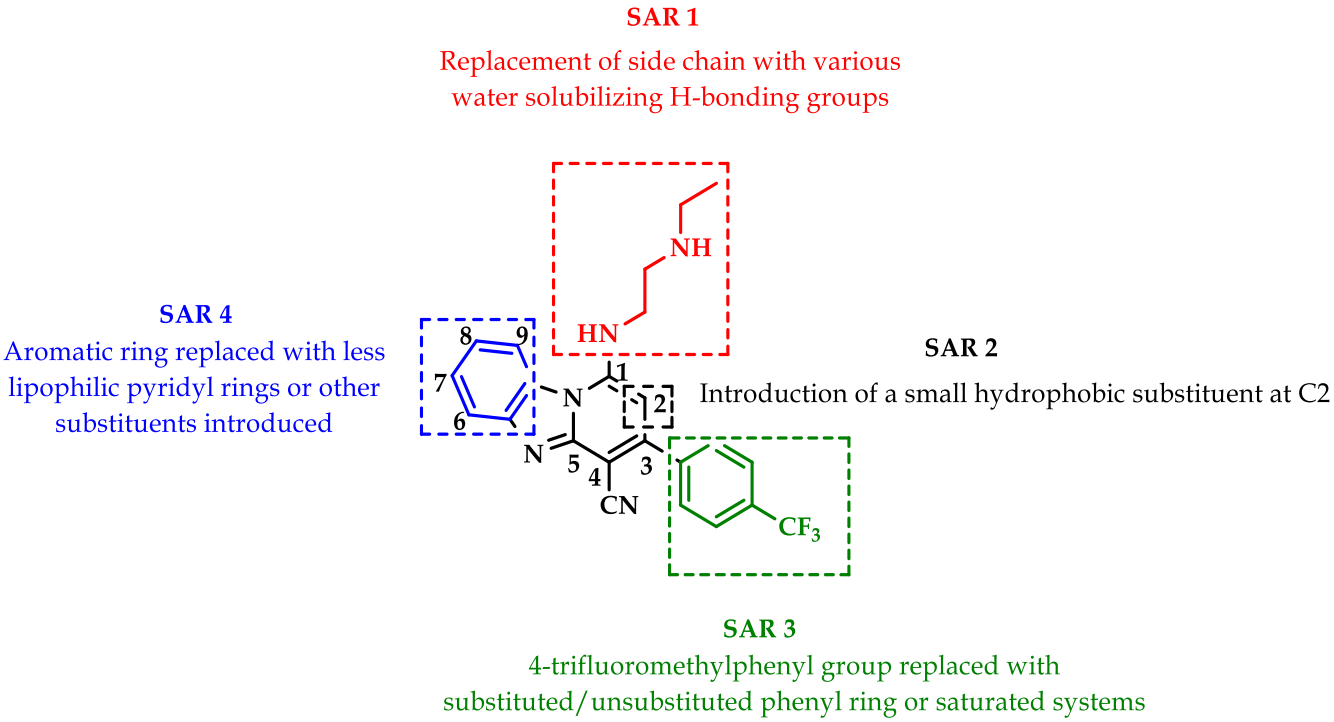

Figure 1.15: Chemical structure of compound **4h** showing the different SAR explorations that aimed at designing compounds with improved pharmacokinetic features

The PBIs have a remarkable structural likeness to CQ, which includes a planar heterocyclic moiety and a basic amine side group. These features make them candidates for *π-π* interactions, which is one of the hallmark features of haem-drug complex formation. As such, PBI derivatives lend themselves evaluable as potential inhibitors of βH formation *in vitro* and HZ formation within *P. falciparum* and *S. mansoni* cells. Additionally, the identification of related benzimidazole and acridine scaffolds as βH inhibitors,[137, 140] provides further rationale for exploring PBIs as potential inhibitors of the HZ formation.

1.9. General Aims & Objectives

The aims of this project were to profile a series of pDBQ and PBI derivatives using *in vitro* and *in silico* analyses in order to determine their physicochemical properties and correlate these with activity of the derivatives against different *P. falciparum* strains. As part of mechanistic investigations, the ability of the compounds to perturb HZ formation was investigated through analysis of their βH inhibiting potential as well as their effect on the fate of parasite-derived haem. In addition, their safety profiles with respect to the inhibition of mammalian cell growth and the hERG channel were evaluated using predictive computational tools as well as through direct experimentation (for the pDBQs). Finally, the *in vivo* antimalarial and antischistosomal efficacy of derivatives with favourable features was tested in the relevant mouse models.

1.9.1. Specific Objectives

The primary objectives of the project with respect to pDBQs and/or PBIs were:

(i) To predict and experimentally determine aqueous solubility, permeability and lipophilicity (LogD).

(ii) To test *in vitro* antiplasmodial activity against CQS and CQR *P. falciparum* strains and their cytotoxicity in Chinese Hamster Ovarian (CHO) cells.

(iii) To test *in vitro* microsomal metabolic stability in mouse and human liver microsomes and identify the resultant metabolites.

(iv) To test ability to inhibit *in vitro* formation of βH as well as HZ formation in synchronised *P. falciparum* cultures.

(v) To use computational prediction and a heterologous expression system to determine hERG toxicity.

(vi) To investigate *in vivo* efficacy in malaria and schistosomiasis mouse models.

Chapter 2

MATERIALS AND GENERAL METHODS

2.1 Materials (Reagents and Solvents)

All materials used were of AR grade or higher and unless specified, used without further purification. The materials are listed according to the methods for which they were needed. All consumables were purchased from Lasec, Millipore, Merck South Africa and Sigma Aldrich. The water used throughout this work was double distilled deionised Millipore® Direct-Q water.

2.1.1. Materials for Biological Experiments

A list of materials is presented in **Tables 2.1 – 2.13**

Table 2.1: Materials used for the tissue culture of *Plasmodium falciparum*

Materials	Supplier
RPMI 1640 with glutamine but without sodium bicarbonate (R6504)	Sigma Life Science
D-(+)-Glucose	Sigma Life Science
(N-2-[hydroxyethyl]piperizine-N′-2-[ethanesulfonic acid]) HEPES	Sigma Life Science
Phosphate buffered saline (PBS) tablet	Sigma Life Science
Albumax II	Gibco
Potassium chloride	Sigma
Sodium bicarbonate	Sigma Life Science
Sodium chloride	Sigma Aldrich
Sodium L-lactate	Sigma Life Science
Gentamicin solution	Sigma Life Science
D- Sorbitol	Sigma Life Science
Sodium dihydrogen phosphate	Merck
Glycerine (1,2,3 – propantriol)	Sigma Aldrich
Oil for immersion lenses	Merck
Giemsa's azur eosin methylene blue solution	Merck
Hypoxanthine	Sigma Life Science

Table 2.2: Materials used for the lactate dehydrogenase (pLDH) antiplasmodial assays

Materials	Supplier
Dimethyl sulfoxide (DMSO)	Merck
Triton X 100	Merck
Saponin	Sigma Life Sciences
Trizma base (Tris)	Sigma Life Sciences
Calcium L-lactate hydrate	Sigma Life Sciences
Phenazine ethosulphate	Sigma Aldrich
Nitro blue tetrazolium salt (NBT)	Sigma Aldrich
Hydrochloric acid 32%	Sigma Aldrich
Ethylenediaminetetraacetic acid (EDTA)	BDH
3-Acetylpyridine adenine dinucleotide (APAD)	Sigma Life Science

Table 2.3: Materials used for *in vitro* and *in vivo* antischistosomal assays

Materials	Supplier
Dimethyl sulfoxide (DMSO)	Fluka
Resazurin	Sigma Aldrich
Medium 199	Invitrogen
RPMI 1640	Invitrogen
5% heat-inactivated fetal calf serum (FCS)	Sigma
Penicillin (100 U/ml)	Sigma Aldrich
Streptomycin (200 µg/ml)	Sigma Aldrich
Phosphate buffered saline (PBS) tablet	Sigma Life Science
Hanks Balanced Salt Solution (HBSS)	Sigma Aldrich
2% amphotericin B	Sigma Aldrich
70% Percoll®	Sigma Aldrich
Sodium chloride (1.5M)	Sigma
5% glucose	Sigma Aldrich
Ethanol	Fischer Scientific
7% Tween 80	Sigma Aldrich
Control: Praziquantel ($C_{19}H_{24}N_2O_2$, Mw = 312.41 g/mol)	Sigma Life Science

Table 2.4: Materials used for the Chinese Hamster Ovarian (CHO) cell cytotoxicity assay

Materials	**Supplier**
45% Dulbecco's Modified Eagle Medium (DMEM)	Gibco
45% HAMS F-12	Gibco
10% inactivated foetal calf serum	Sigma Aldrich
Crystal Violet Dye	Sigma Aldrich
Dimethyl sulfoxide (DMSO)	Merck
3-(4,5)-dimethylthiazol-2-yl)-2,5-diphenyl tetrazolium bromide (MTT)	Thermo Fisher Scientific
Control: Emetine hydrochloride ($C_{29}H_{40}N_2O_4$ .2HCl Mw = 553.56 g/mol)	Sigma

Table 2.5: Materials used for determination of hERG toxicity through QPatch Experiment

Materials	**Supplier**
Dimethyl sulfoxide (DMSO)	Merck
Sodium chloride	Sigma Aldrich
Potassium chloride	Sigma Aldrich
Potassium flouride	Sigma Aldrich
HEPES (N-2-[hydroxyethyl]piperizine-N'-2-[ethanesulfonic acid])	Sigma Life Science
Magnesium chloride	Sigma Aldrich
Calcium chloride	Sigma Aldrich
EGTA (ethylene glycol-bis(β-aminoethyl ether)-N,N,N',N'-tetraacetic acid)	Sigma Aldrich
D-(+)-Glucose	Sigma Aldrich
Magnesium salt of ATP (Mg_2ATP)	Sigma Aldrich
Control: Verapamil hydrochloride ($C_{27}H_{38}N_2O_4$ .HCl Mw = 491.07 g/mol)	Tocris Bioscience

Table 2.6: Materials used for microsomal stability and metabolite identification assays

Materials	Supplier
Human liver microsomes	Xenotech
Mouse liver microsomes	Xenotech
Nicotinamide adenine dinucleotide phosphate (NADPH)	Merck
Potassium dihydrogen phosphate (KH_2PO_4, Mw = 136.09 g/mol)	Merck
Dipotassium hydrogenphosphate (K_2HPO_4, Mw = 174.18 g/mol)	Merck
Dimethyl sulfoxide (DMSO)	Sigma Aldrich
Acetonitrile (LC-MS grade)	Merck/Sigma
Formic acid	Sigma
Ammonium formate	Sigma
Carbamazepine (Mw = 236.3 g/mol)	Sigma
Control 1: Propranolol hydrochloride (Mw = 295.8 g/mol)	Sigma
Control 2: Midazolam maleate salt (Mw = 441.8 g/mol)	AiBST Zimbabwe

Table 2.7: Materials for *in vivo* antimalarial efficacy testing in *P. berghei*-infected mice

Materials	Supplier
Phosphate buffered saline (PBS) tablet	Sigma Life Science
Dimethyl sulfoxide (10%)	Sigma Aldrich
Ethanol (10%)	Fischer Scientific
Propylene glycol (40%)	Sigma Aldrich
Hydroxypropylmethylcellulose (HPMC)	Sigma Aldrich
Purified water (HPLC grade)	Merck Millipore
Control 1: Chloroquine ($C_{18}H_{26}ClN_3.2H_3PO_4$, Mw = 515.87 g/mol)	Sigma Life Science

Table 2.8: Materials used for the detergent mediated β-haematin (βH) inhibition assay

Materials	Supplier
Dimethyl sulfoxide (DMSO)	Sigma Aldrich
Sodium acetate trihydrate	Sigma Aldrich
Acetic acid	Sigma Aldrich
Haemin (> 98%)	Fluka
Acetone	Sigma Aldrich
Pyridine	Sigma Aldrich
Nonidet P-40 (NP-40), 305.5 µM	Pierce Biotechnology
Control 1: Chloroquine ($C_{18}H_{26}ClN_3.2H_3PO_4$, Mw = 515.87 g/mol)	Sigma Life Science
Control 2: Amodiaquine ($C_{20}H_{24}Cl_3N_3O.2H_2O$, Mw = 464.81 g/mol)	Sigma
Control 3: Pyrimethamine ($C_{12}H_{13}ClN_4$ Mw = 248.71 g/mol)	Fluka Analytical

Table 2.9: Materials used for fluorescence-activated cell sorting (FACS) analysis

Materials for FACS analysis	Supplier
Phosphate buffered saline (PBS) tablets	Sigma Life Science
SYBR Green I nucleic acid gel stain	Sigma Aldrich
Trucount ™ Beads	Becton, Dickinson & Company

Table 2.10: Materials used for cellular haem fractionation assay

Materials	Supplier
(N-2-[hydroxyethyl]piperizine-N′-2-[ethanesulfonic acid]) HEPES	Sigma Life Science
Sodium Dodecyl Sulfate (SDS)	Sigma Aldrich
Sodium chloride	Sigma Aldrich
Pyridine	Sigma Aldrich
Sodium hydroxide	Sigma Aldrich
Hydrochloric acid	Sigma

2.1.2. Materials for Physicochemical Experiments

Table 2.11: Materials used for LogD determination at pH 5.0 (Shake Flask Method)

Materials	**Supplier**
2-(N-morpholino) ethanesulfonic acid (MES)	Sigma Aldrich
Dimethyl sulfoxide (DMSO)	Sigma Aldrich
n-Octanol	Sigma Aldrich
Purified water (HPLC grade)	Merck Millipore

Table 2.12: Materials used for LogD determination at pH 7.4 (HPLC Method)

Materials	**Supplier**
n-Octanol	Sigma
Potassium dihydrogen phosphate (KH_2PO_4, Mw = 136.09 g/mol)	Merck
Dipotassium hydrogenphosphate (K_2HPO4, Mw = 174.18 g/mol)	Merck
Dimethyl sulfoxide (DMSO)	Sigma Aldrich
Acetonitrile (LC-MS grade)	Sigma
Formic acid	Sigma
Purified water (HPLC grade)	Merck Millipore
Control 1: Ouabain ($C_{29}H_{44}O_{12}$, Mw = 584.65 g/mol)	Sigma
Control 2: Hydrocortisone ($C_{21}H_{30}O_5$, Mw = 362.46 g/mol)	Sigma
Control 3: Verapamil ($C_{27}H_{38}N_2O_4$, Mw = 454.60 g/mol)	Sigma

Table 2.13: Materials used for Kinetic solubility and membrane permeability assays

Materials	Supplier
MultiScreen Filter plates (Millipore, 0.4 µM PCTE Membrane)	Merck
Potassium dihydrogen phosphate (KH_2PO_4, Mw = 136.09 g/mol)	Merck
Dipotassium hydrogenphosphate (K_2HPO4, Mw = 174.18 g/mol)	Merck
Dimethyl sulfoxide (DMSO)	Sigma Aldrich
Acetonitrile (LC-MS grade)	Anatech
Formic acid	Sigma
Carbamazepine (Mw = 236.3 g/mol)	Sigma
Acetic acid	Merck
Sodium monohydrogen phosphate heptahydrate (Mw = 268.1 g/mol)	Sigma
Lucifer Yellow CH dipotassium salt (Mw = 521.57 g/mol)	Sigma
Control 1: Propranolol hydrochloride (Mw = 295.8 g/mol)	Sigma
Control 2: Testosterone (Mw = 288.42 g/mol)	Sigma
Control 3: Warfarin (Mw = 308.34 g/mol)	Sigma
Control 4: Hydrocortisone (Mw = 362.5 g/mol)	Sigma
Control 5: Reserpine (Mw = 608.7 g/mol)	AiBST Zimbabwe

2.2. Sample Preparation

2.2.1 Tissue culture of *Plasmodium falciparum*

***Incomplete culture medium*:** Incomplete culture medium was prepared by dissolving 10.4 g RPMI 1640 (with glutamine but without sodium bicarbonate), 4 g D-(+)-glucose, 6 g HEPES, 0.088 g hypoxanthine, 5 g albumax II, and 1.2 mL (0.05 g/L) gentamicin in 1 L of distilled water. The solution was pre-filtered through a 0.45 µm filter then sterile-filtered through a 0.22 µm membrane into autoclaved glass bottles before being stored at 4 °C until further use.

***Sodium bicarbonate (5%)*:** The solution was prepared by dissolving 50 g of $NaHCO_3$ in 1 L of distilled water and sterile filtered through a 0.22 µm membrane into 100 mL autoclaved glass bottles before storage at 4 °C until further use.

***Complete culture medium*:** Solution of complete culture medium was prepared by adding 8.4 mL of 5% $NaHCO_3$ to 200 mL of the incomplete culture medium before use then stored at 4 °C until further use.

***5% Sorbitol*:** A solution of 5% D- Sorbitol was prepared by dissolving 50 g of D-sorbitol in 1 L of distilled water. The solution was sterile filtered through a 0.22 µm membrane into 250 mL autoclaved glass bottles and stored at 4 °C until further use.

***Phosphate Buffered Saline (PBS)*:** PBS was prepared by dissolving 1 tablet in 200 mL of distilled water. The final preparation yielded a solution containing 0.01 M phosphate buffer, 0.0027 M KCl and 0.14 M NaCl with a pH of 7.4 at 25 °C.

***Washed O+ human red blood cells*:** The human blood used in the experiments was obtained from the blood bank (Groote Schuur Hospital). The blood was washed by adding wash medium to whole blood in a 1:1 ratio. The solution was centrifuged at 1200 relative

centrifugal force (rcf) for 5 min and the supernatant aspirated. This process was repeated a second time and the washed blood stored at 4 °C.

Giemsa stain (10%): Giemsa stain was prepared before use by diluting the stain 1:10 in PBS.

2.2.2 Antiplasmodial assays

***Malstat solution*:** Malstat was prepared by dissolving 400 µL Triton X100, 4 g L-lactate and 1.32 g Tris buffer in 150 mL of distilled water. To this, 22 mg of APAD was added and the pH adjusted to 9 with 32% HCl. The final volume was made up to 200 mL with distilled water then stored at 4 °C.

***NBT solution*:** A solution of NBT was prepared by dissolving 160 mg of NBT and 8 mg phenazine ethosulphate in distilled water to a final volume of 100 mL. The storage container was covered with foil as NBT is light sensitive and stored at 4 °C.

2.2.3 Detergent mediated assay for β-haematin inhibitors

***DMSO: NP-40: water / 10: 20: 70 (v/v)*:** The solution (20 mL) was prepared by mixing 14 mL of water with 4 mL of NP-40 (305.5 µM) and 2 mL of DMSO and used immediately.

***Acetate buffer (1 M)*:** The acetate buffer was prepared by weighing 4.1 g of sodium acetate and dissolving in approximately 30 mL of water before adding 2.4 mL of acetic acid and diluting the solution to 50 mL with water. The final pH was adjusted to 4.80 using 5 M NaOH.

***Haemin stock solution*:** A 25 mM haemin stock solution was prepared by weighing 16.30 mg of haemin into a 2 mL Eppendorf tube and dissolved in 1 mL of DMSO. The solution was

sonicated for 1 min and 178.80 µL was immediately added to 20 mL of 1 M acetate buffer. The solution was vortexed well and used immediately, ensuring the haem remained uniformly suspended in the buffer during use.

***HEPES buffer pH 7.5 (2 M)*:** A solution of 2 M HEPES buffer was prepared by dissolving 47.66 g of HEPES in 80 mL of distilled water. The pH was adjusted to 7.5 with 5 M NaOH before diluting to a final volume of 100 mL with distilled water. The solution was stored at room temperature.

***Pyridine solution in HEPES (50% v/v)*:** Buffered pyridine was prepared by mixing 10 mL of pyridine with 4 mL of acetone, 4 mL of water and 2 mL of 2 M HEPES (pH 7.5).

2.2.4 Haem-pyridine fractionation assay

***Glutaraldehyde (0.125%)*:** A stock solution of 50 % glutaraldehyde was diluted in a 1: 400 ratio with 0.22 µm filtered PBS (pH 7.5) before use.

***1 × SYBR® green I*:** This solution was prepared away from direct light and used immediately. 1 µL of SYBR Green 10 000 × was added per 10 mL of 0.22 µm filtered PBS (pH 7.5).

2.3. Methods

2.3.1 Tissue culturing of Plasmodium falciparum

The chloroquine sensitive (CQS) strains of *Plasmodium falciparum* NF54 (originally derived from a patient near Schiphol, Amsterdam presumed to be of West African origin) and the chloroquine resistant (CQR) strains Dd2 and K1 obtained from the MR4 were used throughout this study. Parasites were cultured using a modified method of Trager and Jensen.[172] Cultures were maintained under sterile conditions in the prepared washed O+ human RBCs in complete medium at 2% haematocrit.

Assay procedure: Every 24 h, medium with parasitised RBCs (pRBCs) was transferred to sterile 50 mL centrifuge tubes and centrifuged at 750 rcf for 5 min. The supernatant was aspirated and the parasitemia and predominant phase in the remaining pRBC pellet was determined by viewing a Giemsa stained blood smear under a light microscope. Briefly, a thin blood smear on a glass slide from the culture was fixed to the glass with methanol and stained for 10 min with freshly prepared 10% Giemsa stain. The slide was rinsed with tap water and dried before viewing with an oil immersion lens under a light microscope. Parasitemia was determined by counting the number of pRBCs as a percentage of the total number of cells (erythrocytes and pRBCs) counted. Trophozoite cultures were diluted to 5% parasitemia with washed O+ human RBCs while ring cultures were synchronised as described by Lambros and Vanderberg [173] with 5x volume of 5% sorbitol at 37 °C for 10 min. After synchronisation, cultures were centrifuged at 750 rcf for 5 min and the layer of debris corresponding to lysed cells and dead parasites was carefully aspirated off the culture. Lastly 40 mL of complete culture medium was added to 1 mL of pRBC pellet in a 200 mL flat bottomed culture flask and gassed with a mixture of 4% CO_2, 3% O_2, and N_2 for 1 min,

sealed and incubated at 37 °C. The cycle was repeated until parasite material sufficient to set up an assay was obtained.

2.3.2 *Parasite lactate dehydrogenase (pLDH) antiplasmodial assay*

Compound antiplasmodial activity against the *Pf*NF54, *Pf*Dd2 and *Pf*K1 strains of *P. falciparum* was determined via a modified method of the parasite lactate dehydrogenase (pLDH) assay described by Makler *et al*., which colourimetrically measures *Plasmodium* enzyme lactate dehydrogenase.[174] Lactate dehydrogenase (LDH) is present in both the parasite and erythrocyte, and catalyses the conversion of lactate to pyruvate during glycolysis, with nicotinamide adenine dinucleotide (NAD) as a co-enzyme. The activity of NAD in the parasite is indistinguishable from the erythrocyte; during glycolysis, the NAD analogue, 3-acetyl pyridine dinucleotide (APAD) is selectively and rapidly used by *Plasmodium* as a coenzyme instead of NAD and forms APADH. In the presence of APAD, erythrocyte LDH converts lactate to pyruvate at a much slower rate.[174]

Assay procedure: During assay development, plates are supplemented with Malstat™ reagent containing both APAD and lactate and the yellow NBT reagent. Viable parasites rapidly form APADH as the reaction proceeds and this reduces yellow NBT to its purple formazan salt which is measurable at 620 nm and corresponds to parasite viability. The assay was carried out by preparing 2 mg/mL solutions of test samples in 100% DMSO and storing at -20 °C. On the day of use, samples were diluted in medium to a starting concentration of 1000 ng/mL or 100 ng/mL and serially diluted two-fold in medium in 96-well plates. All samples were tested in triplicate at ten concentrations, with 0.2 ng/mL representing the lowest concentration. The blank column contained unparasitised erythrocytes at 1% haematocrit while the positive control and the drug testing wells all contained pRBCs at 2% parasitaemia and 1% haematocrit. The highest concentration of

DMSO to which the parasites were exposed was 0.5%. The plates were covered with a sterile lid and gassed in an airtight chamber with a mixture of 4% CO_2, 3% O_2, and N_2 for 5 min and incubated at 37 °C for 48 h. After incubation, the plates were frozen at -20 °C then thawed (to facilitate cell lysis) and developed by adding 100 µL of Malstat solution and 25 µL of NBT to 15 µL of the re-suspended pRBC pellet. The absorbance of each well on the plate was measured at 620 nm using a Modulus™ Microplate Multimode Reader (Turner Biosystems) and IC_{50} values determined using non-linear dose-response curve fitting analysis via Graph Pad Prism v.4.0 software.

2.3.3 Cytotoxicity assay

Compounds were screened for in vitro cytotoxicity against a Chinese Hamster Ovarian (CHO) mammalian cell-line, using the 3-(4,5-dimethylthiazol-2-yl)-2,5-diphenyltetrazoliumbromide (MTT)-assay which measures cellular growth and survival, and compares well with other available assays.[175] The tetrazolium salt MTT was used to measure all growth and chemosensitivity. In active mitochondria, the tetrazolium ring is cleaved, thus only viable cells are able to reduce the water-soluble yellow coloured MTT to water-insoluble purple coloured formazan.

Assay procedure: The assay was conducted by first preparing the test compounds to 20 mg/mL stock solutions in 100% DMSO followed by further dilutions in complete medium. The initial concentration of the compounds was 100 µg/mL, which was serially diluted in complete medium with 10-fold dilutions to give 6 concentrations, the lowest being 0.001 µg/mL. Emetine was used as the reference drug in this experiment and the same dilution technique was applied to the control, and testing performed in triplicate on each occasion. The 50% inhibitory concentration (IC_{50}) values were obtained from full dose-response

curves, using non-linear dose-response curve fitting analysis via GraphPad Prism v.4 software (GraphPad Software Inc., La Jolla, USA).

2.3.4. Microsomal Metabolic Stability and Metabolite Identification

The microsomal stability of the test compounds was investigated using a single point metabolic stability assay described by Di and colleagues, which involves incubation with human and/or mouse liver microsomes in the presence of phosphate buffer and NADPH (as co-factor) at 37 °C.[176]

Assay procedure: Test compounds (1 µM) were incubated at 37 °C in a solution containing 0.35 mg/ml microsomes (MLM; male Mouse BALB/c, Xenotech, or HLM, mixed gender, Xenotech) and metabolic reactions were initiated by the addition of NADPH (1 mM) in phosphate buffered saline (100 mM, pH 7.4), and incubated for 30 min. The samples were then prepared by ice-cold acetonitrile precipitation containing 0.1 µM carbamazepine (internal standard), centrifuged and filtered for LC-MS analysis. The incubations of compounds and controls (midazolam and MMV390048) were performed in triplicates. LC-MS/MS analysis were then performed on a 4000 QTRAP® (AB Sciex) equipped with a Turbo V™ ion source and coupled to an Agilent 1200 Rapid Resolution HPLC system (600 bar, Agilent technologies, USA). Aliquots (2 µL) of samples stored on a sample tray set at 8°C were injected onto a Kinetex C18 column, 2.1 mm x 50 mm, 2.6 µm particles (Phenomenex) or Kinetex PFP, 2.1 mm x 50 mm, 2.6 µm particles (Phenomenex) at 40°C. Compounds were separated using a gradient solvent system consisting of 0.1% formic acid and 0.1% formic acid in acetonitrile. The relative loss of parent compound over the course of the incubation was monitored by LC-MS/MS and results reported as % remaining after 30 min incubation.

Phase 1 metabolite profiling was conducted by incubating 10 μM of the test compounds at 37 °C in a solution containing 1 mg/mL mouse liver microsomes (MLM male BALB/C, Xenotech), magnesium chloride (5 mM) and NADPH (1 mM) in phosphate buffered saline (100 mM, pH 7.4), for 1 h while shaking. The samples were then prepared by protein precipitation using 2 volumes of acetonitrile, centrifuged and filtered for LC-MS/MS analysis. Controls containing all the sample constituents (not incubated), and in which NADPH or microsomes were individually excluded were also prepared and handled similarly to the test sample. LC-MS/MS analysis was performed on the same LC-MS/MS instrument as used for metabolic stability analysis where 10 μL of samples stored on a sample tray set at 8 °C were injected onto a Supelco Ascentis C18 column, (4.6 mm x 150 mm, 2.6 μm particles) at 40 °C. Metabolites were separated using a gradient solvent system consisting of 0.1% formic acid in water (A) and 0.1% formic acid in acetonitrile (B). The gradient was as follows: 10% B for 0.5 min, 10 - 90% B for 8.5 min, 90% B held for 3 min, and returned to initial conditions for 4 min to re-equilibrate the column. The flow rate was 0.4 mL/min. The total run time per sample was 16 min. All mass scans were operated under electrospray positive ionisation mode and the operation parameters were as follows: curtain gas, 30 psi; collision gas, 6 psi; nebulizer gas (GS1), 50 psi; turbo gas (GS2), 60 psi; source temperature, 500 °C; ion- spray voltage, 5000 V; declustering potential, 46V for 675615/31 and 121V for 674850/19; collisionally activated dissociation (CAD) gas setting: high. Enhanced mass spectrum was used as a survey scan to trigger information dependent acquisition of MS/MS spectra. Metabolites formed were identified by comparison of chromatograms at 30 min with chromatograms at time 0 and with no NADPH controls using Lightsight v2.3. The tentative metabolite identities were deduced by comparison of the product ion spectra of the $[M+H]^+$ ions of each metabolite with that of parent compound using Analyst 1.5.1. The retention time and fragmentation pattern was also compared to that of synthetic standards, where available, to confirm the identity.

2.3.5. Detergent mediated β-haematin inhibition assay

Cellular lipid-mediated inhibition of HZ formation can be mimicked synthetically under physiological conditions in a detergent-mediated assay which substitutes neutral lipids for the commercially available lipophilic detergent NP-40 and used to assess the efficiency of a compound to inhibit βH formation.[97] Based on a pyridine haemochrome inhibition method developed by Ncokazi and Egan, this assay quantifies, at an absorbance of 405 nm, unreacted haematin that complexes with pyridine.[96]

Assay procedure: Stock solutions of control and test compounds were prepared to 20 mM in 100% DMSO (CQ diphosphate salt was, however, prepared to the same initial concentration in HPLC grade water). A 100 µL solution containing water/305.5 µM NP-40/DMSO at a v/v ratio of 7:2:1, respectively, was added to every well in columns 1-11 of the 96-well micro titre plate while 140 µL of water and 40 µL of 305.5 µM NP-40 were added to column 12 to mediate the formation of βH. Twenty microliters of drug (20 mM) was added to column 12 and 100 µL of this solution serially diluted up to column 2 to create a concentration range, with column 1 left as a blank (0 µM of compound). A hundred microliters of freshly prepared homogenous suspension of haematin in 1 M acetate buffer pH 4.8 was added to all wells, including the blank column, such that the final concentration of haematin in all wells was 100 µM. Plates were then covered and incubated for ~5 h at 37 °C in a Labcon 508 IU incubator. Post incubation, 32 µL of 50 % pyridine solution (20% water, 20% acetone, 10% 2M HEPES buffer (pH 7.4), 50% pyridine) was added to all wells, followed by addition of 60 µL of acetone to help in the dispersion of the haematin. Plates were read at 405 nm using a SpectraMax plate reader after 5 s of shaking. The 50% βH inhibitory concentration for each test compound was computed from the blank corrected absorbance values at 405 nm using a

sigmoidal dose-response curve fitting analysis via Graph Pad Prism v.4.0 software (GraphPad Software Inc., La Jolla, USA).

2.3.6. Cellular Haem Fractionation Assay

This is a cellular fractionation technique based on the ability of neutral aqueous pyridine to selectively form a low spin haem-pyridine complex with 'free' haem in the presence of HZ,[96] and examines the dose-dependent effect (if any) of an inhibitor on the fate of total haem in the parasite. True inhibitors of HZ formation like CQ exhibit a dose-dependent signature characterised by a decrease in the cellular content of HZ matched by a corresponding rise in both 'free' haem and haemoglobin (Hb).[89]

2.3.6.1. Parasite Incubation and Harvesting

Sorbitol-synchronised ring stage *Pf*NF54 parasites (5% parasitemia and 2% haematocrit) were incubated at 37 °C in varying concentrations of test compounds and controls for 32 h. The assay was then stopped, the cultures centrifuged at 750 rcf for 5 min and the supernatant containing cell debris and a black layer on top of the pRBC pellet was discarded. A 10% (v/v) Giemsa stained blood smear of each culture was viewed under a light microscope to confirm the presence of trophozoites. Trophozoites were isolated afterwards through lysis by adding 1.8 mL of PBS pH 7.5 and 100 µL of 1% saponin to the settled erythrocyte pellet, left to stand for 2 min then spun at 750 rcf for 15 min. The supernatant was carefully aspirated off and this wash repeated 3 more times with 0.5 mL PBS to remove all traces of Hb and the trophozoite pellet re-suspended in 100 µL PBS. To set up a counting plate, 10 µL of the re-suspended trophozoite pellet was added to 190 µL of counting diluent (10 mL 0.22 µM filtered PBS pH 7.5, 2.5 µL of 50% gluteraldehyde and 50 µL DNAse). This counting plate was stored at 4 °C and used for cell counting through flow

assisted cell sorting (FACS) analysis the next day. The plate containing the remaining 90 µL of the trophozoite pellet was then stored at −80 °C.

2.3.6.2. Flow Assisted Cell Sorting (FACS) Analysis

Cell counts in each well of the counting plate were determined using fluorescent staining and flow cytometry.[177-179] Samples were prepared by diluting 100 µL of cells from the counting plate with 800 µL of 1 x SYBR Green I in PBS pH 7.5 and incubated at 37 °C for 30 min in the dark. Each sample was subsequently spiked with 100 µL of Trucount™ beads such that each sample contained a known fixed amount of fluorescent beads in a final volume of 1 mL. Samples were mixed well in a vortex machine and analysed on a Becton Dickinson FACS Calibur using SSC/FL1 530 nm with CellQuestPro software. All samples were analysed using FlowJo software version 10 (Tree Star Inc). The concentration of cells in the acquisition tube was calculated according to equation 1:

$$CF = (T/B) \times CB \qquad \textbf{(Equation 1)}$$

Where:

CF = concentration of cells per mL as determined with flow cytometry

T = number of trophozoites gated

B = number of fluorescent beads gated

CB = concentration of fluorescent Trucount™ beads in the acquisition tube per mL (calibrated bead count per acquisition is unique to each lot of Trucount™ tubes obtained from the supplier)

Gating was established for trophozoite populations, rings and cell debris. However, it was difficult to distinguish rings from the debris accumulated during the isolation and harvesting procedure hence only intact trophozoites gated were used to determine cell counts, with 10,000 events typically counted for each sample.

2.3.6.3. Measurements of different haem species/fractions

This analysis was done on the plate containing the remaining 90 µL of the trophozoite pellet from **section 2.3.6.1.** Samples were thawed and 50 µL of water was added before 5 min of sonication. This was followed by addition of 50 µL of 0.2M HEPES buffer (pH 7.5) and 50 µL water then centrifuged at 3600 rpm for 20 min. To the separated supernatant, 50 µL of 4% SDS was added, the sample sonicated, and incubated at 25 ^{o}C (30 min). Fifty microliters of 0.3 M NaCl and 50 µL of 25% pyridine (v/v) were added and the UV−visible spectrum of this fraction (Hb) was recorded. Fifty microliters of water was added to the pellet, followed by 50 µL of 4% SDS. After re-suspending the pellet, the solution was sonicated and incubated (30 min) at 25 ^{o}C. Fifty microliters of 0.2 M HEPES, 50 µL of 0.3 M NaCl, and 50 µL of 25% pyridine were added and the sample centrifuged. The supernatant was diluted to 300 µL with water and the UV−visible spectrum recorded (haem fraction). The remaining pellet was treated with 50 µL of water and 50 µL of 0.3 M NaOH, sonicated (15 min), and incubated (30 min) at 25 ^{o}C. Fifty microliters of 0.2 M HEPES, 50 µL of 0.3 M HCl, and 50 µL of 25% pyridine were added and the supernatant was diluted to 300 µL. The UV−visible spectrum of this fraction (HZ) was recorded and percentages of the three haem species i.e Hb, haem and HZ fractions determined from the absorbance values.

2.3.6.4. Haem standard curve

To quantify the total amount of haem in each fraction, a haem standard curve was prepared from a 100 µg/mL haem standard solution of haematin (porcine) in 0.3 M NaOH. The standard solution was serially diluted in a 96-well plate with 100 µL 0.3 M NaOH as a blank. Each haematin standard was diluted with 50 µL of each of the following solutions: 4% (w/v) SDS, 0.3 M NaCl, 0.2 M HEPES pH 7.5, 0.3 M HCl, 25% pyridine in 0.2 M HEPES pH 7.5 and water. All measurements were performed in triplicate and the visible spectra of haem as

Fe(III)haem-pyridine complex was measured in a multi-well plate reader. The amount of haem present in each sample was determined using a calibration curve and amount of haem per cell subsequently calculated by dividing the total haem in each fraction by the number of cells determined in each fraction. All results were expressed as the amount of haem Fe (fg) per cell.

2.3.7. Speed of Action (Killing Kinetics) Assay

This experiment involves measuring the time-scaled effect of a compound on parasite viability by determining its speed of action from the ratio of IC_{50} after either 24 h or 48 h of incubation against the standard 72h.[180]

Assay procedure: Unsynchronised *Pf*NF54 cultures (80% rings) of pRBC at 2% haematocrit and 0.5% parasitemia with 5 μM hypoxanthine were exposed to 2-fold serial dilutions of the compounds. For each compound, three incubation times were employed: 72 (standard assay time), 48 and 24 h. In the case of the 24 h assay, [^{3}H] hypoxanthine was added during the last 8 h while in the case of the 72- and 48-h assays, radioactive labelling was done for the last 24 h. After incubation and addition of [^{3}H] hypoxanthine, plates were harvested on glass fiber filters (Wallac 1450-421) using a cell harvester 96 (TOMTEC, Perkin Elmer). Filters were dried and melt-on scintillator sheets (MeltiLex A, PerkinElmer 1450-441) used to determine the incorporation of [^{3}H]-hypoxanthine on a microbeta counter (Perkin Elmer). The data were normalised using the incorporation of the positive control, (PRBC without drug) and IC_{50} values were determined using GraFit version 5 (Erithacus Software Ltd, UK). This assay was validated by inclusion of 3 standard antimalarials – CQ, artesunate (AS) and (pyrimethamine) PYR, with known speeds of action and performed in at least three independent experiments. The IC_{50} values at 24 and 72 h were expressed as a ratio to highlight any shifts between early or late stage activities, i.e. a ratio close to 1 would be

indicative of comparable activity between the two periods while a larger value clearly deviating from unity hints at late stage activity.

2.3.8. In vivo Efficacy Screening in Plasmodium berghei-infected mice

All efficacy studies were approved by the respective institutional animal experimentation ethics committees at the University of Cape Town and Swiss Tropical and Public Health Institute. Testing was conducted at the Swiss Tropical and Public Health Institute. The antimalarial activity of the test compounds was assessed for groups of 3 (treatment group) and 5 (untreated control group) female NMRI mice (20 - 22 g) intravenously infected on day 0 with a GFP-transfected *Plasmodium berghei* ANKA strain (donated by A. P. Waters and C. J. Janse, Leiden University, The Netherlands) (2 x 10^7 pRBCs per mL) (Roche).

Assay procedure: Compounds were formulated in SSV (70/30 Tween 80/ethanol and diluted 10 x with water) and administered orally in four consecutive daily doses (24, 48, 72 and 96 h after infection) at either 30 mg/kg or 100 mg/kg. Blood smears were collected and stained on day 4 after infection and degree of infection (parasitemia expressed as per cent infected erythrocytes) was determined using microscopy and FACS on the FACSCalibur™ instrument using CellQuestPro software. Antimalarial activity was calculated as the difference between the mean per cent parasitemia for the control and treated groups expressed as a per cent relative to the control group. The survival time in days was also recorded up to 30 days after infection. A compound was considered curative if the animal survived to day 30 after infection with no detectable parasites.

2.3.9. Antischistosomal Screening

All antischistosomal screening was carried out at the Swiss Tropical and Public Health Institute in Basel, Switzerland. Animal studies were carried out in accordance with Swiss national and cantonal regulations on animal welfare at the Swiss Tropical and Public Health Institute (Basel, Switzerland) under the permission number 2070.

2.3.9.1. In vitro screening against newly transformed schistosomula (NTS)

Compounds and control (praziquantel) were dissolved in 100% DMSO to obtain stock solutions of 10 mM. *Schistosoma mansoni* cercariae, obtained from infected intermediate host snails, *Biomphalaria glabrata*, were mechanically transformed to newly transformed schistosomulae (NTS) by placing the snails under light to stimulate cercarial shedding.[181] The cercarial suspension was collected and tails separated from the heads by rinsing three times with cold Hank's Balanced Salt Solution. The NTS were then incubated overnight in culture medium and used the next day where 100 were then incubated in each well of a 96-well plate with culture medium and the test compound for a final well volume of 250 µL. Culture medium was composed of Medium 199 (Invitrogen, Carlsbad, CA) supplemented with 5% fetal calf serum (iFCS, 100 U/mL) and 1% penicillin/streptomycin mixture (Invitrogen, 100 U/mL). Compounds were tested at 10 µM in triplicate with NTS incubated in no more than 1% DMSO serving as control. NTS were kept in an incubator at 37 °C and 5% CO_2 for up to 72 h after which the condition of the NTS was microscopically evaluated using a scale from 3 (normal activity and no tegument alteration) to 0 (dead, completely granulated). IC_{50} determination assays for the compounds were subsequently performed in the same manner.

2.3.9.2. In vitro screening against Adult S. mansoni worms

Female NMRI mice (age 3 weeks, weight ca. 14 g) were purchased from Charles River (Sulzfeld, Germany) and allowed to adapt for 1 week under controlled conditions (22 °C, 50% humidity, 12 h light, and free access to water and rodent diet) before experimental handling. To obtain adult schistosomes, mice were infected subcutaneously with 80 - 100 cercariae. The mice were then euthanised after 7 - 8 weeks with CO_2 and the worms collected from the hepatic portal and mesenteric veins. Two pairs of adult worms were incubated in each well of a 24-well plate with 2 mL culture medium and the test compound. Culture medium was composed of RPMI 1640 (Invitrogen, Carlsbad, CA) supplemented with 5% foetal calf serum (iFCS, 100 U/ml) and 1% penicillin/streptomycin mixture (Invitrogen, 100 U/mL). Only compounds with > 70% activity against NTS were evaluated against adult worms at 10 µM with incubation at < 1% DMSO used as control. Worms were kept in an incubator at 37 °C and 5% CO_2 for up to 72 h after which their condition was microscopically evaluated using a scale from 3 (normal activity and no tegument alteration) to 0 (dead, completely granulated). IC_{50} determination was conducted for compounds with >60% activity. For the *in vitro* drug sensitivity assays, all viability scores were averaged across replicates and normalised to the average viability scores of the control wells (Microsoft Office Excel 2010). IC_{50} values were calculated using CompuSyn2® (ComboSyn Inc., Paramus, New Jersey, 2007).

2.3.9.3. In vivo studies in S. mansoni-infected mice

Female mice (NMRI strain) were purchased from Charles River, Germany, kept under environmentally controlled conditions (temperature ~ 25 °C; humidity ~70%; 12 h light and 12 h dark cycle) with free access to water and rodent diet and acclimatised for one week before infection. Groups of 3– 4 NMRI mice harbouring chronic schistosomal infection were

treated 49 days post-infection with single oral doses of 400 mg/kg of test compounds dissolved in 7% Tween 80 and 3% ethanol in water (v/v/v) while untreated mice served as controls. At 21 days post-treatment, animals were euthanised by the CO_2 method and dissected. Surviving schistosomes residing in the mesenteric veins and the liver were counted and sexed.

2.3.10. Determination of hERG toxicity

Inhibition of the hERG channel can often be predicted using computational techniques. However, due to the promiscuous inhibition of the hERG channel by therapeutically and structurally diverse drugs, and the high flexibility of the hERG protein, computational prediction of inhibition can only be used as guide and should often be complemented with experimental data.

2.3.10.1. Computational prediction using StarDrop ™

StarDrop™ was used to predict hERG pIC_{50}s of the compounds whereby molecules were imported into the analysis software in spatial data file (sdf) format and the hERG pIC_{50} directly predicted. Chloroquine, dihydroartemisinin, halofantrine and desbutyl-halofantrine, all of whose predicted ranges of pIC_{50}s are known, were used as control.

2.3.10.2. Experimental determination of hERG toxicity using QPatch Clamp System

Experimental analysis was performed by Metrion Biosciences, UK on the QPatch gigaseal automated patch clamp platform. Chinese hamster ovarian (CHO) cells stably expressing hERG protein were prepared for assays using proprietary dissociation protocols designed to optimise cell health, yield and assay quality. Test compounds (including verapamil hydrochloride as positive control) were screened at four concentrations (0.3, 1, 3 and 10 µM) against a minimum of three separate CHO cells. The percent inhibition values from each cell

were used to construct concentration-response curves employing a four parameter logistic fit with 0 and 100% inhibition levels fixed at very low and very high concentrations, respectively, and a free Hill slope factor. The IC_{50} and Hill coefficient were then determined, with only data with Hill slopes within 0.5< nH <2.0 included. The IC_{50} data was then reported as the mean ± standard deviation (S.D.) of at least 3 separate cells (n ≥ 3).

2.3.11. Kinetic solubility assay

The aqueous solubility of all test compounds was determined at pH 6.5 using a kinetic solubility assay based on a miniaturised shake flask method previously described.[182]

Assay Procedure: The assay was performed by first preparing 10 mM stock solutions of reserpine (6.09 mg/mL), hydrocortisone (3.63 mg/mL) and each of the test compounds in 100% DMSO. This was followed by preparation of 100 mL PBS at pH 6.5 by weighing out 0.8 g NaCl, 0.2 g KCl, 0.115 g $Na_2HPO_4.7H_2O$ and 0.2 g KH_2PO_4 into a volumetric flask, topping up to the 100 mL mark then adjusting the pH to 6.5. Next, fasted state simulated intestinal fluid (FaSSIF) buffer was prepared by dissolving 2.042 g KH_2PO_4 and 3.728 g KCl in approximately 400 mL of HPLC grade water. Addition of 50 mL of 0.1M NaOH followed before the buffer was brought to the mark with water and adjusted to pH 6.5. The stock solutions were then used to prepare calibration standards in DMSO, and to spike (1:50) duplicate aqueous samples of FaSSIF buffer with a final DMSO concentration of 2%. Once the samples and standards were prepared, the plates were mixed for 2 h on an orbital shaker at 200 rpm at 25 °C. The plates were then centrifuged at 3500 rpm for 15 minutes at 22 ^{o}C and the solutions filtered and analysed by means of HPLC-DAD (Agilent 1200 Rapid Resolution HPLC with a diode array detector). Best fit calibration curves were constructed using the calibration standards, which were used to determine the samples' aqueous solubility. Solubility is reported in the range 0 – 220 µM and ranked as '*very low*' if < 5 µM,

'*low*' if 5 -49 µM, '*moderate*' if 50 -150 µM and '*high*' if > 150 µM. At pH 6.5, the controls reserpine and hydrocortisone have solubility concentrations of < 5µM and >150 µM, respectively.

2.3.12. Membrane Permeability Assay

The parallel artificial membrane permeability assay (PAMPA) is an *in vitro* model of passive, trans-cellular permeability of drug-like compounds to screen for their oral absorption potential across a hexadecane liquid layer at physiologically relevant pH's representative of the gastro-intestinal tract. Apparent permeability (P_{app}) is determined by detecting the appearance of the test compound in the acceptor compartment of the artificial membrane plate following incubation.

Assay Procedure: The PAMPA assay was performed in triplicate in 96-well MultiScreen Filter plates (Millipore, 0.4 µM PCTE Membrane). Membrane filters were pre-coated with 5% hexadecane in hexane and allowed to dry prior to the assay. Membrane integrity marker, Lucifer yellow was added to the apical wells of the pre-coated MultiScreen plate donor/drug solutions containing test compound. Phosphate buffer (pH7.4) was added to the 96-well acceptor plate. 10 mM test compound was used to spike (1 µM) the donor buffer at physiologically relevant pH's (pH 4, 6.5 and 8), the donor plate slotted into the acceptor plate and incubated (4 h at room temperature) with gentle shaking (40 - 50 rpm). Following the incubation, sample from the acceptor wells and theoretical equilibrium wells were transferred to the analysis plate and matrix matched with blank donor buffer. Acetonitrile containing internal standard (carbamazepine, 0.0236 µg/mL) was added to all samples and they were analysed by LC-MS/MS (Agilent Rapid Resolution HPLC, AB SCIEX 4500 MS). The normalised (analyte/internal) peak areas were used to calculate the P_{app}. Membrane integrity was assessed by calculating the P_{app} of Lucifer Yellow (acceptable values <50 nM/s) using a Modulus microplate reader (Excitation 490nm/Emission 510 - 570nm)

(Wohnsland and Faller, 2001). The permeability data was then classed according to the *low* (< -6.5), *moderate* (-6.5 to -5.5) and *high* (> -5.5) categories.

2.3.13. Determination of lipophilicity (LogD)

2.3.13.1. LogD (pH 5.0) determination using shake-flask method

For the determination of the distribution coefficient (Log D) between organic and aqueous phases at pH 5.0, compounds were evaluated by the shake-flask method at room temperature. Compounds were dissolved in DMSO to constitute 10 mM stock solutions. Each compound was mixed in a glass tube with equal volumes of pre-saturated 0.02 M 2-(N-morpholino) ethanesulfonic acid (MES) buffer and *n*-octanol to achieve a final concentration of 75 μM. This solution was then shaken vigorously for 2 h, centrifuged at 3,500 rpm and allowed to equilibrate for 6 h. Each phase was then carefully separated and final drug concentrations in each layer determined by computing absorbance values measured with the extinction coefficients obtained from linear Beer's Law UV-vis spectroscopy plots in each phase within the concentration range tested. The concentrations in the two phases were used to obtain LogD at pH 5.0 using equation 2 shown below.

$$\mathbf{LogD_{5.0}} = \mathbf{Log}\ \frac{[\text{Compound in } n\text{-octanol}]\ \mu M}{[\text{Compound in MES buffer}]\ \mu M} \quad \textbf{Equation 2}$$

2.3.13.2. LogD (pH 7.4) determination using HPLC method

For LogD measurements at pH 7.4, HPLC analysis was used instead since signal to noise ratio confounded UV-vis spectroscopic analysis of compound concentrations in the aqueous layer which were very low. In this analysis, the standards verapamil, hydrocortisone and

ouabain were included as controls. A 10 mM stock solution of each compound was prepared in DMSO and 10 µL of this was used to spike a 1:1 mixture of phosphate buffer (pH 7.4) and *n*-octanol in a square-welled 96-deep-well plate. The solutions were shaken vigorously (1500 rpm) on an orbital shaker for 2 h at room temperature and thereafter, centrifuged (3500 rpm, 2700× *g*) in order to fully separate the two immiscible phases. Carefully, 300 µL from each layer was transferred to a new analysis plate and analysed on the HPLC-DAD (Agilent 1200 Rapid Resolution HPLC) with 0.1 % formic acid in 95 % acetonitrile as the organic mobile phase and 0.1 % formic acid in 5 % acetonitrile as the aqueous mobile phase. $LogD_{7.4}$ was calculated from the areas of integrated UV chromatogram peaks using equation 3 below

$$\mathbf{LogD_{7.4}} = \mathbf{Log}\ \frac{\text{(peak area of } n\text{-octanol phase/}n\text{-octanol phase injected volume)}}{\text{(peak area of buffer phase/buffer phase injected volume)}} \quad \text{Eqn 3}$$

2.3.14. Calculation of vacuolar accumulation ratios (VARs)

Since the digestive vacuolar pH in the malaria parasite is regulated to an acidic value to provide optimal conditions for haemoglobin degradation, the potential vacuolar accumulation ratio (VAR) for drugs can be calculated from their distribution coefficients (LogD) in the vacuole (pH 5.0) and the aqueous medium external to the cell (pH 7.4). This can be predicted from equation 4 below proposed by Warhurst and co-workers.[119]

$$\mathbf{VAR = Antilog\ (LogD_{7.4} - LogD_{5.0})} \qquad \textbf{Equation 4}$$

2.3.15. Software

GraphPad Prism version 4 (GraphPad Software Inc., La Jolla, USA) for windows was used to analyse all data and calculate statistical significance. ChemDraw Professional v15.0.0.0.16 (PerkinElmer) was used to generate chemical structures and figures. All flow cytometry data was analysed using FlowJo software version 10 for which Tree Star Inc. donated an annual subscription (Tree Star Inc). StarDrop™ and MarvinSketch v5.9.4 were used to make *in silico* predictions. The bibliography was created using EndNote X7.4 (Thomson Reuters).

Chapter 3

PYRIDO-DIBEMEQUINES: A REVERSED-CHLOROQUINE ANTIMALARIAL SCAFFOLD WITH HAEMOZOIN-INHIBITING ACTIVITY

3.1 Chapter Overview

This chapter explores the relationship between seven pyrido-dibemequine (pDBQ) derivatives and their mechanistic inhibition of βH, within the context of their biological and physicochemical properties. As introduced in *Chapter 1*, rCQ compounds combine the basic pharmacophore for haem-binding and inhibition of HZ formation (4-amino-7-chloroquinoline) and a resistance reversal pharmacophore. The feasibility of this approach has since been confirmed by different studies that have generated various modifications of these compounds,[129, 157, 183] among them dibemequines (DBQs) - a series containing a 4-amino-7-chloroquinoline with a dibenzylmethylamine side chain, exemplified in **Figure 3.1**. Indeed, these compounds were shown to possess strong *in vitro* antiplasmodial and *in vivo* antimalarial activity, and also inhibited *Pf*CRT-mediated extrusion of CQ from the parasite digestive vacuole (DV).[127]

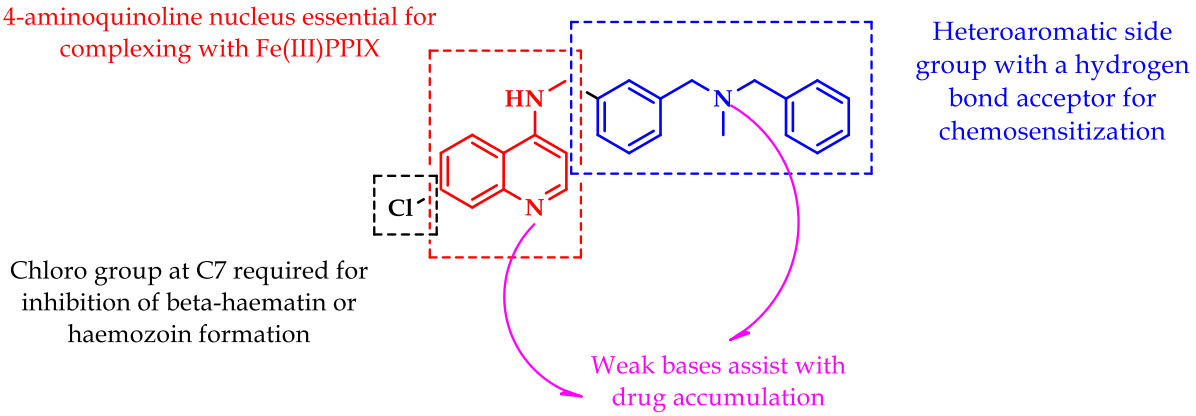

Figure 3.1: Structure-activity relationship profile of the prototype dibemequine molecule with the quinoline nucleus (red grid) hybridised to the resistance reversal moiety (blue grid)

In an attempt to further improve the physicochemical and biological properties of these compounds, a number of modifications were made to the prototype molecule. First, one of the aromatic rings on the dibenzylmethylamine side chain was replaced with a pyridine to

improve aqueous solubility due to the higher polarity of pyridine. This would also introduce an additional protonatable centre that would be anticipated to serve as an extra hydrogen bond acceptor and consequently improve vacuolar drug accumulation through pH trapping. Secondly, the chloro-substituent at carbon 7 (C7) on the 4-aminoquinoline nucleus was replaced by a cyano group in an effort to afford analogues with reduced molecular weight (MW) and lipophilicity while retaining βH inhibition activity (**Figure 3.2**). The lowered lipophilicity and MW could reduce the potential for hERG inhibition and improve druggability in multiple other ways such as decreasing plasma protein binding and lowering potential of the compounds to inhibit cytochrome p450 (CYP) enzymes.[144]

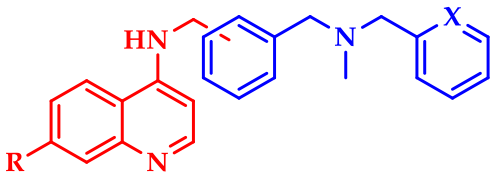

R: Cl, CN

X: CH, N

Figure 3.2: Generic structure of one of the new series of dibemequine molecule

Six of the seven compounds evaluated in this section of the thesis were synthesised as free bases by Dr Mukesh Joshi, while one compound, due to previous solubility challenges with its corresponding free base, was synthesised as a hydrochloride salt by dissolving in a 1.25 M solution of HCl in methanol, followed by evaporation of the solvent *in vacuuo* (**Figure 3.3**).

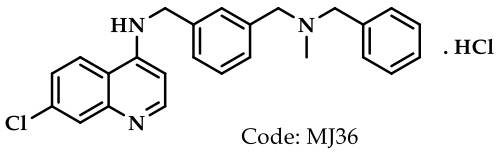

Code: MJ36
Compound: 1
Mol. Formula: $C_{25}H_{24}ClN_3$.HCl
% Purity: 99

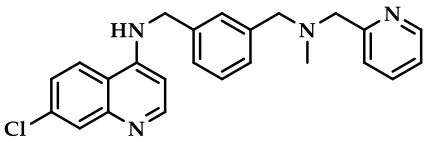

Code: MJ43
Compound: 2
Mol. Formula: $C_{24}H_{23}ClN_4$
% Purity: 99

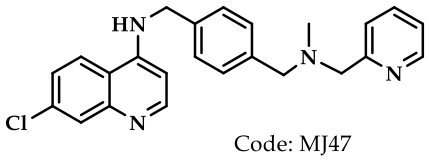

Code: MJ47
Compound: 3
Mol. Formula: $C_{24}H_{23}ClN_4$
% Purity: 99

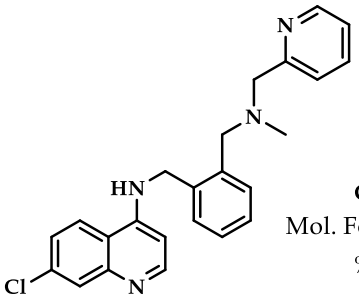

Code: MJ49
Compound: 4
Mol. Formula: $C_{24}H_{23}ClN_4$
% Purity: 99

Code: MJ124
Compound: 5
Mol. Formula: $C_{25}H_{23}N_5$
% Purity: 99

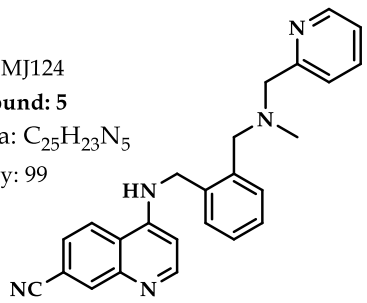

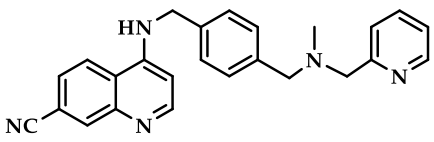

Code: MJ125
Compound: 6
Mol. Formula: $C_{25}H_{23}N_5$
% Purity: 99

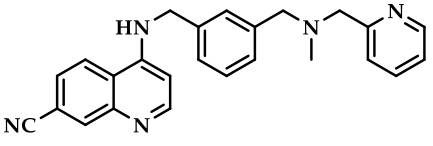

Code: MJ126
Compound: 7
Mol. Formula: $C_{25}H_{23}N_5$
% Purity: 99

Figure 3.3: Chemical structures of the 7 derivatives evaluated in this chapter of the project.

Using direct experimental analyses and predictive *in silico* simulations, this chapter describes in detail the physicochemical features and biological activity of these 7 pDBQ compounds and provides a full cellular haem fractionation profile of each in an effort to establish their HZ-inhibiting mechanism of action (MoA). Finally, data on biotransformation analysis of the compounds and potential for hERG toxicity is explored. All results are subsequently discussed and a conclusion on the chapter presented.

3.2. Materials and Methods

All materials and methods used throughout this chapter are described in detail in *Chapter 2*. The compounds discussed herein were synthesised and characterised by Dr. Mukesh Joshi.

3.3. Results and Discussion

3.3.1. Aqueous Solubility.

Solubility is a key determinant of absorption, and by extension, bioavailability of orally-administered drugs.[184] Often, poorly soluble compounds are riddled with setbacks including false negative bioassay results *in vitro* due to precipitation, poor absorption and difficulty in intravenous administration. They also present challenges in formulation design and an increased likelihood for adverse effects due to the need for frequent, high-dose administration. Since oral administration presents the cheapest and most convenient route, focus has been on prioritising the optimisation of solubility, among other physicochemical properties. There was no correlation between the predicted and experimental solubility (R^2 = 0.0933, p = 0.5053) of the pDBQs, and this is likely attributable to the differential pH in assay conditions. Indeed, experimental solubility (pH 6.5) was higher than that predicted (pH 7.4),

with compounds **3**, **4** and **5** showing comparable solubility to hydrocortisone (**Table 3.1**) as the compounds are likely to exist in their ionised form at lower pH. The solubilities of these compounds therefore show that they are likely to stay in solution under assay conditions, hence supporting the signals obtained from biological evaluations as a true reflection of their activity. Though substitution at C7 on the quinoline ring did not seem to influence solubility, there was a discernible pattern of increasing solubility related to the left hand ring of the side chain, with the *para*- and *ortho*- analogues in both the chloro- and cyano-substituted sets of compounds exhibiting higher solubility than the *meta*-. As anticipated, the introduction of a pyridine in place of the right hand phenyl ring in the dibenzylmethylamine side group improved aqueous solubility relative to **1**. This is likely due to the nitrogen center in the pyridine ring being available for H-bonding to water molecules.

3.3.2. Determination of artificial membrane permeability.

Excluding first-pass hepatic metabolism, oral bioavailability is most highly dependent on intestinal absorption, which in turn is a function of compound solubility and membrane permeability.[185] Therefore, *in vitro* permeability assays can be invoked to help in the interpretation of both *in vivo* pharmacokinetic data as well as cell-based assay results. Permeability of the pDBQs was determined using the PAMPA assay, which uses phospholipid-coated filters to estimate membrane permeability over different physiological pH values representative of the gastrointestinal tract. As described in **section 2.4.5** of *Chapter 2*, logarithm of apparent permeability (Log P_{app}) values > -5.5 were classified as '*high*' while Log P_{app} < -6.5 was considered '*low*'. Compounds exhibiting LogP_{app} values ranging from -6.5 to -5.5 were classified as '*moderately permeable*'. All the compounds had high permeability (Log P_{app} > -5.5) at the physiologically relevant pH 6.5 (**Table 3.1**). This indicates that greater permeation and absorption would be expected in the lower gut than in other parts of the gastrointestinal tract (GIT). However, this assertion is likely to hold true when only passive

diffusion is taken into account. Neither the modifications on the core quinoline ring nor on the side group appeared to have any significant influence as all compounds had comparatively high permeability at pH 6.5.

Table 3.1: The aqueous solubility, membrane permeability and lipophilicity of the 7 pDBQs

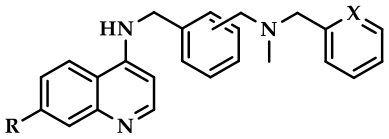

			Kinetic Solubility [a] **(μM)**		**Permeability $LogP_{app}$ (SD)**	**Lipophilicity** [b]		
Compound	**R**	**X**	**Observed**	**Predicted**	**pH 6.5**	**cLogP**	**$LogD_{7.4}$**	**$LogD_5$**
1	Cl	CH	51.8	3.0	-3.60 (0.16)	5.60	3.56	1.33
2 (*meta*-)	Cl	N	59.8	15.1	-4.10 (0.26)	4.46	2.47	0.82
3 (*para*-)	Cl	N	196.6	11.7	-4.56 (0.10)	4.46	2.85	0.84
4 (*ortho*-)	Cl	N	164.7	14.5	-4.56 (0.03)	4.46	3.79	0.90
5 (*ortho*-)	CN	N	172.4	17.0	-4.01 (0.06)	3.71	3.80	0.81
6 (*para*-)	CN	N	143.5	13.8	-4.60 (0.04)	3.71	2.84	0.99
7 (*meta*-)	CN	N	72.4	17.4	-3.60 (0.16)	3.71	2.75	0.85
Warfarin					-3.80 (0.35)			
Propranolol					-4.40 (0.28)			
Testosterone					-3.70 (0.33)			
Reserpine			<5					
Hydrocortisone			>150	520			1.50	
Verapamil							2.50	

[a] Kinetic solubility was determined at pH 6.5 in 0.1M phosphate buffered saline while predicted solubility was obtained from StarDrop by computing the antilog of the LogS provided at pH 7.4

[b] cLogP was predicted using MarvinSketch v5.9.4 while LogD was experimentally determined using HPLC analysis (for pH 7.4) and shake-flask method with UV-spectroscopy (for pH 5).

3.3.3. Predicted and Experimental Lipophilicity.

In the absence of special transport mechanisms, the accumulation of weak bases like CQ in a particular organelle can be described in terms of their physicochemical behaviour through the partitioning theory.[186, 187] Indeed, the flux of a molecule at the interface of two immiscible solvents is largely influenced by its lipophilicity. The lipophilic, diprotic CQ is believed to passively diffuse across membranes in its unprotonated form and accumulate after protonation in the parasite DV. However, an obvious challenge associated with high compound lipophilicity is the negative effect on aqueous solubility, where poorly-soluble drug candidates increasingly rely on enabled formulations to overcome dissolution- and solubility-limited oral bioavailability. The partition (cLogP) and distribution coefficients (LogD) of a molecule observed in a water/*n*-octanol system have therefore been adopted as standard indices of lipophilicity, and these can be quantitatively related to a molecule's SAR, physicochemical or biological behaviors.

With regards to predicted cLogP, compound **2**, **3** and **4** (chloro- at C7) and **5**, **6** and **7** (cyano- at C7) showed no quantitative differences (**Table 3.1**) presumably due to the isostructural nature of each group and identical protonation pattern when the compounds are in their neutral state. However, a clear deviation was observed relative to **1** (cLogP = 5.60), and this could be explained by the presence of the less lipophilic pyridyl group compared to the phenyl hydrophobic rings in the side-chain structure of **1**. Compounds **5**, **6** and **7** had an even more diminished cLogP due to the presence of the nitrile at C7 which has greater electron-withdrawing nature but less lipophilicity than a chloro- group. Analysis of the relationship between cLogP and predicted solubility (pH 7.4) reveals a strong correlation between decreasing solubility and increasing cLogP (R^2 = 0.8085, p = 0.0061). Though this trend was still maintained when the analysis was performed using experimental solubility

(pH 6.5), the correlation diminished (R^2 = 0.1503, p = 0.3902). A more structurally diverse and larger sample set would probably be more revealing.

Results for $LogD_{7.4}$ for the compounds ranged from 2.47 – 3.80 (mean: 3.15 ± 0.55), with compound **5** exhibiting the highest distribution coefficient (3.80) and compound **1**, the lowest (2.47). This narrow range in the LogD at cytosolic pH can be explained by the minimal variation in their acid dissociation constants (pKas). In view of the acidic milieu existing in the *P. falciparum* DV, LogD at pH 5.0 was also determined. These values were markedly lower (mean: 0.93 ± 0.19) and showed minimal differences. The acidic environment of the DV results in substantial ionisation of the aromatic and aliphatic N of these compounds, with enhanced aqueous solubility as shown by the marked drop in vacuolar LogD (**Table 3.1**). Therefore the compounds are trapped within the DV, causing their concentration to increase in the low pH environment.

3.3.4. Antiplasmodial Activity and Correlation with Physicochemical Properties

The compounds were screened for antiplasmodial activity against the CQS (*Pf*NF54) and CQR (*Pf*Dd2 and *Pf*7G8) strains of *P. falciparum* and the results are presented in **Table 3.2**. All compounds showed potent antiplasmodial activity in the nanomolar range against both parasite strains (IC_{50} range CQS: 14.4 – 126.6, CQR^{Dd2}: 44.5 – 162 and CQR^{7G8}: 69.6 – 307.1). Chloro-substituted analogues (**1 – 4**) had higher potency across all strains (mean ± SE IC_{50} CQS: 34.4 ± 8.3 nM, CQR^{Dd2}: 114.0 ± 23.8 nM and CQR^{7G8}: 113.0 ± 25.5 nM) than the cyano-substituted analogues (**5 - 7**) (mean ± SE IC_{50} CQS: 90.6 ± 12.9 nM, CQR^{Dd2}: 132.3 ± 22.0 nM and CQR^{7G8}: 178.2 ± 64.5 nM). This was an unsurprising observation as it has been previously shown that halogens exert optimum influence at C7 on the quinoline ring due to their strong lipophilicity and a moderately strong electron-withdrawing capacity.[100]

Table 3.2: Antiplasmodial activity and cytotoxicity profiles of the 7 pDBQ derivatives

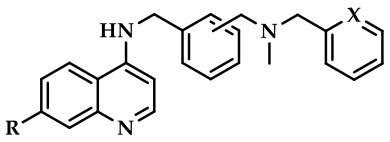

			IC_{50} (nM)					Cytotoxicity	
Compound	**R**	**X**	**NF54**	**Dd2**	**7G8**	**R.I ^{Dd2}**	**R.I ^{7G8}**	**CHO_{IC50} (µM)**	**S. Index**
1	Cl	CH	14.4	44.5	69.6	3.1	4.8	9.5	660.2
2 (*meta*-)	Cl	N	30.1	124.0	83.8	4.1	2.8	8.3	275.1
3 (*para*-)	Cl	N	38.5	150.7	114.2	3.9	3.0	15.7	408.0
4 (*ortho*-)	Cl	N	54.4	136.6	184.3	2.5	3.4	40.2	739.8
5 (*ortho*-)	CN	N	116.3	162.0	307.1	1.4	2.6	27.6	237.1
6 (*para*-)	CN	N	76.4	145.5	115.3	1.9	1.5	11.2	145.9
7 (*meta*-)	CN	N	79.1	89.4	112.1	1.1	1.4	50.6	639.5
Chloroquine[b]			8.3	226.4	88.7	27.3	10.7		
Artesunate			5.6	14.3	7.7	2.6	1.4		
Emetine								0.095	

R.I = Resistance index = [IC_{50} CQR strain] ÷ [IC_{50} CQS strain];

CHO = Chinese Hamster Ovarian cells;

S. Index= Selectivity index = [IC_{50} CHO] ÷ [IC_{50} NF54]; Chloroquine diphosphate salt [b]

Against *Pf*Dd2, all compounds were more active than CQ while only compounds **1** and **2** were more potent against *Pf*7G8. This could be due to any one or more of the seven amino acids that differ between the forms of *Pf*CRT expressed in the two strains (**Table 3.3**) and/or the differential regulation in the pathways that compensate for these mutations in the strains.[188] In addition, while most of these derivatives affirmed their designation as rCQs

through an appreciably higher activity than CQ against *Pf*Dd2, their potency was lower compared to some published rCQs.[129, 134, 157] It is possible that this discrepancy reflects inherent differences in the CQR strains evaluated, variations in antiplasmodial testing protocols (with the confounding influence of starting parasitemia) or even dissimilarities in the choice of chemosensitising scaffolds in these studies. Nonetheless, these derivatives were more active against *Pf*Dd2 compared to some pentacycloundecylamine analogues (*Pf*Dd2 IC_{50}: 28 – 253 nM) [183] and more importantly, exhibit considerably lower lipophilicity than most of their published counterparts.

There was no indication of cross-resistance between the compounds and CQ in the two strains of CQR parasites as indicated by their low resistance indices. This potential low cross-resistance with CQ could be due to the modifications on the quinoline scaffold using a RA side chain thereby possibly allowing for direct interaction of the molecule with *Pf*CRT^{CQR} in a manner unattainable with CQ.

Table 3.3: Resistance-conferring polymorphisms within different *Pfcrt* and *Pfmdr1* codons in CQS^{NF54}, CQR^{7G8} and CQR^{Dd2}

		***Pf*CRT Codons**									***Pf*MDR1 Codons**				
Strain	**Origin**	**72**	**74**	**75**	**76**	**220**	**271**	**326**	**356**	**371**	**86**	**184**	**1034**	**1042**	**1246**
NF54	Amsterdam	C	M	N	K	A	Q	N	I	R	N	F	S	D	D
7G8	Brazil	S	M	N	T	S	Q	D	L	R	N	F	C	D	Y
Dd2	Thailand	C	I	E	T	S	E	S	T	I	Y	Y	S	N	D

Additionally, the compounds showed low cytotoxicity in the mammalian cell line (CHO cells) with a selectivity index range between 146 and 740 (**Table 3.2**). There was, however, no discernible trend in toxicity attributable to any structural features of the molecules. Emetine

(control), a potent inhibitor of protein synthesis in eukaryotic cells exhibited cellular toxicity at very low concentrations (IC_{50} = 0.095 µM).

Analysis of the correlation between antiplasmodial activity and lipophilicity showed a direct association between the two, meaning that the most lipophilic compound is likely to diffuse through the intracellular membrane barriers and into the site of action. With regards to cLogP (**Figure 3.4a**), this association was strongest and significant for *Pf*NF54 (R^2 = 0.9005; p = 0.0011) compared to *Pf*Dd2 (R^2 = 0.5160; p = 0.0690) and *Pf*7G8 (R^2 = 0.3420; p = 0.1679) in which the parasite resistance machineries are likely to be in play thus reducing local drug concentrations. This trend was maintained when a correlation was attempted with $LogD_5$ (**Figure 3.4b**) which is physiologically more relevant with respect to activity of these compounds in the DV. Though the R^2 value improved in *Pf*Dd2 (R^2 = 0.7032; p = 0.0184), it slightly diminished in *Pf*NF54 (R^2 = 0.4639; p = 0.0920) and *Pf*7G8 (R^2 = 0.2903; p = 0.2121).

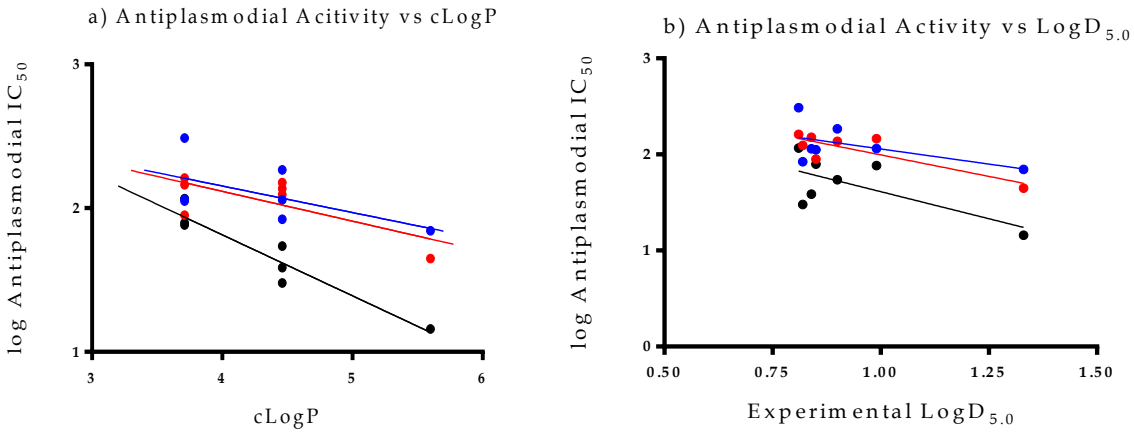

Figure 3.4: Plot showing the association between compounds' predicted lipophilicity and antiplasmodial activity against *Pf*NF54 (black solid dots), *Pf*Dd2 (red solid dots) and *Pf*7G8 (blue solid dots). Plots **a**) and **b**) show associations with cLogP and $LogD_5$, respectively.

3.3.5. β-Haematin Inhibition and Correlations with Antiplasmodial Activity

Due to the presence of the planar quinoline ring system, these compounds were able to inhibit βH formation in a CQ-like manner in the *in vitro* NP-40-based assay that mimics the conditions of the parasite's DV. The derivatives were equipotent to AQ but slightly more active than CQ (**Table 3.4**). There was no pattern in the activity of this series of compounds implying that the inhibition of βH formation is likely contingent primarily on the presence of the planar quinoline core common to all the derivatives. The orientation of the adjacent side chain on the quinoline nucleus did not have any significant influence on βH inhibition activity (βHIA) presumably due to the presence of aromatic ring systems in the dibenzylmethylamine scaffold.

Table 3.4: βH inhibition (βHI) and antiplasmodial activity of the 7 pDBQ derivatives

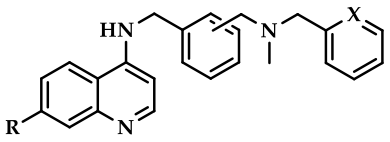

Compound	R	X	βHIA IC_{50} (SD)	*Pf*NF54 IC_{50}	Lipophilicity	
			μM	μM	$LogD_{7.4}$	cLogP [a]
1	Cl	CH	13.4 (1.8)	0.014	3.56	5.60
2 (*meta*-)	Cl	N	20.8 (0.6)	0.030	2.47	4.46
3 (*para*-)	Cl	N	17.2 (0.3)	0.039	2.85	4.46
4 (*ortho*-)	Cl	N	17.9 (3.2)	0.054	3.79	4.46
5 (*ortho*-)	CN	N	16.6 (0.4)	0.116	3.80	3.71
6 (*para*-)	CN	N	24.8 (2.1)	0.076	2.84	3.71
7 (*meta*-)	CN	N	16.7 (0.1)	0.079	2.75	3.71
Chloroquine			26.0 (3.4)	0.008		3.93
Amodiaquine			13.9 (2.3)			4.53
Pyrimethamine			*No inhibition*	0.021		

[a] cLogP predicted using MarvinSketch v5.9.4

Substituting the nitrile for a chloro group at C7 did not appear to impact activity either. Indeed, the influence of different functional groups at C7 on βHIA has been previously investigated using CQ as a model.[100] The ideal properties of best candidate groups at this position for inhibition of βH formation included moderately strong electron-withdrawing capacity and strong lipophilicity, a combination best exhibited by halogens.[100] The electron-withdrawing potentials of cyano and chloro groups compare, hence no radical difference in the βHIA of the analogues from the two groups (mean ± SE βHIA IC_{50} chloro analogues: 17.3 ± 1.5 µM and cyano analogues; 19.4 ± 2.7 µM). Investigations on association between βHIA and compound lipophilicity showed weak but positive correlations (**Figure 3.5a**), which were, however, not significant ($LogD_{7.4}$: R^2 = 0.2608; p = 0.2416, $LogD_5$: R^2 = 0.1202; p = 0.4461, cLogP: R^2 = 0.2943; p = 0.2084).

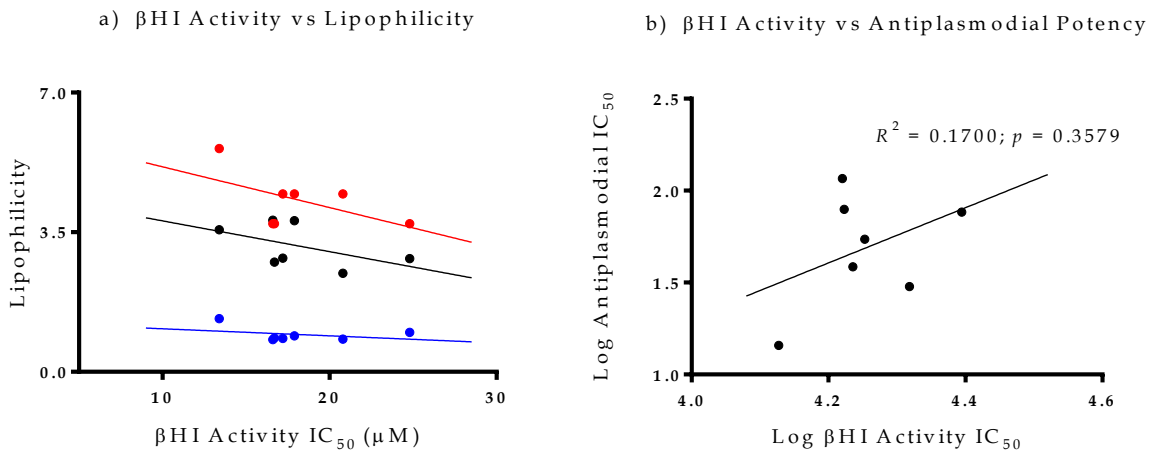

Figure 3.5: Plot of correlation between βHI activity and **a**) lipophilicity and **b**) antiplasmodial activity. In **a**), association between βHI activity and $LogD_{7.4}$, $LogD_5$ and cLogP are represented in black, blue and red, respectively.

Further, analysis of the relationship between antiplasmodial activity and inhibition of βH formation reveals a general trend of decreasing biological activity as βHIA decreases (**Figure**

3.5b). This correlation was nonetheless weak and not statistically significant (R^2 = 0.1700; p=0.3579), implying there could be additional factors to HZ inhibition that influence biological activity. The hypothesis that HZ inhibition correlated with antiplasmodial activity was first tested by Dorn and co-workers by analysing a set of common antimalarials including quinoline methanols, 4-aminoquinolines, acridines, and non-quinolines.[27] In their analysis, the authors established linearity between potency of inhibition of HZ formation and antiplasmodial IC_{50}s using the *Pf*NF54 strain. In contrast, however, Hawley and colleagues, using a similar series of quinoline methanols, 4-aminoquinolines, and acridines on *Pf*3D7 and *Pf*K1 observed no apparent correlation between the two activities when comparing raw IC_{50} data for either the CQS or CQR strains.[86] However, after correcting for accumulation in the DV, Hawley *et al.*, observed a correlation, but only for the CQS strain. Similarly, Kaschula and colleagues, using a series of 2-carbon side chain 4-aminoquinoline derivatives with variable functional groups at C7, also only observed a correlation between antiplasmodial activity and βHIA after the antiplasmodial IC_{50} was scaled to the relative vacuolar accumulation ratio (VAR).[100] In these studies, though, the use of dissimilar chemotypes (e.g., quinolines versus acridines), differences in strains of *P. falciparum* analysed and the non-physiological conditions in the HZ formation assays can be highlighted as reason for the inconsistent results, a more plausible explanation could be the requirement for such molecules to accumulate to very high concentrations within the parasite DV for antiplasmodial, but not necessarily βH inhibition effect. Since these compounds theoretically inhibit HZ formation, the VAR (and by extension the accumulation-normalised IC_{50}) would be the more informative property to correlate with βHIA. Nonetheless, a better understanding of the correlation between antiplasmodial IC_{50} activity and HZ inhibition would require more detailed chemical information on the nature of solid-state aggregates of haem and planar quinoline-based compounds like these pDBQs.

3.3.6. Vacuolar Accumulation

As a follow up on the results of Hawley *et al.* and Kaschula *et al.* that observed linear correlation between βHI and antiplasmodial activity in CQS strains upon correction for differential drug accumulation in the DV, the vacuolar accumulation of the pDBQs was investigated. Since the wide structural diversity of the compounds examined was one of the critical factors that complicated interpretation of results in the previously mentioned studies, the pDBQs provided an opportunity to test for possible correlation using a series of isostructural analogues with a wide range of antiplasmodial IC_{50}s. Additionally, these derivatives span the effective dibasic and tribasic character and thus would be expected to diverge in calculated VARs. Vacuolar accumulation was determined by calculating the antilogarithm of the difference in the experimentally determined LogD values at external and DV pH considered to be 7.4 and 5.0, respectively. The use of the Henderson-Hasselbalch equation, often invoked to predict VAR, was avoided due to its reliance on acid dissociation constants which are not accurately predicted and the potentially confounding assumptions inherent to this method whereby the equation assumes that these weak bases, once protonated, become membrane impermeable. The VAR values ranged from 44.7 to 997.2 (**Table 3.5**), with derivatives having *ortho*- orientation of the RA side group exhibiting highest accumulation in the vacuole (compound **4** and **5**; VAR = 776.2 and 997.2, respectively). Though compounds **2**, **6** and **7** exhibited the lowest accumulation ratio in the vacuole (44.7 – 79.4), their antiplasmodial activities still ranked among the highest, potentially due to other intrinsic features (like solubility and permeability) that confer on them better inhibitory interactions with parasite proteins.

Interestingly, analysis of the VAR with antiplasmodial activity revealed a strong significant correlation in the CQR strain, *Pf*7G8 (R^2 = 0.8475; p = 0.0033) but not in *Pf*NF54 (R^2 = 0.3218; p = 0.1842) or the other CQR strain, *Pf*Dd2 (R^2 = 0.1721; p = 0.3548). Further, no association was

observed with βHIA when the accumulation ratios were scaled using *in vitro* IC_{50} values for *Pf*NF54 (R^2 = 0.0127; p = 0.8097), *Pf*Dd2 (R^2 = 0.0160; p = 0.7872) or even *Pf7*G8 (R^2 = 0.0744; p = 0.5541), further confirming that while accumulation in the organelle is requisite for antiplasmodial activity, it is not a key factor in activity. Rather, as noted in section 3.3.5, the ability of this group to inhibit parasite growth hinges dominantly on their lipophilicity.

Table 3.5: The vacuolar accumulation, βHI and antiplasmodial activity of the 7 pDBQs

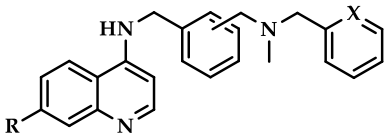

Compound	R	X	VAR [a]	βHIA IC_{50} (μM)	*Pf*NF54 (nM)	VAR x NF54 IC_{50} (μM)
1	Cl	CH	169.8	13.4 ± 1.8	14.4 ± 4.2	2.45
2 (*meta*-)	Cl	N	44.7	20.8 ± 0.6	30.1 ± 5.0	1.36
3 (*para*-)	Cl	N	102.3	17.2 ± 0.3	38.5 ± 4.8	3.94
4 (*ortho*-)	Cl	N	776.2	17.9 ± 3.2	54.4 ± 5.5	42.23
5 (*ortho*-)	CN	N	997.2	16.6 ± 0.4	116.3 ± 17.2	115.97
6 (*para*-)	CN	N	70.8	24.8 ± 2.1	76.4 ± 4.0	5.41
7 (*meta*-)	CN	N	79.4	16.7 ± 0.1	79.1 ± 4.9	6.28

[a] VAR values were calculated using the equation VAR = Antilog($LogD_{7.4}$ – $LogD_{5.0}$)

3.3.7. Cellular Haem-Pyridine Fractionation Profiles

3.3.7.1. Analysis of Chloroquine and Pyrimethamine standards

As mentioned in *Chapter 1*, the processes of Hb degradation and inhibition of haem detoxification are potential targets of such antimalarial classes as quinolines, aryl alcohols, artemisinin, and other peroxides. The dose-dependent effect (if any) of an inhibitor on the fate of total haem in the parasite can be examined by investigating the different fractions/species of haem extracted from *P. falciparum* cells treated with varying doses of drug.[89] Established inhibitors of HZ formation, like CQ, exhibit a dose-dependent signature characterised by a decrease in the fraction of HZ matched by a corresponding rise in both 'free' haem and Hb. Inhibitors like pyrimethamine (PYR), however, that exert their antiplasmodial effect through other targets do not exhibit this pattern. The morphological effect of treating the cells with different drug concentrations can be visualised either on Giemsa-stained slides through microscopy or through flow cytometry (FACs) analysis. To ascertain the fidelity of the cellular fractionation assay, the haem profiles of CQ and PYR were first assessed according to the method detailed in *Chapter 2*. These profiles constitute each haem species (present as Hb, 'free' haem or HZ) expressed in terms of the amount of haem iron (Fe) per cell in femtogram (fg). The control amounts of 'free' haem and HZ indicate the levels of each that are produced and tolerated by the parasite under normal physiological conditions, and in the absence of drug. A significant dose-dependent decrease in HZ and corresponding significant increase in 'free' haem, compared to the control, is therefore representative of HZ inhibitors. Significant differences in measured amounts of haem Fe (fg) relative to the control were calculated using Student's 2-tailed t-test at the 95% confidence interval, and plotted with asterisks to indicate statistical significance, where * $p< 0.05$; ** $p< 0.01$; *** $p< 0.001$.

FACs analysis of the trophozoites shows clear differences in cell size and complexity, between untreated cells and those treated with 3x CQ IC_{50} (**Figure 3.6**). The side-scattered (SSC) shift shows that CQ treated cells are less complex and dense, compared to the control cells while the forward-scattered (FSC) shift shows that treated cells are smaller than the untreated controls. The shift in SYBR Green I fluorescent intensity shows that the CQ-treated cells have less nucleic acid content than the control cells, indicating the presence of less mature cells. These observations provide evidence of stunted maturity of cells from CQ treatment compared to untreated, and that there are fewer trophozoites present in the treated sample. This indicates that at higher concentrations of CQ, and a significantly raised level of 'free' haem, CQ-treated cells are unable to mature and survive to the same extent as the untreated cells. Since the process of Hb uptake and digestion is active in early stages of the parasite as rings,[189] inhibition of HZ formation through CQ treatment therefore impairs the cells' ability to competently transition into the succeeding cycle stages, consequently impacting on their morphology and DNA-making ability.

PYR-treated cells, on the other hand, did not appear to be radically affected by drug treatment, with the FSC, SSC and SYBR Green shifts appearing comparable to the untreated controls. A plausible explanation for this would be that since PYR has a slow speed-of-kill that mainly acts on the late trophozoite and schizont stages,[190] the 32 h treatment assay is unlikely to capture the inability of the abnormal schizonts to mature and release viable merozoites. These observations further validate the target differences between CQ and PYR.

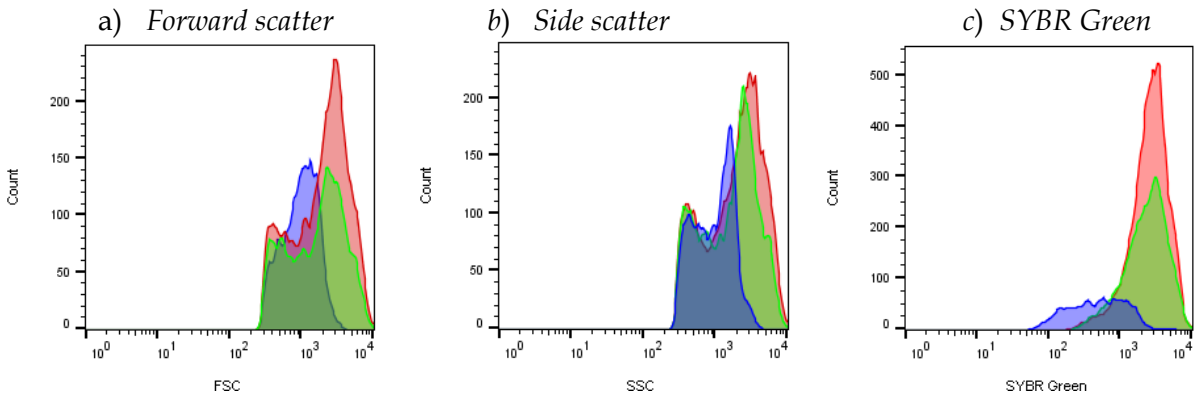

Figure 3.6: Flow cytometry histograms showing changes in cell size (FSC plot), complexity (SSC plot) and nucleic acid content (SYBR Green plot) of *Pf*NF54 trophozoite population treated with 3x IC_{50}s of CQ (blue) and PYR (green) overlaid against untreated control (red).

The haem profiles showed a dose-dependent increase in 'free' haem, which was significant from 2 to 3x CQ IC_{50}, compared to the control (**Figure 3.7**). The average (± SE) amount of 'free' haem present in the control was 3.54 ± 0.52 fg of haem Fe per cell while the amount present at 3x CQ IC_{50} was 6.91 ± 0.77 fg. This increase in toxic 'free' haem corresponded to a significant decreased in HZ, at the equivalent IC_{50} multiples (**Figure 3.7a-b**). The parasite survival curve overlaid with 'free' haem Fe levels showed a trend of increasing 'free' haem corresponding to a decreasing parasite survival (**Figure 3.7c**), thus confirming that CQ is indeed an inhibitor of HZ formation.

As a negative control, PYR, was included to illustrate the robustness of this haem-pyridine fractionation assay. The 'free' haem and HZ profiles for PYR-treated *Pf*NF54 cells show a plateau in haem levels with increasing PYR concentration. In addition, no significant differences in haem Fe were observed relative to the control. Unlike CQ-treated cells, PYR treatment did not lead to a dose-dependent increase in 'free' haem and a corresponding decrease in HZ (**Figure 3.7d-e**). Even at higher PYR concentrations, there was no significant

increase in 'free' haem compared to the untreated cells, indicating that cells are able to grow and survive, as they would under normal physiological conditions. The parasite survival curve overlaid with 'free' haem Fe levels shows no correlation between the two parameters (**Figure 3.7f**). These results corroborate the observations with the FACs analysis where PYR-treated cells did not appear to differ from untreated controls in size, complexity or nucleic acid content, and correlate with PYR's MoA involving inhibition of the trophozoite-specific dihydrofolate reductase–thymidylate synthetase,[191] an event only marginally captured within the 32-h PYR incubation period of these cells. This data demonstrates that PYR is not an inhibitor of HZ formation and by extension affirm the fidelity of the haem-pyridine fractionation assay.

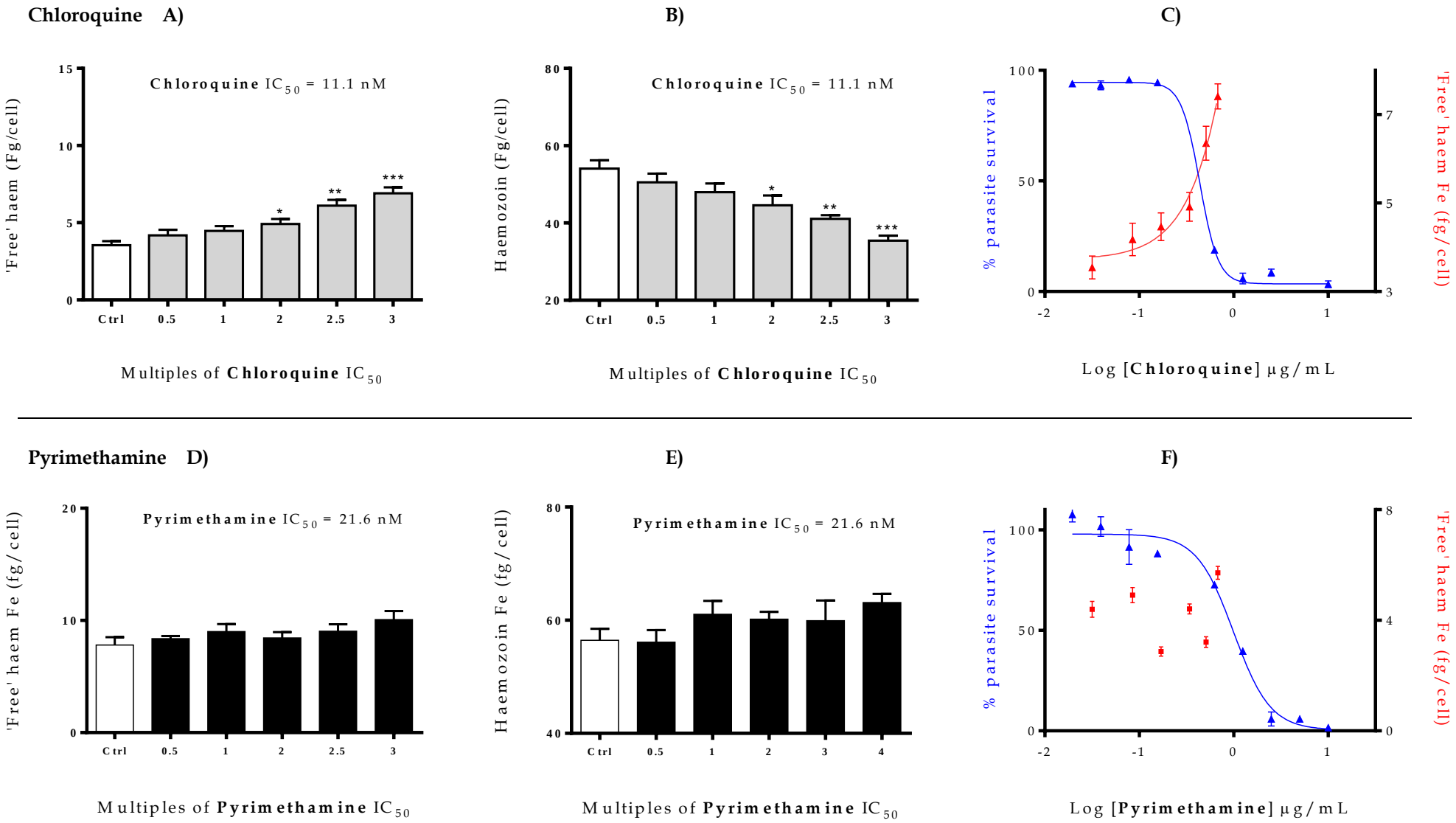

Figure 3.7: Haem fractionation profiles of CQ and PYR in synchronised drug-treated and control *Pf*NF54 parasites. Plots **a, d**) and **b, e**) respectively show 'free' haem and HZ represented in terms of iron (Fe) measured in fg/cell with asterisks indicating statistical significance relative to control (*$p < 0.05$; **$p < 0.01$ and ***$p < 0.001$). Plots **c**) and **f**) represent parasite survival (blue) overlaid against 'free' haem Fe (red) plots and clearly show an unambiguous trend of increasing levels of 'free' haem corresponding with parasite death only in CQ (true inhibitor) but not in PYR.

3.3.7.2. Analysis of Cellular Haem Fractionation Profiles

All the compounds showed similar morphological profiles on analysis using flow cytometry, and on this rationale, FACs histogram data is presented for three compounds (**1**, **2** and **6**) which respectively represent all the various modifications of the scaffold's SAR. Similar to the CQ profiles discussed in **section 3.3.7.1**, the flow cytometry analysis of the trophozoites treated with the three compounds showed shifts in cell size and complexity between the untreated cells and those treated with 3x IC_{50} of the test compounds. However, these differences were not as extreme (**Figure 3.8**) as those observed in CQ-treated *Pf*NF54 cells, and could be indicative of differential sensitivity of the parasite strain to CQ and these test compounds (**CQ** IC_{50} = 11.1 nM; compound **2** IC_{50} = 30.1 nM and compound **6** IC_{50} = 116.3 nM). The SSC shifts showed that treated cells were less complex and dense for all the 3 compounds compared to the control (**Figure 3.8b, e** and **h**) while the FSC shifts revealed that they were comparatively smaller (**Figure 3.8a, d** and **g**). There were slight shifts in SYBR Green I fluorescent intensities indicating that treated cells had less nucleic acid content than untreated cells (**Figure 3.8c, f** and **i**). Put together, these observations indicate that the cells treated with 3x IC_{50} of the pDBQs had grown and matured to a lesser degree than the untreated cells.

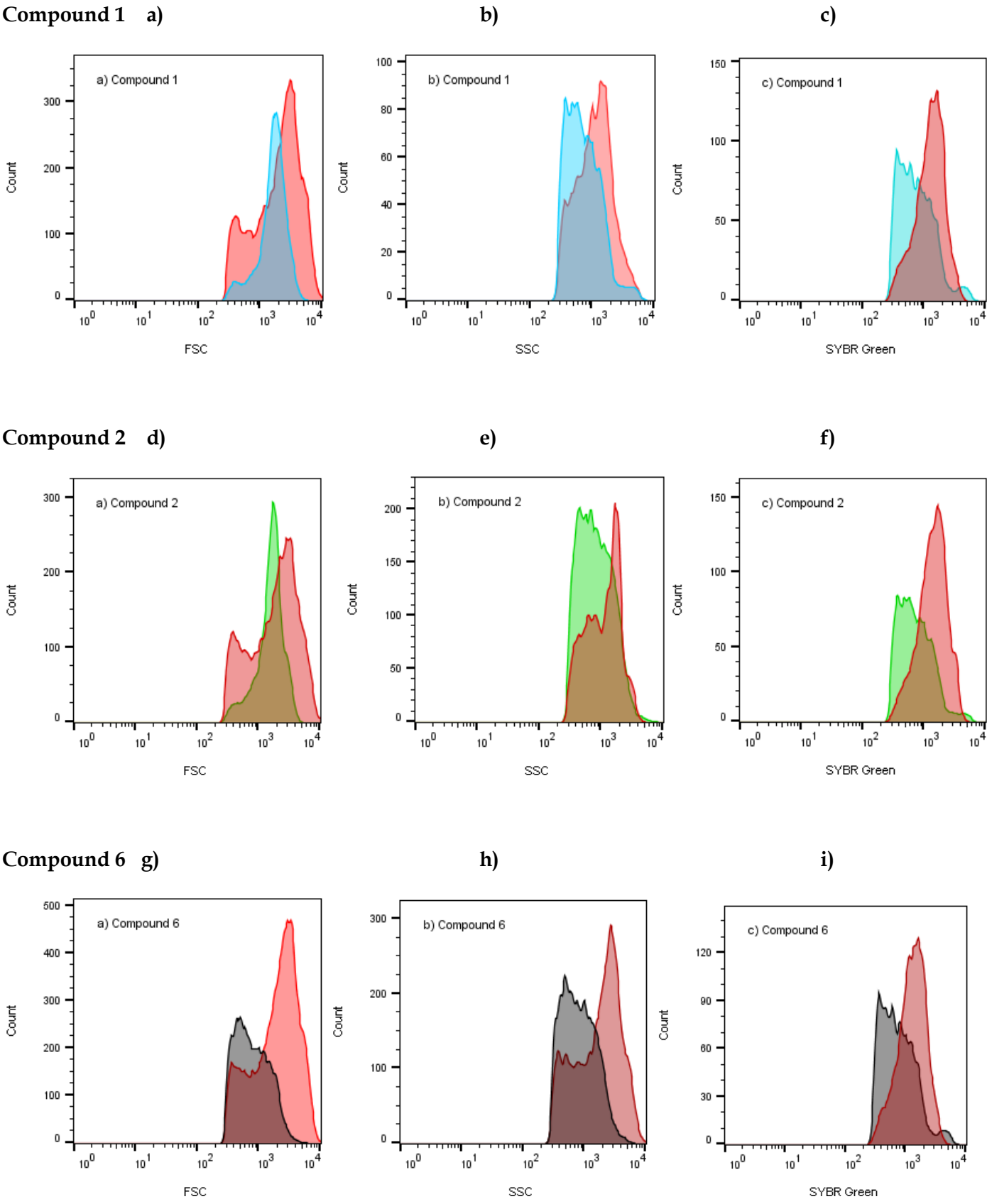

Figure 3.8: Flow cytometry histograms showing changes in cell size (FSC plot: **a**, **d** and **g**), complexity (SSC plot: **b, e** and **h**) and nucleic acid content (SYBR Green plot: **c, f** and **i**) of *Pf*NF54 trophozoite population treated with 3x IC_{50}s of compound **1** (blue), **2** (green) and **6** (grey) overlaid against untreated controls (red).

The 'free' haem profiles show a dose dependent increase in 'free' haem, which was significant from 0.5x IC_{50} (in compound **6** and **7**) to 3x IC_{50} (all compounds), compared to the control (**Figure 3.9**). These increases in 'free' haem corresponded to significant decreases in HZ, at the equivalent IC_{50}s in most of the compounds. In compound **2** and **5**, however, this decrease was only significant at 3x compound IC_{50} even though declining trends in HZ levels were observed. Two lines of evidence strongly support the fact that this anomaly is likely an artefact of experimental error rather than absence of inhibitory activity. First, βHI results provide a baseline hint that these two compounds are likely to inhibit HZ formation in a physiological setting as they had marginally higher activity (compound **2** and **5** βHI IC_{50}: 20.8 μM and 16.6 μM, respectively) compared to CQ (βHI IC_{50}: 26.0 μM) in the detergent-based assay (**Table 3.4**). Second, there were marked error margins, (denoted by the standard deviations on the plots), on the recorded levels of HZ in the treated cells, which could have statistically masked the decrease. Nonetheless, the parasite survival curves for all the compounds overlaid with the 'free' haem levels showed that an increase in 'free' haem Fe indeed corresponded to a decrease in parasite survival (**Figure 3.9**). In general, these results clearly demonstrate that the pDBQs, as a class, are inhibitors of HZ formation. However, possible existence of other auxiliary modes of action for these compounds cannot be discounted. Indeed, though it is widely accepted that such quinoline-containing compounds act primarily by preventing haem detoxification, other mechanisms for the action of quinoline-based and related compounds have been proposed and include inhibition of food vacuole lipase and aspartic proteases [192, 193] as well as protein synthesis.[194]

Compound 1 **a)**

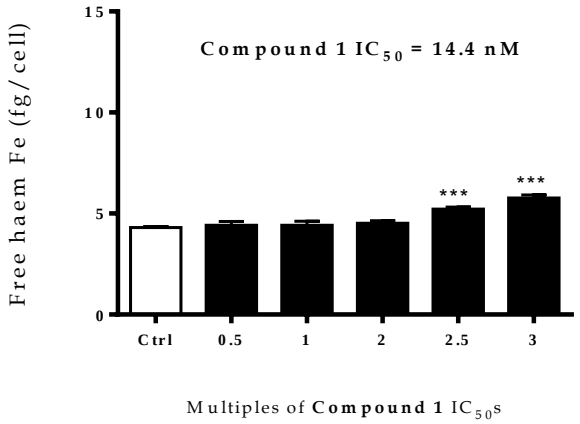

b)

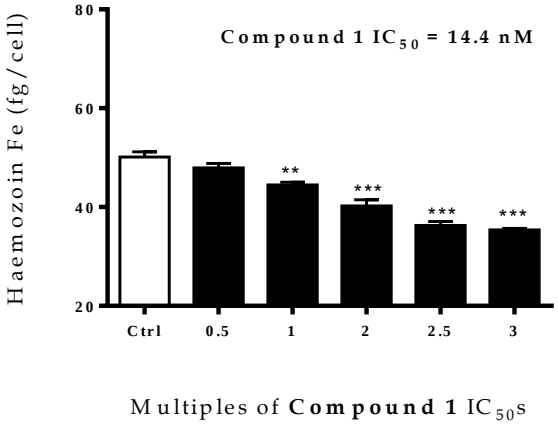

c)

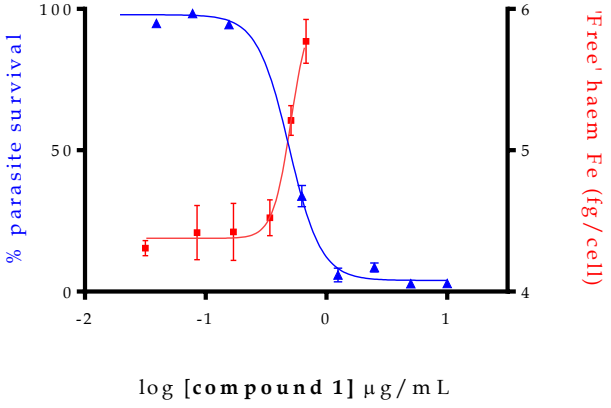

Compound 2 **d)**

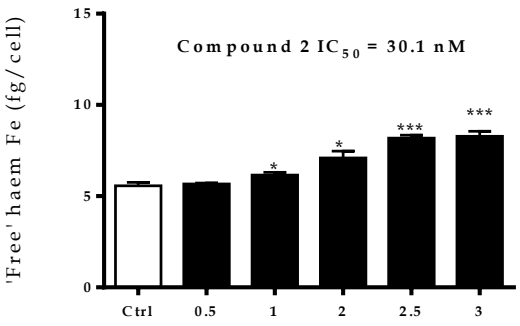

e)

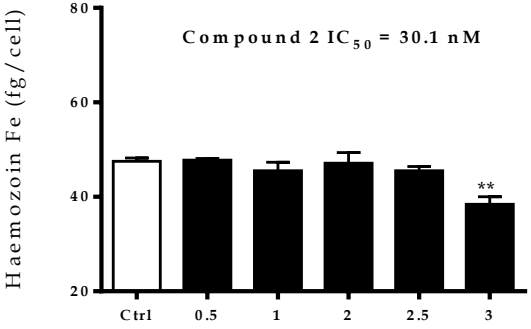

f)

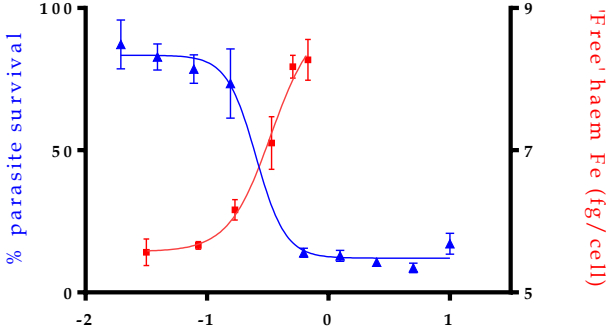

Compound 3 **g)**

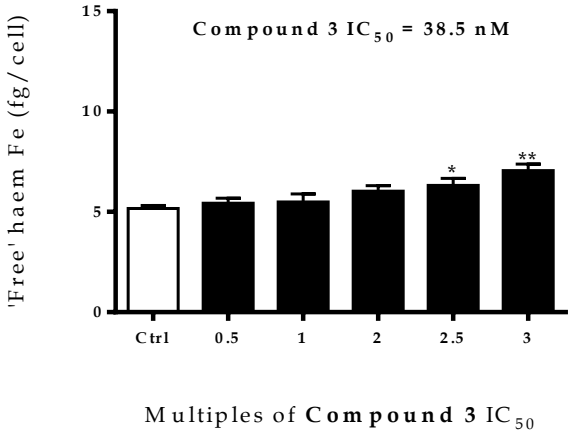

h)

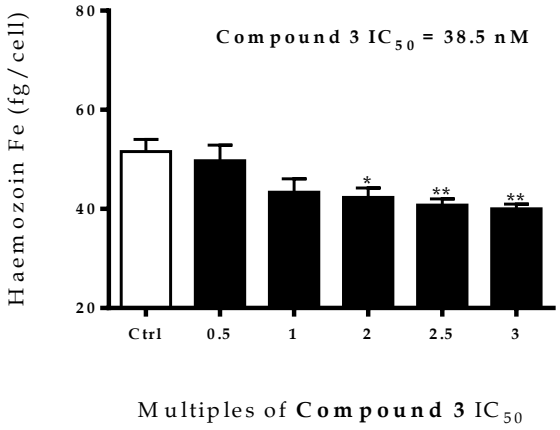

i)

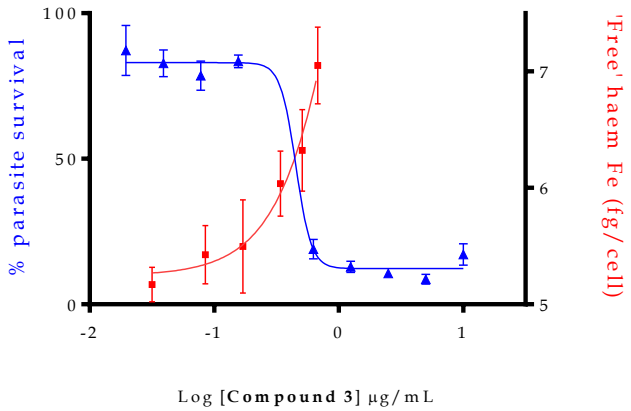

Compound 4 **j)**

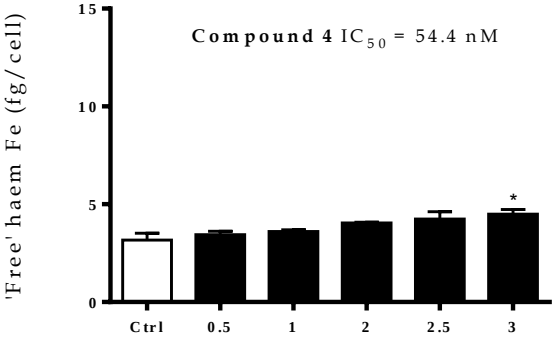

k)

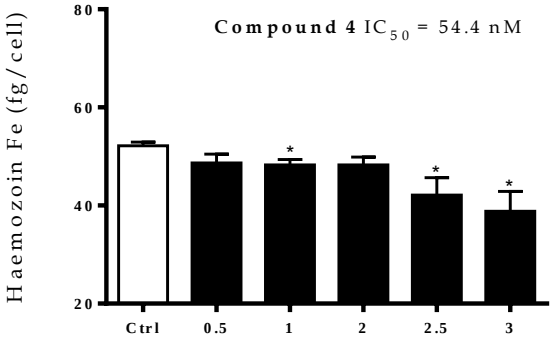

l)

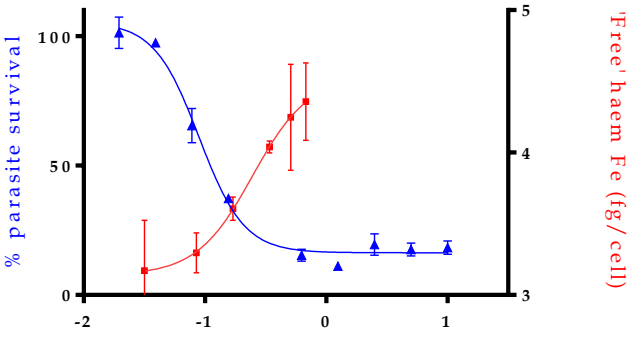

Compound 5 m)

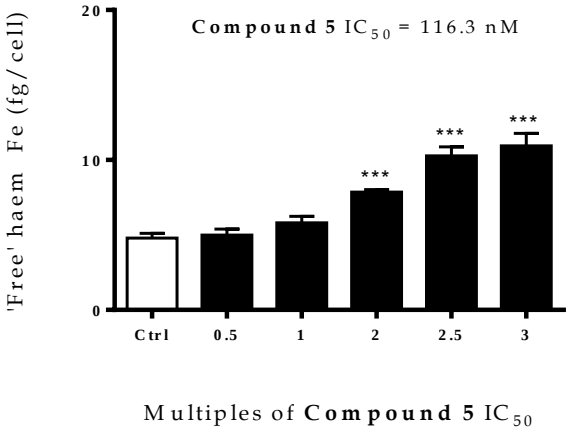

n)

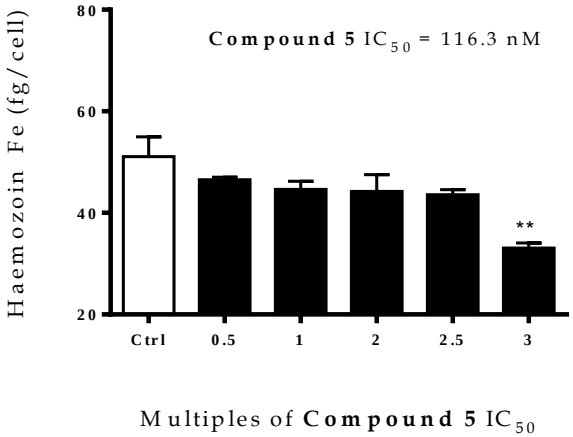

o)

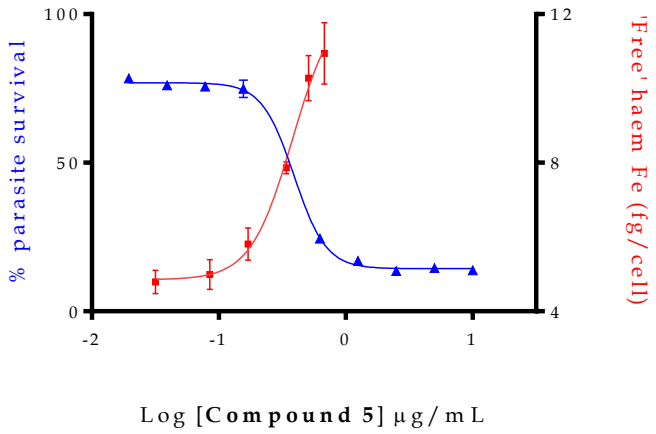

Compound 6 p)

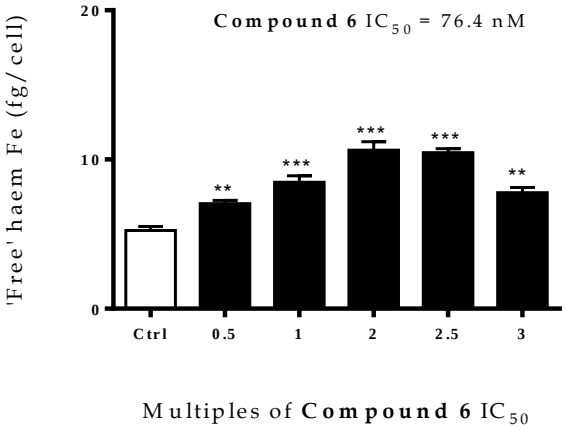

q)

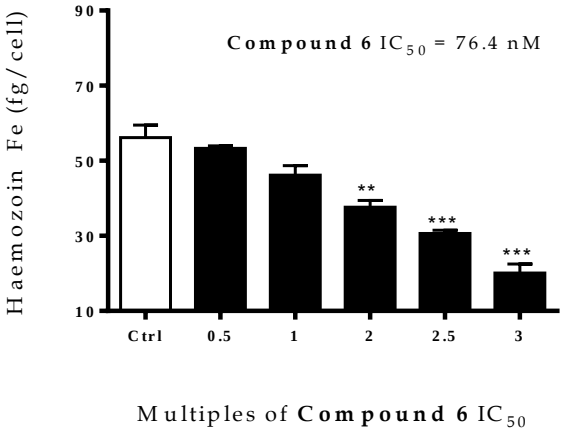

r)

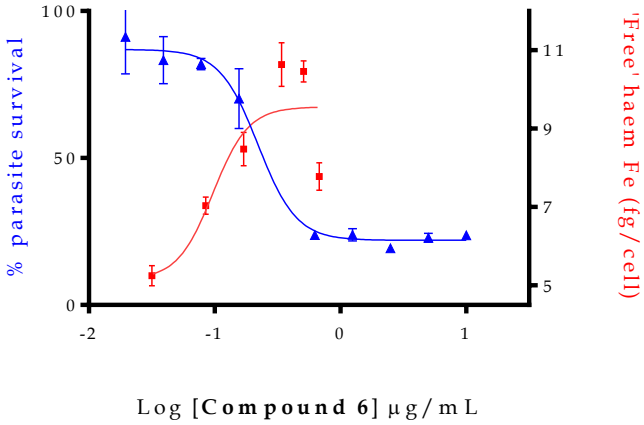

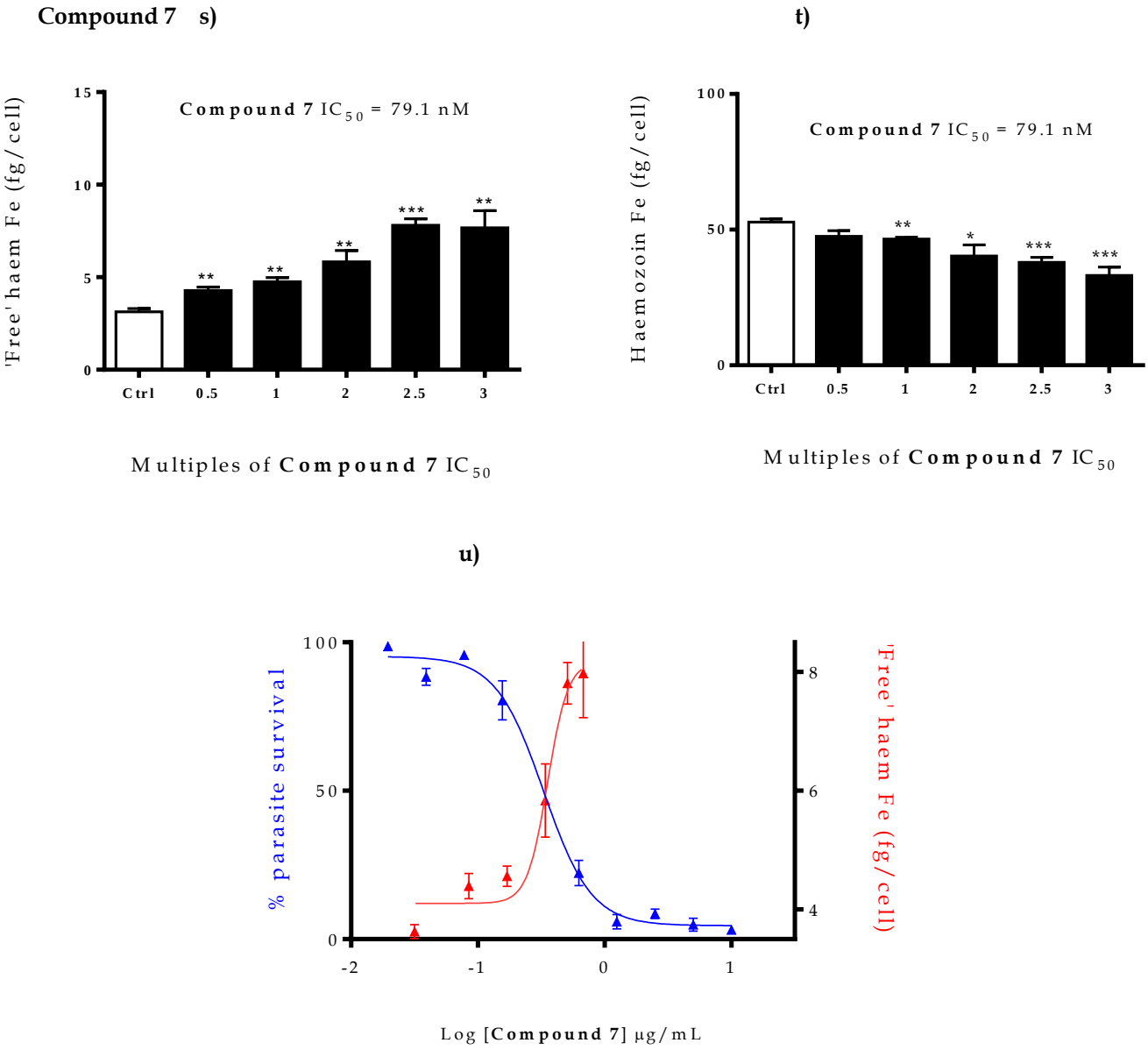

Figure 3.9: Haem fractionation profiles of compounds **1-7** in synchronised drug-treated and control *Pf*NF54 parasites. Plots **a, d, g, j, m, p** and **s**), show levels of toxic 'free' haem represented in terms of iron(Fe) measured in fg/cell while plots **b, e, h, k, n, q** and **t**) show haemozoin levels. The asterisks indicate statistical significance relative to control (*$p < 0.05$; ** $p < 0.01$ and *** $p < 0.001$). Plots **c, f, i, l, o, r** and **u**) represent parasite survival (blue) overlaid against 'free' haem Fe (red) plots and clearly show unambiguous trends of increasing levels of 'free' haem corresponding with parasite death in all the compounds.

3.3.8. Potential for hERG Channel Inhibition

As noted in *Chapter 1*, acquired long-QT syndromes occur quite often, and are commonly caused by pharmacologically and structurally diverse compound classes that reduce currents through hERG channels. Consequently, lead compounds are routinely tested early in the drug development process to flag any potential risk for hERG channel inhibition.[195]

3.3.8.1. In silico Prediction of hERG Channel Toxicity

Prediction of hERG inhibition is very challenging, in part due to the promiscuity of the larger inner vestibule of the hERG channel, which provides more space for structurally diverse drugs to block this channel. Also, there is no detailed X-ray crystal structure for the hERG protein, hence structural details for the hERG channel are inferred by analogy with other ion channels, computational analyses, and mutagenesis studies. *In silico* prediction therefore provides a guide into likelihood of toxicity potential. All predictions of hERG channel inhibition potential of the derivatives were done using StarDrop™ software. One of the challenges for hERG blockage prediction is the lack of a definite threshold for discrimination of hERG blockers from non-blockers.[196, 197] Halofantrine (HLF) and its major metabolite N-desbutylhalofantrine (dbHLF) have previously been associated with QT interval prolongation and with fatal and non-fatal arrhythmias in patients without known underlying cardiac abnormalities.[198, 199] Though considered safe antimalarials, HLF and dbHLF have been shown to block wildtype hERG channels stably expressed in HEK 293 cells in a concentration-dependent manner with IC_{50}s of 0.018 μM and 0.072 μM, respectively.[198, 200] This nanomolar range toxicity suggests that the gain in the safety margin for QT interval prolongation-related cardiotoxicity is minimal, and as such, HLF and dbHLF were included in the analysis and scored as known controls with high inhibition indices while CQ and dihydroartemisinin (DHA) were included as low-inhibition controls. DHA

has previously been reported to have little cardiac toxicity [141] and low *in vitro* inhibition IC_{50} of 9.62 μM [200] while CQ IC_{50} have been reported between the range of 1.0 - 2.5 μM.[198] Inhibition potency was reported as pIC_{50}, which is modelled in the program using the negative logarithm of literature IC_{50} values (in molar units) of 168 chemically diverse molecules with patch-clamp inhibition data. Therefore, more potent compounds present with higher pIC_{50} values. The test compounds had pIC_{50}s within a narrow range of 6.22 – 6.55, with the controls HLF and dbHLF predictably more potent than the pDBQs while CQ and DHA had lower inhibition values as expected (**Table 3.6**).

Discernibly, there was a trend in potency relative to substituent orientation whereby the *para*-substituted compounds **3** and **6** exhibited highest pIC_{50}s (6.43 and 6.39, respectively) compared to the other analogues in the group with a pyridine ring substitution on the RA side chain. This implies that the *para*- aromatic substitution potentially increases access into of the high-affinity internal binding site of the hERG channel to exert stronger blockage. Interestingly, the possibility of reducing hERG potency by modifying the pattern of aromatic substitution on compounds has been previously explored, and results from mutagenesis and molecular modeling studies on clofilium and ibutilide analogues suggested that phenyl ring *para*-substituents strongly affect binding.[201]

Table 3.6: Predicted hERG inhibition IC_{50}s versus molecular weights and lipophilicity of the 7 pDBQ derivatives and 4 reference antimalarials

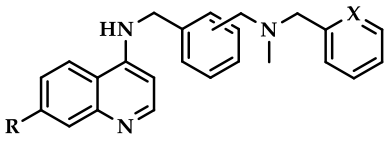

Compound	R	X	pIC_{50} [a]	Mol. Weight	Log P [b]	Log $D_{7.4}$ [b]
1	Cl	CH	6.55	439.4	5.67	4.04
2 (*meta*-)	Cl	N	6.23	402.9	4.51	4.01
3 (*para*-)	Cl	N	6.43	402.9	4.51	4.01
4 (*ortho*-)	Cl	N	6.28	402.9	4.51	4.00
5 (*ortho*-)	CN	N	6.23	395.5	3.80	3.47
6 (*para*-)	CN	N	6.39	395.5	3.80	3.47
7 (*meta*-)	CN	N	6.22	395.5	3.80	3.48
Chloroquine			6.00	319.9	3.81	0.88
Dihydroartemisinin			4.27	284.4	2.84	2.84
Halofantrine			7.37	500.4	8.06	5.46
***N*-desbutylhalofantrine**			6.52	444.3	6.35	3.90

[a] pIC_{50} values were determined using StarDrop™

[b] cLogP and $LogD_{7.4}$ were predicted using MarvinSketch v5.9.4

Previously, it has been hypothesised that compounds with lower lipophilicity and MW are likely to exhibit less toxicity to the hERG potassium channel.[144] While the substitution of a chloro with a nitrile at the C7 position in this series allowed for retention of their βHI potential, it simultaneously yielded a set of compounds with reduced MW and lipophilicity (**Table 3.6**), thus permitting an opportunity to test the predicted hERG inhibition versus lipophilicity and MW hypothesis. A liner regression analysis of hERG pIC_{50}s versus both

measures of lipophilicity on the derivatives yielded a positive correlation between increasing potency of inhibition and lipophilicity. This association was, however, stronger in the cLogP analysis (R^2 = 0.5052; p = 0.0734) compared to LogD (R^2 = 0.1722; p = 0.3545) but significant in neither. When the 4 control compounds were included in the analysis, the strength of the association markedly improved, and was significant in the cLogP analysis (**Figure 3.10a**), suggesting that the weak correlations observed with the derivatives alone are likely a statistical reflection of small sample size with a narrow range of pIC_{50} values, rather than lack of association. Analysis of the association between hERG pIC_{50} and MW similarly showed a strong trend of diminishing potency with decreased MW. Note, however, these correlations must be treated with caution, since lipophilicity and MW may be parameters used by the StarDrop™ program in predicting hERG pIC_{50}s.

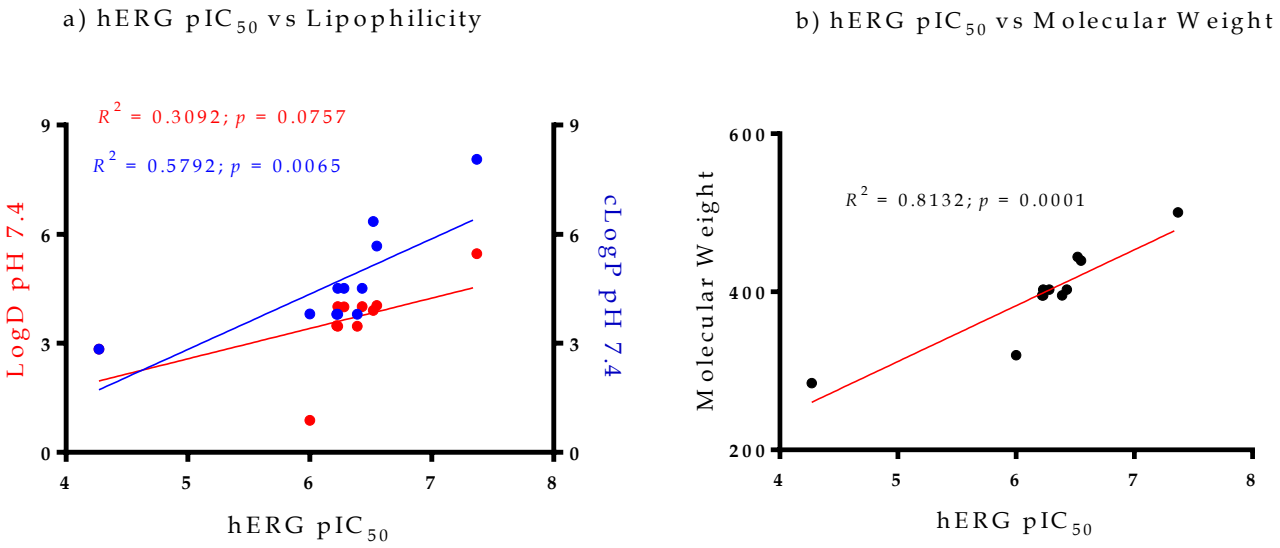

Figure 3.10: Linear regression analysis plots showing the correlation between hERG pIC_{50}s and $LogD_{7.4}$ (solid red circles) and cLogP (solid blue circles) in **a**) as well as molecular weights (solid black circles) in **b**).

3.3.8.2. Experimental Determination of hERG Channel Toxicity

While *in silico* predictions play an important role in providing an approximate indication of a compound's potential for the hERG liability, they can only model to a limited degree the physiological contributions of ventricular repolarisation, channel promiscuity, potential interactions with other ion channels and compound MoA towards hERG channel inhibition. Owing to these complexities, complementation of computational predictions with experimental analysis is customarily recommended.

Due to cost constraints and *in silico* results that showed no significant differences in the pIC_{50}s of the compounds, one derivative (compound **4**) was selected as representative for experimental analysis to determine hERG inhibition potential of this scaffold. Using verapamil hydrochloride as positive control, compound **4** was screened at four concentrations (0.3, 1, 3 and 10 μM) against a minimum of three separate CHO cells stably expressing hERG and the percent inhibition values from each cell was used to construct concentration-response curves. There was a concentration-dependent blockade of hERG protein by compound **4**. At 0.3 μM, the compound was half as inhibitive as the control (mean %Inhibition ± SE: 16.6 ± 0.55 vs 33.9 ± 4.15), and this difference was significant ($p < 0.0001$, unpaired t-test). However, at higher test concentrations, there was no significant difference between the toxicity of compound **4** and verapamil (**Figure 3.11**), In fact, at 10 μM, compound **4** was marginally more toxic – causing 96.2% inhibition compared to the control (94.3%), though this could be indicative of residual inhibition whereby the concentration is too high to reliably measure the true extent of inhibition.

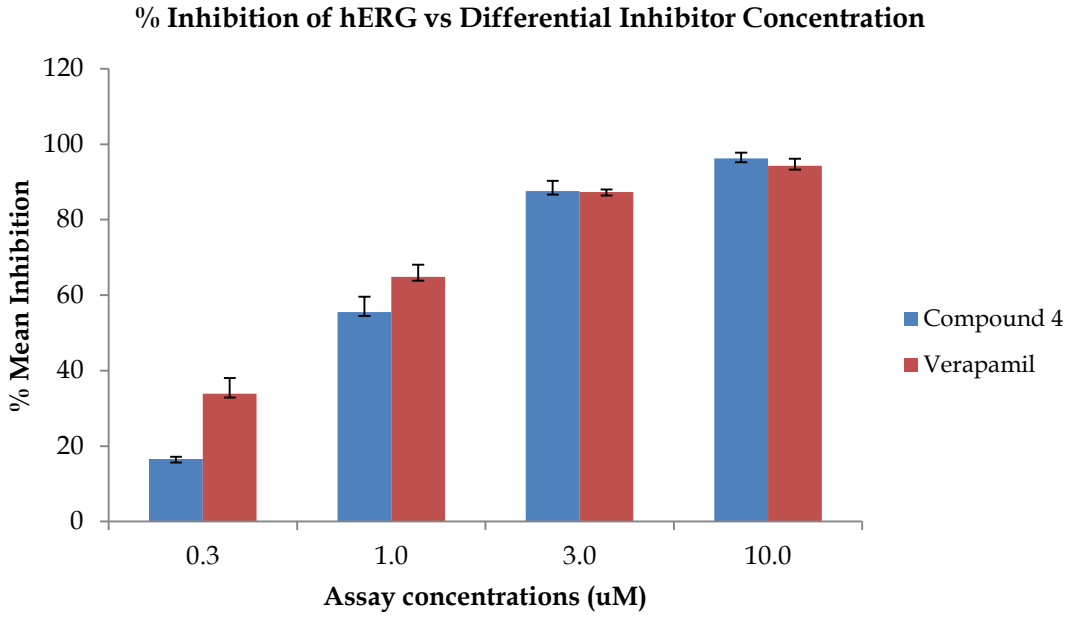

Figure 3.11: Mean percent inhibition of hERG protein expressed in CHO cells at varying concentrations of compound **4** and verapamil hydrochloride.

For compound **4** and the control, this inhibition was further quantified by measuring the IC_{50} values of at least three separate cells (n >3). Data from individual cells were then pooled to obtain mean inhibition IC_{50}s (± SD mean), and are presented in **Table 3.7**. Compound **4** (IC_{50}: 0.87 µM) seemed to inhibit hERG at a comparable potency to verapamil (IC_{50}: 0.56 µM) under the test conditions and these values, on conversion to pIC_{50}s, were consistent with the predicted values obtained from StarDrop™ analysis in **Table 3.6**. The IC_{50} of verapamil under the assay conditions was within range of previously published values of 0.143 – 0.831 µM obtained using heterologous expression systems in HEK 293 and CHO cells.[202-205] This wide range in *in vitro* activity possibly reflects properties of the different expression systems and highlights the problem of endogenous influences in heterologous expression systems. Determination of the approximate free therapeutic serum level ranges of the pDBQs would have been informative as they would provide a pointer of whether the observed inhibitory

activity of compound **4** on hERG occurs at clinically relevant concentrations. Nevertheless, the caveat that data from *in vitro* experiments must be extrapolated to the clinical situation with caution must still be upheld.

Table 3.7: Experimental and predicted hERG inhibition for compound **4** and verapamil

Compound	Structure	Experimental Inhibition (μM) [a]		Predicted Inhibition
		IC_{50} ± SD	pIC_{50}	pIC_{50} [b]
4	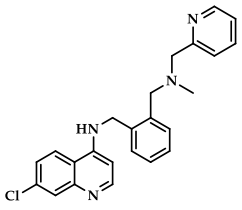	0.87 ± 0.08	6.060	6.279
Verapamil		0.56 ± 0.08	6.252	6.155

[a] Experimental IC50 were determined from inhibition of hERG protein expressed in CHO cells and corresponding pIC_{50} obtained as negative logarithm of these IC_{50} values converted to milimolar units.

[b] Predicted pIC_{50}s were determined using StarDrop™

3.3.9. In vitro Metabolism Studies in Mouse Liver Microsomes

3.3.9.1. Microsomal Metabolic Stability

Extensive and rapid metabolism of a compound to less active or inactive metabolites is a liability as it can lead to reduced efficacy. Though *in vitro* metabolic stability can be assessed using recombinant CYP enzymes, microsomes, hepatocytes or liver fractions,[206] microsomes are the most widely preferred due to their ease of preservation, amenability to HTS and stability of their enzymatic activity even after prolonged storage.[207] The microsomal

metabolic stability of the 7 derivatives was assessed in mouse liver microsomes (MLMs) using a single point assay. All the compounds were rapidly metabolised with less than 5% of the parent remaining after 30 minutes of incubation at 0.1 mg/mL microsomal protein (**Table 3.8**). The compounds exhibited short degradation half-lives (Mean $t_{1/2}$: 5.65 min) and high hepatic clearance ratios (>0.90), suggesting significant susceptibility to hepatic metabolism.

Table 3.8: *In vitro* metabolic stability of analogues **1 - 7** in mouse liver microsomes (MLMs)

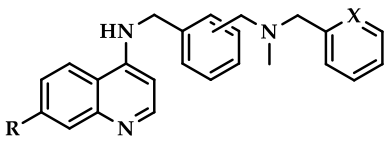

Compound	R	X	% remaining (after 30 min)	Projected Half Life (min)	Intrinsic Clearance CL (mL/min/kg)	Predicted Hepatic Extraction Ratio
1	Cl	CH	3.57	6.15	1107	0.92
2 (*meta*-)	Cl	N	2.96	5.89	1139	0.93
3 (*para*-)	Cl	N	2.08	5.35	1250	0.93
4 (*ortho*-)	Cl	N	2.32	5.49	1224	0.93
5 (*ortho*-)	CN	N	2.08	5.35	1249	0.93
6 (*para*-)	CN	N	3.63	6.22	1101	0.90
7 (*meta*-)	CN	N	1.91	5.10	1349	0.94
Midazolam			1.33	4.74	1425	0.94
MMV390048			93.55	172.25	42	0.32

This high rate of metabolism was comparable to the benzodiazepine, midazolam (1.33% remaining after 30 min). No metabolism occurred in the absence of NADPH or microsomes in the control set ups, implying that the observed bioactivation was primarily a function of cytochrome p450 enzyme-mediated phase 1 metabolism. Varying the position of the

dibenzylmethylamine side chain from *ortho*-, to *meta*- or *para*- did not seem to influence compound stability as would sometimes be expected, whereby substituent orientations would sterically hinder or permit enzyme access into metabolically labile sites of the molecule. This high metabolic susceptibility has implications on *in vivo* efficacy as plasma exposure of the compounds is likely to be poor and bioavailability low upon dosing.

3.3.9.2. Metabolite Identification

To further understand the structural basis of this rapid compound clearance, all the compounds were subjected to metabolite identification studies. In this analysis, mass spectroscopy data from the metabolic stability assay of each compound were screened for the presence of fragments corresponding to putative metabolites and routes/sites of metabolism inferred. Notably, the fragmentation pattern appeared to be conserved in all derivatives in the series regardless of the substitution at C7 on the quinoline ring or orientation of the side group, with *N*-dealkylation on the tertiary amine appearing to be the most predominant route of metabolism as metabolite 2 was present in highest proportion in all compounds. Other metabolites detected included products from oxidation of either the quinoline or pyridyl ring, denoted by a +16 shift in mass (metabolite 5). *N*-dealkylation and a combination of oxidative deamination (metabolite 6) and aldehyde reduction (metabolite 3) and oxidation of aldehyde to carboxylic acid (metabolite 4) were also observed as depicted in **Figure 3.12**. The physicochemical, biological and mechanistic properties of the resultant metabolites will be discussed in the next chapter.

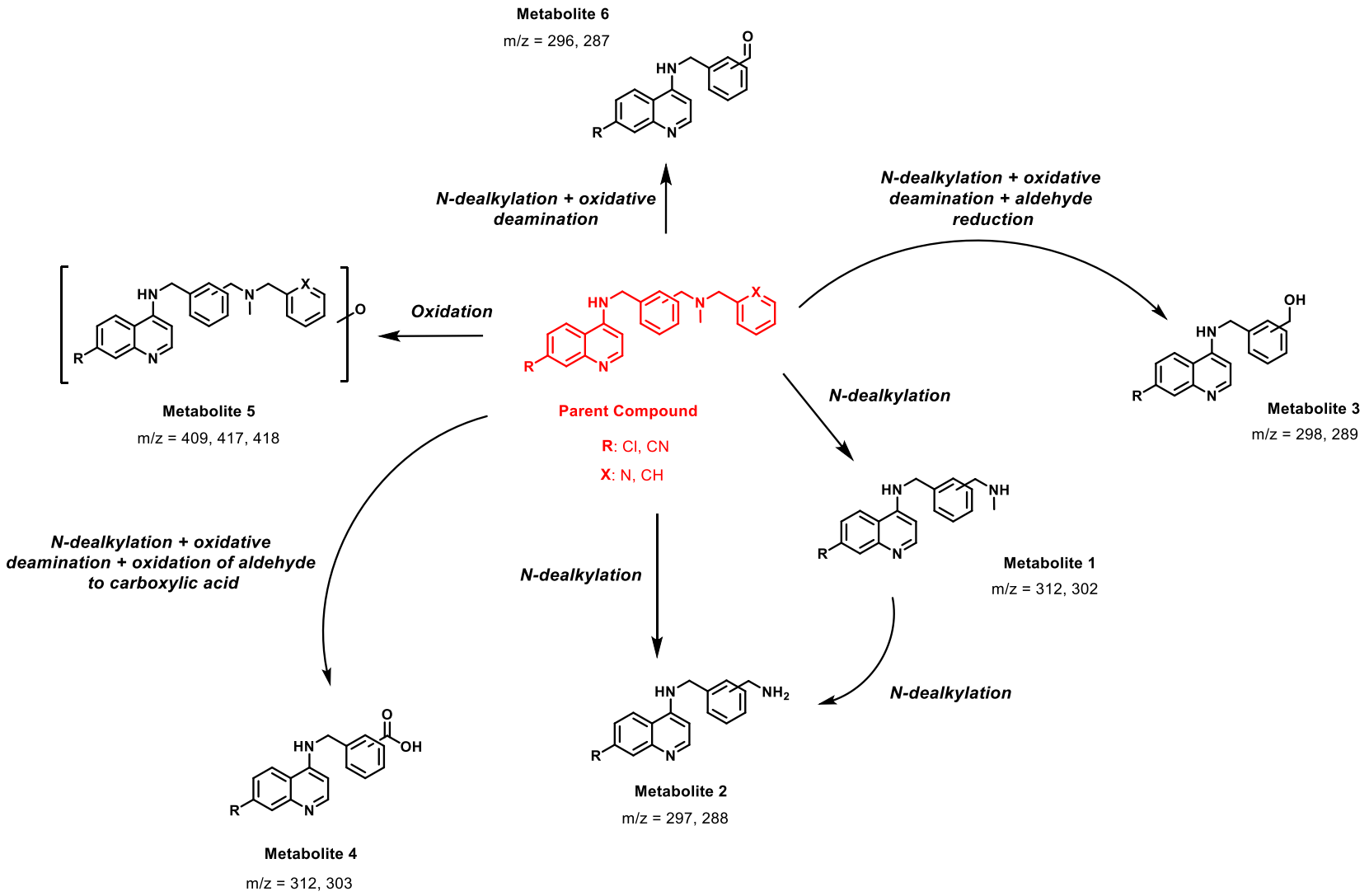

Figure 3.12: Fragmentation patterns of the prototype molecule with putative metabolite structures and masses (in positive mode)

3.4. Summary and Conclusion

This chapter evaluated the physicochemical properties, biological activities and mechanistic inhibition potential against βH/HZ of seven rCQ compounds bearing a dibenzylmethylamine side group hybridised to a quinoline ring. The results from these analyses have been supplemented by microsomal metabolism as well as predicted and experimental hERG data.

In summary, the compounds exhibited moderate to high solubility at pH 6.5, with significant improvement in compounds **2 – 7** which, unlike **1**, bore a pyridine ring substituent in place of one of the phenyl rings thus allowing for enhanced H-bonding to water molecules. The compounds also exhibited high membrane permeability at the physiologically-relevant pH 6.5, indicating that greater permeation and absorption would be expected in the lower GIT. As predicted, cLogP analysis showed that compound **1**, lacking the less lipophilic pyridyl group and having higher MW, was most lipophilic followed by the 7-chloro analogues. There was a correlation between decreasing predicted solubility and increasing cLogP, though the strength of this association diminished when the analysis was extended to experimental solubility data. Additionally, the compounds exhibited a narrow range in LogD at both cytosolic and vacuolar pH, presumably due to the minimal variation in their acid dissociation constants. LogD values at pH 5.0 were markedly lower with even less variation since the vacuolar acidic environment results in substantial ionisation of the aromatic and aliphatic N of these compounds, hence reducing lipophilicity while correspondingly enhancing solubility.

The compounds also showed antiplasmodial activity in the low nanomolar range against CQS and CQR strains of *P. falciparum*, with no discernible cross-resistance with CQ and the chloro-substituted analogues having higher potency across all strains. However, though all

the compounds were more potent than CQ against *Pf*Dd2, only **1, 2** and **7** exhibited indiscriminate activity with clear potency against *Pf*NF54, *Pf*Dd2 and *Pf*7G8 probably consistent with their designation as rCQs. Antiplasmodial activity directly correlated with lipophilicity, meaning that the most lipophilic compounds were likely to diffuse through the intracellular membrane barriers and into the site of action.

Mechanistically, the compounds possessed active inhibition of βH formation, with a mean IC_{50} comparable to AQ. This βH inhibition potential did not, however, correlate with antiplasmodial activity, presumably due to the requirement for vacuolar accumulation for the latter. Predicted VAR was highest in compound **5** and lowest in **2**, and this strongly correlated with antiplasmodial activity against *Pf*7G8 but not *Pf*NF54 or *Pf*Dd2. No association was observed, however, between *in vitro* βHIA and the IC_{50}-scaled equivalent of VAR, highlighting the dominance of lipophilicity in biological activity. Analysis of the cellular haem-pyridine fractionation profiles of the compounds revealed that they all exhibit CQ-like signatures when incubated with synchronised ring stage *P. falciparum* cells. First, this was characterised by impaired cell morphology and DNA-synthesising ability of cultures treated with 3x compound IC_{50}, implying damage to the cells' competence to mature and transition into the next cycle. Secondly, the compounds exhibited a dose-dependent decrease in the fraction of haem present as HZ and this matched a corresponding rise in the 'free' haem fraction. Overlay plots revealed diminishing parasite survival directly correlating with increasing amounts of 'free' haem for each compound, further affirming their activity as inhibitors of HZ formation. However, possible existence of other MoAs for these compounds cannot be discounted.

Predictive analyses of hERG inhibition potential indicated that though the compounds' activities were in the same order of magnitude as CQ - and significantly better than HLF, they still exhibited a notable hERG liability in comparison to DHA. Fitting with a previous

hypothesis, predicited activity against hERG correlated with both lipophilicity and compound MW. Experimental evaluation of the hERG inhibition potential on compound **4**, elected to represent the whole series, illustrated a verapamil-like liability, which would need to be addressed if the compound was to be progressed further. Finally, the compounds also showed a high susceptibility to microsomal metabolism, with < 5% of the parent compound remaining after 30 minutes incubation with mouse liver microsomes. The metabolic modification pattern appeared to be conserved in all the derivatives in the series regardless of the substitution at C7 on the quinoline ring or orientation of the side group, with *N*-dealkylation on the tertiary amine appearing to be the predominant route of metabolism, even though other metabolites were also observed.

In conclusion, the evaluation of the physicochemical, biological and mechanistic properties of the seven pDBQs illustrates room for improvement of their activity and reduction in their hERG and metabolic liabilities, while retaining their inhibitory mechanistic potency against HZ formation. In the next chapter, a similar spectrum of analysis will be extended to the resultant pDBQ metabolites generated in this chapter.

Chapter 4

PYRIDO-DIBEMEQUINE METABOLITES: HAEMOZOIN-INHIBITING DERIVATIVES WITH IMPROVED BIOLOGICAL ACTIVITY AND PHYSICOCHEMICAL PROPERTIES

4.1 Chapter Overview

In this chapter, the biological activities, drug-like properties and mechanistic inhibition of βH and HZ by the pDBQ metabolites are examined. These profiles are compared to, and contrasted with, the parent pDBQ compounds. As introduced in *Chapter 3*, CYP-mediated NADPH-dependent phase 1 microsomal metabolism can either generate active or inactive/less active metabolites. Instructively, the Food and Drug Administration (FDA) guideline on "Safety Testing of Drug Metabolites" defines a 'pharmacologically active metabolite' as one with pharmacological activity at the target receptor, and whose activity may be greater than, equal or less than the parent drug exposure.[208] In malaria chemotherapy, it is not uncommon for these biotransformations to result in more active agents, as evident in literature with examples of antimalarial metabolites with enhanced activity or drug-like features superior to their parents. For instance, dihydroartemisinin (DHA) is the principal metabolite and most active of all artemisinin derivatives and is considered to be responsible for the antimalarial activity of artesunate (AS).[209] The proguanil-related PS-15 is metabolised to its putative metabolite, WR99210 (**Figure 4.1**), whose potency and lack of *in vivo* cross-resistance with CQ, PYR, and cycloguanil has been documented.[210] The activity of primaquine (PMQ) is also thought to depend on the formation of active metabolite(s), as evidenced by the observation that PMQ remains inactive *in vitro*, presumably due to the absence of the active metabolites involved in its MoA.

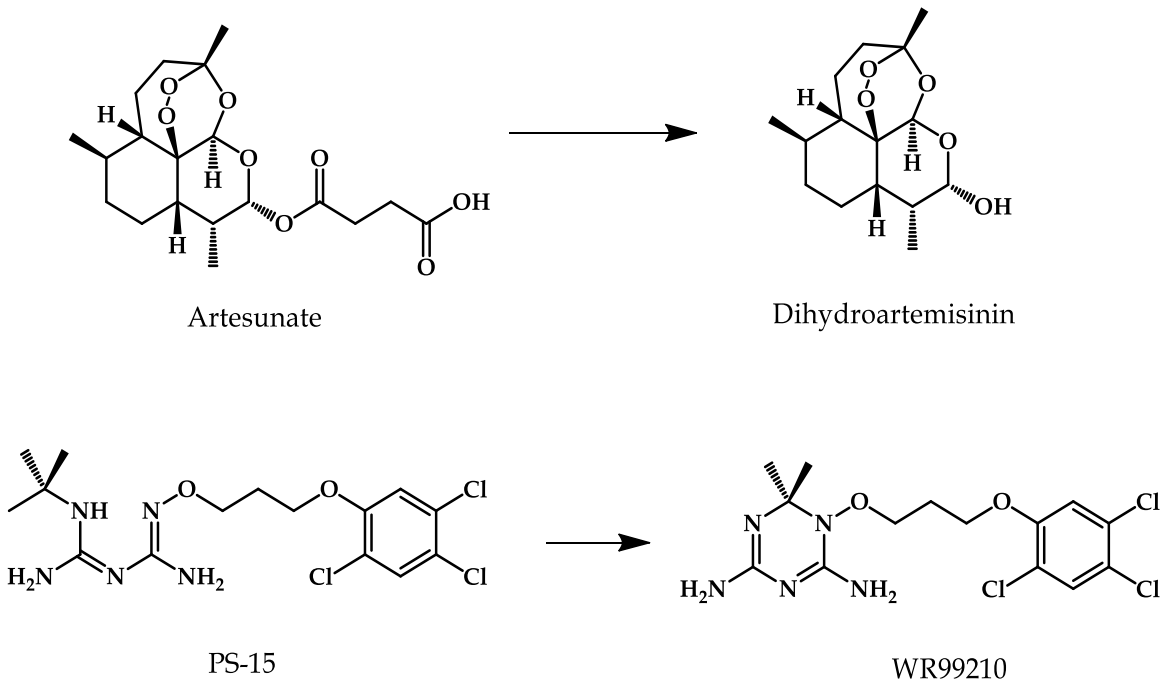

Figure 4.1: Chemical structures of artesunate and PS-15 and their respective active metabolites, dihydroartemisinin and WR99210

The FDA guideline further defines a 'major metabolite' as one that accounts for plasma levels greater than 10% of the administered dose or systemic exposure in humans.[208] Although all the metabolites generated in *Chapter 3* technically fit within the definition of pharmacologically active metabolites, only the products of *N*-dealkylation were consistently observed in all compounds and constituted ~65% of the metabolites in each compound. As such, these were the compounds that were considered the major metabolites, and consequently prioritised for synthesis and analysis in this chapter.

The contention that the aforementioned metabolites are likely to possess enhanced biological activity and favourable drug-like features was informed by two hypotheses. First, phenylequine (PQN), a structural phenyl analogue of ferroquine (FQ), which retains the requisite components for efficacy of a 4-aminoquinoline (i.e. the 7-chloro group and weakly basic amino groups), has been previously reported to be potent against the CQS and CQR

strain of *P. falciparum*.[211] The metabolite scaffold assessed in this chapter bore a striking structural likeness to PQN, with the tertiary nature of the terminal nitrogen in PQN representing the only difference between them in the case of the 7-chloro derivatives (**Figure 4.2**). Secondly, since biotransformation through *N*-dealkylation effectively lowers the molecular weight, and by extension lipophilicity, this would potentially improve aqueous solubility while also potentially minimising the likelihood for inhibition of the hERG channel, decrease plasma protein binding and lower CYP enzyme inhibition.[144]

a) Phenylequine

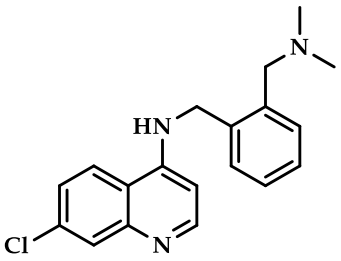

IC_{50} D10 = 13.2 nM

IC_{50} K1 = 6.9 nM

b) Major metabolite scaffolds

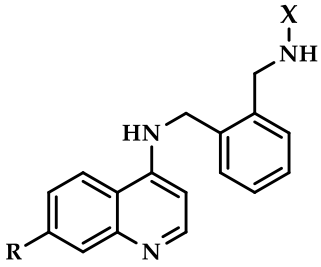

R = Cl, CN

X = H, CH_3

Blackie et al. / Bioorg. Med. Chem. Lett. 2010:20(3):1078-80.[211]

Figure 4.2: Structures of (**a**) phenylequine and (**b**) the major metabolite scaffold evaluated in this *Chapter*.

The seven compounds evaluated in this section of the thesis were synthesised as free bases and are structurally represented in **Figure 4.3**. This chapter details the experimental and computational characterisation of the physicochemical properties and biological activity of these 7 pDBQ metabolites and, as with the parent compounds, assesses the HZ-inhibiting MoA of each. In addition, further biotransformation analyses of the metabolites in both MLMs and HLMs are reported, as is experimental hERG channel inhibition data. All results are subsequently discussed and compared with the parent pDBQs.

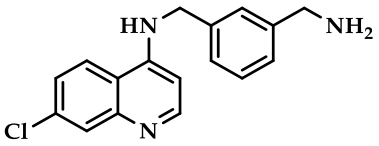

Code: MJmet01
Compound: 8
Mol. Formula: $C_{17}H_{16}ClN_3$
% Purity: 95.9

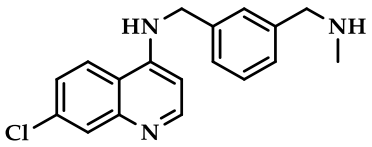

Code: MJmet02
Compound: 9
Mol. Formula: $C_{18}H_{18}ClN_3$
% Purity: 95.1

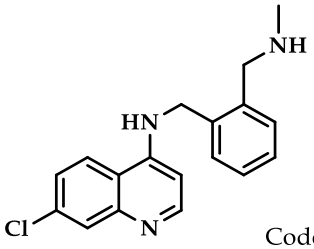

Code: MJmet03
Compound: 10
Mol. Formula: $C_{18}H_{18}ClN_3$
% Purity: 95.3

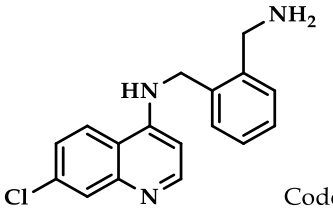

Code: MJmet04
Compound: 11
Mol. Formula: $C_{17}H_{16}ClN_3$
% Purity: 95.2

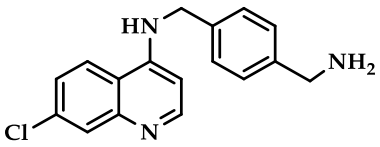

Code: MJmet05
Compound: 12
Mol. Formula: $C_{17}H_{16}ClN_3$
% Purity: 95.4

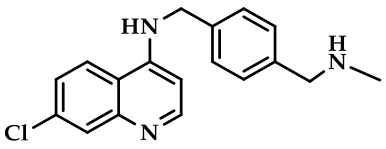

Code: MJmet06
Compound: 13
Mol. Formula: $C_{18}H_{18}ClN_3$
% Purity: 95.9

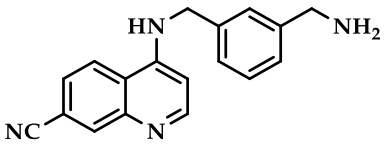

Code: MJmet07
Compound: 14
Mol. Formula: $C_{18}H_{16}N_4$
% Purity: 96.1

Figure 4.3: Chemical structures of the 7 pDBQ metabolites evaluated in this chapter.

4.2. Materials and Methods

All materials and methods used in this chapter are described in detail in *Chapter 2*. The compounds discussed herein were synthesised and characterised by Dr. Malkeet Kumar.

4.3. Results and Discussion

4.3.1. Physicochemical Properties and drug-likeness.

The results of the predicted and experimentally determined physicochemical properties are shown in **Table 4.1**. In general, the metabolites had good solubility that ranged between medium (50 -150 μM) for **8**, **10, 11** and **14** to high (≥ 150 μM) for **9**, **12** and **13**. This kinetic solubility (pH 6.5) profile was comparable to that observed in the parent compounds.

Permeability of the pDBQ metabolites was determined using the PAMPA assay at pH 6.5 and a permeability class assigned as described in **section 2.4.5** in *Chapter 2*. Apart from compound **12,** which had low membrane permeability, the remaining metabolites either had moderate (**8** and **14**) or high permeability (**9**, **10**, **11** and **13**) as shown in **Table 4.1** As with the parent compounds, permeation of these metabolites would therefore be expected in the lower GIT.

Table 4.1: Solubility, membrane permeability and lipophilicity of the pDBQ metabolites

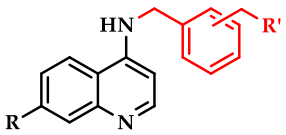

Compound	R	R′	Kinetic Solubility [a] (μM)	Permeability Log P_{app} (SD)	Lipophilicity [b]		
			Observed	pH 6.5	cLogP	$LogD_{7.4}$	$LogD_5$
2 (*meta*-)	Cl	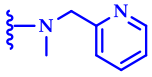	59.8	-4.10 (0.26)	4.46	2.47	0.82
8 (*meta*-)	Cl		122.3	-5.90 (0.02)	3.06	0.84	-0.896
9 (*meta*-)	Cl		200.0	-5.00 (0.12)	3.49	0.95	-0.918
4 (*ortho*-)	Cl	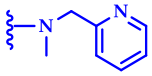	164.7	-4.56 (0.03)	4.46	3.79	0.90
10 (*ortho*-)	Cl		90.0	-5.20 (0.06)	3.49	0.95	-0.918
11 (*ortho*-)	Cl		125.0	-4.30 (0.04)	3.06	0.85	-0.862
3 (*para*-)	Cl	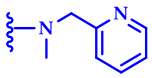	196.6	-4.56 (0.10)	4.46	2.85	0.84
12 (*para*-)	Cl		165.0	-7.00 (0.10)	3.06	0.69	-0.833
13 (*para*-)	Cl		200.0	-4.00 (0.20)	3.49	0.69	-0.991
7 (*meta*-)	CN	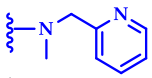	72.4	-3.60 (0.16)	3.71	2.75	0.85
14 (*meta*-)	CN		53.5	-6.50 (0.21)	2.31	0.54	-0.908
Warfarin				-3.80 (0.35)			
Propranolol				-4.40 (0.28)			
Testosterone				-3.70 (0.33)			
Reserpine			<5				
Hydrocortisone			>150			1.50	
Verapamil						2.50	

[a] Kinetic solubility was determined at pH 6.5

[b] cLogP was predicted using MarvinSketch v5.9.4 while LogD was experimentally determined using HPLC analysis (for pH 7.4) and shake-flask method with UV-spectroscopy (for pH 5).

Data on the parent compounds is included for comparison and highlighted in blue font

The high lipophilicity observed for the parent pDBQs in the previous chapter was partly attributable to the presence of the largely nonpolar quinoline core and heterocyclic rings in the side chain. The microsomal cleavage of one of the side chain rings would be anticipated to yield molecules with lower lipophilicity. This was interrogated through prediction of cLogP using MarvinSketch v5.9.4 and experimental determination of LogD at pH 5 and 7.4. cLogP values for the metabolites ranged between 2.31 and 3.49, and were markedly lower compared to the parent pDBQs (range: 3.71 - 5.60). Compound **14** exhibited the lowest cLogP of all the metabolites due to the less lipophilic nitrile substitution at C7 unlike the chloro substituent at the same position. These metabolites thus conform to Lipinski's "rule of five'" with respect to lipophilicity, cLogP of <5. Correlation of cLogP and predicted solubility yielded a strong and significant association of increasing solubility with diminishing cLogP (R^2 = 0.7824; p < 0.0082), and this was consistent with the observed association in the parent pDBQs (R^2 = 0.8085, p = 0.0061). $LogD_{7.4}$ ranged from 0.54 – 0.95 (mean ± SE: 0.79 ± 0.06), with compound **14** again exhibiting the lowest distribution coefficient (**Table 4.1**). $LogD_{5.0}$ values were even lower (mean ± SE: -0.90 ± 0.02) and showed minimal differences. These favourable partitioning and distribution coefficients in the metabolites, which correlate with improved aqueous solubility, represent an improvement over the parent compounds.

4.3.2. Antiplasmodial Activity.

The antiplasmodial effects of the metabolites were then determined against CQS (*Pf*NF54) and CQR (*Pf*Dd2) *P. falciparum* strains and are summarised in **Table 4.2.** Against *Pf*NF54, all the compounds, except **12,** were potent with IC_{50}s below 41 nM. Apart from **12**, each of the metabolites was either comparably or more active than the parent pDBQ against *Pf*NF54,

with the potency of **9**, **10** and **13** within the range of CQ and AS activity. Though this potency was maintained against *Pf*Dd2, the activity of **8**, **12** and **14** diminished and mirrored that of CQ. While it was expected that the parent pDBQs maintained activity against CQR strains due to their RA side chains, the observed activity of the metabolites against *Pf*Dd2 may be speculated to be on the basis of dissimilar interaction with resistance proteins or higher toxicity in their MoA as discussed later. While the drop in activity against *Pf*Dd2 suggests an influence of resistance mechanism against the molecules, the potency of **9**, **10**, **11** and **13**, and the resistance indices suggest that this is not similar in extent to that influencing CQ activity.

There was no association between aqueous solubility and antiplasmodial activity against CQS (R^2 = 0.0153) or CQR (R^2 = 0.0001) parasite strains. However, there was a trend of increased activity against both strains with high compound cLogP, though this was weak and not significant in either strain (CQS: R^2 = 0.0495; p = 0.6316 and CQR: R^2 = 0.1392; p = 0.4097). The same pattern was observed when $LogD_{7.4}$ was substituted into the analysis instead, suggesting that antiplasmodial activity may depend on lipophilicity in these compounds as with the parents and possibly reflects the ability of the most lipophilic compounds to best diffuse through intracellular membranes to the site of action, but the effect is dramatically diminished in the metabolites. It was therefore of interest to investigate the possible MoA of these derivatives.

The selectivity indices of these metabolites ranged from 58.4 to 4,983.6, with compound **12** showing highest likelihood of toxicity in the CHO cells (S. Index = 58.4). Notably, except for **14**, atleast one of each metabolite pair showed an improvement in cytotoxicity index compared to the parent compound, with the greatest improvement observed between compound **8** (S. Index = 4,983.6) and it parent, **2** (S. Index = 275.1).

Table 4.2: Antiplasmodial activity and cytotoxicity profiles of the pDBQ metabolites

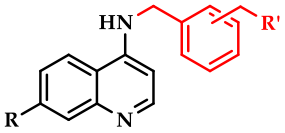

Compound	R	R′	IC_{50} (nM)			Cytotoxicity	
			*Pf*NF54	*Pf*Dd2	R. Index *Pf*Dd2	CHO_{IC50} (µM)	S. Index
2 (*meta*-)	Cl	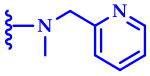	30.1	124.0	4.1	8.3	275.1
8 (*meta*-)	Cl		33.8	255.7	7.6	168.2	4,983.6
9 (*meta*-)	Cl		11.5	78.2	6.8	5.0	432.7
4 (*ortho*-)	Cl	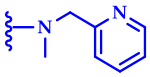	54.4	136.6	3.4	40.2	739.8
10 (*ortho*-)	Cl		9.8	51.2	5.2	10.7	1,093.6
11 (*ortho*-)	Cl		24.7	63.0	2.6	7.4	298.8
3 (*para*-)	Cl	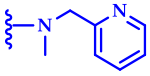	38.5	150.7	3.0	15.7	408.0
12 (*para*-)	Cl		230.8	953.6	4.1	13.5	58.4
13 (*para*-)	Cl		9.2	55.3	6.0	5.7	616.8
7 (*meta*-)	CN	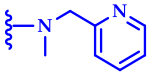	79.1	89.4	1.4	50.6	639.5
14 (*meta*-)	CN		40.7	335.6	8.2	12.5	307
CQ [b]			8.3	226.4	27.3		
Artesunate			5.6	14.3	2.6		
Emetine						0.095	

R. Index = Resistance index = [IC_{50} CQR strain] / [IC_{50} CQS strain]; CHO = Chinese Hamster Ovarian cells; S. Index= Selectivity index = [IC_{50} CHO] / [IC_{50} *Pf*NF54];

[b] Chloroquine diphosphate salt

Data on the parent compounds is included for comparison and highlighted in blue font

4.3.3. Mechanistic Evaluation

Interestingly, though the biotransformation of the parent pDBQs led to various modifications to the compounds (in addition to N-dealkylation), the fundamental pharmacophore responsible for βH/HZ inhibition i.e. chloro/nitrile- substitution at C7 and planar 4-aminoquinoline nucleus was still intact in the resultant metabolites. Moreover, the quinoline rings and the attached benzylamine/benzylmethylamine side groups in the metabolites are still capable of adopting a planar conformation thus leaving the metabolites potentially capable of inhibition of βH and HZ formation.

4.3.3.1. β-Haematin Inhibition and Correlation with Antiplasmodial Activity

All the metabolites retained potency against the formation of βH, with IC_{50} values ranging from 15.0 to 24.2 μM, and comparable to those of AQ and CQ (**Table 4.3**). There was no significant difference between the mean inhibition IC_{50}s of the metabolites and the parent compounds (Mean ± SEM: 19.1 ± 1.6 vs 18.2 ± 1.4; $p = 0.6641$, unpaired t-test), a likely result of the preservation of the quinoline core and its C7 substituents responsible for inhibition of HZ/βH formation.

Table 4.3: βH inhibition (βHI) and antiplasmodial activity of the pDBQ metabolites

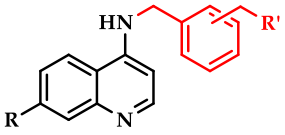

Compound	R	R′	βHIA IC_{50} (SD) μM	*Pf*NF54 IC_{50} μM
2 (*meta*-)	Cl	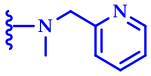	20.8 (0.6)	0.030
8 (*meta*-)	Cl		15.3 (0.2)	0.034
9 (*meta*-)	Cl		15.0 (2.7)	0.012
4 (*ortho*-)	Cl	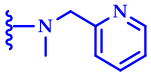	17.9 (3.2)	0.054
10 (*ortho*-)	Cl		21.9 (1.7)	0.010
11 (*ortho*-)	Cl		24.2 (2.9)	0.025
3 (*para*-)	Cl	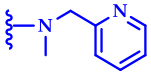	17.2 (0.3)	0.039
12 (*para*-)	Cl		15.1 (0.6)	0.231
13 (*para*-)	Cl		23.8 (4.2)	0.009
7 (*meta*-)	CN	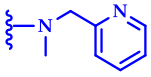	16.7 (0.1)	0.079
14 (*meta*-)	CN		18.6 (1.8)	0.041
Chloroquine			26.0 (3.4)	0.008
Amodiaquine			13.9 (2.3)	
Pyrimethamine			*No inhibition*	0.021

Data on the parent compounds is included for comparison and highlighted in blue font

As observed with the parent compounds, analysis of the association between βH inhibition and antiplasmodial activity against *Pf*NF54 did not yield any significant association (**Figure 4.4**). Again, this could either be due to the cell-free design of the βH inhibition assay that

limits true reflection of the environment involved in whole cell parasite inhibition including factors such as membrane permeation or accumulation or that instead, antiplasmodial activity better correlates with other indicators of MoA. In summary, the metabolites proved as potent as the parent pDBQs against formation of βH albeit this did not correlate with their *in vitro* antiplasmodial activity thus motivating analysis of their accumulation potential as a possible factor in their parasite growth inhibition activity.

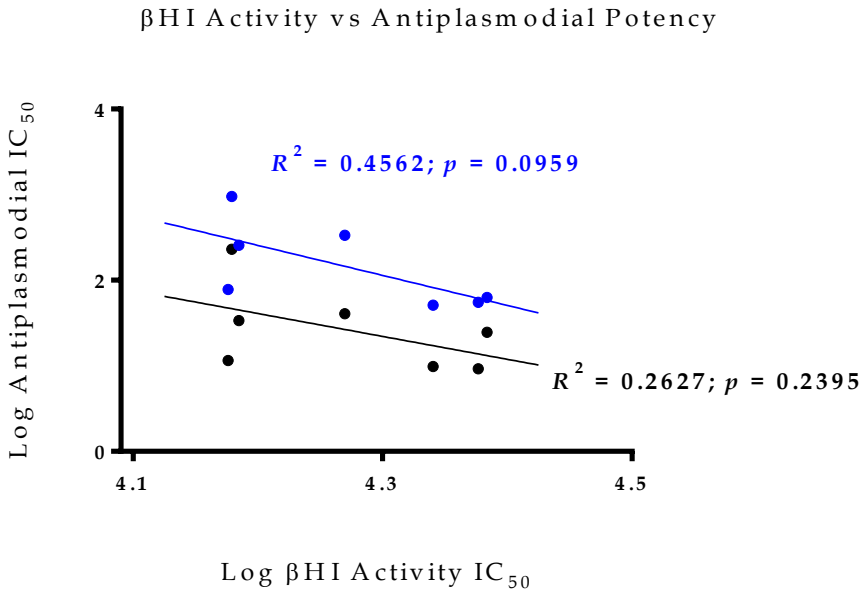

Figure 4.4: Correlation between βHI and antiplasmodial activity for the pDBQ metabolites in CQS (black plot) and CQR parasites (blue plot).

4.3.3.2. Vacuolar Accumulation

The cleavage of the ethylpyridine/ethylbenzene moiety from the chemosensitising side group of the parent pDBQs during metabolism would be expected to disrupt the optimal chemosensitisation SAR of these molecules. While an unsurprising CQ-like diminished activity against *Pf*Dd2 was observed for **8**, **12** and **14,** the remaining metabolites still maintained significant activity against the CQR strain in spite of this structural distortion in

ability to circumvent the parasite resistance machinery. Thus, an investigation predicting whether these derivatives accumulate to higher concentrations was conducted and correlated with antiplasmodial and βHI activity.

As shown in **Table 4.4**, the compounds (unlike the parent pDBQs) had only two protonatable centers and their predicted VAR ranged between 28.1 and 73.8. The metabolites (mean VAR ± SE: 51.9 ± 6.7) seemed to accumulate to a lesser degree than their parent compounds (mean ± SE: 320.1 ± 149.0), with compounds **10** and **11** exhibiting ~10-fold less accumulation potential compared to their parent derivative, **4**. This could be due to the difference in the number of protonatable centres between the metabolites (2 centres) and the parent pDBQs (3 centres) or differences in pKa of equivalent centres. The VAR correlated with antiplasmodial activity against both *Pf*NF54 (R^2 = 0.3084; p = 0.1956) and *Pf*Dd2 (R^2 = 0.4110; p = 0.1207), although none of these associations was significant. Analysis of the VAR-normalised IC_{50}s with βHI activity still yielded weak and non-significant associations in both the CQS (R^2 = 0.2476; p = 0.2558) and CQR (R^2 = 0.4370; p = 0.1059) strains, implying that accumulation – though important in achieving threshold inhibitory concentrations, may not be the driving determinant of the potent activity of these metabolites. The lack of correlation between the normalised accumulation ratios and βH inhibition suggests that the mechanism of drug accumulation is complex, even in the CQS *Pf*NF54 strain, and cannot be captured by the simple pH trapping hypothesis. These results further suggest that the antiplasmodial activity of these HZ inhibitors is not necessarily reduced by the loss of the basic pyridine moieties from their parent structures.

Table 4.4: The vacuolar accumulation, βHI and antiplasmodial activity of the 7 pDBQ metabolites

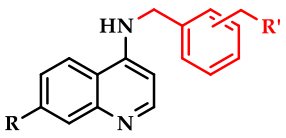

Compound	R	R′	VAR [a]	βHIA IC_{50} (μM)	*Pf*NF54 (nM)	VAR x NF54 IC_{50} (μM)
2 (*meta-*)	Cl	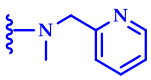	44.7	20.8 ± 0.6	30.1 ± 5.0	1.36
8 (*meta-*)	Cl		54.5	15.3 ± 0.2	33.8 ± 0.1	5.74
9 (*meta-*)	Cl		73.8	15.0 ± 2.7	11.5 ± 1.5	0.51
4 (*ortho-*)	Cl	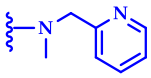	776.2	17.9 ± 3.2	54.4 ± 5.5	42.23
10 (*ortho-*)	Cl		73.8	21.9 ± 1.7	9.8 ± 1.1	1.00
11 (*ortho-*)	Cl		51.5	24.2 ± 2.9	24.7 ± 5.9	19.17
3 (*para-*)	Cl	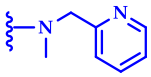	102.3	17.2 ± 0.3	38.5 ± 4.8	3.94
12 (*para-*)	Cl		33.3	15.1 ± 0.6	230.8 ± 24.0	230.15
13 (*para-*)	Cl		48.0	23.8 ± 4.2	9.2 ± 4.0	0.65
7 (*meta-*)	CN	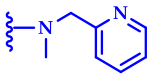	79.4	16.7 ± 0.1	79.1 ± 4.9	6.28
14 (*meta-*)	CN		28.1	18.6 ± 1.8	40.7 ± 1.6	3.23

[a] VAR values were calculated using the equation VAR = Antilog($LogD_{7.4}$ – $LogD_{5.0}$)

Data on the parent compounds is included for comparison and highlighted in blue font

It has previously been hypothesised that the ability of quinoline analogues to accumulate to high inhibitory concentrations in the DV can be attributed to their ability to avoid recognition by the CQ resistance mechanism altogether or directly block *Pf*CRT-mediated extrusion thus enabling toxic levels of the drug to accumulate in both CQS and CQR strains.[212] In the latter scenario, the drug may exert a second antiplasmodial effect in CQR

parasites as a consequence of inhibiting the normal function of the transporter. Employing kinetic analyses to investigate the interaction of *Pf*CRT with CQ, QN, QND and verapamil, Bellanca and colleagues showed that different drugs are likely to interact with distinct sites within a poly-specific substrate recognition cavity of *Pf*CRT^{Dd2}, resulting in different levels of affinity and transport efficiency.[213] This suggests that even with modest modification to the structure, there may be scope for minimisation or complete elimination of a drug's interaction with *Pf*CRT^{Dd2}, thus allowing the drug to escape the resistance mechanism altogether. It is not unreasonable to speculate that the biotransformation of the parent pDBQs inadvertently introduce subtle structural modifications to afford metabolites with dissimilar interactions with *Pf*CRT^{Dd2} to the parent compounds. This, however, can only be directly tested with investigations of the interactions of the parent pDBQs and the metabolites with *Pf*CRT, for example, in a *Xenopus laevis* oocyte expression system.[214]

The VAR-normalised IC_{50}s ranged from 0.52 to 3.41, consistent with the parent compounds. However, this parameter only yielded negative associations when correlated with βHI activity in both CQS (R^2 = 0.2701; p = 0.2318) and CQR (R^2 = 0.4898; p = 0.0800) strains, implying that accumulation – though important in achieving threshold inhibitory concentrations, may not be the driving determinant of the potent activity of these metabolites especially against *Pf*Dd2. The lack of correlation between the calculated or normalised accumulation ratios and βH inhibition suggested that the mechanism of drug accumulation is far complex, even in the CQS *Pf*NF54 strain, than can be captured by the simple pH trapping model. These results further showed that antiplasmodial activity of HZ inhibitors is not necessarily reduced by cleaving off of basic moieties from the parent structures.

4.3.3.3. Morphological Effect of Treating Synchronised Cultures

Since the cycle stage at which compounds interfere with plasmodial growth can give an insight into their MoA, the morphological effect of treating cells with a high concentration of the metabolites was investigated through FACs analysis with the aim of ascertaining if these derivatives impair growth of plasmodial cells in the same manner and stage as their parents. FACs histogram data presented in **Figure 4.5** reveal that all the compounds caused similar shifts in cell size, complexity and nucleic acid content when cells where treated with 3x compound IC_{50}. The SSC shifts showed that treated cells were less complex and dense for all the compounds compared to the control (**Figure 4.5a**) while the FSC shifts revealed that they were comparatively smaller (**Figure 4.5b**). There were slight shifts in SYBR Green I fluorescent intensities indicating that treated cells had less nucleic acid content than untreated cells (**Figure 4.5c**). These observations suggest that, in a manner not unlike the profiles of CQ and the pDBQ parent compounds, the metabolite-treated cells had stunted growth and matured to a lesser degree than the untreated cells.

a) Forward scatter

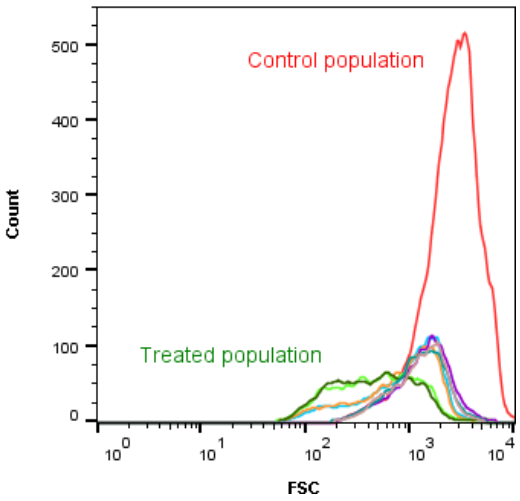

b) Side scatter

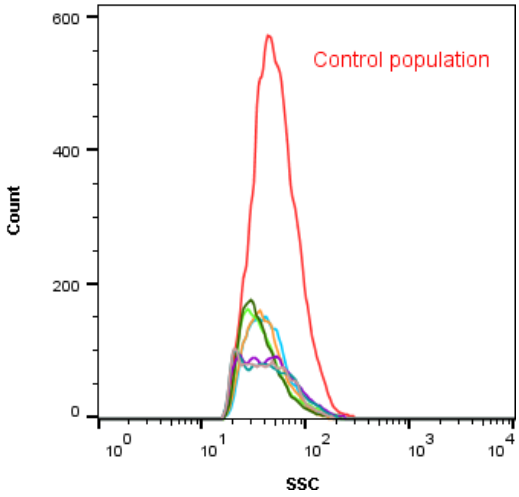

c) SYBR Green

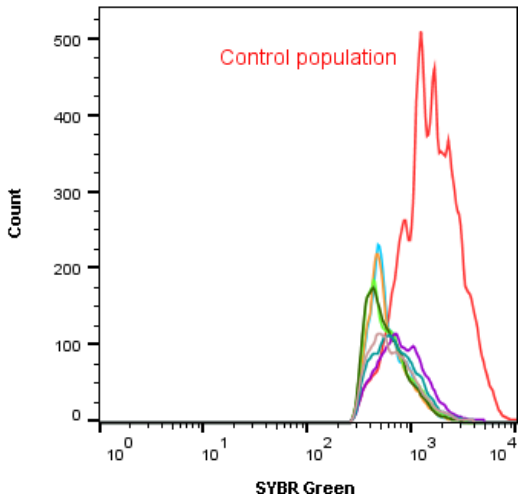

Figure 4.5: FACs histograms showing changes in cell size (a), complexity (b) and nucleic acid content (c) of *Pf*NF54 trophozoite population after treatment of synchronised rings with 3x IC_{50}s of each metabolite overlaid against untreated controls. The red plot represents the untreated control cells while the treated population are represented by the cyan plot (compound **8**), yellow (compound **9**), green (compound **10**), orange (compound **11**), blue (compound **12**), purple (compound **13**) and fluorescent green (compound **14**)

4.3.3.4. Haem-Pyridine Fractionation Profiles

As follow up on the βH inhibition results to ascertain if these metabolites are genuine inhibitors of HZ formation in the cells, a haem-pyridine fractionation assay was conducted. The haem profiles show a dose-dependent increase in 'free' haem, which was significant from 0.5x IC_{50} (in compound **8**) to 3x IC_{50} (all compounds), compared to the control (**Figure 4.6**). As with CQ and the parent pDBQs, these increases in 'free' haem levels corresponded to significant decreases in HZ in all the metabolites. In compound **11,** this decrease was,

however, only significant from between 2.5 and 3x compound IC_{50} even though declining trends in HZ levels were observed. The parasite survival curves for all the compounds overlaid with the 'free' haem Fe showed corresponding increases in 'free' haem Fe with a drop in parasite survival. While not discounting the possible existence of other MoAs, these results together with *in vitro* βH inhibition data suggest that these pDBQ metabolites are true inhibitors of HZ formation.

Compound 8 **a)**

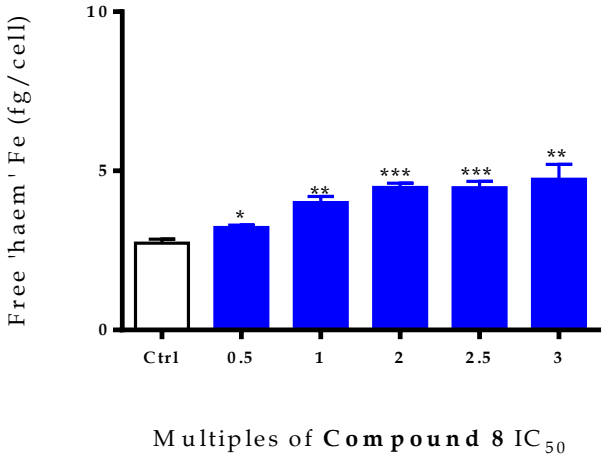

b)

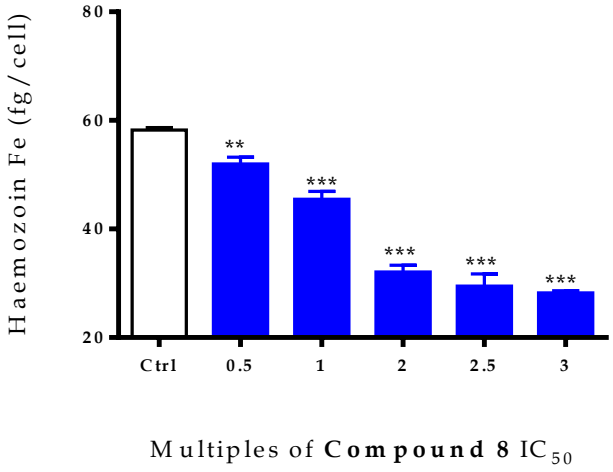

c)

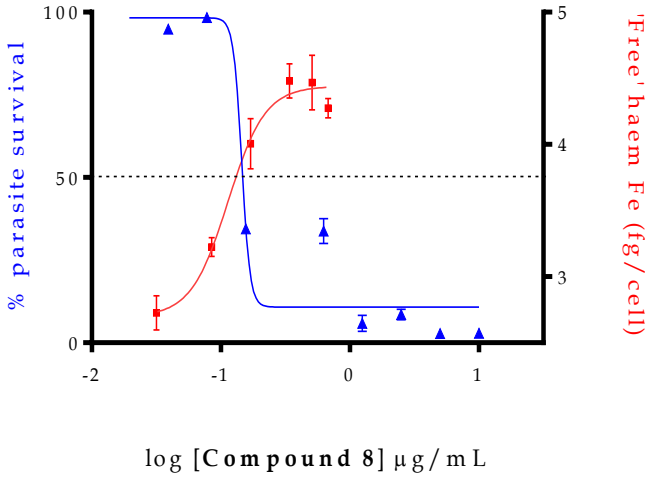

Compound 9 **d)**

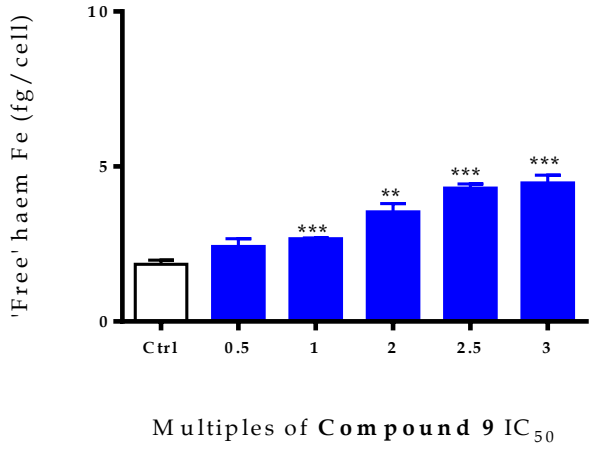

e)

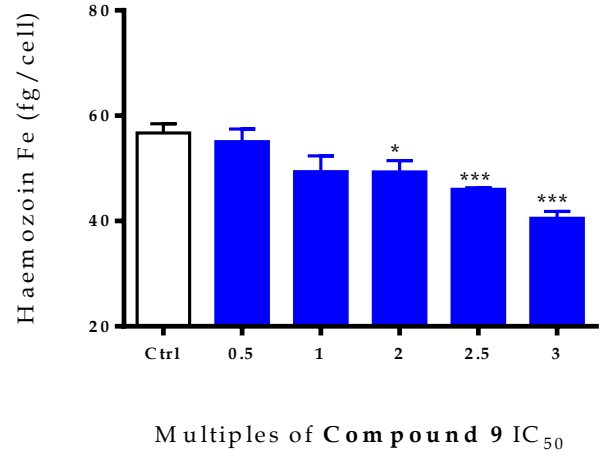

f)

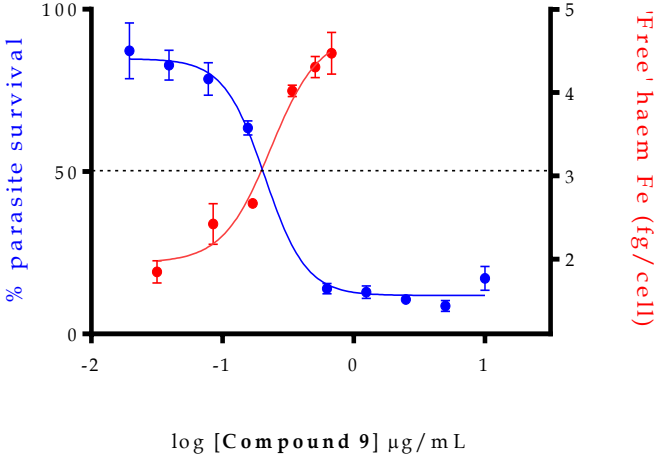

Compound 10 **g)**

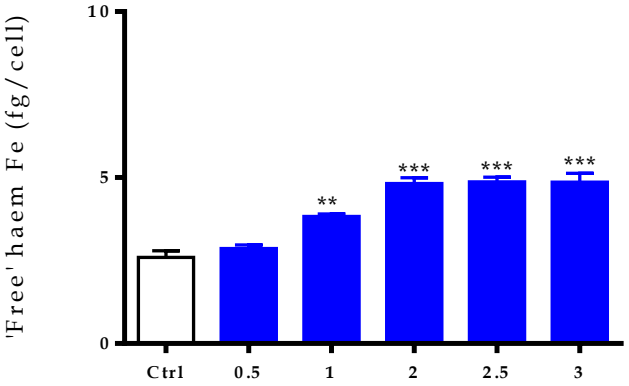

Multiples of **Compound 10** IC_{50}

h)

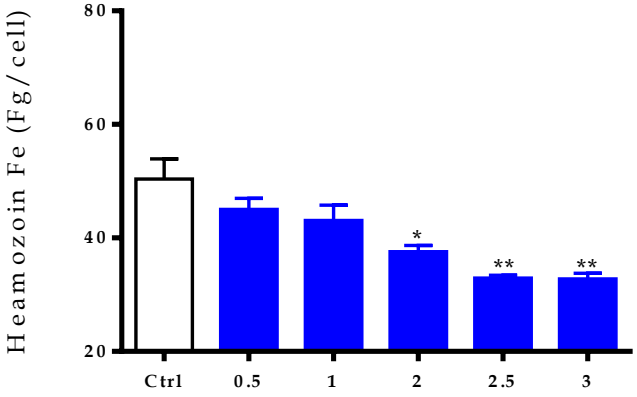

Multiples of **Compound 10** IC_{50}

i)

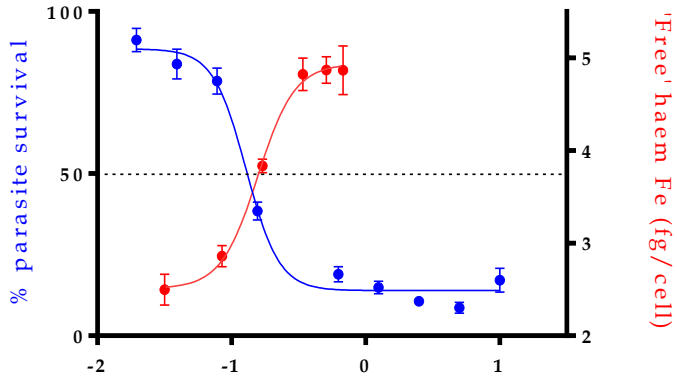

log [**Compound 10**] µg/mL

Compound 11 **j)**

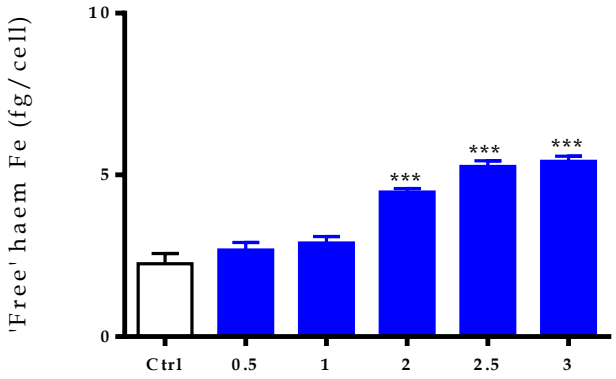

Multiples of **Compound 11** IC_{50}

k)

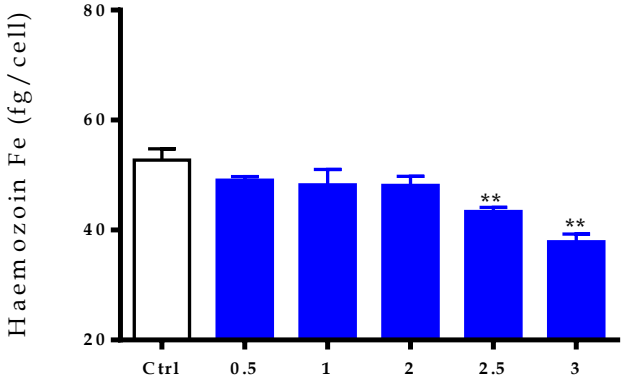

Multiples of **Compound 11** IC_{50}

l)

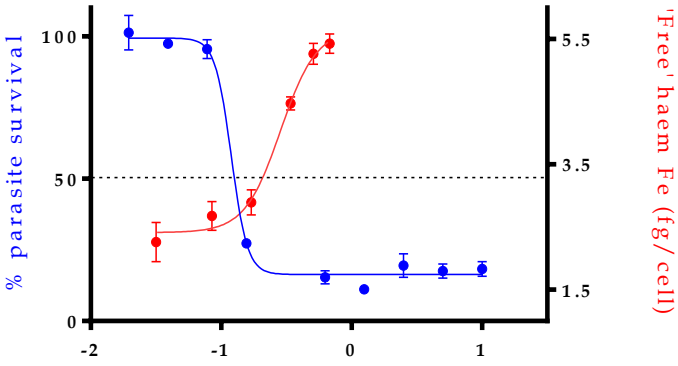

log [**Compound 11**] µg/mL

Compound 12 **m)**

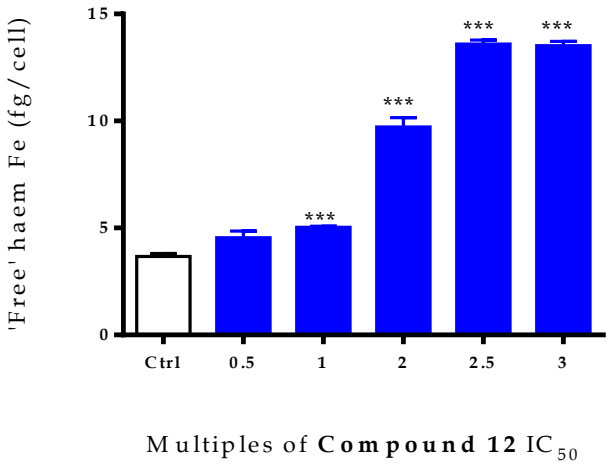

n)

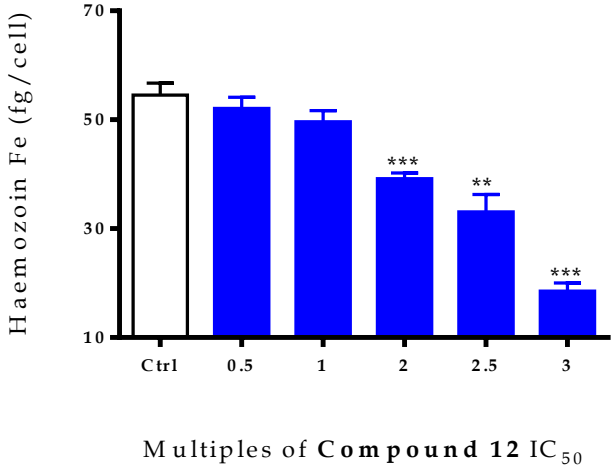

o)

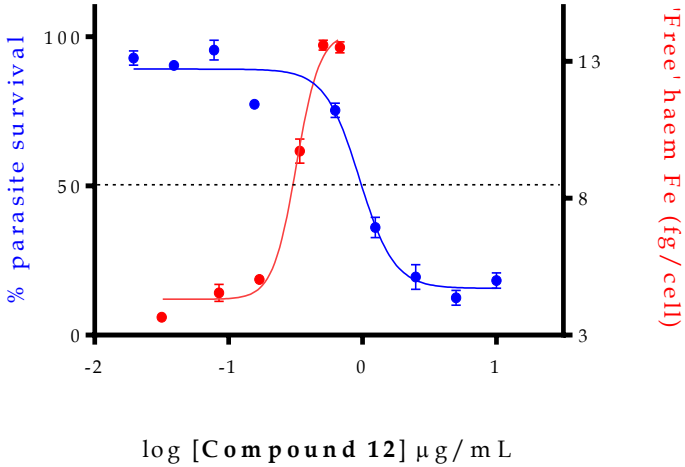

Compound 13 **p)**

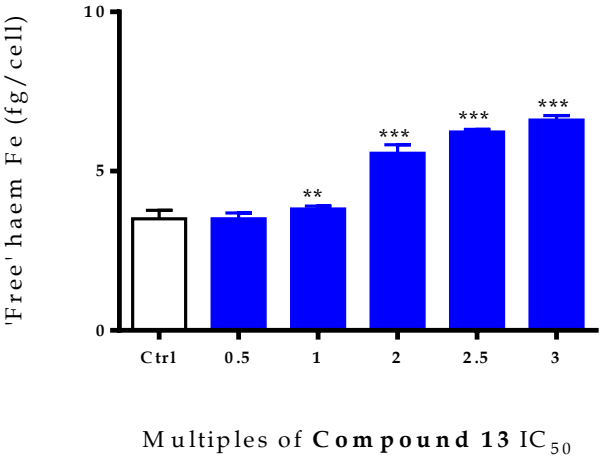

q)

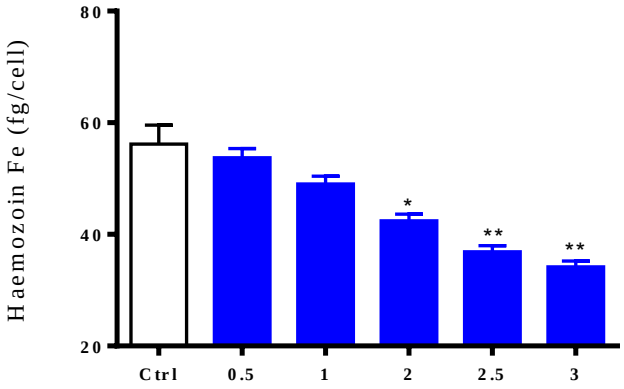

r)

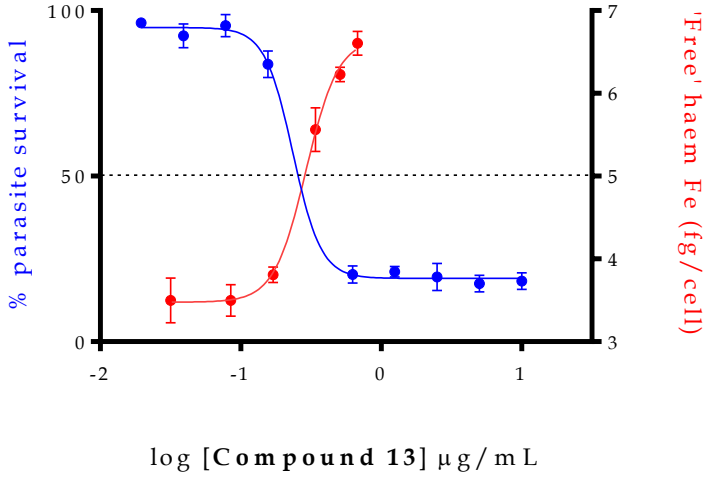

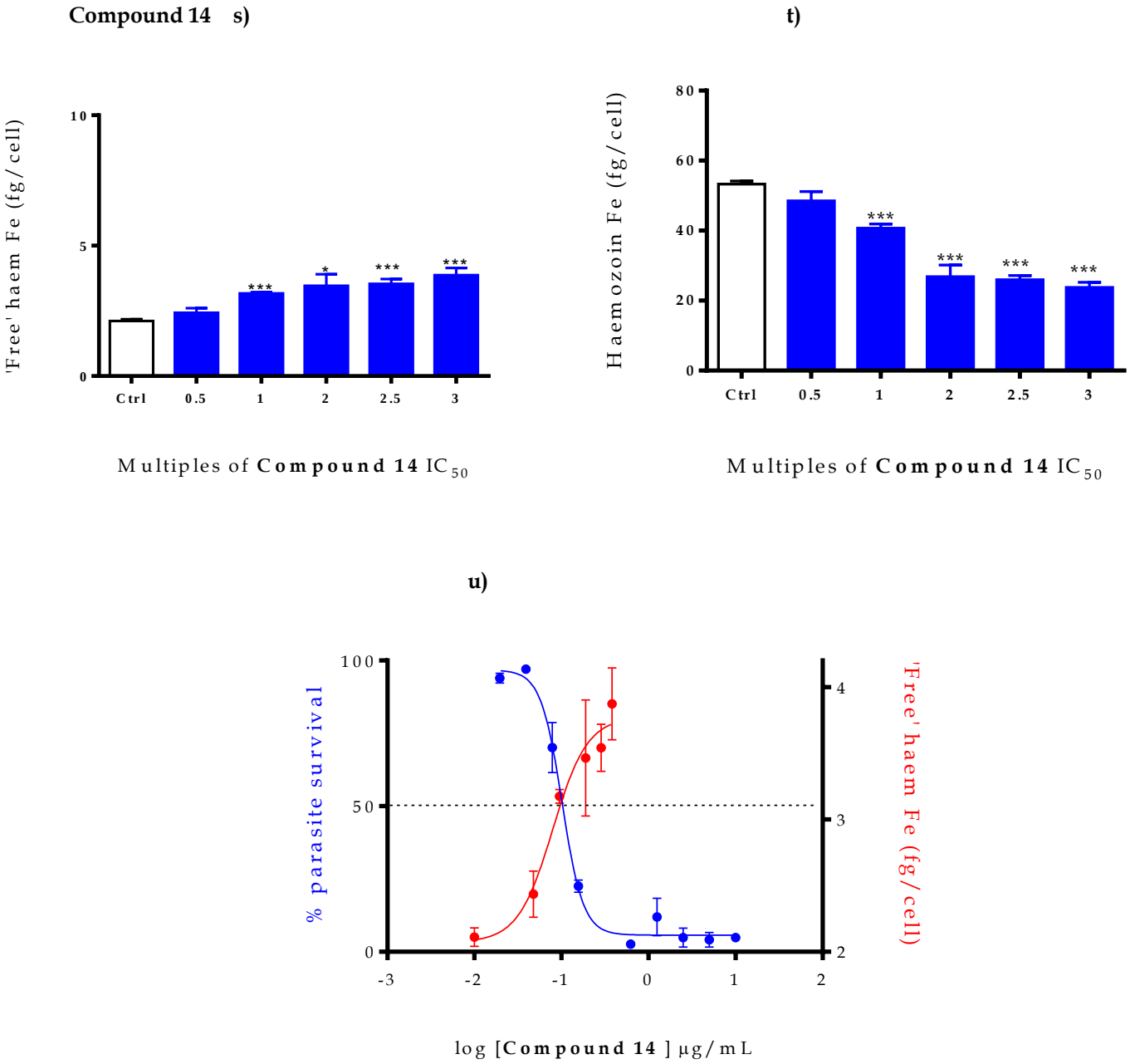

Figure 4.6: Haem fractionation profiles of compounds **8-14** in synchronised drug-treated and control *Pf*NF54 parasites. Plots **a, d, g, j, m, p** and **s**), show levels of toxic 'free' haem represented in terms of iron(Fe) measured in fg/cell while plots **b, e, h, k, n, q** and **t**) show haemozoin levels. The asterisks indicate statistical significance relative to control (*$p < 0.05$; ** $p < 0.01$ and *** $p < 0.001$). Plots **c, f, i, l, o, r** and **u**) represent parasite survival (blue) overlaid against 'free' haem Fe (red) plots and clearly show unambiguous trends of increasing levels of 'free' haem corresponding with parasite death in all the compounds.

4.3.3.5. Effect of 'Free' Haem Levels

In an attempt to further explain the enhanced activity of these metabolites against the CQS strain relative to their parents, a comparative analysis of the 'free' haem levels produced in the parasites at different drug concentrations was performed. In this analysis, the mean 'free' haem Fe (fg/cell) present at each drug concentration was obtained for the metabolites and parent pDBQs, analysed using an unpaired t-test for possible differences and plotted in **Figure 4.7**. Though compounds belonging to the quinoline scaffold customarily require only a small increase in "free" haem to induce parasite death, the metabolites seemed to require comparatively lower levels of 'free' haem than the parent pDBQs to induce killing, though they both encompassed the quinoline scaffold. In fact, omission of **12** as an outlier (mean 'free' haem range: 4.54 – 13.60 fg/cell and IC_{50}: 230.8 nM) yields significant differences in all but the 2x IC_{50} dose, thus highlighting that the effectiveness of these metabolites over their parents could be due to formation of a more toxic and soluble 'drug-haem' complexes.

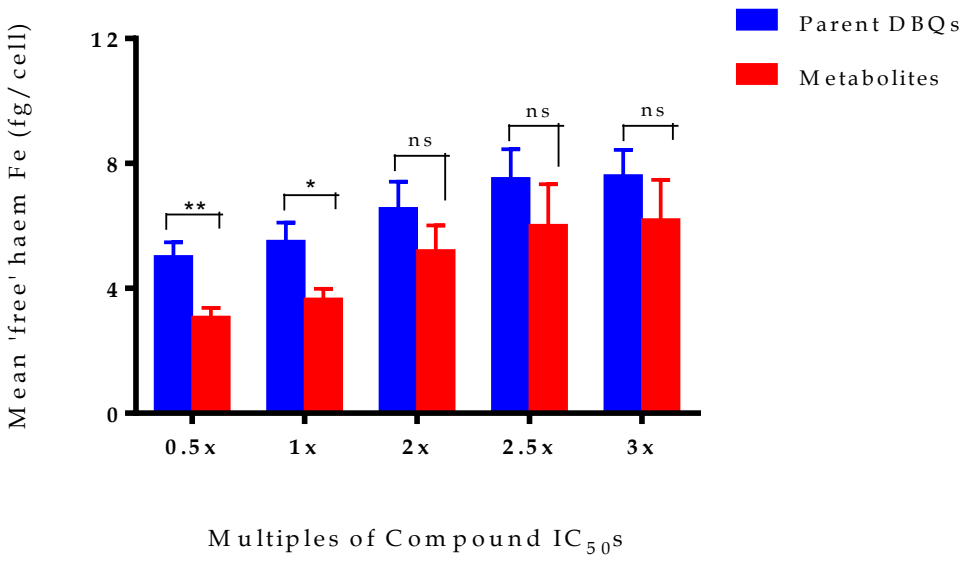

Figure 4.7: Comparative mean levels of 'free' haem Fe measured in fg/cell in synchronised parasites treated with varying doses of metabolites and parent pDBQs. Asterisks denote statistical significance relative to parent drug (*$p < 0.05$; **$p < 0.01$ and ns = not significant).

4.3.4. Metabolic Stability in Mouse and Human Liver Microsomes

As further assessment of the biological activity of the metabolites in light of their drug-like potential and owing to the extensive and rapid metabolism of the parent pDBQs, it was imperative to test the metabolic stability of the metabolites. In addition to investigations of stability in MLM, the metabolites were also assessed in human liver microsomes (HLM). All compounds exhibited a high metabolic stability in both MLM and HLM with >75% remaining after 30 min of incubation with the liver microsomes (**Table 4.5**).

The observed high microsomal metabolic stability was a significant improvement from the poor metabolic stability observed in the parent compounds described in the previous chapter. Compound **9** however, showed an anomalous result in MLM, with only 19% of the compound remaining after 30 min of incubation. While this still represented a substantial improvement from compounds **1** and **2** (its parents), it was unclear why this was inconsistent with the MLM incubation results for the other metabolites. Nonetheless, the good microsomal stability of these metabolites suggested that further efforts on metabolite identification were not necessary.

Table 4.5: Metabolic stability of the metabolites in mouse and human liver microsomes

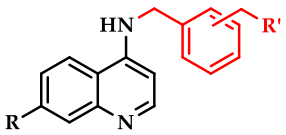

Compound	R	R′	Species	% remaining (after 30 min)	Projected Half Life (min)	Intrinsic Clearance CL (mL/min/kg)[a]	Hepatic Extraction Ratio
2 (*meta-*)	Cl	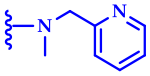	Mouse	3.57	5.9	1139	0.93
8 (*meta-*)	Cl	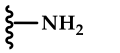	Mouse	99.9	>150		
			Human	91.3	>100		
9 (*meta-*)	Cl		Mouse	19.0	12.5	545	0.86
			Human	86.2	>100	14	<0.42
4 (*ortho-*)	Cl	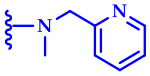	Mouse	2.32	5.5	1224	0.93
10 (*ortho-*)	Cl	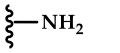	Mouse	97.0	>100	10	<0.33
			Human	98.9	>100	1	<0.42
11 (*ortho-*)	Cl		Mouse	98.5	>100	5	<0.33
			Human	95.0	>100	4	<0.42
3 (*para-*)	Cl	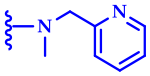	Mouse	2.08	5.4	1250	0.93
12 (*para-*)	Cl	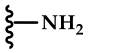	Mouse	91.5	>100	60	0.40
			Human	98.9	>100	1	<0.42
13 (*para-*)	Cl		Mouse	90.4	>100	33	<0.33
			Human	94.6	>100	15	<0.42
7 (*meta-*)	CN	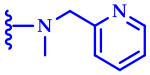	Mouse	1.91	4.7	1349	0.94
14 (*meta-*)	CN	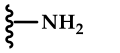	Mouse	99.0	>150		
			Human	87.9	>100		
Midazolam			Mouse	1.33	4.74	1425	0.94
			Human				
MMV390048			Mouse	93.55	172.25	42	0.32
			Human				

Data on the parent compounds is included for comparison and highlighted in blue font

[a] Data not corrected for protein binding

4.3.5. Inhibition of the hERG Channel

Metabolites likely to be in circulation, and structurally related to the parent drugs require investigation for activity against any off-target receptor to which the parent drugs possess activity.[215] Since it is likely that the high *in vitro* activity, good aqueous solubility and microsomal metabolic stability of these compounds could translate to good *in vivo* efficacy from high systemic exposure, these metabolites may cause effects on off-target receptors/enzymes by virtue of their inadvertently high concentration. Coupled with a nominal affinity by weak bases, this risk is particularly heightened for the hERG channel. *In silico* and experimental hERG inhibition studies were therefore extended to these metabolites.

4.3.5.1. In silico Analysis of hERG Channel Inhibition

The metabolites had pIC_{50}s ranging between 4.98 (compound **14**) and 5.70 (compound **13**). This predicted inhibition range was more favourable than CQ and the standard high inhibition controls, halofantrine (HLF) and desbutyl-halofantrine (dbHLF). In fact, the inhibition potential of **14** was not significantly different from DHA, and mirrored their comparable molecular weight and partitioning coefficients (**Table 4.6**). Crucially, each metabolite was predicted to possess a reduced risk for hERG channel inhibition compared to its corresponding parent compound and, collectively, the mean pIC_{50} for the metabolites was significantly lower than that of the parent pDBQs (mean ± SE: 5.29 ± 0.11 vs 6.33 ± 0.05; $p < 0.0001$, unpaired t-test).

Table 4.6: Predicted hERG inhibition IC_{50}s versus molecular weights and predicted lipophilicity of the metabolites compared to the parent pDBQs and 4 reference antimalarials

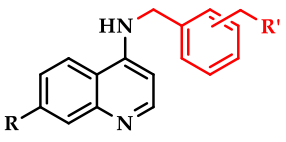

Compound	R	R′	pIC_{50} [a]	Mol. Weight	cLogP [b]	Log $D_{7.4}$ [b]
2 (*meta-*)	Cl	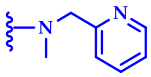	6.23	402.9	4.51	4.01
8 (***meta-***)	Cl		5.02	297.8	3.06	0.80
9 (***meta-***)	Cl		5.53	311.8	3.49	1.06
4 (*ortho-*)	Cl	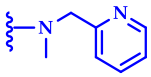	6.28	402.9	4.51	4.00
10 (***ortho-***)	Cl		5.55	311.8	3.49	1.07
11 (***ortho-***)	Cl		5.04	297.8	3.06	0.84
3 (*para-*)	Cl	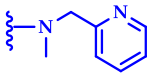	6.43	402.9	4.51	4.00
12 (***para-***)	Cl		5.19	297.8	3.06	0.78
13 (***para-***)	Cl	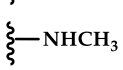	5.70	311.8	3.49	1.05
7 (*meta-*)	CN	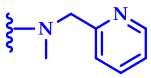	6.22	395.5	3.80	3.48
14 (***meta-***)	CN		4.98	288.4	2.31	0.27
Chloroquine			6.00	319.9	3.81	0.88
Dihydroartemisinin			4.27	284.4	2.84	2.84
Halofantrine			7.37	500.4	8.06	5.46
***N*-desbutylhalofantrine**			6.52	444.3	6.35	3.90

[a] pIC_{50} values were determined using StarDrop™

[b] cLogP and $LogD_{7.4}$ were predicted using MarvinSketch v5.9.4

Data on the parent compounds is included for comparison and highlighted in blue font

Because the interaction of drugs with membrane phospholipids is driven, in part, by lipophilicity as well as electrostatic interactions with both acidic and basic moieties on phosphate head groups,[216, 217] correlation analysis between cLogP/LogD and pIC_{50}s, similar to those performed on the parent compounds were extended to these metabolites. There was a direct and significant correlation between predicted hERG channel inhibition and these lipophilicity indices, with the association stronger in cLogP than LogD (**Figure 4.8a**). Indeed, apart from flexibility (number of rotatable bonds) and topological surface area, lipophilicity has been successfully used in predicting hERG blockage in some models.[218] A similar observation was made for compound molecular weight (**Figure 4.8b**), and confirms findings of a recent study that positively correlated the most potent hERG inhibitors to increased cLogP, rotatable bonds and molecular weight on approximately 300 000 compounds contained in Molecular Library Small Molecular Repository library.[219] These predictive analyses thus demonstrate that hERG liability tends to be more pronounced in compounds that are more hydrophobic with high molecular weight, features more observed in the parent compounds than metabolites. Again, care must be taken, given that these factors are probably used in the prediction software.

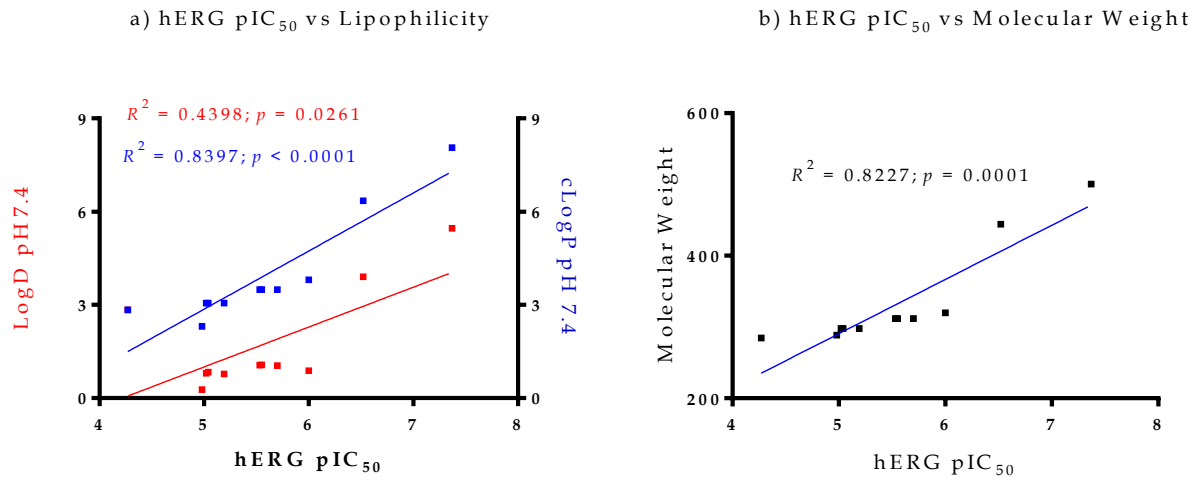

Figure 4.8: Linear regression analysis plots of the correlation between predicted hERG pIC_{50}s and $LogD_{7.4}$ (red) and cLogP (blue) in **a**) as well as molecular weights (black) in **b**)

4.3.4.2. Experimentally-determined hERG Channel Inhibition

In addition to compound **4** described in *Chapter 3*, the experimental inhibition potentials of two of its metabolites, **10** and **11**, were also determined using similar assay conditions thus allowing for direct comparison of the toxicity of the metabolites in relation to the parent compound. As with **4**, there was a concentration-dependent blockade of hERG by compounds **10** and **11**. This is in agreement with a previous clinical study where a high dose regimen of HLF (72 mg kg^{-1}) was reported to induce dose-dependent QT prolongation in all 61 patients treated,[220] and *in vitro* findings of a concentration-dependent block of hERG channels by HLF and dbHLF.[198, 199] There was no significant difference in the levels of channel inhibition between the two metabolites in all the four tested concentrations, perhaps suggestive of the fact that there were no radical differences in the lipophilicities and MW.

At 0.3 µM, the metabolites were 3-fold less toxic compared to the control (%Mean Inhibition ± SD: 10.4 ± 0.65 vs 33.9 ± 4.15), and this difference was significant ($p < 0.0001$, unpaired t-test). In fact, a similar fold difference between the metabolites and verapamil was still observed at 1.0 µM test concentration (%Mean Inhibition ± SD: 22.4 ± 0.74 vs 64.9 ± 3.21). At 3.0 µM, there was a significant 2-fold toxicity difference between the metabolites and their parent, **4** (%Mean Inhibition ± SD: 43.6 ± 0.64 vs 87.6 ± 2.70; $p < 0.0001$, unpaired t-test). Though the metabolites still maintained comparatively lower hERG channel inhibition at the highest test concentrations (10.0 µM), this was not significantly different from the toxicity observed from compound **4** or verapamil (**Figure 4.9**).

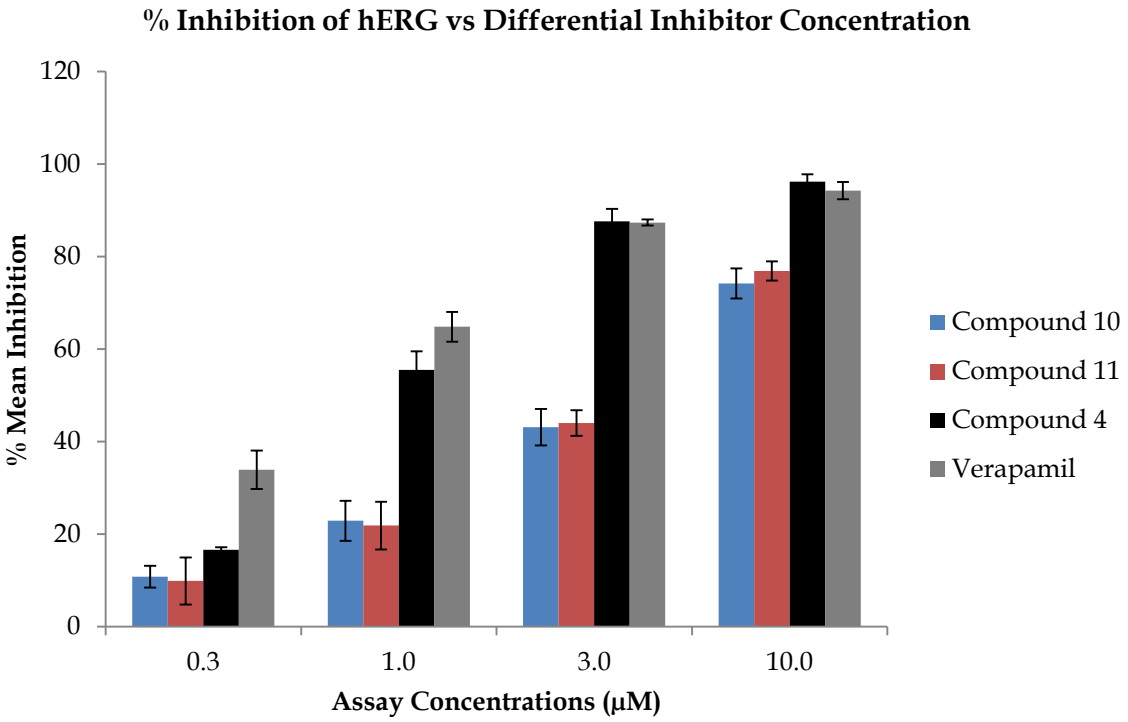

Figure 4.9: Percent mean inhibition of hERG protein expressed in CHO cells at varying concentrations of the metabolites (**10** and **11**), their parent compound (**4**) and verapamil.

Similar to the analysis conducted on **4** in the previous chapter, these proportional inhibitions were further quantified by measuring the IC_{50} values of at least three separate cells (n >3)

and presented as mean inhibition IC_{50}s (± SD mean) in **Table 4.7**. Again, the metabolites were approximately 5-fold less toxic (Mean IC_{50} ± SD: 3.56 ± 0.16) compared to their parent (Mean IC_{50} ± SD: 0.87 ± 0.08) or verapamil (Mean IC_{50} ± SD: 0.56 ± 0.08), and the pIC_{50} equivalents of these discreet experimental IC_{50}s were in agreement with the predicted values.

Table 4.7: Experimental and predicted hERG inhibition for compounds **10** and **11** compared to **4** and verapamil

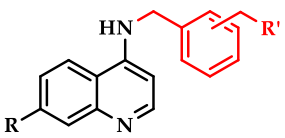

Compound	R	R′	Experimental Inhibition		Predicted Inhibition
			IC_{50} ± SD (μM)	pIC_{50}	pIC_{50}
10 (*ortho*-)	Cl		3.67 ± 0.70	5.44	5.55
11 (*ortho*-)	Cl		3.45 ± 0.50	5.46	5.04
4 (*ortho*-)	Cl	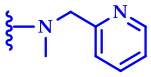	0.87 ± 0.08	6.06	6.28
Verapamil			0.56 ± 0.08	6.25	6.16

[a] Experimental IC_{50} were determined from inhibition of hERG protein expressed in CHO and corresponding pIC_{50} obtained as negative logarithm of these IC_{50} values converted to milimolar units.

[b] Predicted pIC_{50}s were determined using StarDrop™

Data on the parent compounds is included for comparison and highlighted in blue font

Obviously, this diminished risk of potential cardiotoxicity by the metabolites is of clinical significance, and would make even better sense if interpreted in a pharmacokinetic context.

Curiously, in HLF, it has been shown that QT interval significantly correlates with high plasma levels of the parent drug, but not its major metabolite, dbHLF.[221] In fact, in an earlier report of serious HLF cardiotoxicity, plasma concentration was measured at syncope or time of death and approximated to be 1.6 μM in the two study patients.[220] Tellingly, therapeutic plasma HLF concentration in patients receiving HLF treatment is 1.67 - 2.98 μM,[222, 223] thus highlighting the possibility of drug-induced cardiotoxicity occurring at therapeutic concentrations of the drug. Owing to their *in vitro* potency, good solubility and metabolic stability in liver microsomes, these metabolites, unlike their parent compounds, could potentially achieve therapeutic levels at lower plasma concentrations that do not border the hERG inhibition range. However, it is important to urge caution especially when extrapolating to *in vivo* settings. First, these *in vitro* analyses do not comprehensively account for the proportion of drug bound to serum proteins versus the free fraction likely to elicit therapeutic or toxic effects. Secondly, it is indeed conceivable that the potency of blockade of the native human hERG channel by these metabolites (and the parent pDBQ) may be different from that observed against the hERG protein expressed in heterologous cell lines. Nonetheless, these data encouragingly show a favourable cardiotoxicity profile for the metabolites relative to the parent pDBQ, hence confirming their drug-likeness and potential for further development. The molecular basis of this lowered risk of potential cardiotoxicity by the metabolites compared to the parent compounds is beyond the scope of this thesis. Nevertheless, it is noteworthy that the number of compounds evaluated is limited and precludes meaningful delineation of structure-property relationships.

4.4. Summary and Conclusion

In this chapter, seven metabolites arising from *N*-dealkylation of the parent pDBQ compounds were investigated for their biological activity and drug-like physicochemical properties as well as their mechanistic potential to inhibit formation of βH and HZ. In *chapter 3*, the parent compounds were shown to possess moderate to high permeability, moderate to high aqueous solubility at pH 6.5 and high lipophilicity. The metabolites maintained similar solubility and permeability profiles, though with significantly reduced lipophilicity. The metabolites also exhibited improved biological activity and cytotoxicity profiles. The compounds were active against both CQS and CQR strains in the nanomolar range, though activity against CQR parasites seemed to diminish in compounds **12** and **14** compared to the parent drugs (**Figure 4.10**). This antiplasmodial activity, as with the parents, was shown to be a function of lipophilicity and possibly reflected the ability of the most lipophilic compound to best diffuse through the multiple intracellular membranes to the site of action.

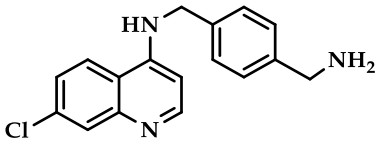

12

*Pf*Dd2 IC_{50} = 953.6 nM

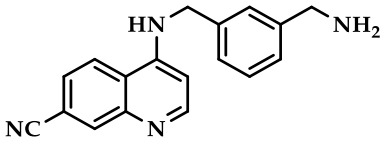

14

*Pf*Dd2 IC_{50} = 335.6 nM

Figure 4.10: Chemical structures of compound **12** and **14** and their activity against *Pf*Dd2

Though a mechanistic investigation of this activity noted potent inhibition of βH formation in these compounds, there was no correlation between this phenomenon and antiplasmodial activity or predicted vacuolar accumulation of the metabolites in the parasite DV. It is possible therefore that upon high accumulation within the DV, these metabolites interact with *Pf*CRT^{PfDd2} in a manner dissimilar to their parents or CQ, resulting in different levels of

affinity and transport efficiency. This suggests that modest structural modifications could result in minimising drug interaction with *Pf*CRT^{PfDd2}, allowing for evasion of the resistance machinery. Cellular haem-pyridine fractionation analyses further showed profiles of dose-dependent increases in 'free' haem significantly corresponding to decreases in HZ levels in the metabolites. The mean levels of 'free' haem Fe were significantly lower in these metabolites than the parents, suggesting that their potency could be due to the formation of more soluble and toxic drug-heam complexes than the parent pDBQs. These haem Fe levels overlaid on parasite growth showed an inverse trend, which confirmed these metabolites as genuine inhibitors of HZ formation in the parasite, though possible existence of auxiliary MoAs cannot be conclusively ruled out.

Microsomal metabolic stability analyses showed that all the metabolites were highly stable in both MLM and HLM with >75% remaining after 30 min of incubation, a significant improvement from the high microsomal metabolic lability of the parents described in the previous *Chapter*. Compound **9** however, registered an anomalous result in MLM, with only 19% of the compound remaining after 30 min of incubation. Predictive and experimental analyses of hERG inhibition potential highlighted a significant improvement in the cardiotoxicity risk profiles of compounds **10** and **11** (**Figure 4.11**). These compounds were on average 5-fold less toxic (Mean IC_{50}: 3.56 ± 0.16) compared to their parent (Mean IC_{50}: 0.87 ± 0.08) or verapamil (Mean IC_{50}: 0.56 ± 0.08), a reduction in toxicity likely attributable directly to reduction in lipophilicity and compound mass, and possible disruption of the binding between the aromatic residue of the channel and aromatic substituents on the drugs

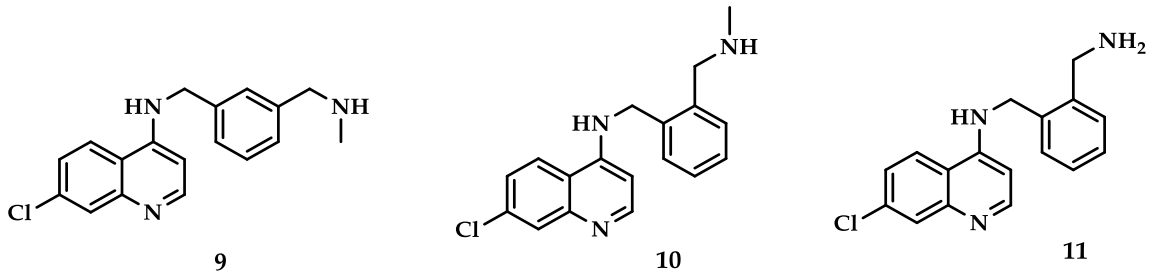

Figure 4.11: Chemical structures of compounds **9**, **10** and **11**

In conclusion, the data collected on the physicochemical, biological and mechanistic properties of these seven pDBQ metabolites highlight favourable drug-like features comprising good aqueous solubility, permeability and a lowered lipophilicity. Further analyses on the interaction between these compounds and *Pf*CRT *in situ* as well as insight on the nature of the complex they form with 'free' haem would be instructive. The improved microsomal metabolic stability, cardiotoxicity profiles and other drug-like features of the compounds make them superior to their parent molecules.

Chapter 5

PYRIDO[1, 2-*a*]BENZIMIDAZOLE: A PLANAR NON-QUINOLINE β-HAEMATIN INHIBITING ANTIMALARIAL CHEMOTYPE

5.1 Chapter Overview

Though inhibition of haem detoxification has been extensively explored against *P. falciparum* through classical aminoquinolines and other scaffolds known to interact with 'free' haem molecules, the detoxification machinery is also present in *Schistosoma mansoni* and other hematophagous organisms as described in *Chapter 1*. As noted in *Chapters 3* and *4*, the quinoline-based pDBQs and their metabolites are endowed with a SAR profile that allows for inhibition of βH/HZ formation and they are able to structurally adopt a planar conformation crucial for haem-drug complex formation. This chapter explores the physicochemical features, biological activities and mechanistic profiles of ten (10) novel pyrido[1,2-*a*]benzimidazole (PBI) derivatives in *P. falciparum* and *S. mansoni*. The PBIs were hypothesised to potentially inhibit HZ formation in both organisms owing to their structural likeness to CQ, which includes a planar heterocyclic moiety, a halo-substituent and a basic amine side group, which would make them candidates for *π-π* interactions - another hallmark feature of haem-drug complex formation.

PBIs, previously investigated for antibacterial, antifungal, antiviral and antitumor activities,[169] were recently shown to be a novel antimalarial chemotype.[170] In this study by Ndakala *et al.*, the lead compound, **15** (**Figure 5.1**), showed high *in vitro* antiplasmodial activity (IC_{50} *Pf*NF54: 0.11 µM and IC_{50} *Pf*K1: 0.12 µM) and promising *in vivo* oral efficacy (95% reduction in parasitemia at 4 x 50 mg/kg p.o) in the rodent *P. berghei* model. However, pharmacokinetic (PK) studies indicated saturation in oral absorption at low doses, presumably due to poor solubility, which limited oral efficacy.

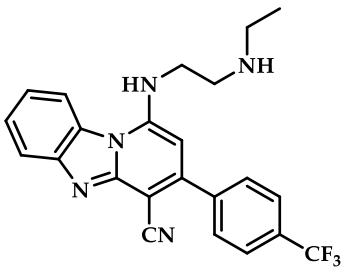

15

*Pf*NF54 = 0.11 μM

*Pf*K1 = 0.12 μM

in vivo *P. berghei* (HCl salt: p.o) 4×25 mg/kg = 95.7%

0/3 malaria infected mice cured

Figure 5.1: Original lead compound, **15**, with activity against the CQS (*Pf*NF54) and CQ/multidrug-resistant (*Pf*K1) *P. falciparum* strains.

Ten derivatives were therefore selected for SAR investigations around the basic structure of compound **15** (**Figure 5.2**) and synthesised to explore the biological and physicochemical effects of modifications around parts of the scaffold not previously investigated. SAR_1 comprised replacement of the alkylamino side chain in **15** with various moieties containing water-solubilising H-bonding groups, encompassing imidazole (**16**), hydroxypyrrolidine (**17**) or piperidinyl (**18**). SAR_2 involved introduction of small hydrophobic substituents at C2, which were envisaged to result in distortion of molecular planarity thus lowering the crystal packing energies, and consequently potentially improving aqueous solubility.[171] In this regard, to afford **19**, fluorine was preferred since, due to its small size, it is less likely to interfere with protein-drug interactions but more likely to increase the dihedral angle without loss of biological activity.[171] SAR_3 comprised two derivatives bearing replacement of the 4-trifluoromethylphenyl (4-CF_3Ph) at C3 with *meta*- (**20**) or di-substituted (**21**) phenyl rings. Finally, SAR_4 involved introduction of substituents on the previously unexplored left

hand side (LHS) aromatic ring, including mono- (**22**) and di-chloro substituents (**23** and **24**) at C7, C8 and C9.

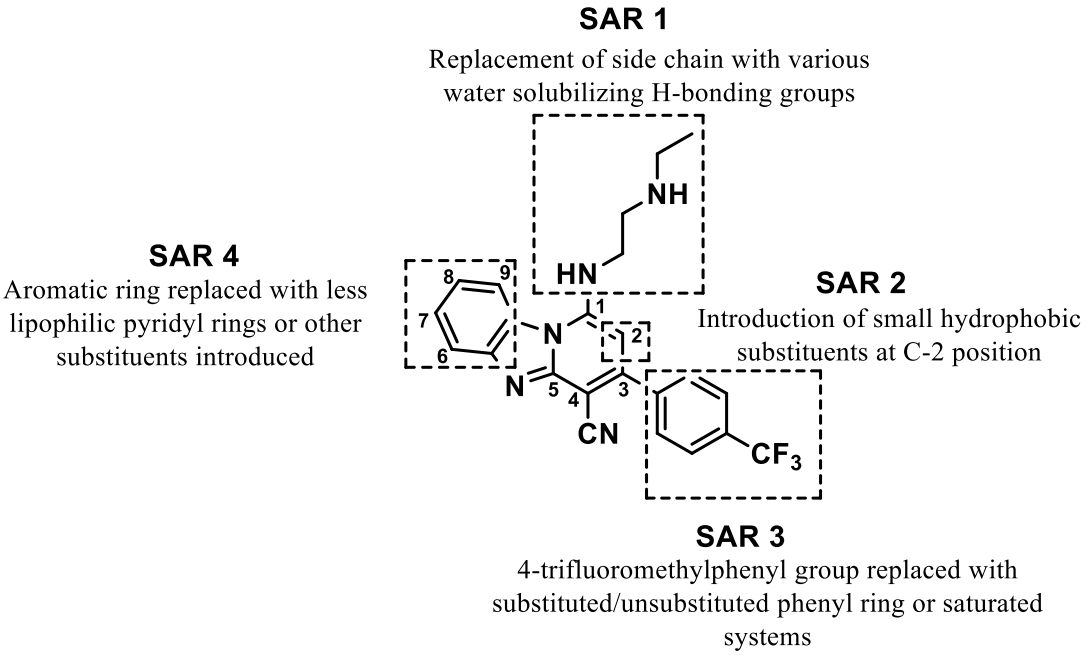

Figure 5.2: Chemical structure of the prototype PBI molecule showing the different SAR exploration that afforded the various compounds analysed in this chapter

All derivatives, shown in **Figure 5.3**, were first evaluated for aqueous solubility and membrane permeability at pH 6.5 and lipophilicity at pH 7.4. This was followed by assessment of their cytotoxicity in CHO cells, *in vitro* antiplasmodial activity against both CQS and CQR strains and *in vivo* efficacy in *P. berghei*-infected mice for 3 derivatives. Inhibition of βH/HZ as their potential MoA, the killing kinetics, hERG channel inhibition potential and the metabolic stability of these PBIs in MLMs and HLMs were also explored. Additionally, the *in vitro* and *in vivo* antischistosomal activity of these compounds is also described in this chapter. All results are subsequently discussed and a conclusion on the chapter presented.

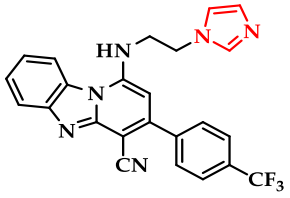

Code: KP27
Compound: 16
Mol. Formula: $C_{24}H_{17}F_3N_6$
% Purity: 97

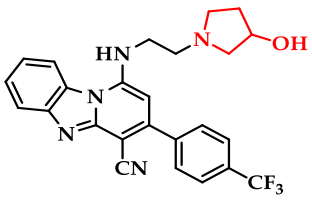

Code: KP64
Compound: 17
Mol. Formula: $C_{25}H_{22}F_3N_5O$
% Purity: 99

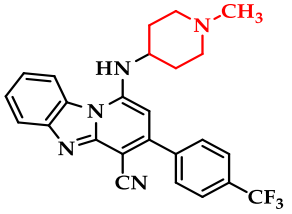

Code: FJC4
Compound: 18
Mol. Formula: $C_{25}H_{22}F_3N_5$
% Purity: 99

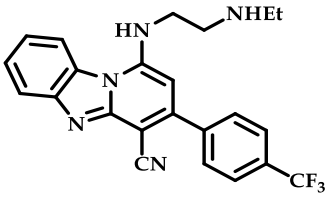

Code: KP4
Compound: 15
Mol. Formula: $C_{23}H_{20}F_3N_5$
% Purity: 99

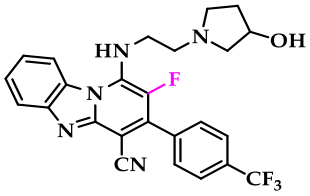

Code: LB34
Compound: 19
Mol. Formula: $C_{25}H_{21}F_4N_5O$
% Purity: 98

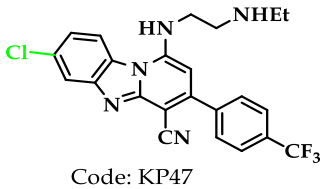

Code: KP47
Compound: 22
Mol. Formula: $C_{23}H_{19}ClF_3N_5$
% Purity: 98

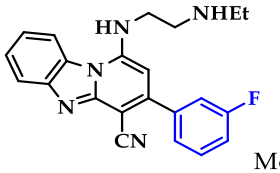

Code: CWP02
Compound: 20
Mol. Formula: $C_{22}H_{20}FN_5$
% Purity: 99

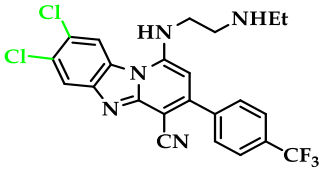

Code: KP63
Compound: 23
Mol. Formula: $C_{23}H_{18}Cl_2F_3N_5$
% Purity: 98

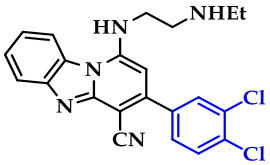

Code: KP75
Compound: 21
Mol. Formula: $C_{22}H_{19}Cl_2N_5$
% Purity: 99

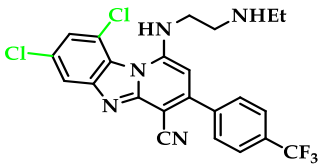

Code: KP68
Compound: 24
Mol. Formula: $C_{23}H_{18}Cl_2F_3N_5$
% Purity: 99

Figure 5.3: Chemical structures of the 10 PBIs obtained from SAR_1 (red), SAR_2 (pink), SAR_3 (blue) and SAR_4 (green) modifications

5.2 Materials and Methods

All materials and methods used throughout this chapter are listed and exhaustively described in *Chapter 2*. The compounds discussed herein were synthesised and characterised by Dr. Kawaljit Singh, Mr. Ferdinand Ndubi, Ms. Linley Barnard and Mr. Chad Wilkinson, and have been reported elsewhere in published literature.[224, 225]

5.3 Results and Discussion

5.3.1 Solubility, membrane permeability, lipophilicity and metabolic stability

Though the lead compound (**15**) in the Ndakala *et al.* study showed good antiplasmodial activity and promising oral efficacy, pharmacokinetics (PK) hinted at saturation in oral absorption at low doses, presumably due to poor dissolution. This necessitated further optimisation of the lead PBI to identify derivatives with better PK profiles - hypothetically achievable through improving aqueous solubility and/or permeability while maintaining metabolic stability. Results of the evaluation of the physicochemical properties of these derivatives are presented in **Table 5.1**. Generally, none of the SAR_1 modifications led to any improvement in aqueous solubility as all the compounds exhibited low solubility (<5 μM). However, relative to **15**, solubility improved for all the other analogues. For instance, fluoro-substitution at C2 (compound **19**) resulted in significant improvement in solubility (80 μM). This was unsurprising since introduction of the fluoro substituent at this position was anticipated to distort the planarity of the compound and thus lower the energy barrier to dissolution in aqueous media. Replacement of the 4-CF_3Ph group at C3 with a fluoro-substituted phenyl ring (**20**) also led to moderate improvement in solubility (25 μM), while only subtle improvements were observed in the chloro- analogues of SAR_4 (**21;** 10 μM, **23;** 10 μM and **24;** 20 μM).

Table 5.1: Solubility, membrane permeability and lipophilicity of the PBI compounds

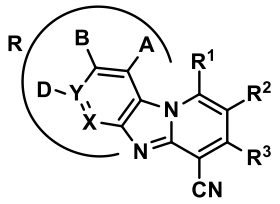

Compound	R	R^1	R^2	R^3	Kinetic Solubility (μM) [a]	$LogD_{7.4}$ [b]		Permeability Log P_{app}, (SD) [c]
						Experimental	Predicted	pH6.5
15		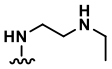	**H**	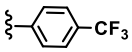	<5	2.61	1.80	-4.3, (0.28)
16		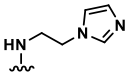	**H**	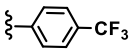	<5	3.62	3.95	-4.9, (0.19)
17		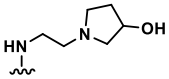	**H**	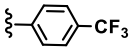	<5	3.33	2.03	-3.8, (0.25)
18		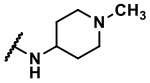	**H**	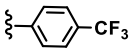	<5	2.60	2.76	-5.0, (0.22)
19		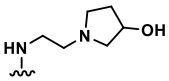	**F**	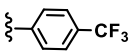	80	3.17	2.70	-3.8, (0.27)
20		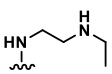	**H**		25	1.89	1.07	-4.0, (0.18)
21		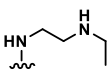	**H**	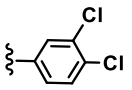	20	2.74	2.13	-4.6, (0.10)
22	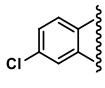	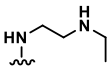	**H**	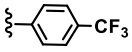	10	3.29	2.41	-6.5, (0.12)
23	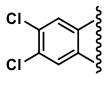	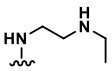	**H**	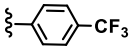	10	3.55	3.01	-4.9, (0.18)
24	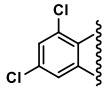	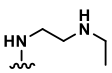	**H**	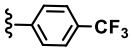	20	3.56	3.01	-5.3, (0.26)
Reserpine					<5			
Hydrocortisone					>150	1.50	1.28	
Verapamil						2.50	2.79	
Warfarin								-3.8, (0.35)
Propranolol								-4.4, (0.28)

[a] Kinetic solubility was determined at pH 6.5.

[b] Experimental LogD was determined using HPLC analysis at pH 7.4 while the predicted values were obtained from MarvinSketch™ version5.9.4.

[c] Low permeability; log P_{app} <-6.5; moderate; log P_{app} -6.5 to -5.5; high; log P_{app} >-5.5

Membrane permeability generally ranged from moderate to high at pH 6.5 for all the derivatives and the different substituents did not have any significant influence on this parameter. Considering only passive diffusion, this range of permeability suggests that permeation through the lower GIT is unlikely to be a limiting factor in the oral absorption of these compounds. Experimental $LogD_{7.4}$ ranged from 1.89 to 3.62, and was observed to be relatively higher (mean ± SE: 3.03 ± 0.18) compared to the quinoline scaffold described in *Chapter 3* and *4*. The experimental values correlated well with predicted data (R^2 = 0.6348; p = 0.0058). Since all the SAR_1 derivatives gave poor solubility signals below 5 µM, correlation analysis with $LogD_{7.4}$ were restricted to SAR_2 – SAR_4 compounds, and these yielded no association (R^2 = 0.0039; p = 0.9063).

From the hepatic extraction ratios, which are normalised for blood flow and incubation time, there was no significant interspecies difference in microsomal stability in the compounds **Table 5.2**. All compounds tested in HLMs (**15**, **18**, **20**, **21**, **22**, **23** and **24**) were stable while only 5 retained stability (> 75% remaining) after 30 min incubation in MLMs. Fluoro-substitution at C2 (**19**) was detrimental to metabolic stability in MLMs (37%) compared to its unsubstituted counterpart **15**. Dichloro- substitution on the phenyl ring **(21)** in SAR_3 was not favorable in either MLMs or HLMs, while fluoro-substitution at the *para* position on the phenyl ring yielded a derivative (**20**) stable in both microsomal species. Halo-substitution on the LHS of molecules (SAR_4) proved efficient in improving microsomal metabolic stability as all the analogues in this category were stable in MLMs and HLMs (**Table 5.2**).

Table 5.2: Metabolic stability of the PBI derivatives in mouse and human liver microsomes

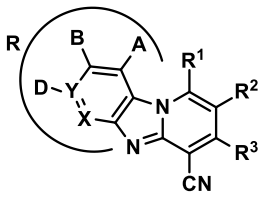

Compound	R	R¹	R²	R³	Species	Single Point Metabolic Stability (30 min)		
						% Remaining	Half Life (min)	Extraction Ratio
15		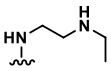	**H**	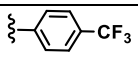	Mouse	97	>100	<0.17
					Human	84	>100	0.48
16		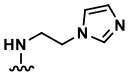	**H**	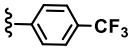	Mouse	60	40	0.68
17		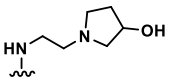	**H**	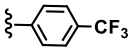	Mouse	51	31	0.73
18		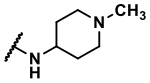	**H**	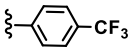	Mouse	63	60	0.58
					Human	75	71	0.60
19		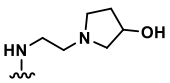	**F**	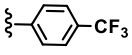	Mouse	37	28	0.75
20		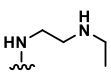	**H**		Mouse	100	>100	<0.17
					Human	89	>100	0.37
21		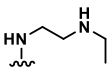	**H**	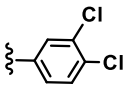	Mouse	65	51	0.62
					Human	60	40	0.73
22	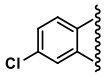	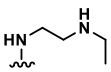	**H**	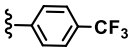	Mouse	75	73	0.54
					Human	87	>100	0.42
23	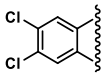	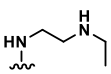	**H**	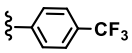	Mouse	81	>100	0.39
					Human	95	>100	0.20
24	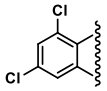	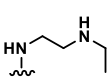	**H**	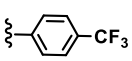	Mouse	87	>100	0.34
					Human	87	>100	0.41
Midazolam					Mouse	1.3	4.7	0.94
					Human	0.1		
MMV390048					Mouse	94	172.3	0.32
					Human	93	>100	0.22

5.3.2 Antiplasmodial activity and cytotoxicity

Though subsequent SAR analyses around the compounds identified by Ndakala *et al.* were primarily aimed at improving physicochemical properties that would boost oral bioavailability, it was essential to maintain, or possibly enhance the antiplasmodial activity and selectivity of the subsequent analogues. The derivatives were therefore evaluated for *in vitro* activity against the CQS strains, *Pf*NF54 and CQR strains, *Pf*Dd2 and *Pf*K1 as well as against CHO cells for cytotoxicity. Against *Pf*NF54, all the compounds exhibited IC_{50} values less than 1μM, with compound **24** being most active (IC_{50}; 20 nM) and **18** least (IC_{50}; 440 nM). Against the CQR strains, IC_{50}s ranged between 20 and 1,020 nM.

With regard to SAR_1, **17**, bearing a 3-hydroxypyrrolidinyl replacement of the N-ethyl group of the aminoalkyl side chain was the most potent against in this series (IC_{50}: 40 nM) with a 3-fold improvement in activity compared to **15** (IC_{50}; 120 nM). This compound still retained potent activity against both CQR strains (*Pf*Dd2 IC_{50}; 40 nM and *Pf*K1 IC_{50}; 90 nM). Compounds **15** and **16** - bearing a terminal imidazole moiety also showed submicromolar potency against the two resistant strains (**Table 5.3a**). Since the aqueous solubility in this set of compounds was not encouraging, it is likely that their activity is due to their high lipophilicity (mean ± SE: cLogP; 3.91 ± 0.18) and permeability (mean ± SE: -4.5 ± 0.28).

Table 5.3a: *In vitro* antiplasmodial activity and cytotoxicity results of SAR_1 analogues

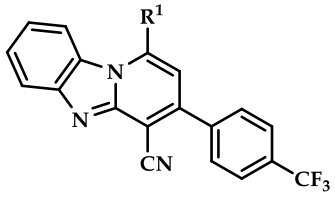

Compound	R^1	Antiplasmodial Activity IC_{50} (nM)			R.I Dd2	R.I K1	Cytotoxicity (CHO)	
		NF54	Dd2	K1			IC_{50} (µM)	S.I
15	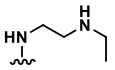	120	440	110	3.7	0.9	1.56	13
16	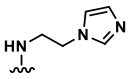	380	570	790	1.5	2.1	10.5	28
17	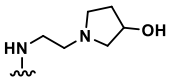	40	90	30	2.3	0.8	6.12	153
18	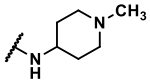	440	900	1,020	2.0	2.3	5.98	14
Chloroquine		8.0	240	230	30	28.8	35.8	4,475
Artesunate		6.0	4.0	1.0	0.7	0.2	-	-
Emetine		nd	nd	nd	-	-	0.095	-

CQS = *Pf*NF54; CQR = *Pf*Dd2 and *Pf*K1

R.I. = Resistance index = IC_{50} CQR strain/IC_{50} CQS strain

CHO = Chinese Hamster Ovarian cells.

S.I. = Selective index = IC_{50} CHO/IC_{50} *Pf*NF54

Substitution with piperidinyl moiety (**18**) did not yield any change in compound selectivity compared to **15.** However, there was a 2- and 12-fold increase in selectivity relative to **15** in the imidazole (**16**) and hydroxypyrrolidine (**17**)-containing derivative, respectively

In SAR_2, activity of the 2-F derivative (**19**) against *Pf*NF54 was improved by introduction of the 3-hydroxypyrrolidinyl side chain (**Table 5.3b**), consistent with the observations from SAR_1 involving compound **17**. The compound showed comparable activity to **15,** with significantly better selectivity. Though activity dropped against *Pf*Dd2, potency was still maintained against *Pf*K1, highlighting the different genomic backgrounds of resistance alleles in the two strains.

Table 5.3b: *In vitro* antiplasmodial activity and cytotoxicity results of SAR_2 analogues

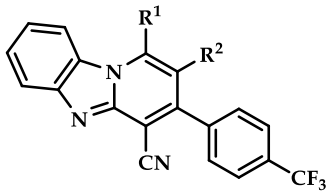

Compound	R^1	R^2	Antiplasmodial Activity IC_{50} (nM)			R.I Dd2	R.I K1	Cytotoxicity (CHO)	
			NF54	Dd2	K1			IC_{50} (µM)	S.I
15	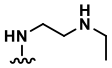	**H**	120	440	110	3.7	0.9	1.56	13
19	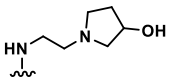	**F**	190	620	170	3.3	0.9	207.1	1,090
Chloroquine			8.0	240	230	30	28.8	35.8	4,475
Artesunate			6.0	4.0	1.0	0.7	0.2	-	-
Emetine			nd	nd	nd	-	-	0.095	-

CQS = *Pf*NF54; CQR = *Pf*Dd2 and *Pf*K1

R.I. = Resistance index = IC_{50} CQR strain/IC_{50} CQS strain

CHO = Chinese Hamster Ovarian cells

S.I. = Selective index = IC_{50} CHO/IC_{50} *Pf*NF54

Replacing the 4-CF_3Ph in **15** with *meta*- and di-chloro substituted derivatives in SAR_3 led to retention of activity against *Pf*NF54 as shown in **Table 5.3c**. Compound **21** was equipotent against both strains of the parasite while the activity of **20** only diminished against *Pf*K1. There was, however, no improvement in selectivity in this series.

Table 5.3c: *In vitro* antiplasmodial activity and cytotoxicity results of SAR_3 analogues

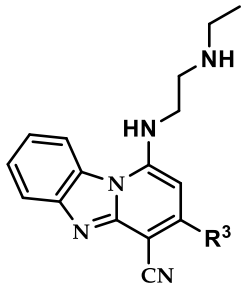

Compound	R³	Antiplasmodial Activity IC_{50} (nM)			R.I Dd2	R.I K1	Cytotoxicity (CHO)	
		NF54	Dd2	K1			IC_{50} (µM)	S.I
15	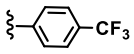	120	440	110	3.7	0.9	1.56	13
20		380	420	1,000	1.1	2.6	5.18	13
21	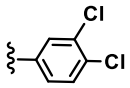	110	380	120	3.5	1.1	1.55	14
Chloroquine		8.0	240	230	30	28.8	35.8	4,475
Artesunate		6.0	4.0	1.0	0.7	0.2	-	-
Emetine		nd	nd	nd	-	-	0.095	-

CQS = *Pf*NF54; CQR = *Pf*Dd2 and *Pf*K1

R.I. = Resistance index = IC_{50} CQR strain/IC_{50} CQS strain

CHO = Chinese Hamster Ovarian cells.

S.I. = Selective index = IC_{50} CHO/IC_{50} *Pf*NF54

Regarding SAR_4, mono- (**22**) or dichloro- substitutions (**23** and **24**) at C7, C8 or C9 were well tolerated, providing significant improvements in selectivity and antiplasmodial activity against all strains tested (**Table 5.3d**). This could be due to their high lipophilicity (mean ± SE: $LogD_{7.4}$; 3.47 ± 0.09), and attendant ability to permeate through phospholipid membranes

Table 5.3d: *In vitro* antiplasmodial activity and cytotoxicity results of SAR_4 analogues

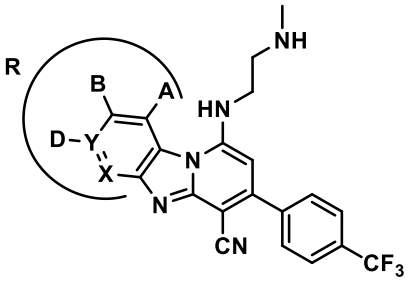

Compound	R	Antiplasmodial Activity IC_{50} (nM)			R.I Dd2	R.I K1	Cytotoxicity (CHO)	
		NF54	Dd2	K1			IC_{50} (µM)	S.I
15		120	440	110	3.7	0.9	1.56	13
22	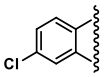	30	90	30	3.0	1.0	8.71	362
23	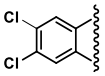	20	40	20	1.0	2.0	3.39	188
24	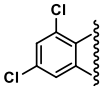	30	70	40	3.2	1.3	11.20	431
Chloroquine		8.0	240	230	30	28.8	35.8	4,475
Artesunate		6.0	4.0	1.0	0.7	0.2	-	-
Emetine		nd	nd	nd	-	-	0.095	-

CQS = *Pf*NF54; CQR = *Pf*Dd2 and *Pf*K1

R.I. = Resistance index = IC_{50} CQR strain/IC_{50} CQS strain

CHO = Chinese Hamster Ovarian cells. S.I. = Selective index = IC_{50} CHO/IC_{50} *Pf*NF54

There was no indication of significant cross-resistance between these PBIs and CQ in the two CQR strains as indicated by their low resistance indices (**Tables 5.3a-d**). RI values close to unity denoted activity regardless of parasite susceptibility while loss of activity due to resistance development or likelihood of resistance development would be characterised by large RIs. As depicted in **Figure 5.4A and B**, the PBIs show little deviation from the diagonal line which represents a RI value of 1, and are clearly differentiated from CQ in the analyses of both CQR strains. Promising drug leads would customarily have low RI, implying they are less recognised by the parasite's resistance machinery. Therefore, the difference in RI between these compounds and CQ suggests that their mechanism of resistance may be different from one involving reduction in vacuolar accumulation (like CQ), which would make them affected by the protein transporters responsible for lower accumulation of CQ within the parasite.

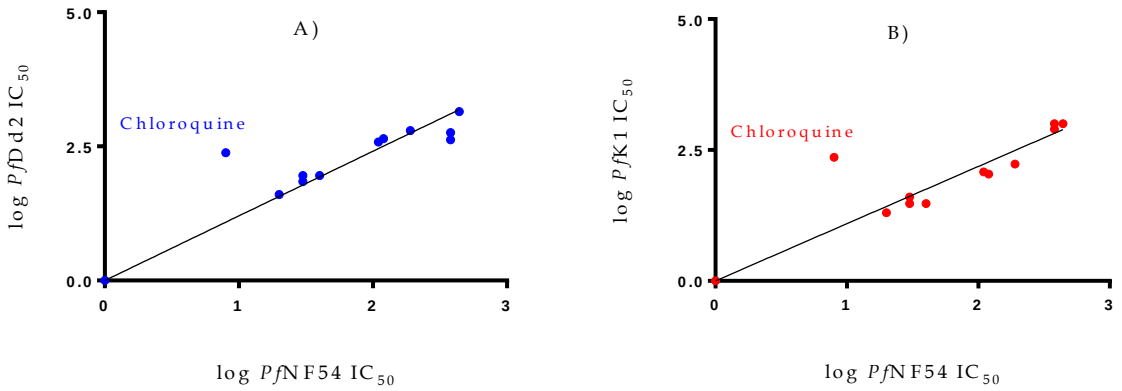

Figure 5.4: Resistance index (RI) expressed as the correlation of the *in vitro* antiplasmodial activity against *Pf*NF54 and *Pf*Dd2 (blue plot) and *Pf*K1 (red plot).

5.3.3 In Vivo Efficacy against P. berghei-infected mice

Based on their potent blood stage antiplasmodial activity, high selectivity, moderate solubility and high microsomal stability, **20**, **23** and **24,** were selected for *in vivo* efficacy studies. Testing was conducted at the Swiss Tropical and Public Health Institute where the compounds were initially administered four times in daily oral doses of 50 mg/kg. If mice were cured, lower doses (4 x 30 mg/kg, 4 x 10 mg/kg and 4 x 3 mg/kg) were subsequently evaluated.

Suppression of parasitemia as a percentage of the untreated control and the effects of the test compounds on mouse survival is shown in **Table 5.4**, with compound considered curative if the animal survived to day 30 after infection with no detectable parasites. Compound **20** showed weak efficacy (61%) with a single cure at 4 x 50 mg/kg, while **23** and **24** were completely curative at 4 x 50 mg/kg, with **23** in fact proving better at 4 x 30 mg/kg. At lower doses (4 x 10 mg/kg and 4 x 3 mg/kg), the mice were not cured (mean survival days ± SE: 17.5 ± 0.5) although parasitemia was still reduced by > 99%. The potent oral *in vivo* efficacy of the two analogues was encouraging and indicative of good oral bioavailability possibly due to the lack of first pass metabolism. It could also imply a reasonably low volume of distribution, which affords sufficient free unbound drug concentration in systemic circulation to achieve parasitemia reduction in parasitised erythrocytes. The ideal profile for new antimalarials comprises orally active compounds that can cure the disease with a 3-day regimen using once-a-day dosing.[2] Indeed, these analogues demonstrate the potential to meet this requirement.

Table 5.4: Effect of compounds **20**, **23** and **24** on suppression of parasitemia and mouse survival

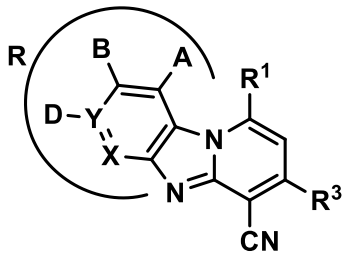

Compound	R	R^1	R^3	Oral Dose [a] (mg/kg)	% Reduction in parasitemia (MSD) [b]	Cured/ Infected
20		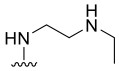		4 x 50	61.0 (24)	1/3
23	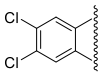	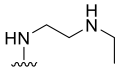	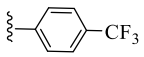	4 x 50 4 x 30 4 x 10 4 x 3	98.0 (30) 99.7 (30) 99.6 (18) 99.5 (17)	3/3 3/3 0/3 0/3
24	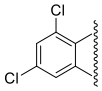	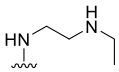	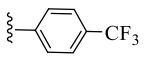	4 x 50 4 x 30 4 x 10 4 x 3	98.0 (30) 99.4 (30) 99.4 (18) 99.4 (16)	3/3 2/3 0/3 0/3
Chloroquine				4 x 30	99.9 (24)	0/10
Control				-	- (4) [c]	

[a] Test compounds were formulated in 90/10 Tween80/ethanol (v/v), diluted 10 times with water and administered orally once per day on 4 consecutive days (4, 24, 48, and 72 h after infection).

[b] MSD = mean survival time in days.

[c] Mice with < 40 % parasitemia reduction were euthanised on day 4 to prevent death otherwise occurring at day 6.

5.3.4. Possible Mechanism(s) of Action

Following the good *in vitro* antiplasmodial activity and *in vivo* oral efficacy of compounds based on this scaffold, investigations on potential MoAs were conducted. These comprised analyses on the speed of action of these compounds when *P. falciparum* cultures were incubated with fixed drug concentrations to obtain insights into possible lifecycle stage at which the compounds are likely to be most active. Further, their CQ-like planar architecture allowed for studies on *in vitro* inhibition of βH formation and cellular haem fractionation experiments.

5.3.4.1. Analysis of Speed of Killing

Standard *in vitro* parasite growth inhibition assays expose parasites to drugs for specific periods of time and assess the viability of the remaining parasites by measuring labelled nucleic acids or enzymatic activity. The rapidity of parasite killing in these assays is crucial as it can hint at the MoA of different compounds.[226] The effect of 8 PBIs (**15, 16, 17, 18, 19, 20, 22** and **23**), representing all the four SAR groups, on parasite viability over time was measured to determine their speed of action as described in detail in **section 2.4.11** of *Chapter 2*. Correlation analyses were further performed between compound killing rate and potency against *Pf*NF54. The IC_{50} values of PYR, **17** and **19** were 6-, 18- and 22- fold, respectively, higher at 24 h than at 72 h (**Figure 5.5**), indicating that these compounds possess a slow-acting parasiticidal effect and likely impair late-stage processes in the parasite's 48-h cycle. CQ, AS, **15**, **18** and **20** seemed to exhibit fast-acting modes (24 h/IC_{50} 72 h IC_{50} ratios < 1.5) hence likely inhibit ring stage and trophozoite-associated events. However, compounds **16**, **22** and **23** could neither be classified as fast or slow since they had an activity ratio between 1.5 and 2. Since these PBIs share a common core scaffold, it is plausible that the observed differences in the speed of parasiticidal effect are a consequence of the various modifications introduced onto the prototype molecule, **15**, hence enabling

acces or binding to different protein or enzymes and consequently eliciting distinct MoAs as hinted by the disparate IC_{50}s in both CQS and CQR strains. In fact, both slow-acting derivatives (**17** and **19**) contain the 3-hydroxypyrrolidine group indicating that they could share a similar MoA different from the other derivatives.

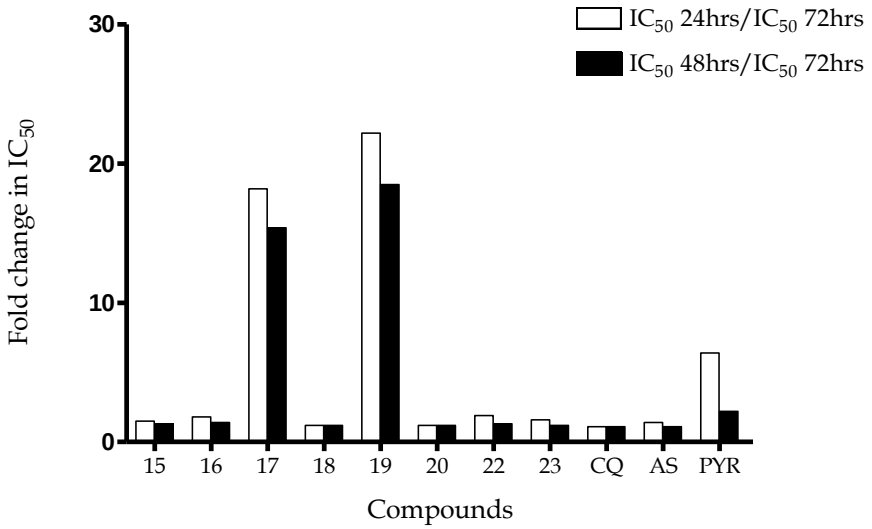

Figure 5.5: Plot showing fold change in activity of compounds at different speed assay durations relative to 72 h assay.

Overall, there was neither a bias in the phenotypic screen for any particular killing speed nor significant correlation between compound speed of action and their antiplasmodial potency against *Pf*NF54 (**Figure 5.6**), implying that the PBIs display a fairly broad spectrum of killing speeds that cannot directly be predicted by their efficiency in blocking [^{3}H] hypoxanthine incorporation. However, the number of compounds evaluated in this analysis is statistically low and the inferences must be considered with caution.

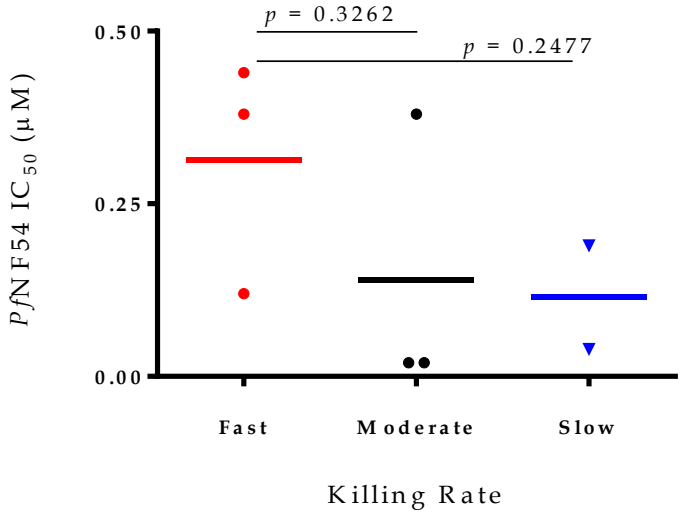

Figure 5.6: Compound killing rate versus potency against *Pf*NF54 compared between groups to determine if potency could be a predictor for speed of action.

5.3.4.2. Inhibition of β-haematin Formation and Haem-Pyridine Speciation

As earlier mentioned, the ability to adopt a flat conformation makes this class of compounds candidates for π-π interactions, which alongside hydrogen bonding and direct coordination to the Fe(III) centre of the haem monomer, constitute the key interactions between inhibitors and Fe(III)PPIX during haem-drug complex formation.[90] The compounds were therefore first evaluated for their ability to inhibit βH formation.

All derivatives except **19** (βHIA IC_{50}; 119.9 µM) were active against formation of βH, with IC_{50}s below 100 µM. Among the actives, compound **24** was the most potent (βHIA IC_{50}; 7.0 µM) and **17** the least (βHIA IC_{50}; 85.3 µM) as shown in **Table 5.5**. Due to their planarity, these compounds are presumed to be able to π-stack with ferriprotoporphyrin IX leading to formation a haem-drug complex. The presence of the fluoro- group at C2 in **19** possibly disrupts the planarity of the molecule hence accounting for the observed low activity. It

could also relate to the 3-hydroxyprolidine side chain common to both compounds **17** and **19**, which are the least active in the group.

Table 5.5: βH inhibition activity of the PBI derivatives and controls

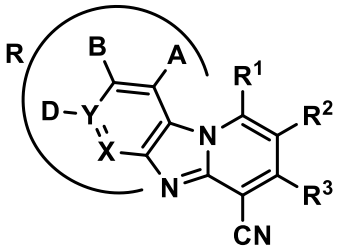

Compound	R	R¹	R²	R³	βHIA IC_{50} (Mean ± SE) μM
15		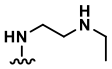	**H**	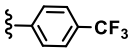	40.5 ± 0.4
16		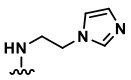	**H**	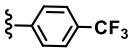	8.0 ± 0.2
17		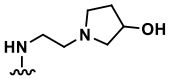	**H**	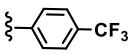	85.3 ± 1.4
18		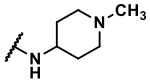	**H**	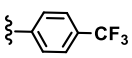	47.6 ± 5.4
19		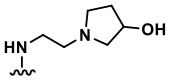	**F**	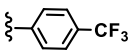	119.9 ± 21.7
20		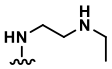	**H**		32.1 ± 2.4
21		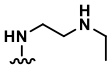	**H**	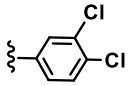	19.2 ± 2.9
22	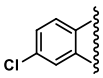	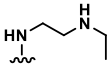	**H**	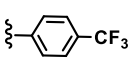	14.5 ± 4.2
23	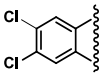	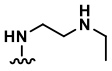	**H**	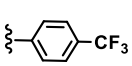	30.7 ± 4.7
24	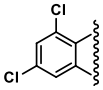	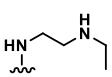	**H**		6.8 ± 1.6
Chloroquine					25.0 ± 2.2
Amodiaquine					15.9 ± 1.4
Pyrimethamine					*No Inhibition*

However, without a detailed structural investigation of these intramolecular interactions, this remains only speculative. There was no discernible trend in activity that could be correlated to the substituents. However, though analysis of the βHI activity with speed of kill of the molecules did not reveal any direct statistical trends, it was noted that the hydroxypyrrolidine-bearing compound **17** and **19**, which grouped together in the 'slow-acting' category also showed the weakest βHI activity. The abilities of these compounds to inhibit βH formation therefore appear to depend on the presence of a planar ring system, aliphatic hydrophobicity and the availability of a protonation site (ionisability) in a fashion too complex to predict from the limited number of compounds evaluated in this chapter and without the guide of an X-ray crystal structure.

Though the analysis of the association between *in vitro* antiplasmodial activities versus inhibition of βH formation indicated a general trend of decreasing antiplasmodial potency as βH inhibition activity decreases, this correlation was extremely weak and not significant (**Figure 5.7**). Again, this could possibly reflect the limitations in comparing data from the cell-free NP-40 assay to signals from intracellular assays that data on antiplasmodial drug activity represents.

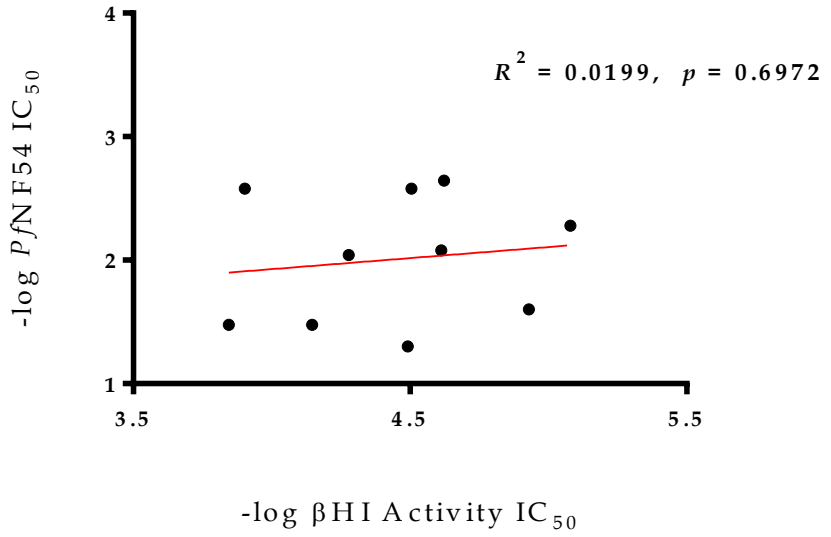

Figure 5.6: Correlation between PBI activity against *Pf*NF54 and βH inhibition activity.

To further interrogate if these βH inhibition signals are genuine reflections of potential for intracellular inhibition of HZ formation, a set of four PBI derivatives were subjected to the cellular haem fractionation assay used to characterise pDBQs and their metabolites in the previous two chapters. Five compounds, **15**, **17**, **19**, **21** and **22**, were chosen as representatives of all the four different SAR groups. Compound **19**, in addition, represented a negative control with no observed inhibitory activity in the detergent-based assay.

Only compounds **15** and **22** showed significant changes in 'free' haem that were associated with both decrease in levels of HZ in a dose-dependent manner relative to untreated controls. Similarly, increases in 'free' haem were correlated with parasite survival in only these two derivatives (**Figure 5.7**). No significant changes in toxic 'free' haem or HZ levels with increasing drug concentrations were, however, observed for **17, 19** and **21** (**Figure 5.7**). The lack of HZ inhibition by **17** and **19,** which both show weak to negligible βH inhibition activity is consistent with the results of the βH inhibition assay, and thus further validates

the fidelity of this haem fractionation assay in identifying true negatives especially in non-quinoline scaffolds. Interestingly, this is consistent with speed of killing results which also alludes to a different target for these compounds. Taken together, the discordant results observed from these derivatives representing different SAR groups suggests that inhibition of HZ formation could be one but not the sole or primary target of this class of compounds; their flat conformation possibly allowing for weak haem-drug complex formation through only π-π interactions as was recently reported for certain benzamide analogues.[227] This would be unlike HLF and QN, for instance, which reportedly exhibit hydrogen bonding and coordination to Fe(III)PPIX, in addition to $\pi-\pi$ interactions.[90, 228]

Compound 15 **a)**

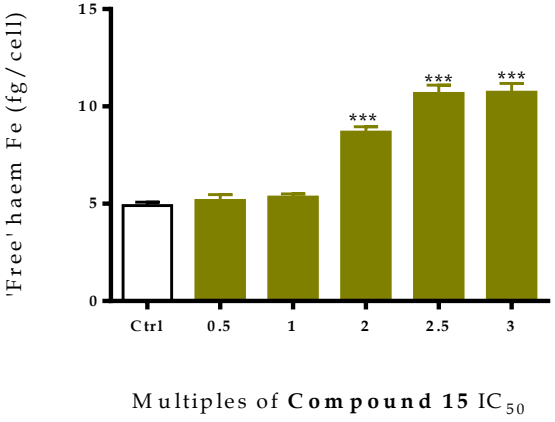

b)

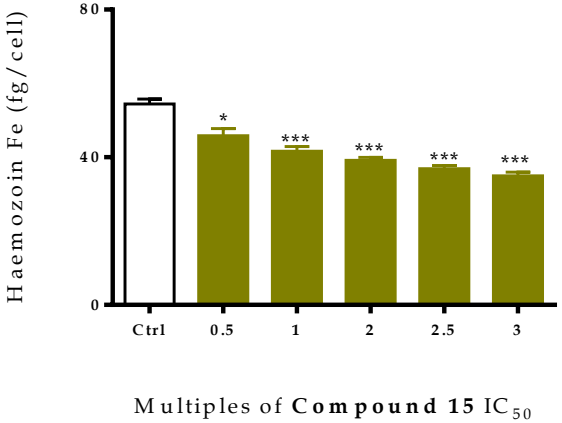

c)

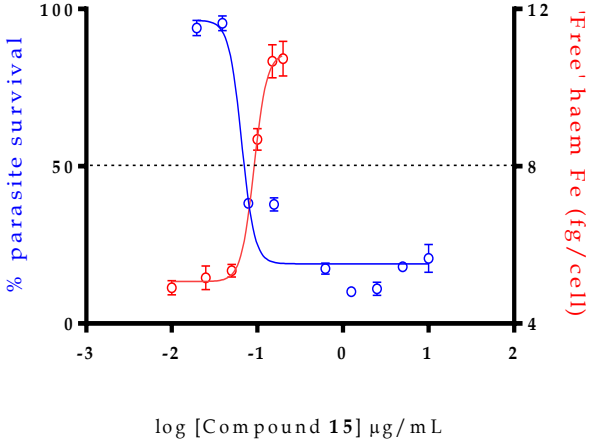

Compound 17 **d)**

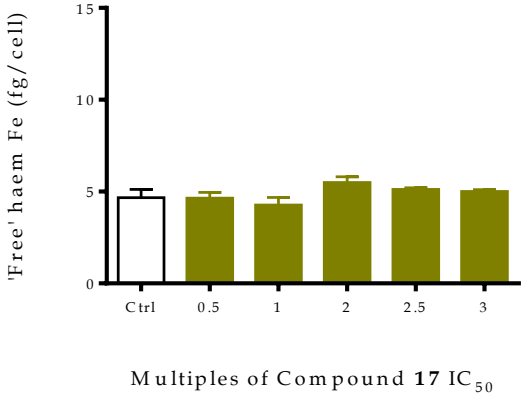

e)

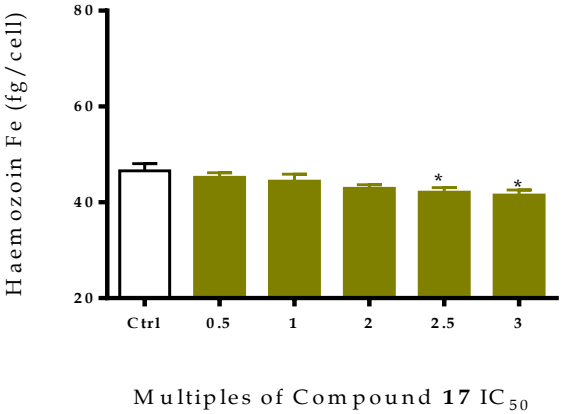

f)

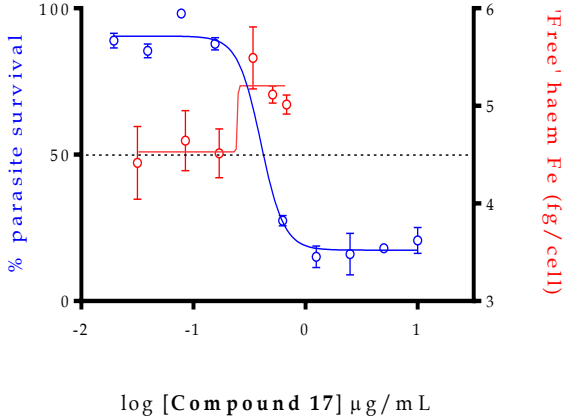

Compound 19 **g)**

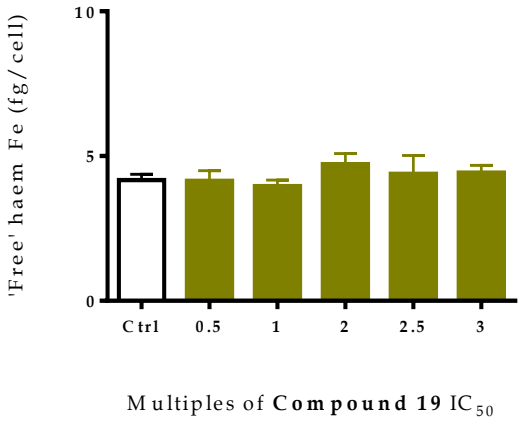

h)

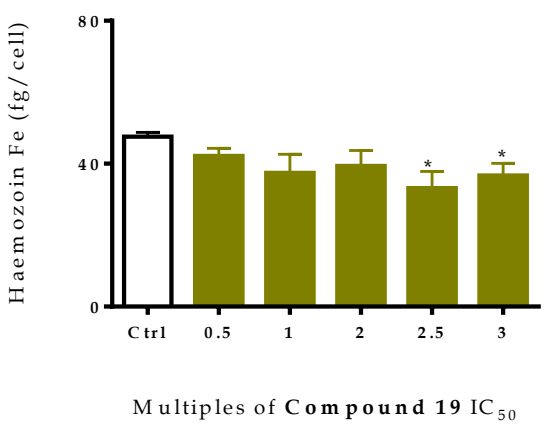

i)

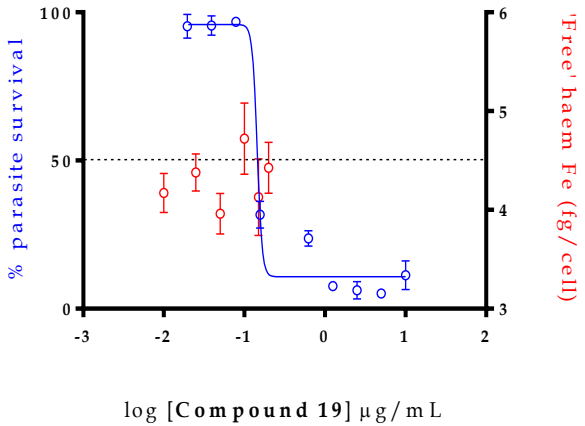

Compound 21 **j)**

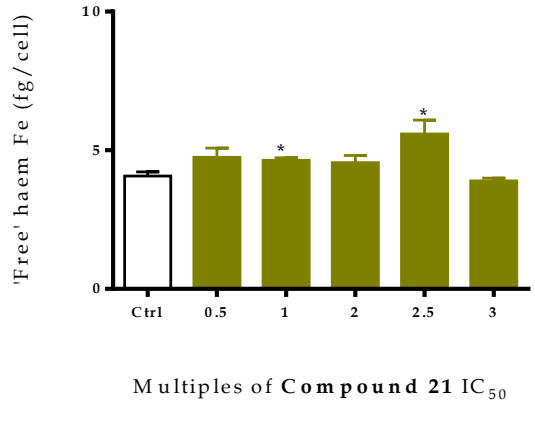

k)

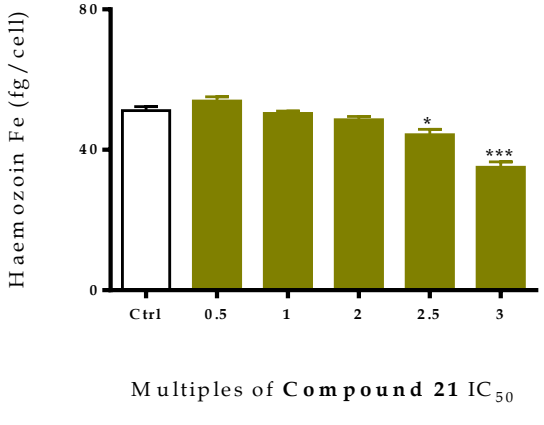

l)

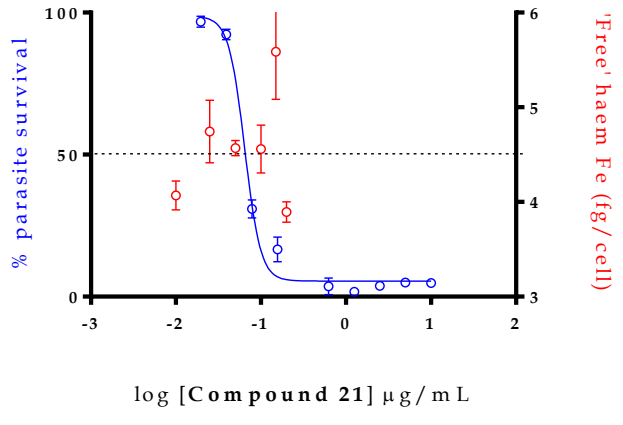

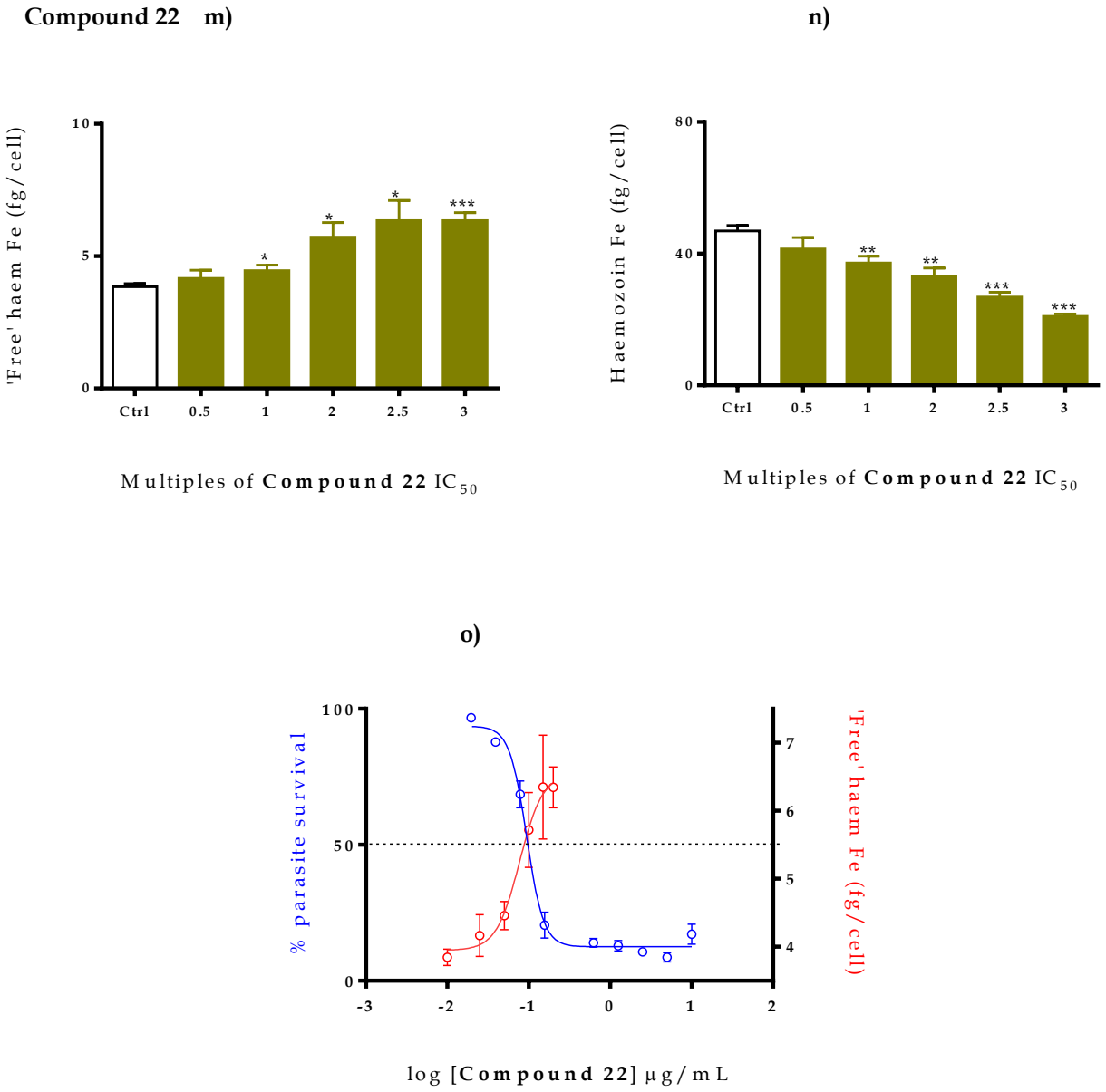

Figure 5.7: Haem fractionation profiles of compounds **15, 17, 19, 21** and **22** in synchronised drug-treated and control *Pf*NF54 parasites. Plots **a, d, g, j** and **m**), show levels of toxic 'free' haem represented as Fe measured in fg/cell while plots **b, e, h, k** and **n**) show HZ levels. The asterisks indicate statistical significance relative to control (*p < 0.05; ** p < 0.01 and *** p < 0.001). Plots **c, f, i, l** and **o**) represent parasite survival (blue) overlaid against 'free' haem Fe (red) plots.

This leaves the intriguing prospect that the PBIs could act, at least in part, through an as yet unidentified mechanism. Indeed, some PBI compounds have previously been reported to inhibit the biosynthesis of β-1,6-glucan, a key component of the mycetes cell wall.[229] Although the possible presence of β-glucan synthase orthologue(s) in *P. falciparum* or *S. mansoni* cannot be excluded, plasmodial and schistosomal genomes do not appear to contain genes encoding the enzymes traditionally associated with β -glucan synthesis due to the evolutionary irrelevance of cell walls in the two organisms. In addition, inhibition of the pore-forming protein perforin in mammalian cells by 1-amino-2, 4-dicyanopyrido[1,2-*a*]benzimidazoles has also been reported.[230] This is interesting as the *P. falciparum* proteome harbours perforin-like proteins (PLPs) known to be involved in permeabilising the erythrocyte membrane during egress of either gametocytes or merozoites.[231] More recently, an hydroxyl derivative 2-ethyl-1-hydroxy-3-methyl-pyrido[1,2-a]benzimidazole-4-carbonitrile (GNF7686) with potent *in vitro* activity against *Trypanosoma cruzi*, was also shown to act through inhibition of cytochrome b - a component of cytochrome bc1 or complex III [232] and a well-established antimalarial target. All these different MoAs by various PBI derivatives highlight a scenario where some PBIs may inhibit HZ formation while others inhibit other different targets.

5.3.5 Antischistosomal Activity

5.3.5.1. In vitro Antischistosomal Activity against Juvenile and Adult Worms

As earlier mentioned, *S. mansoni* like *P. falciparum*, has evolved the biocrystallisation of haem molecules into HZ as a detoxification mechanism to rid themselves of the toxicity of 'free' haem.[233, 234] Inhibition of this pathway therefore presents a vulnerable target and towards this aim, organometallic complexes, natural products and a number of repositioned antimalarial agents have variously been explored as antischistosomal agents and recently

reviewed.[235-237] On the basis of the previously discussed hypothesis that PBIs can inhibit formation of βH due to their structural conformation, and results from the *in vitro* NP-40 assay, the antischistosomal activity of 9 of the derivatives was evaluated against newly transformed schistosomula (NTS) and adult worms as described in **section 2.4.13** in *Chapter 2*. Analogues that showed favourable *in vitro* activity were examined for *in vivo* efficacy in experimental mice.

All derivatives tested exhibited an inhibition range of 95.7 to 100% against NTS proliferation, thus allowing for subsequent evaluation against adult worms where 7/9 derivatives still retained >60% worm mortality (**Table 5.6**). IC_{50} determination was also carried out for these compounds, and ranged between 0.32 to 3.94 µM and 1.62 to 10.14 µM, against NTS and adult worms, respectively. Compounds **24** and **21** were the most potent (IC_{50}s: 1.62 and 1.69 µM, respectively) against the adult worms, which could suggest presence of chloro- group(s) on either side of the ring system is favoured for activity. Analogues based on piperidine **(18)** or imidazole **(16)** substitutions in place of the ethylamine group were inactive, implying these modifications are not tolerated for antischistosomal activity. Though all derivatives seemed more potent against the juvenile parasites (mean IC_{50} ± SE: 1.97 ± 0.36), activity diminished against the adult worms (mean IC_{50} ± SE: 4.38 ± 1.49). This could be due to presence of completely developed proteins and/or pathways in the adult worms that can tolerate drug pressure or even extrude it, before lethal concentrations are achieved, unlike in the juvenile.

Table 5.6: *In vitro* effect of PBI compounds against juvenile and adult stages of *S. mansoni*

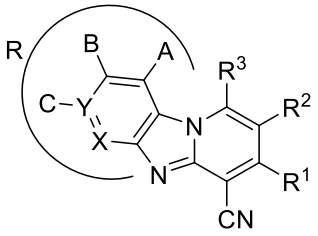

Compound	R	R¹	R²	R³	Against NTS		Against Adult Worms	
					% Effect	IC_{50} (µM)	% Effect	IC_{50} (µM)
15		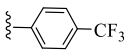	**H**	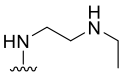	100	0.78	100	2.41
16		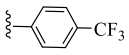	**H**	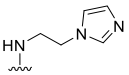	100	2.28	100	10.14
17		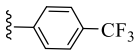	**H**	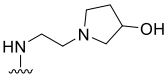	97.4	3.83	79	10.02
18		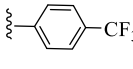	**H**	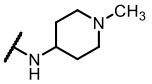	96.1	3.83	53	*nd*
19		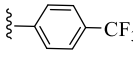	**F**	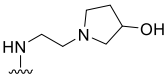	95.7	3.94	54	*nd*
21		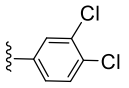	**H**	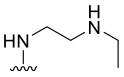	100	0.32	100	1.69
22	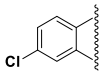	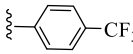	**H**	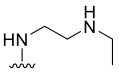	100	1.88	100	2.41
23	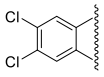	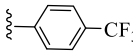	**H**	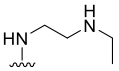	100	0.42	100	2.08
24	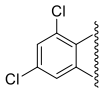	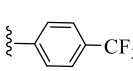	**H**	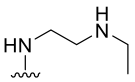	100	0.46	100	1.62
PZQ					100		100	0.02

PZQ = Praziquantel

nd = Not determined

It is worth noting that compounds **17**, **18** and **19**, which had the least potency against both juvenile and adult worms, were also observed in **section 5.3.4.2** as weakest βH inhibitors. A correlation of *in vitro* βH activity with antischistosomal activity revealed a general trend of increasing βH activity with antischistosomal activity against adult *S. mansoni* (**Figure 5.8**). Though positive, these associations were weak and not significant, implying either possible

presence of additional mechanisms involved in the antischistosomal activity of this class of compounds, or factors that affect the localisation of these compounds in the worm gut. This is consistent with recent findings involving the antimalarials CQ, MFQ and QN, which were shown to exhibit antischistosomal activity that did not correlate with their HZ inhibition property,[238] with MFQ in fact demonstrated to interfere with glycolysis in NTS.[239] It is noteworthy that, unlike in *P. falciparum*, HZ formation proceeds extracellularly in *S. mansoni* and is thought to be possibly initiated by, or involve proteins, lipids and other hydrophobic components in the gut of the parasite.[40] It is therefore conceivable that these PBIs inhibit HZ formation in *Schistosoma* in a manner dissimilar to *Plasmodium* by interacting with any of these targets, resulting in the perturbation of the crystal growth microenvironment.

a) b)

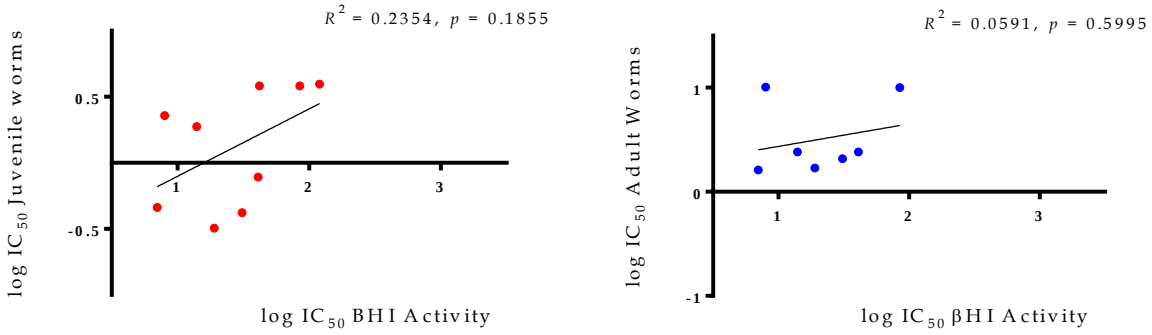

Figure 5.8: Correlation between PBI antischistosomal and βH inhibition activity of **a**) 9 PBI compounds exhibiting a broad spectrum of anti-NTS activity and **b**) 7 compounds with activity against adult worms.

5.3.5.2. In vivo efficacy against S. mansoni-infected mice

Compounds **15, 21, 23** and **24,** which showed the best *in vitro* activity against NTS (IC_{50} range: 0.32 to 0.78 µM) and adult worms (IC_{50} range: 1.62 to 2.41 µM) were evaluated for efficacy against *S. mansoni*-infected mice as described in **section 2.4.13** in *Chapter 2*.

Compound **15** showed no reduction in total worm burden at 400 mg/kg (**Table 5.7**). Though all compounds showed only weak activity with < 50% reduction in both total and female worm burden, there was nonetheless a general trend of higher female worm reduction (FWR) which further corroborates their impressive *in vitro* IC_{50}s and could, by extension, be indicative of a sex-specific inhibition mode not uncommon among antischistosomal inhibitors.[240]

Table 5.7: Effect on worm burden following single 400 mg/kg oral doses of 4 PBIs administered to mice harbouring adult *S. mansoni* infection.

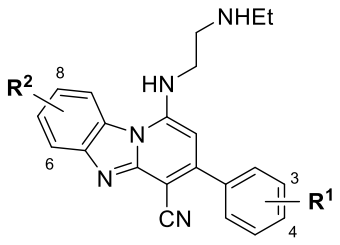

Compound Code	R^1	R^2	No. mice investigated (n)	No. mice cured (n)	Mean number of worms (SD)		TWR (%)	FWR (%)
					Males	Females		
Control	-		9	-	17.3 (8.7)	14.2 (8.4)	-	-
15	4-CF_3	H	3	0	18.7 (3.1)	14.3 (6.8)	0.0	0.0
21	3,4-diCl	H	4	0	8.0 (2.6)	8.3 (2.2)	48.3	41.9
23	4-CF_3	6,7-diCl	4	0	12.8 (5.3)	10.3(4.8)	26.7	27.8
24	4-CF_3	6,8-diCl	4	0	12.0 (2.7)	7.5 (3.9)	38.1	47.2

SD = Standard deviation

TWR = Total worm reduction

FWR = Female worm reduction

5.3.6. Predicted hERG Channel Inhibition Potential

Like the quinoline-based pDBQs and their metabolites, these PBIs also classify as weak bases whose molecular weights and lipophilicity can influence a range of absorption-related parameters, including likelihood for hERG channel inhibition.[144] Predictions were therefore made on the ability of these molecules to inhibit the hERG channel and this risk was correlated with their molecular weights and lipophilicity. Compared to the pDBQs and their metabolites, the PBIs had higher pIC_{50}s that ranged from 6.11 to 7.50 and averaged 6.66 ± 0.14 (**Table 5.8**). This comparatively elevated risk for cardiotoxicity was however not associated with cLogP (R^2 = 0.1773; p = 0.2256), LogD (R^2 = 0.0689; p = 0.4639) or molecular weight (R^2 = 0.1133; p = 0.3416). Considering the structural and pharmacological diversity of hERG inhibitors and the flexibility of the hERG protein, there are likely to be several modes and sites of interaction, making the prediction of ligand–protein interaction extremely complex. Indeed, it has been shown that other molecular properties like aromaticity,[241] polar surface area and hydrogen bond donors/acceptors [242] also constitute key features of hERG-inhibiting compounds. Therefore, it is important to remember that the predictions are not solely based on differences in these parameters since these, on their own, cannot sufficiently elucidate the dynamics of hERG channel inhibition.

Table 5.8: Predicted hERG inhibition IC_{50}s and predicted lipophilicity of the PBIs

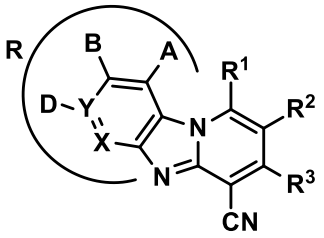

Compound	R	R^1	R^2	R^3	pIC_{50} [a]	Mol. Weight	cLogP [b]	$LogD_{7.4}$ [b]
15		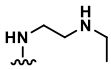	**H**	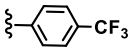	6.46	423.9	4.10	1.80
16		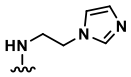	**H**	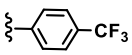	6.70	446.4	4.01	3.95
17		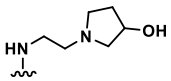	**H**	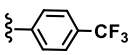	7.07	465.5	3.38	2.03
18		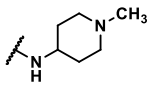	**H**	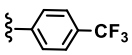	7.50	449.5	4.13	2.76
19		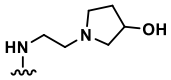	**F**	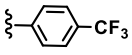	7.24	483.5	3.53	2.70
20		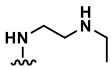	**H**		6.28	373.4	3.36	1.07
21		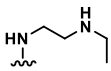	**H**	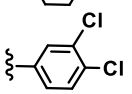	6.11	424.3	4.43	2.13
22	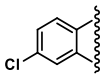	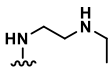	**H**	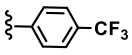	6.45	457.9	4.70	2.41
23	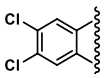	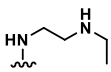	**H**	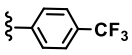	6.42	492.3	5.31	3.01
24	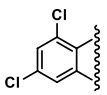	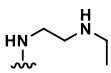	**H**	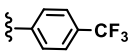	6.40	492.3	5.31	3.01
Chloroquine					6.00	319.9	3.81	0.88
Dihydroartemisinin					4.27	284.4	2.84	2.84
Halofantrine					7.37	500.4	8.06	5.46
***N*-desbutylhalofantrine**					6.52	444.3	6.35	3.90

[a] pIC_{50} values were determined using StarDrop™

[b] cLogP and $LogD_{7.4}$ were predicted using MarvinSketch v5.9.4

5.4. Summary and Conclusion

In this chapter, 10 derivatives of the PBI scaffold, identified in a previous study as having promising antimalarial potential, were evaluated for their biological as well as physicochemical properties, and characterised for their mechanistic potential to disrupt HZ inhibition in *P. falciparum* and *S. mansoni*. Investigations were based on SAR analyses referenced on the frontrunner compound, **15**, and showed that though the compounds had an overall high permeability, only SAR 2-4 modifications led to modest improvements in solubility. Lipophilicity was measured by experimental determination of LogD at pH 7.4 and averaged (± SE) 3.04 ± 0.18. These values correlated well with computationally predicted LogD results (R^2 = 0.6348; p = 0.0058). Moderate to excellent metabolic stability was observed in mouse and human liver microsomes, particularly in **20** (**Figure 5.9**) and the 3 SAR_4 compounds.

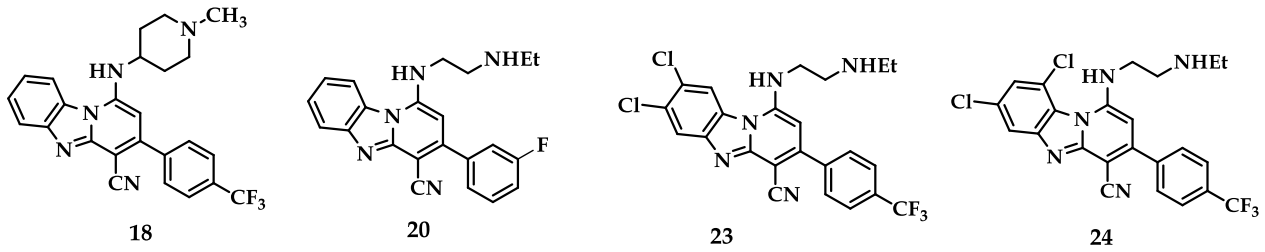

Figure 5.9: Chemical structures of compounds **18**, **20**, **23** and **24**.

All compounds except **18** (**Figure 5.9**) had submicromolar activity against both CQS and CQR strains, with the SAR_4 derivatives bearing halo-substitutions on the LHS of the PBI core, showing the best antiplasmodial activity and highest selectivity. There was no indication of cross resistance between these derivatives and CQ, hinting at possible divergence in their MoA, and by extension mechanism of resistance. This antiplasmodial activity data, coupled with solubility and metabolic stability results, informed the selection

of **15**, **23** and **24** for *in vivo* efficacy studies in *P. berghei*-infected mice where **23** and **24** resulted in >99% suppression of parasitemia and complete cures in treated mice.

To gain greater insight into the potential antiplasmodial MoA of these compounds, killing kinetics were quantified using viability time-course profiles, which were compared with antimalarials known to have fast (CQ, AS) or slow (PYR) rates of action. Of the 8 analogues selected for investigation, 3 were fast-acting, 2 were slow while the other 3 showed intermediate activity. Fast-acting compounds have already been a focus in therapeutic development as they rapidly stop disease progression, avoid severe complications and have recently been shown to have reduced propensity for evolution of resistance.[243] This would make **15**, **18** and **20**, which likely inhibit early-stage events in the *P. falciparum* life cycle, attractive candidates for future antimalarial development in this regard. The fairly even distribution in speeds of activity highlighted a non-preferential killing signature and hinted at a broad spectrum in the activity and MoA of this class compounds. Mechanistic characterisation to explore βH potential of these compounds, owing to their ability to adopt a planar conformation, was also explored. All compounds had IC_{50}s within an active range of inhibition except **19**, hypothesised to harbour disrupted planarity from the 2-F substitution. Though no direct statistical association was observed between βH inhibition and speed of parasite growth inhibition, a pattern was noted whereby the weakest βH inhibiting compounds (**17** and **19**) grouped together as slow-acting derivatives and both bore the 3-hydroxypyrrolidine substituent. Further, correlations were compound-specific as **21** (**Figure 5.10**), which was determined to have βH and antiplasmodial IC_{50} activity, did not appear to inhibit HZ formation in CQS *P. falciparum* as shown in the cellular haem fractionation results (**Figure 5.7**). Although HZ inhibition may occur with some derivatives (as evidenced by the mechanistic profiles of **15** and **22**), the PBIs as a class of compounds most likely have alternative (and perhaps even more dominant) MoA(s) occurring elsewhere

in the lifecycle where HZ inhibition is not involved. A complete understanding of the correlation between antiplasmodial activity and HZ inhibition would require more detailed chemical information on the nature of solid-state aggregates of haem and these PBIs.

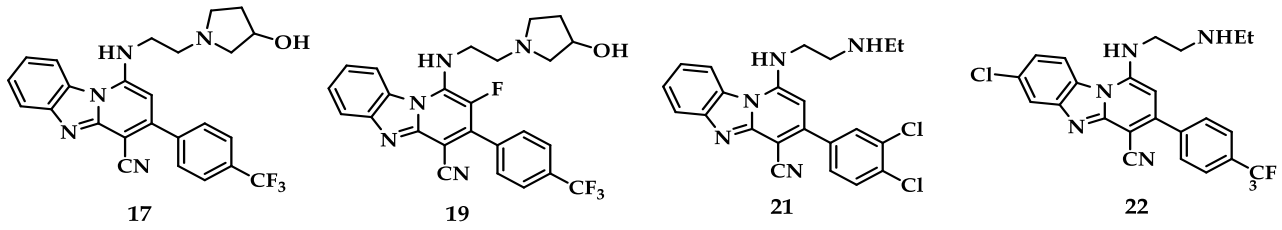

Figure 5.10: Chemical structures of compounds **17**, **19**, **21** and **22**

Finally, 9 derivatives were tested for their antischistosomal activity based on the presence of comparable haem detoxification machinery in *S. mansoni*. All the derivatives showed good activity against the juvenile worms (mean IC_{50} ± SE: 1.97 ± 0.36) but were less active against adult worms (mean IC_{50} ± SE: 4.38 ± 1.49), probably due to complete assembly of the proteome in the adult worms. There was a positive but weak correlation between *in vitro* antischistosomal activity and βH inhibition, suggesting that inhibition of HZ formation could be a contributing mechanism through which these compounds exert their antischistosomal effect. Further, encouraging efficacy in *S. mansoni*-infected mice was noted in compound **21** (48% TWR and 41% FWR) suggesting further optimisation efforts can deliver derivatives with improved efficacy. The observed antischistosomal property of these PBIs further complements the already-known broad antimicrobial potency of this compound class. The predicted risk of hERG channel inhibition by the PBIs was, however, higher (mean pIC_{50} ± SE: 6.66 ± 0.14) than that of the pDBQs (mean pIC_{50} ± SE: 6.33 ± 0.05) or their metabolites (mean pIC_{50} ± SE: 5.29 ± 0.11), a concern that would need to be addressed in their future development. Evaluation of more PBI derivatives is necessary to delineate

meaningful SAR while direct correlation of anti-parasitic activity and actual inhibition of HZ formation in the worm needs to be established, as do any other additional MoAs involved.

Chapter 6

CONCLUSION AND RECOMMENDATIONS FOR FUTURE STUDIES

6.1 Summary and Conclusion

Despite reports of declining incidence and deaths related to malaria,[3] the disease still remains a major public health concern particularly due to the challenges posed by asymptomatic (chronic) infections [5] and reduced sensitivity to ACTs.[54, 55] There is, therefore, an urgency to explore novel scaffolds to which parasites may not have been exposed and, hence, are less likely to be prone to resistance. In addition, it is important to exploit the merits of established drugs through chemical modifications that harness their pharmacological and pharmacokinetic advantages to help overcome theμir therapeutic shortcomings. CQ represents an excellent example of such known drugs. CQ resistance has been shown to be a consequence of reduced vacuolar concentrations due to the efflux activity of the transmembrane transporter, *Pf*CRT, rather than alterations within the HZ formation process – the actual target of the drug. Antimalarial drug design based on molecules that can adopt a CQ-like SAR but remain unrecognisable to the efflux machinery or built on the CQ sub-structure but permit local accumulation has the potential to address the challenge of antimalarial drug resistance. Crucially, these compounds should have favourable physicochemical and ADME properties that not only make them efficacious, but safe and convenient to administer.

The aim of this project was to establish the physicochemical, biological and mechanistic profiles of a set of molecules within the pyrido-dibemequine (pDBQ) and pyrido [1,2-*a*] benzimidazole (PBI) series in the context of antiplasmodial and antischistosomal activity. The structural framework of the pDBQ and PBI derivatives analysed in this project was informed by prototype molecules previously reported by Zishiri *et al.* and Ndakala *et al.*, respectively.[127, 170] Specifically, the project set out to i) investigate the solubility, permeability, lipophilicity, metabolic stability and potential for cardiotoxicity of pDBQs, their metabolites

and PBIs using computational and experimental techniques, ii) determine their *in vitro* and *in vivo* antiplasmodial/antischistosomal activity and correlate these with their respective physicochemical properties and, iii) as part of mechanistic investigations, ascertain their βH inhibiting potential and extend this probe to intracellular inhibition of HZ formation.

Due to the presence of two hydrophobic aromatic rings (the dibenzylmethylamine side group) and a hydrogen bond acceptor (quinoline N-atom), consistent with the proposals of Bhattacharjee *et al*.,[126] the pDBQs were hypothesised to possess resistance reversal activity. Moreover, the intact 4-amino-7-chloroquinoline moiety was envisaged to facilitate haem-binding and inhibition of HZ formation in line with the requirements in the SAR model proposed by Egan *et al*. for the activity of CQ-like molecules.[99] Modification of this original molecule by replacing one of the aromatic rings on the dibenzylmethylamine side chain with a pyridine and substituting the –Cl at C7 with –CN afforded compounds **2 – 7** (**Figure 6.1**).

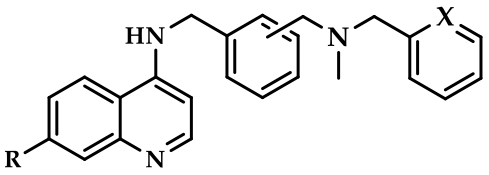

R = Cl; **X** = CH : **1**

R = Cl; **X** = N : **2, 3** and **4**

R = CN; **X** = N : **5, 6** and **7**

Figure 6.1: Chemical structure of the pDBQ molecules (**1 – 7**) analysed in this project

The compounds exhibited moderate (50 – 150 μM) to high (> 150 μM) aqueous solubility, with the introduction of a pyridine for one of the aromatic rings in the RA side group appearing to be responsible for the improved aqueous solubility, presumably due to the

availability of the pyridine nitrogen for H-bonding with water molecules. All the pDBQs also had high permeability (> -4.5) at pH 6.5, suggesting the possibility of enhanced permeation and absorption in the lower GIT if only passive diffusion is considered. The mean (± SE) LogD for the compounds at pH 7.4 was 3.15 ± 0.55 and even lower (0.93 ± 0.19) at pH 5.0. Analysis of cLogP showed compounds **5 - 7** had the lowest cLogP, presumably due to the greater electron-withdrawing but less lipophilic nature of the –CN compared to –Cl group at C7. There was also a strong inverse correlation between cLogP and predicted solubility (R^2 = 0.8085, p = 0.0061). The compounds additionally displayed nanomolar antiplasmodial activity, and though their activity against *Pf*Dd2 was better (mean IC_{50}: 121.8 nM) than CQ (IC_{50}: 226.4 nM) it was comparatively lower than other rCQs reported elsewhere. The resistance indices of the compounds further indicated a lack of cross resistance between these compounds and CQ. All compounds further showed potent inhibition of βH formation *in vitro*, and this mechanistic feature was confirmed through inhibition of HZ formation in a cellular haem fractionation experiment. The predicted and experimentally-determined hERG inhibition potential of the compounds showed that while compound **4** might present a hERG liability, the rapid metabolism would probably mean that it is unlikely to be present at toxic levels thus easing out concerns of hERG liability. Besides, the pDBQs exhibited very low metabolic stability with <5% of compound remaining after 30 min of incubation in mouse liver microsomes, with N-dealkylation identified as the main route of metabolism.

The resultant metabolites represented a set of compounds with reduced molecular weight yet retaining the fundamental SAR of CQ (**Figure 6.2**). They exhibited an aqueous solubility profile at pH 6.5 that was comparable to that of the parent compounds and also showed a moderate to high membrane permeability.

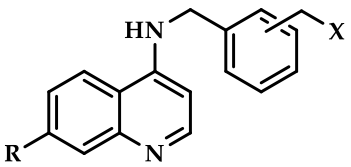

R = Cl; **X** = NH_2 : **8, 11** and **12**

R = Cl; **X** = NH-CH_3 : **9, 10** and **13**

R = CN; **X** = NH_2 : **14**

Figure 6.2: Chemical structure of the pDBQ metabolites (**8 – 14**) analysed in this project

As anticipated, the microsomal cleavage of one of the side chain rings of the parent pDBQs contributed to the low lipophilicity among these metabolites as evidenced by the reduced cLogP (mean: 3.14) and $LogD_{7.4}$ (mean: 0.79). Interestingly, 4/7 of these metabolites showed improved activity against *Pf*Dd2 (IC_{50} < 80 nM) even though they no longer had the RA side group in their structures. It could be speculated that this is because they interact with *Pf*CRT in a dissimilar manner to either CQ or their parent compounds, or that they are better at haem-drug complex formation. Indeed, like the parent pDBQs, the metabolites effectively inhibited formation of βH and further confirmed this mechanistic feature by inhibiting HZ formation in a CQ-like manner within the cell. Intriguingly, though quinoline-based compounds ordinarily require only a small increase in "free" haem to induce parasite death, the metabolites seemed to require comparatively lower levels of 'free' haem than the parent pDBQs to induce killing. This phenomenon could probably explain, at least in part, their potency even against CQR strains. The metabolites were additionally stable in both human and liver microsomes, with >75% of compound remaining after 30 min of incubation with the liver microsomes.

Table 6.1: Comparative summary of the physicochemical and biological features between the parent pDBQs and their metabolites

	Parent pDBQs	pDBQs Metabolites
	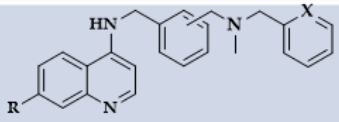	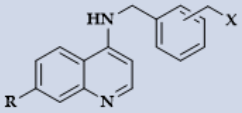
1. Physicochemical Properties		
Molecular weight	396 - 439	288 - 311
Aqueous solubility (μM)	52 - 197	54 - 200
Permeability pH 6.5	Moderate - High	Moderate - High
cLogP (mean)	4.30	3.14
$LogD_{7.4}$	3.15	0.79
2. Biological Activity		
Antiplasmodial Activity (nM)	*Pf*NF54 Mean IC_{50}: 58	*Pf*NF54 Mean IC_{50}: 52
Selectivity Index range	146 - 740	58 - 4984
Microsomal metabolic stability in mice	< 5%	>90%
hERG channel Inhibition IC_{50} (μM)	0.87	3.45 – 3.67
3. Mechanistic Features		
β-haematin Mean IC_{50} (μM)	18.2	19.1
Intracellular inhibition of HZ formation	Yes	Yes

Experimental and *in silico* analyses revealed a significantly improved hERG channel inhibition profile among this set of compounds relative to their parent compounds, and mirrored their reduced molecular weights and lipophilicity. Each metabolite was predicted to possess a reduced risk for hERG channel inhibition compared to its corresponding parent compound and, collectively, the mean pIC_{50} for the metabolites was significantly lower than that of the parent pDBQs (Mean ± SE: 5.29 ± 0.11 vs 6.33 ± 0.05; $p < 0.0001$, unpaired t-test). Experimentally, the metabolites (**10** and **11**) were approximately 5-fold less toxic (Mean IC_{50} ± SD: 3.56 ± 0.16) compared to their parent, **4** (Mean IC_{50} ± SD: 0.87 ± 0.08) or verapamil

(Mean IC_{50} ± SD: 0.56 ± 0.08), and the pIC_{50} equivalents of these experimental IC_{50}s were consistent with predicted values. As a caveat, however, this data is best evaluated in the context of cardiac safety indices which consider these discrete IC_{50} values in the light of the free therapeutic plasma levels of the compounds. These favourable physicochemical and biological features in the metabolites position them as improved molecules relative to the parent compounds (**Table 6.1**).

In an aim to explore non-quinoline scaffolds with potential to inhibit the same HZ formation pathway as CQ-like compounds, investigations were centred on SAR analyses on the frontrunner PBI compound, **15** (**Figure 6.3**).

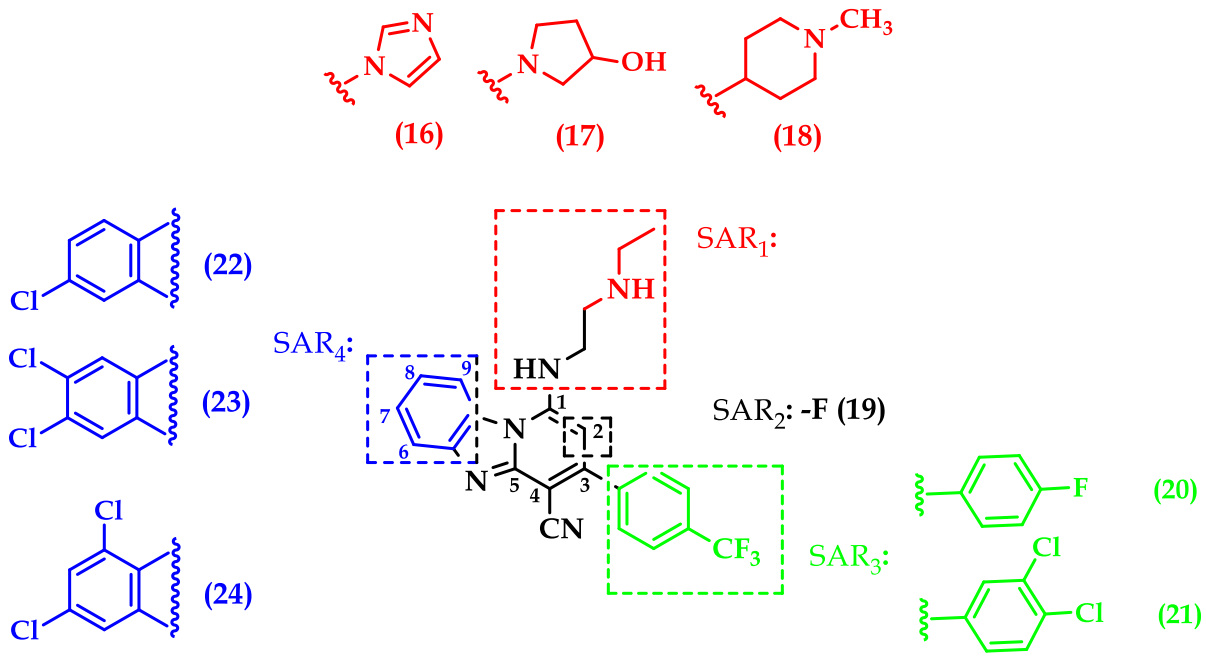

Figure 6.3: Structure of compound **15** showing the different SAR exploration around it

The PBIs tested showed only modest improvement in aqueous solubility, relative to **15** and had moderate lipophilicity with an average LogD value of 3.04 ± 0.18 at pH 7.4. The

compounds similarly had moderate to excellent metabolic stability in mouse and human liver microsomes, particularly **20** and the 3 SAR_4 compounds, **22**, **23** and **24**. All derivatives, except **18,** had submicromolar activity against both CQS and CQR strains, with the SAR_4 derivatives (**22**, **23** and **24**) – bearing halo-substituents on the LHS of the PBI core, showing the best antiplasmodial activity (mean IC_{50} against *Pf*NF54 = 26.7 nM and *Pf*K1 = 30.0 nM) and highest selectivity (188 – 341). Based on antiplasmodial activity, solubility and metabolic stability data, compounds **15**, **23** and **24** were evaluated for *in vivo* efficacy in *P. berghei*-infected mice where **23** and **24** led to >99% suppression of parasitemia and complete cures of the mice. Analysis of the killing kinetics of a select set of derivatives revealed an even distribution in speeds of activity thus highlighting a non-preferential killing signature and hinting at a broad spectrum in activity. Due to their ability to adopt a planar conformation, the PBIs showed βH inhibiting activity though this did not translate into intracellular inhibition of HZ formation in all the derivatives as only two (**15** and **22**) of the five compounds tested exhibited increases in 'free' haem levels that corresponded with reduction in HZ. Since the HZ formation pathway also exists in *S. mansoni*, derivatives were tested for antischistosomal activity against young and adult worms. All the derivatives showed excellent *in vitro* activity against the juvenile worms (Mean IC_{50} ± SE: 1.97 ± 0.36 μM) but were less active against adult worms (Mean IC_{50} ± SE: 4.38 ± 1.49 μM). Additionally, *in vivo* efficacy in *S. mansoni*-infected mice was noted in compound **21** (48% TWR and 41% FWR), suggesting further lead optimisation efforts can potentially deliver derivatives with improved *in vivo* activity.

In conclusion, the pDBQs analysed in this project represent a set of compounds which exhibit potent antiplasmodial activity and target a vulnerable pathway in *P. falciparum* yet are compromised by poor microsomal metabolic stability and potential for cardiotoxicity. The resultant metabolites, on the other hand, appeared to be endowed with improved

features while crucially still retaining the ability to inhibit HZ formation. The metabolites **10** and **11**, in particular, showed good solubility, low lipophilicity, high metabolic stability in MLM and HLM), sub-100 nM potency against CQS and CQR strains as well as an improved hERG toxicity profile compared to their parent. The observed antiplasmodial and antischistosomal properties of the PBIs in this project further confirm and complement the already-known broad antimicrobial potency of this class of compounds. Specifically, compounds **21 – 24** would be of interest for further optimisation due to their high selectivity and *in vivo* antimalarial and antischistosomal efficacy in relevant animal models. The potential hERG inhibiting risk of these compounds would, however, need to be addressed.

6.2. Recommendations for Future Studies

6.2.1. Evaluation of *In vivo* Efficacy of the Metabolites in *P. berghei*-infected models

As earlier shown, the pDBQ metabolites share high structural similarity to phenylequine (PQN) whose hydrochloride salt, in a previous report, showed 100% and 99.5% suppression of parasitemia at 4 x 30mg/kg against *P. berghei* ANKA strain and *P. yoelli*, respectively.[211] It would be worth investigating the *in vivo* efficacy of these metabolites in animal models. Compound **10** (**Figure 6.4**) would be of particular interest since it ranked as the most potent against both *Pf*NF54 and *Pf*Dd2, and its solubility (90 μM), permeability (high) and metabolic stability (>90%) are likely to enhance bioavailability and hence contribute to efficacy. Its high selectivity, second only to compound **8**, also gives it a favourable cytotoxicity profile.

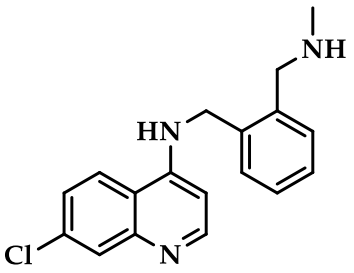

Compound **10**

Solubility**: 90 µM**

Membrane permeability**: High**

Met stability %**: HLM; 98.9** and **MLM; 97**

Antiplasmodial IC_{50} (nM)**:** *Pf*NF54 **- 9.8** and *Pf*Dd2 **- 51.2**

Selectivity Index**: 1,094**

Figure 6.4: Chemical structure and summary physicochemical and biological properties of compound **10** that favour consideration for *in vivo* efficacy testing.

6.2.2. Target Identification in the PBIs

While their ability to adopt a planar architecture possibly allows the PBIs to interact with haem molecules and, in the process, even inhibit formation of HZ formation, this study did not find conclusive evidence that this is the irrefutable MoA of this class of compounds. It would be thus prudent to explore different approaches to identify their genuine targets. Some ideas include;

6.2.2.1. Analysis of stage-specificity.

Coupling the speed of kill experiment with an assay to determine the blood stage specific activity of the PBIs would give insight into whether the compounds are more potent during early (rings) or late stages (trophozoites and schizonts). This is informative in two ways as,

first, it would provide clues as to which proteins the compounds target due to stage-specific expression in the *P. falciparum* proteome.[244] Secondly, it is a window into the potential mechanism of resistance as a particular stage of the parasite may be able to be quiescent to the effect of the drug only to resume growth later, a phenomenon aptly illustrated by quiescent ring stage parasites tolerant to artemisinin.[245]

6.2.2.2. Analysis of DNA Intercalation.

At least at non-physiologically relevant concentrations, CQ can interact with DNA. Using proton nuclear magnetic resonance (H-NMR) technique, CQ was observed to preferentially bond with the double-stranded DNA, with the G-C base pairs as its special binding sites.[246] Though this hypothesis of intercalation no longer holds as the MoA of CQ, it can still be extended to, and tested in, other planar molecules, which might possess a CQ-like ability to intercalate into DNA and compromise replication. A practical approach to investigate this would involve treating parasite-extracted DNA with PBIs followed by polymerase chain reaction (PCR) amplification of the DNA fragment and finally calculating the percent amplification efficiency relative to positive (known DNA binder like centanamycin) and negative (DMSO) controls. Drug: DNA adducts would block *Taq* polymerase activity and prevent amplification by PCR of the treated DNA. An alternative approach would involve staining of nucleic acid with a DNA-specific intercalating dye such as methyl green. Agents that displace methyl green from DNA-methyl green complex, would constitute binders, and can subsequently be detected spectrophotometrically by a decrease in absorbance at 620 nm and loss of colour.[247]

6.2.2.3. Investigation of Inhibition of Permeation Pathways in P. falciparum.

Within the host cell membrane, *P. falciparum* induces new permeation pathways (NPPs) which have the characteristics of anion-selective channels and are permeable to chemically

diverse inorganic and organic ions essential for its survival. Such NPPs are also likely to be crucial for egress of mature parasites from the erythrocyte to facilitate re-invasion. Some antiplasmodial compounds have been shown to inhibit these NPPs (and subsequent haemolysis),[248] and because inhibition of pore-forming proteins constitutes a putative target for PBIs, it would be of interest to test this hypothesis. In theory, since the channels induced in the infected cell membrane would allow in sorbitol when parasitised erythrocytes are suspended in an isosmotic sorbitol solution leading to cell swelling and haemolysis, blockage of these parasite-induced transport channels in *P. falciparum*-infected erythrocytes would demonstrate a mechanistic inhibition property by the PBIs.

6.2.2.4. Drug Affinity Responsive Target Stability (DARTS) Studies

A more holistic and comprehensive strategy involving identification of the target of small molecules through exploiting drug-protein binding interaction without chemical modification is drug affinity responsive target stability (DARTS).[249] This strategy provides a platform where small molecules stabilise their target protein structures, resulting in resistance to protease treatment as depicted in **Figure 6.5**. The PBIs (ligands) would be incubated with parasite lysate (containing global *Plasmodium* proteome) and through negative enrichment, non-target proteins would be degraded by proteolysis leaving behind bound target proteins rendered protease-resistant. Inhibitor and control (vehicle)-treated proteins would be resolved by sodium dodecyl sulphate - polyacrylamide gel electrophoresis (SDS-PAGE) to identify bands whose abundance differ between the inhibitor-treated and control sample - which would then be excised, digested with enzyme (trypsin) and analysed by LC-MS/MS for mass characterisation and potential identification.

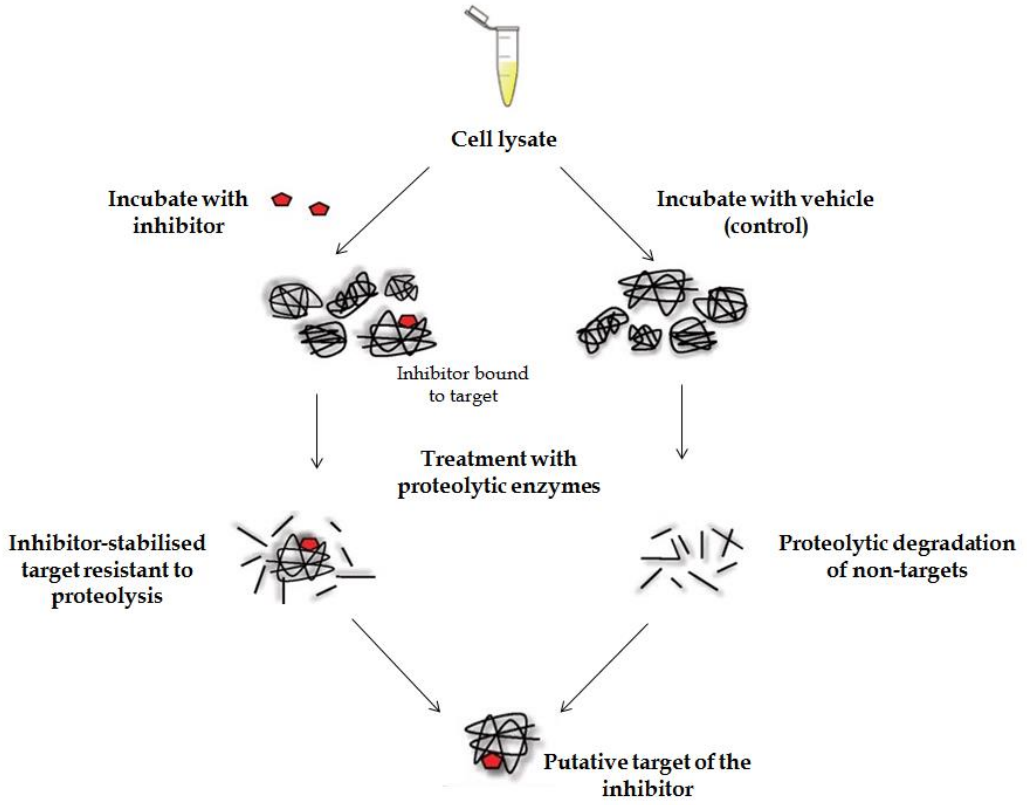

Figure 6.5: Model illustration of DARTS approach whereby cell lysates are incubated with native drug and then treated with proteases. The 'target' proteins are negatively enriched due to their drug-induced protease resistance while non-target proteins are digested away.

6.2.2.5. In vitro Selection of Mutants

This experiment is premised on the hypothesis that the resultant 'resistant' phenotype would be a consequence of gene amplification/deletion or point mutations either in target genes or related ones that offset the mutational costs on the target genes. Drug pressure would therefore be induced using variously substituted PBIs for a specific number of cycles (at least 30) and global genomic changes investigated using whole genome sequencing and real time PCR (RT-PCR) to probe mutations and gene amplification events. The use of different derivatives is argued for on the basis that common mutations observed (if any) would be a consequence of the core scaffold and not the side group modification, and thus represent true reflections of the possible target of the entire class.

Chapter 7

REFERENCES

1. Greenwood, B. M.; Bojang, K.; Whitty, C. J.; Targett, G. A. Malaria. *Lancet* **2005,** *365*, 1487-1498.

2. Ridley, R. G. Medical need, scientific opportunity and the drive for antimalarial drugs. *Nature* **2002,** *415*, 686-693.

3. World Health Organization (WHO). *World Malaria Report 2016*; Geneva, Switzerland (accessed 4th August 2017).

4. World Health Organization (WHO). *World Malaria Report 2015*; Geneva, Switzerland (accessed 4th August 2017).

5. Lindblade, K. A.; Steinhardt, L.; Samuels, A.; Kachur, S. P.; Slutsker, L. The silent threat: asymptomatic parasitemia and malaria transmission. *Expert Rev Anti Infect Ther* **2013,** *11*, 623-639.

6. Baton, L. A.; Ranford-Cartwright, L. C. Spreading the seeds of million-murdering death: metamorphoses of malaria in the mosquito. *Trends Parasitol* **2005,** *21*, 573-580.

7. Francis, S. E.; Sullivan, D. J., Jr.; Goldberg, D. E. Hemoglobin Metabolism in the Malaria Parasite *Plasmodium falciparum*. *Annu. Rev. Microbiol.* **1997,** *51*, 97-123.

8. Greenwood, B. M.; Fidock, D. A.; Kyle, D. E.; Kappe, S. H.; Alonso, P. L.; Collins, F. H.; Duffy, P. E. Malaria: progress, perils, and prospects for eradication. *J Clin Invest* **2008,** *118*, 1266-1276.

9. Tilley, L.; Dixon, M. W.; Kirk, K. The Plasmodium falciparum-infected red blood cell. *Int J Biochem Cell Biol* **2011,** *43*, 839-842.

10. Bannister, L. H.; Mitchell, G. H. The malaria merozoite, forty years on. *Parasitology* **2009,** *136*, 1435-1444.

11. Ginsburg, H. Some reflections concerning host erythrocyte-malarial parasite interrelationships. *Blood Cells* **1990,** *16*, 225-235.

12. Bannister, L. H.; Hopkins, J. M.; Fowler, R. E.; Krishna, S.; Mitchell, G. H. A brief illustrated guide to the ultrastructure of Plasmodium falciparum asexual blood stages. *Parasitol Today* **2000,** *16*, 427-433.

13. Lew, V. L.; Tiffert, T.; Ginsburg, H. Excess hemoglobin digestion and the osmotic stability of Plasmodium falciparum-infected red blood cells. *Blood* **2003,** *101*, 4189-4194.

14. Morrison, D. B.; Jeskey, H. A. Alterations in some constituents of the monkey erythrocyte infected with Plasmodium knowlesi as related to pigment formation. *J Natl Malar Soc* **1948,** *7*, 259-264.

15. Roth, E. F., Jr.; Brotman, D. S.; Vanderberg, J. P.; Schulman, S. Malarial pigment-dependent error in the estimation of hemoglobin content in Plasmodium falciparum-infected red cells: implications for metabolic and biochemical studies of the erythrocytic phases of malaria. *Am J Trop Med Hyg* **1986,** *35*, 906-911.

16. Sherman, I. W. Amino acid metabolism and protein synthesis in malarial parasites. *Bull World Health Organ* **1977,** *55*, 265-276.

17. Dorn, A.; Stoffel, R.; Matile, H.; Bubendorf, A.; Ridley, R. G. Malarial haemozoin/beta-haematin supports haem polymerization in the absence of protein. *Nature* **1995,** *374*, 269-271.

18. Egan, T. J.; Combrinck, J. M.; Egan, J.; Hearne, G. R.; Marques, H. M.; Ntenteni, S.; Sewell, B. T.; Smith, P. J.; Taylor, D.; van Schalkwyk, D. A.; Walden, J. C. Fate of haem iron in the malaria parasite Plasmodium falciparum. *Biochem J* **2002,** *365*, 343-347.

19. Maines, M. D. Heme oxygenase: function, multiplicity, regulatory mechanisms, and clinical applications. *FASEB J* **1988,** *2*, 2557-2568.

20. Tenhunen, R.; Marver, H. S.; Schmid, R. The enzymatic conversion of heme to bilirubin by microsomal heme oxygenase. *Proc Natl Acad Sci U S A* **1968,** *61*, 748-755.

21. Egan, T. J.; Chen, J. Y.; de Villiers, K. A.; Mabotha, T. E.; Naidoo, K. J.; Ncokazi, K. K.; Langford, S. J.; McNaughton, D.; Pandiancherri, S.; Wood, B. R. Haemozoin (beta-haematin)

biomineralization occurs by self-assembly near the lipid/water interface. *FEBS Lett* **2006,** *580*, 5105-5110.

22. Slater, A. F.; Cerami, A. Inhibition by chloroquine of a novel haem polymerase enzyme activity in malaria trophozoites. *Nature* **1992,** *355*, 167-169.

23. Bendrat, K.; Berger, B. J.; Cerami, A. Haem polymerization in malaria. *Nature* **1995,** *378*, 138-139.

24. Sullivan, D. J., Jr.; Gluzman, I. Y.; Goldberg, D. E. Plasmodium hemozoin formation mediated by histidine-rich proteins. *Science* **1996,** *271*, 219-222.

25. Choi, C. Y.; Cerda, J. F.; Chu, H. A.; Babcock, G. T.; Marletta, M. A. Spectroscopic characterization of the heme-binding sites in Plasmodium falciparum histidine-rich protein 2. *Biochemistry* **1999,** *38*, 16916-16924.

26. Sullivan, D. J. Theories on malarial pigment formation and quinoline action. *Int J Parasitol* **2002,** *32*, 1645-1653.

27. Dorn, A.; Vippagunta, S. R.; Matile, H.; Bubendorf, A.; Vennerstrom, J. L.; Ridley, R. G. A comparison and analysis of several ways to promote haematin (haem) polymerisation and an assessment of its initiation in vitro. *Biochem Pharmacol* **1998,** *55*, 737-747.

28. Fitch, C. D.; Cai, G. Z.; Chen, Y. F.; Shoemaker, J. D. Involvement of lipids in ferriprotoporphyrin IX polymerization in malaria. *Biochim Biophys Acta* **1999,** *1454*, 31-37.

29. Tripathi, A. K.; Garg, S. K.; Tekwani, B. L. A physiochemical mechanism of hemozoin (beta-hematin) synthesis by malaria parasite. *Biochem Biophys Res Commun* **2002,** *290*, 595-601.

30. Jackson, K. E.; Klonis, N.; Ferguson, D. J.; Adisa, A.; Dogovski, C.; Tilley, L. Food vacuole-associated lipid bodies and heterogeneous lipid environments in the malaria parasite, Plasmodium falciparum. *Mol Microbiol* **2004,** *54*, 109-122.

31. Palacpac, N. M.; Hiramine, Y.; Mi-ichi, F.; Torii, M.; Kita, K.; Hiramatsu, R.; Horii, T.; Mitamura, T. Developmental-stage-specific triacylglycerol biosynthesis, degradation and

trafficking as lipid bodies in Plasmodium falciparum-infected erythrocytes. *J Cell Sci* **2004,** *117*, 1469-1480.

32. Vielemeyer, O.; McIntosh, M. T.; Joiner, K. A.; Coppens, I. Neutral lipid synthesis and storage in the intraerythrocytic stages of Plasmodium falciparum. *Mol Biochem Parasitol* **2004,** *135*, 197-209.

33. Pisciotta, J. M.; Coppens, I.; Tripathi, A. K.; Scholl, P. F.; Shuman, J.; Bajad, S.; Shulaev, V.; Sullivan, D. J., Jr. The role of neutral lipid nanospheres in Plasmodium falciparum haem crystallization. *Biochem J* **2007,** *402*, 197-204.

34. Ambele, M. A.; Sewell, B. T.; Cummings, F. R.; Smith, P. J.; Egan, T. J. Synthetic Hemozoin (beta-Hematin) Crystals Nucleate at the Surface of Neutral Lipid Droplets that Control Their Sizes. *Cryst Growth Des* **2013,** *13*.

35. Pisciotta, J. M.; Sullivan, D. Hemozoin: oil versus water. *Parasitol Int* **2008,** *57*, 89-96.

36. Jani, D.; Nagarkatti, R.; Beatty, W.; Angel, R.; Slebodnick, C.; Andersen, J.; Kumar, S.; Rathore, D. HDP-a novel heme detoxification protein from the malaria parasite. *PLoS Pathog* **2008,** *4*, e1000053.

37. Chugh, M.; Sundararaman, V.; Kumar, S.; Reddy, V. S.; Siddiqui, W. A.; Stuart, K. D.; Malhotra, P. Protein complex directs hemoglobin-to-hemozoin formation in Plasmodium falciparum. *Proc Natl Acad Sci U S A* **2013,** *110*, 5392-5397.

38. Oliveira, M. F.; d'Avila, J. C.; Torres, C. R.; Oliveira, P. L.; Tempone, A. J.; Rumjanek, F. D.; Braga, C. M.; Silva, J. R.; Dansa-Petretski, M.; Oliveira, M. A.; de Souza, W.; Ferreira, S. T. Haemozoin in Schistosoma mansoni. *Mol Biochem Parasitol* **2000,** *111*, 217-221.

39. Correa Soares, J. B.; Maya-Monteiro, C. M.; Bittencourt-Cunha, P. R.; Atella, G. C.; Lara, F. A.; d'Avila, J. C.; Menezes, D.; Vannier-Santos, M. A.; Oliveira, P. L.; Egan, T. J.; Oliveira, M. F. Extracellular Lipid Droplets Promote Hemozoin Crystallization in the Gut of the Blood Fluke *Schistosoma mansoni*. *FEBS Lett.* **2007,** *581*, 1742-1750.

40. Oliveira, M. F.; Kycia, S. W.; Gomez, A.; Kosar, A. J.; Bohle, D. S.; Hempelmann, E.; Menezes, D.; Vannier-Santos, M. A.; Oliveira, P. L.; Ferreira, S. T. Structural and Morphological Characterization of Hemozoin Produced by *Schistosoma mansoni* and *Rhodnius prolixus*. *FEBS Lett.* **2005,** *579*, 6010-6016.

41. Agnandji, S. T.; Lell, B.; Soulanoudjingar, S. S.; Fernandes, J. F.; Abossolo, B. P.; Conzelmann, C.; Methogo, B. G.; Doucka, Y.; Flamen, A.; Mordmuller, B.; Issifou, S.; Kremsner, P. G.; Sacarlal, J.; Aide, P.; Lanaspa, M.; Aponte, J. J.; Nhamuave, A.; Quelhas, D.; Bassat, Q.; Mandjate, S.; Macete, E.; Alonso, P.; Abdulla, S.; Salim, N.; Juma, O.; Shomari, M.; Shubis, K.; Machera, F.; Hamad, A. S.; Minja, R.; Mtoro, A.; Sykes, A.; Ahmed, S.; Urassa, A. M.; Ali, A. M.; Mwangoka, G.; Tanner, M.; Tinto, H.; D'Alessandro, U.; Sorgho, H.; Valea, I.; Tahita, M. C.; Kabore, W.; Ouedraogo, S.; Sandrine, Y.; Guiguemde, R. T.; Ouedraogo, J. B.; Hamel, M. J.; Kariuki, S.; Odero, C.; Oneko, M.; Otieno, K.; Awino, N.; Omoto, J.; Williamson, J.; Muturi-Kioi, V.; Laserson, K. F.; Slutsker, L.; Otieno, W.; Otieno, L.; Nekoye, O.; Gondi, S.; Otieno, A.; Ogutu, B.; Wasuna, R.; Owira, V.; Jones, D.; Onyango, A. A.; Njuguna, P.; Chilengi, R.; Akoo, P.; Kerubo, C.; Gitaka, J.; Maingi, C.; Lang, T.; Olotu, A.; Tsofa, B.; Bejon, P.; Peshu, N.; Marsh, K.; Owusu-Agyei, S.; Asante, K. P.; Osei-Kwakye, K.; Boahen, O.; Ayamba, S.; Kayan, K.; Owusu-Ofori, R.; Dosoo, D.; Asante, I.; Adjei, G.; Chandramohan, D.; Greenwood, B.; Lusingu, J.; Gesase, S.; Malabeja, A.; Abdul, O.; Kilavo, H.; Mahende, C.; Liheluka, E.; Lemnge, M.; Theander, T.; Drakeley, C.; Ansong, D.; Agbenyega, T.; Adjei, S.; Boateng, H. O.; Rettig, T.; Bawa, J.; Sylverken, J.; Sambian, D.; Agyekum, A.; Owusu, L.; Martinson, F.; Hoffman, I.; Mvalo, T.; Kamthunzi, P.; Nkomo, R.; Msika, A.; Jumbe, A.; Chome, N.; Nyakuipa, D.; Chintedza, J.; Ballou, W. R.; Bruls, M.; Cohen, J.; Guerra, Y.; Jongert, E.; Lapierre, D.; Leach, A.; Lievens, M.; Ofori-Anyinam, O.; Vekemans, J.; Carter, T.; Leboulleux, D.; Loucq, C.; Radford, A.; Savarese, B.; Schellenberg, D.; Sillman, M.; Vansadia, P. First results of phase 3 trial of RTS,S/AS01 malaria vaccine in African children. *N Engl J Med* **2011,** *365*, 1863-1875.

42. Richie, T. L.; Billingsley, P. F.; Sim, B. K.; James, E. R.; Chakravarty, S.; Epstein, J. E.; Lyke, K. E.; Mordmuller, B.; Alonso, P.; Duffy, P. E.; Doumbo, O. K.; Sauerwein, R. W.; Tanner, M.; Abdulla, S.; Kremsner, P. G.; Seder, R. A.; Hoffman, S. L. Progress with Plasmodium falciparum sporozoite (PfSPZ)-based malaria vaccines. *Vaccine* **2015,** *33*, 7452-7461.

43. Dahl, E. L.; Rosenthal, P. J. Apicoplast translation, transcription and genome replication: targets for antimalarial antibiotics. *Trends Parasitol* **2008,** *24*, 279-284.

44. Nzila, A. The past, present and future of antifolates in the treatment of Plasmodium falciparum infection. *J Antimicrob Chemother* **2006,** *57*, 1043-1054.

45. Toovey, S. Mefloquine neurotoxicity: a literature review. *Travel Med Infect Dis* **2009,** *7*, 2-6.

46. Winter, R. W.; Kelly, J. X.; Smilkstein, M. J.; Dodean, R.; Hinrichs, D.; Riscoe, M. K. Antimalarial quinolones: synthesis, potency, and mechanistic studies. *Exp Parasitol* **2008,** *118*, 487-497.

47. Baird, J. K.; Hoffman, S. L. Primaquine therapy for malaria. *Clin Infect Dis* **2004,** *39*, 1336-1345.

48. Rieckmann, K. H.; McNamara, J. V.; Kass, L.; Powell, R. D. Gametocytocidal and sporontocidal effects of primaquine upon two strains of Plasmodium falciparum. *Mil Med* **1969,** *134*, 802-819.

49. Crockett, M.; Kain, K. C. Tafenoquine: a promising new antimalarial agent. *Expert Opin Investig Drugs* **2007,** *16*, 705-715.

50. Llanos-Cuentas, A.; Lacerda, M. V.; Rueangweerayut, R.; Krudsood, S.; Gupta, S. K.; Kochar, S. K.; Arthur, P.; Chuenchom, N.; Mohrle, J. J.; Duparc, S.; Ugwuegbulam, C.; Kleim, J. P.; Carter, N.; Green, J. A.; Kellam, L. Tafenoquine plus chloroquine for the treatment and relapse prevention of Plasmodium vivax malaria (DETECTIVE): a multicentre, double-blind, randomised, phase 2b dose-selection study. *Lancet* **2014,** *383*, 1049-1058.

51. Walsh, D. S.; Looareesuwan, S.; Wilairatana, P.; Heppner, D. G., Jr.; Tang, D. B.; Brewer, T. G.; Chokejindachai, W.; Viriyavejakul, P.; Kyle, D. E.; Milhous, W. K.; Schuster, B. G.; Horton, J.; Braitman, D. J.; Brueckner, R. P. Randomized dose-ranging study of the safety and efficacy of WR 238605 (Tafenoquine) in the prevention of relapse of Plasmodium vivax malaria in Thailand. *J Infect Dis* **1999,** *180*, 1282-1287.

52. Walsh, D. S.; Wilairatana, P.; Tang, D. B.; Heppner, D. G., Jr.; Brewer, T. G.; Krudsood, S.; Silachamroon, U.; Phumratanaprapin, W.; Siriyanonda, D.; Looareesuwan, S. Randomized trial of 3-dose regimens of tafenoquine (WR238605) versus low-dose primaquine for preventing Plasmodium vivax malaria relapse. *Clin Infect Dis* **2004,** *39*, 1095-1103.

53. Wilson, D. W.; Langer, C.; Goodman, C. D.; McFadden, G. I.; Beeson, J. G. Defining the timing of action of antimalarial drugs against Plasmodium falciparum. *Antimicrob Agents Chemother* **2013,** *57*, 1455-1467.

54. Dondorp, A. M.; Nosten, F.; Yi, P.; Das, D.; Phyo, A. P.; Tarning, J.; Lwin, K. M.; Ariey, F.; Hanpithakpong, W.; Lee, S. J.; Ringwald, P.; Silamut, K.; Imwong, M.; Chotivanich, K.; Lim, P.; Herdman, T.; An, S. S.; Yeung, S.; Singhasivanon, P.; Day, N. P.; Lindegardh, N.; Socheat, D.; White, N. J. Artemisinin Resistance in *Plasmodium falciparum* Malaria. *N. Engl. J. Med.* **2009,** *361*, 455-467.

55. Noedl, H.; Se, Y.; Schaecher, K.; Smith, B. L.; Socheat, D.; Fukuda, M. M. Evidence of Artemisinin-resistant Malaria in western Cambodia. *N. Engl. J. Med.* **2008,** *359*, 2619-2620.

56. Lu, F.; Culleton, R.; Zhang, M.; Ramaprasad, A.; von Seidlein, L.; Zhou, H.; Zhu, G.; Tang, J.; Liu, Y.; Wang, W.; Cao, Y.; Xu, S.; Gu, Y.; Li, J.; Zhang, C.; Gao, Q.; Menard, D.; Pain, A.; Yang, H.; Zhang, Q.; Cao, J. Emergence of Indigenous Artemisinin-Resistant Plasmodium falciparum in Africa. *N Engl J Med* **2017,** *376*, 991-993.

57. Foley, M.; Tilley, L. Quinoline antimalarials: mechanisms of action and resistance and prospects for new agents. *Pharmacol Ther* **1998,** *79*, 55-87.

58. Sloboda, A. E.; Powell, D.; Poletto, J. F.; Pickett, W. C.; Gibbons, J. J., Jr.; Bell, D. H.; Oronsky, A. L.; Kerwar, S. S. Antiinflammatory and antiarthritic properties of a substituted quinoline carboxylic acid: CL 306,293. *J Rheumatol* **1991,** *18*, 855-860.

59. Nakamura, T.; Oka, M.; Aizawa, K.; Soda, H.; Fukuda, M.; Terashi, K.; Ikeda, K.; Mizuta, Y.; Noguchi, Y.; Kimura, Y.; Tsuruo, T.; Kohno, S. Direct interaction between a quinoline derivative, MS-209, and multidrug resistance protein (MRP) in human gastric cancer cells. *Biochem Biophys Res Commun* **1999,** *255*, 618-624.

60. de Souza, M. V.; Pais, K. C.; Kaiser, C. R.; Peralta, M. A.; de, L. F. M.; Lourenco, M. C. Synthesis and in vitro antitubercular activity of a series of quinoline derivatives. *Bioorg Med Chem* **2009,** *17*, 1474-1480.

61. Font, M.; Monge, A.; Ruiz, I.; Heras, B. Structure-activity relationships in quinoline Reissert derivatives with HIV-1 reverse transcriptase inhibitory activity. *Drug Des Discov* **1997,** *14*, 259-272.

62. Santos-Magalhaes, N. S.; Mosqueira, V. C. Nanotechnology applied to the treatment of malaria. *Adv Drug Deliv Rev* **2010,** *62*, 560-575.

63. Smith, E. R.; Klein-Schwartz, W. Are 1-2 dangerous? Chloroquine and hydroxychloroquine exposure in toddlers. *J Emerg Med* **2005,** *28*, 437-443.

64. Lind, D. E.; Levi, J. A.; Vincent, P. C. Amodiaquine-induced agranulocytosis: toxic effect of amodiaquine in bone marrow cultures in vitro. *Br Med J* **1973,** *1*, 458-460.

65. Neftel, K. A.; Woodtly, W.; Schmid, M.; Frick, P. G.; Fehr, J. Amodiaquine induced agranulocytosis and liver damage. *Br Med J (Clin Res Ed)* **1986,** *292*, 721-723.

66. Kaur, K.; Jain, M.; Reddy, R. P.; Jain, R. Quinolines and structurally related heterocycles as antimalarials. *Eur J Med Chem* **2010,** *45*, 3245-3264.

67. Arinaitwe, E.; Sandison, T. G.; Wanzira, H.; Kakuru, A.; Homsy, J.; Kalamya, J.; Kamya, M. R.; Vora, N.; Greenhouse, B.; Rosenthal, P. J.; Tappero, J.; Dorsey, G. Artemether-

lumefantrine versus dihydroartemisinin-piperaquine for falciparum malaria: a longitudinal, randomized trial in young Ugandan children. *Clin Infect Dis* **2009,** *49*, 1629-1637.

68. Grande, T.; Bernasconi, A.; Erhart, A.; Gamboa, D.; Casapia, M.; Delgado, C.; Torres, K.; Fanello, C.; Llanos-Cuentas, A.; D'Alessandro, U. A randomised controlled trial to assess the efficacy of dihydroartemisinin-piperaquine for the treatment of uncomplicated falciparum malaria in Peru. *PLoS One* **2007,** *2*, e1101.

69. Tran, T. H.; Dolecek, C.; Pham, P. M.; Nguyen, T. D.; Nguyen, T. T.; Le, H. T.; Dong, T. H.; Tran, T. T.; Stepniewska, K.; White, N. J.; Farrar, J. Dihydroartemisinin-piperaquine against multidrug-resistant Plasmodium falciparum malaria in Vietnam: randomised clinical trial. *Lancet* **2004,** *363*, 18-22.

70. Supan, C.; Mombo-Ngoma, G.; Kombila, M.; Ospina Salazar, C. L.; Held, J.; Lell, B.; Cantalloube, C.; Djeriou, E.; Ogutu, B.; Waitumbi, J.; Otsula, N.; Apollo, D.; Polhemus, M. E.; Kremsner, P. G.; Walsh, D. S. Phase 2a, Open-Label, 4-Escalating-Dose, Randomized Multicenter Study Evaluating the Safety and Activity of Ferroquine (SSR97193) Plus Artesunate, versus Amodiaquine Plus Artesunate, in African Adult Men with Uncomplicated Plasmodium falciparum Malaria. *Am J Trop Med Hyg* **2017,** *97*, 514-525.

71. Chavain, N.; Vezin, H.; Dive, D.; Touati, N.; Paul, J. F.; Buisine, E.; Biot, C. Investigation of the redox behavior of ferroquine, a new antimalarial. *Mol Pharm* **2008,** *5*, 710-716.

72. Ginsburg, H.; Krugliak, M. Quinoline-containing antimalarials--mode of action, drug resistance and its reversal. An update with unresolved puzzles. *Biochem Pharmacol* **1992,** *43*, 63-70.

73. Gyang, F. N.; Poole, B.; Trager, W. Peptidases from Plasmodium falciparum cultured in vitro. *Mol Biochem Parasitol* **1982,** *5*, 263-273.

74. Kwakye-Berko, F.; Meshnick, S. R. Binding of chloroquine to DNA. *Mol Biochem Parasitol* **1989,** *35*, 51-55.

75. Slater, A. F. Chloroquine: mechanism of drug action and resistance in Plasmodium falciparum. *Pharmacol Ther* **1993,** *57*, 203-235.

76. Woodland, J. G.; Hunter, R.; Smith, P. J.; Egan, T. J. Shining new light on ancient drugs: preparation and subcellular localisation of novel fluorescent analogues of Cinchona alkaloids in intraerythrocytic Plasmodium falciparum. *Org Biomol Chem* **2017,** *15*, 589-597.

77. Davidson, M. W.; Griggs, B. G., Jr.; Boykin, D. W.; Wilson, W. D. Mefloquine, a clinically useful quinolinemethanol antimalarial which does not significantly bind to DNA. *Nature* **1975,** *254*, 632-634.

78. Muller, S.; Da'dara, A.; Luersen, K.; Wrenger, C.; Das Gupta, R.; Madhubala, R.; Walter, R. D. In the human malaria parasite Plasmodium falciparum, polyamines are synthesized by a bifunctional ornithine decarboxylase, S-adenosylmethionine decarboxylase. *J Biol Chem* **2000,** *275*, 8097-8102.

79. Konigk, E.; Putfarken, B. Ornithine decarboxylase of Plasmodium falciparum: a peak-function enzyme and its inhibition by chloroquine. *Trop Med Parasitol* **1985,** *36*, 81-84.

80. Van der Zee, J.; Barr, D. P.; Mason, R. P. ESR spin trapping investigation of radical formation from the reaction between hematin and tert-Butyl hydroperoxide. *Free Radic Biol Med* **1996,** *20*, 199-206.

81. Gutteridge, J. M.; Smith, A. Antioxidant protection by haemopexin of haem-stimulated lipid peroxidation. *Biochem J* **1988,** *256*, 861-865.

82. Aft, R. L.; Mueller, G. C. Hemin-mediated oxidative degradation of proteins. *J Biol Chem* **1984,** *259*, 301-305.

83. Aft, R. L.; Mueller, G. C. Hemin-mediated DNA strand scission. *J Biol Chem* **1983,** *258*, 12069-12072.

84. Cohen, S. N.; Phifer, K. O.; Yielding, K. L. Complex Formation between Chloroquine and Ferrihaemic Acid in Vitro, and Its Effect on the Antimalarial Action of Chloroquine. *Nature* **1964,** *202*, 805-806.

85. Egan, T. J.; Ross, D. C.; Adams, P. A. Quinoline anti-malarial drugs inhibit spontaneous formation of beta-haematin (malaria pigment). *FEBS Lett* **1994,** *352*, 54-57.

86. Hawley, S. R.; Bray, P. G.; Mungthin, M.; Atkinson, J. D.; O'Neill, P. M.; Ward, S. A. Relationship between antimalarial drug activity, accumulation, and inhibition of heme polymerization in Plasmodium falciparum in vitro. *Antimicrob Agents Chemother* **1998,** *42*, 682-686.

87. Ginsburg, H.; Famin, O.; Zhang, J.; Krugliak, M. Inhibition of glutathione-dependent degradation of heme by chloroquine and amodiaquine as a possible basis for their antimalarial mode of action. *Biochem Pharmacol* **1998,** *56*, 1305-1313.

88. Loria, P.; Miller, S.; Foley, M.; Tilley, L. Inhibition of the peroxidative degradation of haem as the basis of action of chloroquine and other quinoline antimalarials. *Biochem J* **1999,** *339 (Pt 2)*, 363-370.

89. Combrinck, J. M.; Mabotha, T. E.; Ncokazi, K. K.; Ambele, M. A.; Taylor, D.; Smith, P. J.; Hoppe, H. C.; Egan, T. J. Insights Into The Role of Heme in the Mechanism of Action of Antimalarials. *ACS Chem. Biol.* **2013,** *8*, 133-137.

90. de Villiers, K. A.; Marques, H. M.; Egan, T. J. The Crystal Structure of Halofantrine-Ferriprotoporphyrin IX and the Mechanism of Action of Arylmethanol Antimalarials. *J. Inorg. Biochem.* **2008,** *102*, 1660-1667.

91. Geary, T. G.; Jensen, J. B.; Ginsburg, H. Uptake of [3H]chloroquine by drug-sensitive and -resistant strains of the human malaria parasite Plasmodium falciparum. *Biochem Pharmacol* **1986,** *35*, 3805-3812.

92. Ginsburg, H.; Nissani, E.; Krugliak, M. Alkalinization of the food vacuole of malaria parasites by quinoline drugs and alkylamines is not correlated with their antimalarial activity. *Biochem Pharmacol* **1989,** *38*, 2645-2654.

93. Fitch, C. D.; Yunis, N. G.; Chevli, R.; Gonzalez, Y. High-affinity accumulation of chloroquine by mouse erythrocytes infected with Plasmodium berghei. *J Clin Invest* **1974,** *54*, 24-33.

94. Yayon, A.; Cabantchik, Z. I.; Ginsburg, H. Identification of the acidic compartment of Plasmodium falciparum-infected human erythrocytes as the target of the antimalarial drug chloroquine. *Embo J* **1984,** *3*, 2695-2700.

95. Chou, A. C.; Chevli, R.; Fitch, C. D. Ferriprotoporphyrin IX fulfills the criteria for identification as the chloroquine receptor of malaria parasites. *Biochemistry* **1980,** *19*, 1543-1549.

96. Ncokazi, K. K.; Egan, T. J. A colorimetric high-throughput beta-hematin inhibition screening assay for use in the search for antimalarial compounds. *Anal Biochem* **2005,** *338*, 306-319.

97. Carter, M. D.; Phelan, V. V.; Sandlin, R. D.; Bachmann, B. O.; Wright, D. W. Lipophilic mediated assays for beta-hematin inhibitors. *Comb Chem High Throughput Screen* **2010,** *13*, 285-292.

98. Combrinck, J. M.; Fong, K. Y.; Gibhard, L.; Smith, P. J.; Wright, D. W.; Egan, T. J. Optimization of a multi-well colorimetric assay to determine haem species in Plasmodium falciparum in the presence of anti-malarials. *Malar J* **2015,** *14*, 253.

99. Egan, T. J.; Hunter, R.; Kaschula, C. H.; Marques, H. M.; Misplon, A.; Walden, J. Structure-Function Relationships in Aminoquinolines: Effect of Amino and Chloro Groups on Quinoline-Hematin Complex Formation, Inhibition of Beta-hematin Formation, and Antiplasmodial Activity. *J. Med. Chem.* **2000,** *43*, 283-291.

100. Kaschula, C. H.; Egan, T. J.; Hunter, R.; Basilico, N.; Parapini, S.; Taramelli, D.; Pasini, E.; Monti, D. Structure-activity relationships in 4-aminoquinoline antiplasmodials. The role of the group at the 7-position. *J Med Chem* **2002,** *45*, 3531-3539.

101. Iwaniuk, D. P.; Whetmore, E. D.; Rosa, N.; Ekoue-Kovi, K.; Alumasa, J.; de Dios, A. C.; Roepe, P. D.; Wolf, C. Synthesis and antimalarial activity of new chloroquine analogues carrying a multifunctional linear side chain. *Bioorg Med Chem* **2009,** *17*, 6560-6566.

102. Natarajan, J. K.; Alumasa, J. N.; Yearick, K.; Ekoue-Kovi, K. A.; Casabianca, L. B.; de Dios, A. C.; Wolf, C.; Roepe, P. D. 4-N-, 4-S-, and 4-O-chloroquine analogues: influence of side chain length and quinolyl nitrogen pKa on activity vs chloroquine resistant malaria. *J Med Chem* **2008,** *51*, 3466-3479.

103. De, D.; Krogstad, F. M.; Byers, L. D.; Krogstad, D. J. Structure-activity relationships for antiplasmodial activity among 7-substituted 4-aminoquinolines. *J Med Chem* **1998,** *41*, 4918-4926.

104. Stocks, P. A.; Raynes, K. J.; Bray, P. G.; Park, B. K.; O'Neill, P. M.; Ward, S. A. Novel short chain chloroquine analogues retain activity against chloroquine resistant K1 Plasmodium falciparum. *J Med Chem* **2002,** *45*, 4975-4983.

105. Cheruku, S. R.; Maiti, S.; Dorn, A.; Scorneaux, B.; Bhattacharjee, A. K.; Ellis, W. Y.; Vennerstrom, J. L. Carbon isosteres of the 4-aminopyridine substructure of chloroquine: effects on pK(a), hematin binding, inhibition of hemozoin formation, and parasite growth. *J Med Chem* **2003,** *46*, 3166-3169.

106. Payne, D. Spread of chloroquine resistance in Plasmodium falciparum. *Parasitol Today* **1987,** *3*, 241-246.

107. Fidock, D. A.; Nomura, T.; Talley, A. K.; Cooper, R. A.; Dzekunov, S. M.; Ferdig, M. T.; Ursos, L. M.; Sidhu, A. B.; Naude, B.; Deitsch, K. W.; Su, X. Z.; Wootton, J. C.; Roepe, P. D.; Wellems, T. E. Mutations in the P. falciparum digestive vacuole transmembrane protein PfCRT and evidence for their role in chloroquine resistance. *Mol Cell* **2000,** *6*, 861-871.

108. Sidhu, A. B.; Verdier-Pinard, D.; Fidock, D. A. Chloroquine resistance in Plasmodium falciparum malaria parasites conferred by pfcrt mutations. *Science* **2002,** *298*, 210-213.

109. Summers, R. L.; Nash, M. N.; Martin, R. E. Know your enemy: understanding the role of PfCRT in drug resistance could lead to new antimalarial tactics. *Cell Mol Life Sci* **2012,** *69*, 1967-1995.

110. Krogstad, D. J.; Gluzman, I. Y.; Kyle, D. E.; Oduola, A. M.; Martin, S. K.; Milhous, W. K.; Schlesinger, P. H. Efflux of chloroquine from Plasmodium falciparum: mechanism of chloroquine resistance. *Science* **1987,** *238*, 1283-1285.

111. Lakshmanan, V.; Bray, P. G.; Verdier-Pinard, D.; Johnson, D. J.; Horrocks, P.; Muhle, R. A.; Alakpa, G. E.; Hughes, R. H.; Ward, S. A.; Krogstad, D. J.; Sidhu, A. B.; Fidock, D. A. A critical role for PfCRT K76T in Plasmodium falciparum verapamil-reversible chloroquine resistance. *Embo J* **2005,** *24*, 2294-2305.

112. Bray, P. G.; Mungthin, M.; Hastings, I. M.; Biagini, G. A.; Saidu, D. K.; Lakshmanan, V.; Johnson, D. J.; Hughes, R. H.; Stocks, P. A.; O'Neill, P. M.; Fidock, D. A.; Warhurst, D. C.; Ward, S. A. PfCRT and the trans-vacuolar proton electrochemical gradient: regulating the access of chloroquine to ferriprotoporphyrin IX. *Mol Microbiol* **2006,** *62*, 238-251.

113. Reed, M. B.; Saliba, K. J.; Caruana, S. R.; Kirk, K.; Cowman, A. F. Pgh1 modulates sensitivity and resistance to multiple antimalarials in Plasmodium falciparum. *Nature* **2000,** *403*, 906-909.

114. Koenderink, J. B.; Kavishe, R. A.; Rijpma, S. R.; Russel, F. G. The ABCs of multidrug resistance in malaria. *Trends Parasitol* **2010,** *26*, 440-446.

115. Cowman, A. F.; Galatis, D.; Thompson, J. K. Selection for mefloquine resistance in Plasmodium falciparum is linked to amplification of the pfmdr1 gene and cross-resistance to halofantrine and quinine. *Proc Natl Acad Sci U S A* **1994,** *91*, 1143-1147.

116. Pickard, A. L.; Wongsrichanalai, C.; Purfield, A.; Kamwendo, D.; Emery, K.; Zalewski, C.; Kawamoto, F.; Miller, R. S.; Meshnick, S. R. Resistance to antimalarials in Southeast Asia and genetic polymorphisms in pfmdr1. *Antimicrob Agents Chemother* **2003,** *47*, 2418-2423.

117. Price, R. N.; Uhlemann, A. C.; Brockman, A.; McGready, R.; Ashley, E.; Phaipun, L.; Patel, R.; Laing, K.; Looareesuwan, S.; White, N. J.; Nosten, F.; Krishna, S. Mefloquine resistance in Plasmodium falciparum and increased pfmdr1 gene copy number. *Lancet* **2004,** *364*, 438-447.

118. Holmgren, G.; Gil, J. P.; Ferreira, P. M.; Veiga, M. I.; Obonyo, C. O.; Bjorkman, A. Amodiaquine resistant Plasmodium falciparum malaria in vivo is associated with selection of pfcrt 76T and pfmdr1 86Y. *Infect Genet Evol* **2006,** *6*, 309-314.

119. Warhurst, D. C.; Craig, J. C.; Adagu, I. S.; Guy, R. K.; Madrid, P. B.; Fivelman, Q. L. Activity of Piperaquine and other 4-Aminoquinoline Antiplasmodial Drugs against Chloroquine-sensitive and resistant Blood-stages of *Plasmodium falciparum*. Role of Beta-haematin Inhibition and Drug Concentration in Vacuolar Water- and Lipid-phases. *Biochem. Pharmacol.* **2007,** *73*, 1910-1926.

120. Sa, J. M.; Twu, O.; Hayton, K.; Reyes, S.; Fay, M. P.; Ringwald, P.; Wellems, T. E. Geographic patterns of Plasmodium falciparum drug resistance distinguished by differential responses to amodiaquine and chloroquine. *Proc Natl Acad Sci U S A* **2009,** *106*, 18883-18889.

121. Burgess, S. J.; Selzer, A.; Kelly, J. X.; Smilkstein, M. J.; Riscoe, M. K.; Peyton, D. H. A chloroquine-like molecule designed to reverse resistance in Plasmodium falciparum. *J Med Chem* **2006,** *49*, 5623-5625.

122. Guan, J.; Kyle, D. E.; Gerena, L.; Zhang, Q.; Milhous, W. K.; Lin, A. J. Design, synthesis, and evaluation of new chemosensitizers in multi-drug-resistant Plasmodium falciparum. *J Med Chem* **2002,** *45*, 2741-2748.

123. van Schalkwyk, D. A.; Walden, J. C.; Smith, P. J. Reversal of chloroquine resistance in Plasmodium falciparum using combinations of chemosensitizers. *Antimicrob Agents Chemother* **2001,** *45*, 3171-3174.

124. Kyle, D. E.; Milhous, W. K.; Rossan, R. N. Reversal of Plasmodium falciparum resistance to chloroquine in Panamanian Aotus monkeys. *Am J Trop Med Hyg* **1993,** *48*, 126-133.

125. Oduola, A. M.; Sowunmi, A.; Milhous, W. K.; Brewer, T. G.; Kyle, D. E.; Gerena, L.; Rossan, R. N.; Salako, L. A.; Schuster, B. G. In vitro and in vivo reversal of chloroquine resistance in Plasmodium falciparum with promethazine. *Am J Trop Med Hyg* **1998,** *58*, 625-629.

126. Bhattacharjee, A. K.; Kyle, D. E.; Vennerstrom, J. L.; Milhous, W. K. A 3D QSAR pharmacophore model and quantum chemical structure--activity analysis of chloroquine(CQ)-resistance reversal. *J Chem Inf Comput Sci* **2002,** *42*, 1212-1220.

127. Zishiri, V. K.; Joshi, M. C.; Hunter, R.; Chibale, K.; Smith, P. J.; Summers, R. L.; Martin, R. E.; Egan, T. J. Quinoline antimalarials containing a dibemethin group are active against chloroquinone-resistant Plasmodium falciparum and inhibit chloroquine transport via the P. falciparum chloroquine-resistance transporter (PfCRT). *J Med Chem* **2011,** *54*, 6956-6968.

128. Warhurst, D. C. Polymorphism in the Plasmodium falciparum chloroquine-resistance transporter protein links verapamil enhancement of chloroquine sensitivity with the clinical efficacy of amodiaquine. *Malar J* **2003,** *2*, 31.

129. October, N.; Watermeyer, N. D.; Yardley, V.; Egan, T. J.; Ncokazi, K.; Chibale, K. Reversed Chloroquines Based on the 3,4-dihydropyrimidin-2(1H)-one Scaffold: Synthesis and Evaluation for Antimalarial, Beta-haematin Inhibition, and Cytotoxic Activity. *ChemMedChem* **2008,** *3*, 1649-1653.

130. Musonda, C. C.; Whitlock, G. A.; Witty, M. J.; Brun, R.; Kaiser, M. Chloroquine-astemizole hybrids with potent in vitro and in vivo antiplasmodial activity. *Bioorg Med Chem Lett* **2009,** *19*, 481-484.

131. Solaja, B. A.; Opsenica, D.; Smith, K. S.; Milhous, W. K.; Terzic, N.; Opsenica, I.; Burnett, J. C.; Nuss, J.; Gussio, R.; Bavari, S. Novel 4-aminoquinolines active against chloroquine-resistant and sensitive P. falciparum strains that also inhibit botulinum serotype A. *J Med Chem* **2008,** *51*, 4388-4391.

132. Kumar, A.; Srivastava, K.; Kumar, S. R.; Puri, S. K.; Chauhan, P. M. Synthesis of new 4-aminoquinolines and quinoline-acridine hybrids as antimalarial agents. *Bioorg Med Chem Lett* **2010,** *20*, 7059-7063.

133. Wirjanata, G.; Sebayang, B. F.; Chalfein, F.; Prayoga; Handayuni, I.; Noviyanti, R.; Kenangalem, E.; Poespoprodjo, J. R.; Burgess, S. J.; Peyton, D. H.; Price, R. N.; Marfurt, J. Contrasting ex vivo efficacies of "reversed chloroquine" compounds in chloroquine-resistant Plasmodium falciparum and P. vivax isolates. *Antimicrob Agents Chemother* **2015,** *59*, 5721-5726.

134. Gunsaru, B.; Burgess, S. J.; Morrill, W.; Kelly, J. X.; Shomloo, S.; Smilkstein, M. J.; Liebman, K.; Peyton, D. H. Simplified Reversed Chloroquines To Overcome Malaria Resistance to Quinoline-Based Drugs. *Antimicrob Agents Chemother* **2017,** *61*.

135. Lehane, A. M.; Hayward, R.; Saliba, K. J.; Kirk, K. A verapamil-sensitive chloroquine-associated H+ leak from the digestive vacuole in chloroquine-resistant malaria parasites. *J Cell Sci* **2008,** *121*, 1624-1632.

136. Sandlin, R. D.; Carter, M. D.; Lee, P. J.; Auschwitz, J. M.; Leed, S. E.; Johnson, J. D.; Wright, D. W. Use of the NP-40 detergent-mediated assay in discovery of inhibitors of beta-hematin crystallization. *Antimicrob Agents Chemother* **2011,** *55*, 3363-3369.

137. Sandlin, R. D.; Fong, K. Y.; Wicht, K. J.; Carrell, H. M.; Egan, T. J.; Wright, D. W. Identification of beta-hematin inhibitors in a high-throughput screening effort reveals scaffolds with in vitro antimalarial activity. *Int J Parasitol Drugs Drug Resist* **2014,** *4*, 316-325.

138. Guiguemde, W. A.; Shelat, A. A.; Bouck, D.; Duffy, S.; Crowther, G. J.; Davis, P. H.; Smithson, D. C.; Connelly, M.; Clark, J.; Zhu, F.; Jimenez-Diaz, M. B.; Martinez, M. S.;

Wilson, E. B.; Tripathi, A. K.; Gut, J.; Sharlow, E. R.; Bathurst, I.; El Mazouni, F.; Fowble, J. W.; Forquer, I.; McGinley, P. L.; Castro, S.; Angulo-Barturen, I.; Ferrer, S.; Rosenthal, P. J.; Derisi, J. L.; Sullivan, D. J.; Lazo, J. S.; Roos, D. S.; Riscoe, M. K.; Phillips, M. A.; Rathod, P. K.; Van Voorhis, W. C.; Avery, V. M.; Guy, R. K. Chemical Genetics of *Plasmodium falciparum*. *Nature* **2010,** *465*, 311-315.

139. Heikkila, T.; Ramsey, C.; Davies, M.; Galtier, C.; Stead, A. M.; Johnson, A. P.; Fishwick, C. W.; Boa, A. N.; McConkey, G. A. Design and synthesis of potent inhibitors of the malaria parasite dihydroorotate dehydrogenase. *J Med Chem* **2007,** *50*, 186-191.

140. Fong, K. Y.; Sandlin, R. D.; Wright, D. W. Identification of beta-hematin inhibitors in the MMV Malaria Box. *Int J Parasitol Drugs Drug Resist* **2015,** *5*, 84-91.

141. White, N. J. Cardiotoxicity of antimalarial drugs. *Lancet Infect Dis* **2007,** *7*, 549-558.

142. Chu, K. A.; Yalkowsky, S. H. An interesting relationship between drug absorption and melting point. *Int J Pharm* **2009,** *373*, 24-40.

143. Biot, C.; Taramelli, D.; Forfar-Bares, I.; Maciejewski, L. A.; Boyce, M.; Nowogrocki, G.; Brocard, J. S.; Basilico, N.; Olliaro, P.; Egan, T. J. Insights into the mechanism of action of ferroquine. Relationship between physicochemical properties and antiplasmodial activity. *Mol Pharm* **2005,** *2*, 185-193.

144. Gleeson, M. P. Generation of a set of simple, interpretable ADMET rules of thumb. *J Med Chem* **2008,** *51*, 817-834.

145. Ermondi, G.; Visentin, S.; Caron, G. GRIND-based 3D-QSAR and CoMFA to investigate topics dominated by hydrophobic interactions: the case of hERG K+ channel blockers. *Eur J Med Chem* **2009,** *44*, 1926-1932.

146. Curran, M. E.; Splawski, I.; Timothy, K. W.; Vincent, G. M.; Green, E. D.; Keating, M. T. A molecular basis for cardiac arrhythmia: HERG mutations cause long QT syndrome. *Cell* **1995,** *80*, 795-803.

147. Waring, M. J.; Johnstone, C. A quantitative assessment of hERG liability as a function of lipophilicity. *Bioorg Med Chem Lett* **2007,** *17*, 1759-1764.

148. Siramshetty, V. B.; Nickel, J.; Omieczynski, C.; Gohlke, B. O.; Drwal, M. N.; Preissner, R. WITHDRAWN--a resource for withdrawn and discontinued drugs. *Nucleic Acids Res* **2016,** *44*, D1080-1086.

149. Cavalli, A.; Poluzzi, E.; De Ponti, F.; Recanatini, M. Toward a pharmacophore for drugs inducing the long QT syndrome: insights from a CoMFA study of HERG K(+) channel blockers. *J Med Chem* **2002,** *45*, 3844-3853.

150. Pearlstein, R. A.; Vaz, R. J.; Kang, J.; Chen, X. L.; Preobrazhenskaya, M.; Shchekotikhin, A. E.; Korolev, A. M.; Lysenkova, L. N.; Miroshnikova, O. V.; Hendrix, J.; Rampe, D. Characterization of HERG potassium channel inhibition using CoMSiA 3D QSAR and homology modeling approaches. *Bioorg Med Chem Lett* **2003,** *13*, 1829-1835.

151. Clemessy, J. L.; Favier, C.; Borron, S. W.; Hantson, P. E.; Vicaut, E.; Baud, F. J. Hypokalaemia related to acute chloroquine ingestion. *Lancet* **1995,** *346*, 877-880.

152. Kang, J.; Chen, X. L.; Wang, L.; Rampe, D. Interactions of the antimalarial drug mefloquine with the human cardiac potassium channels KvLQT1/minK and HERG. *J Pharmacol Exp Ther* **2001,** *299*, 290-296.

153. Cavero, I.; Mestre, M.; Guillon, J. M.; Crumb, W. Drugs that prolong QT interval as an unwanted effect: assessing their likelihood of inducing hazardous cardiac dysrhythmias. *Expert Opin Pharmacother* **2000,** *1*, 947-973.

154. Webster, R.; Leishman, D.; Walker, D. Towards a drug concentration effect relationship for QT prolongation and torsades de pointes. *Curr Opin Drug Discov Devel* **2002,** *5*, 116-126.

155. Traebert, M.; Dumotier, B.; Meister, L.; Hoffmann, P.; Dominguez-Estevez, M.; Suter, W. Inhibition of hERG K+ currents by antimalarial drugs in stably transfected HEK293 cells. *Eur J Pharmacol* **2004,** *484*, 41-48.

156. Andrews, S.; Burgess, S. J.; Skaalrud, D.; Kelly, J. X.; Peyton, D. H. Reversal agent and linker variants of reversed chloroquines: activities against Plasmodium falciparum. *J Med Chem* **2010,** *53*, 916-919.

157. Burgess, S. J.; Kelly, J. X.; Shomloo, S.; Wittlin, S.; Brun, R.; Liebmann, K.; Peyton, D. H. Synthesis, structure-activity relationship, and mode-of-action studies of antimalarial reversed chloroquine compounds. *J Med Chem* **2010,** *53*, 6477-6489.

158. Zishiri, V. K.; Hunter, R.; Smith, P. J.; Taylor, D.; Summers, R.; Kirk, K.; Martin, R. E.; Egan, T. J. A series of structurally simple chloroquine chemosensitizing dibemethin derivatives that inhibit chloroquine transport by PfCRT. *Eur J Med Chem* **2011,** *46*, 1729-1742.

159. Bansal, Y.; Silakari, O. The therapeutic journey of benzimidazoles: a review. *Bioorg Med Chem* **2012,** *20*, 6208-6236.

160. Keller, P.; Muller, C.; Engelhardt, I.; Hiller, E.; Lemuth, K.; Eickhoff, H.; Wiesmuller, K. H.; Burger-Kentischer, A.; Bracher, F.; Rupp, S. An Antifungal Benzimidazole Derivative Inhibits Ergosterol Biosynthesis and Reveals Novel Sterols. *Antimicrob Agents Chemother* **2015,** *59*, 6296-6307.

161. Pan, T.; He, X.; Chen, B.; Chen, H.; Geng, G.; Luo, H.; Zhang, H.; Bai, C. Development of benzimidazole derivatives to inhibit HIV-1 replication through protecting APOBEC3G protein. *Eur J Med Chem* **2015,** *95*, 500-513.

162. Chandrasekera, N. S.; Alling, T.; Bailey, M. A.; Files, M.; Early, J. V.; Ollinger, J.; Ovechkina, Y.; Masquelin, T.; Desai, P. V.; Cramer, J. W.; Hipskind, P. A.; Odingo, J. O.; Parish, T. Identification of Phenoxyalkylbenzimidazoles with Antitubercular Activity. *J Med Chem* **2015,** *58*, 7273-7285.

163. Pieroni, M.; Tipparaju, S. K.; Lun, S.; Song, Y.; Sturm, A. W.; Bishai, W. R.; Kozikowski, A. P. Pyrido[1,2-a]benzimidazole-based agents active against tuberculosis (TB), multidrug-resistant (MDR) TB and extensively drug-resistant (XDR) TB. *ChemMedChem* **2011,** *6*, 334-342.

164. Hayashi, S.; Hirao, A.; Nakamura, H.; Yamamura, K.; Mizuno, K.; Yamashita, H. Discovery of 1-[1-(1-methylcyclooctyl)-4-piperidinyl]-2-[(3R)-3-piperidinyl]-1H-benzimidazole: integrated drug-design and structure-activity relationships for orally potent, metabolically stable and potential-risk reduced novel non-peptide nociceptin/orphanin FQ receptor agonist as antianxiety drug. *Chem Biol Drug Des* **2009,** *74*, 369-381.

165. Keri, R. S.; Hiremathad, A.; Budagumpi, S.; Nagaraja, B. M. Comprehensive Review in Current Developments of Benzimidazole-Based Medicinal Chemistry. *Chem. Biol. Drug. Des.* **2015,** *86*, 19-65.

166. Keurulainen, L.; Vahermo, M.; Puente-Felipe, M.; Sandoval-Izquierdo, E.; Crespo-Fernandez, B.; Guijarro-Lopez, L.; Huertas-Valentin, L.; de las Heras-Duena, L.; Leino, T. O.; Siiskonen, A.; Ballell-Pages, L.; Sanz, L. M.; Castaneda-Casado, P.; Jimenez-Diaz, M. B.; Martinez-Martinez, M. S.; Viera, S.; Kiuru, P.; Calderon, F.; Yli-Kauhaluoma, J. A Developability-Focused Optimization Approach Allows Identification of in Vivo Fast-Acting Antimalarials: N-[3-[(Benzimidazol-2-yl)amino]propyl]amides. *J. Med. Chem.* **2015,** *58*, 4573-4580.

167. Saify, Z. S.; Azim, M. K.; Ahmad, W.; Nisa, M.; Goldberg, D. E.; Hussain, S. A.; Akhtar, S.; Akram, A.; Arayne, A.; Oksman, A.; Khan, I. A. New Benzimidazole Derivatives as Antiplasmodial Agents and Plasmepsin Inhibitors: Synthesis and Analysis of Structure-Activity Relationships. *Bioorg. Med. Chem. Lett.* **2012,** *22*, 1282-1286.

168. Camacho, J.; Barazarte, A.; Gamboa, N.; Rodrigues, J.; Rojas, R.; Vaisberg, A.; Gilman, R.; Charris, J. Synthesis and Biological Evaluation of Benzimidazole-5-carbohydrazide Derivatives as Antimalarial, Cytotoxic and Antitubercular Agents. *Bioorg. Med. Chem.* **2011,** *19*, 2023-2029.

169. Rida, S.; Farid, S.; El-Sayed, B. B.; El-Ghazzawi, E.; Kader, O.; Kappe, T. Benzimidazole Condensed Ring Systems. 1. Syntheses and Biological Investigations of Some Substituted Pyrido[1,2-a]benzimidazoles. *J. Heterocycl. Chem.* **1988,** *25*, 1087-1093.

170. Ndakala, A. J.; Gessner, R. K.; Gitari, P. W.; October, N.; White, K. L.; Hudson, A.; Fakorede, F.; Shackleford, D. M.; Kaiser, M.; Yeates, C.; Charman, S. A.; Chibale, K. Antimalarial Pyrido[1,2-a]benzimidazoles. *J. Med. Chem.* **2011,** *54*, 4581-4589.

171. Ishikawa, M.; Hashimoto, Y. Improvement in Aqueous Solubility in Small Molecule Drug Discovery Programs by Disruption of Molecular Planarity and Symmetry. *J. Med. Chem.* **2011,** *54*, 1539-1554.

172. Trager, W.; Jensen, J. B. Human malaria parasites in continuous culture. *Science* **1976,** *193*, 673-675.

173. Lambros, C.; Vanderberg, J. P. Synchronization of Plasmodium falciparum erythrocytic stages in culture. *J Parasitol* **1979,** *65*, 418-420.

174. Makler, M. T.; Ries, J. M.; Williams, J. A.; Bancroft, J. E.; Piper, R. C.; Gibbins, B. L.; Hinrichs, D. J. Parasite lactate dehydrogenase as an assay for Plasmodium falciparum drug sensitivity. *Am J Trop Med Hyg* **1993,** *48*, 739-741.

175. Mosmann, T. Rapid Colorimetric Assay for Cellular Growth and Survival: Application to Proliferation and Cytotoxicity Assays. *J. Immunol. Methods.* **1983,** *65*, 55-63.

176. Di, L.; Kerns, E. H.; Gao, N.; Li, S. Q.; Huang, Y.; Bourassa, J. L.; Huryn, D. M. Experimental design on single-time-point high-throughput microsomal stability assay. *J Pharm Sci* **2004,** *93*, 1537-1544.

177. Bei, A. K.; Desimone, T. M.; Badiane, A. S.; Ahouidi, A. D.; Dieye, T.; Ndiaye, D.; Sarr, O.; Ndir, O.; Mboup, S.; Duraisingh, M. T. A flow cytometry-based assay for measuring invasion of red blood cells by Plasmodium falciparum. *Am J Hematol* **2010,** *85*, 234-237.

178. Jimenez-Diaz, M. B.; Mulet, T.; Gomez, V.; Viera, S.; Alvarez, A.; Garuti, H.; Vazquez, Y.; Fernandez, A.; Ibanez, J.; Jimenez, M.; Gargallo-Viola, D.; Angulo-Barturen, I. Quantitative measurement of Plasmodium-infected erythrocytes in murine models of malaria by flow cytometry using bidimensional assessment of SYTO-16 fluorescence. *Cytometry A* **2009,** *75*, 225-235.

179. Jun, G.; Lee, J. S.; Jung, Y. J.; Park, J. W. Quantitative determination of Plasmodium parasitemia by flow cytometry and microscopy. *J Korean Med Sci* **2012,** *27*, 1137-1142.

180. Le Manach, C.; Scheurer, C.; Sax, S.; Schleiferbock, S.; Cabrera, D. G.; Younis, Y.; Paquet, T.; Street, L.; Smith, P.; Ding, X. C.; Waterson, D.; Witty, M. J.; Leroy, D.; Chibale, K.; Wittlin, S. Fast In Vitro Methods to Determine The Speed of Action and the Stage-specificity of Anti-malarials in *Plasmodium falciparum*. *Malar. J.* **2013,** *12*, 424-430.

181. Manneck, T.; Haggenmuller, Y.; Keiser, J. Morphological Effects and Tegumental Alterations Induced by Mefloquine on Schistosomula and Adult Flukes of *Schistosoma mansoni*. *Parasitology.* **2010,** *137*, 85-98.

182. Hill, A. P.; Young, R. J. Getting Physical in Drug Discovery: A Contemporary Perspective on Solubility and Hydrophobicity. *Drug Discov. Today.* **2010,** *15*, 648-655.

183. Joubert, J.; Fortuin, E. E.; Taylor, D.; Smith, P. J.; Malan, S. F. Pentacycloundecylamines and conjugates thereof as chemosensitizers and reversed chloroquine agents. *Bioorg Med Chem Lett* **2014,** *24*, 5516-5519.

184. Lipinski, C. A.; Lombardo, F.; Dominy, B. W.; Feeney, P. J. Experimental and computational approaches to estimate solubility and permeability in drug discovery and development settings. *Adv Drug Deliv Rev* **2001,** *46*, 3-26.

185. Wexler, D. S.; Gao, L.; Anderson, F.; Ow, A.; Nadasdi, L.; McAlorum, A.; Urfer, R.; Huang, S. G. Linking solubility and permeability assays for maximum throughput and reproducibility. *J Biomol Screen* **2005,** *10*, 383-390.

186. Gulyaeva, N.; Zaslavsky, A.; Lechner, P.; Chlenov, M.; Chait, A.; Zaslavsky, B. Relative hydrophobicity and lipophilicity of beta-blockers and related compounds as measured by aqueous two-phase partitioning, octanol-buffer partitioning, and HPLC. *Eur J Pharm Sci* **2002,** *17*, 81-93.

187. Pehourcq, F.; Jarry, C.; Bannwarth, B. Potential of immobilized artificial membrane chromatography for lipophilicity determination of arylpropionic acid non-steroidal anti-inflammatory drugs. *J Pharm Biomed Anal* **2003,** *33*, 137-144.

188. Adjalley, S. H.; Scanfeld, D.; Kozlowski, E.; Llinas, M.; Fidock, D. A. Genome-wide transcriptome profiling reveals functional networks involving the Plasmodium falciparum drug resistance transporters PfCRT and PfMDR1. *BMC Genomics* **2015,** *16*, 1090.

189. Xie, S. C.; Dogovski, C.; Hanssen, E.; Chiu, F.; Yang, T.; Crespo, M. P.; Stafford, C.; Batinovic, S.; Teguh, S.; Charman, S.; Klonis, N.; Tilley, L. Haemoglobin degradation underpins the sensitivity of early ring stage Plasmodium falciparum to artemisinins. *J Cell Sci* **2016,** *129*, 406-416.

190. Maerki, S.; Brun, R.; Charman, S. A.; Dorn, A.; Matile, H.; Wittlin, S. In vitro assessment of the pharmacodynamic properties and the partitioning of OZ277/RBx-11160 in cultures of Plasmodium falciparum. *J Antimicrob Chemother* **2006,** *58*, 52-58.

191. Bozdech, Z.; Llinas, M.; Pulliam, B. L.; Wong, E. D.; Zhu, J.; DeRisi, J. L. The transcriptome of the intraerythrocytic developmental cycle of Plasmodium falciparum. *PLoS Biol* **2003,** *1*, E5.

192. Ginsburg, H.; Geary, T. G. Current concepts and new ideas on the mechanism of action of quinoline-containing antimalarials. *Biochem Pharmacol* **1987,** *36*, 1567-1576.

193. Vander Jagt, D. L.; Hunsaker, L. A.; Campos, N. M. Comparison of proteases from chloroquine-sensitive and chloroquine-resistant strains of Plasmodium falciparum. *Biochem Pharmacol* **1987,** *36*, 3285-3291.

194. Surolia, N.; Padmanaban, G. Chloroquine inhibits heme-dependent protein synthesis in Plasmodium falciparum. *Proc Natl Acad Sci U S A* **1991,** *88*, 4786-4790.

195. Sanguinetti, M. C.; Tristani-Firouzi, M. hERG potassium channels and cardiac arrhythmia. *Nature* **2006,** *440*, 463-469.

196. Heijman, J.; Voigt, N.; Carlsson, L. G.; Dobrev, D. Cardiac safety assays. *Curr Opin Pharmacol* **2014,** *15*, 16-21.

197. Wang, S.; Li, Y.; Xu, L.; Li, D.; Hou, T. Recent developments in computational prediction of HERG blockage. *Curr Top Med Chem* **2013,** *13*, 1317-1326.

198. Mbai, M.; Rajamani, S.; January, C. T. The anti-malarial drug halofantrine and its metabolite N-desbutylhalofantrine block HERG potassium channels. *Cardiovasc Res* **2002,** *55*, 799-805.

199. Tie, H.; Walker, B. D.; Singleton, C. B.; Valenzuela, S. M.; Bursill, J. A.; Wyse, K. R.; Breit, S. N.; Campbell, T. J. Inhibition of HERG potassium channels by the antimalarial agent halofantrine. *Br J Pharmacol* **2000,** *130*, 1967-1975.

200. Borsini, F.; Crumb, W.; Pace, S.; Ubben, D.; Wible, B.; Yan, G. X.; Funck-Brentano, C. In vitro cardiovascular effects of dihydroartemisin-piperaquine combination compared with other antimalarials. *Antimicrob Agents Chemother* **2012,** *56*, 3261-3270.

201. Perry, M.; Stansfeld, P. J.; Leaney, J.; Wood, C.; de Groot, M. J.; Leishman, D.; Sutcliffe, M. J.; Mitcheson, J. S. Drug binding interactions in the inner cavity of HERG channels: molecular insights from structure-activity relationships of clofilium and ibutilide analogs. *Mol Pharmacol* **2006,** *69*, 509-519.

202. Chouabe, C.; Drici, M. D.; Romey, G.; Barhanin, J.; Lazdunski, M. HERG and KvLQT1/IsK, the cardiac K+ channels involved in long QT syndromes, are targets for calcium channel blockers. *Mol Pharmacol* **1998,** *54*, 695-703.

203. Obejero-Paz, C. A.; Bruening-Wright, A.; Kramer, J.; Hawryluk, P.; Tatalovic, M.; Dittrich, H. C.; Brown, A. M. Quantitative Profiling of the Effects of Vanoxerine on Human Cardiac Ion Channels and its Application to Cardiac Risk. *Sci Rep* **2015,** *5*, 17623.

204. Ridley, J. M.; Dooley, P. C.; Milnes, J. T.; Witchel, H. J.; Hancox, J. C. Lidoflazine is a high affinity blocker of the HERG K(+)channel. *J Mol Cell Cardiol* **2004,** *36*, 701-705.

205. Zhang, S.; Zhou, Z.; Gong, Q.; Makielski, J. C.; January, C. T. Mechanism of block and identification of the verapamil binding domain to HERG potassium channels. *Circ Res* **1999,** *84*, 989-998.

206. Brandon, E. F.; Raap, C. D.; Meijerman, I.; Beijnen, J. H.; Schellens, J. H. An update on in vitro test methods in human hepatic drug biotransformation research: pros and cons. *Toxicol Appl Pharmacol* **2003,** *189*, 233-246.

207. Baranczewski, P.; Stanczak, A.; Kautiainen, A.; Sandin, P.; Edlund, P. O. Introduction to early in vitro identification of metabolites of new chemical entities in drug discovery and development. *Pharmacol Rep* **2006,** *58*, 341-352.

208. FDA), U. S. F. a. D. A. U. Guidance for Industry: Safety Testing of Drug Metabolites. In 2008j.

209. Teja-Isavadharm, P.; Watt, G.; Eamsila, C.; Jongsakul, K.; Li, Q.; Keeratithakul, G.; Sirisopana, N.; Luesutthiviboon, L.; Brewer, T. G.; Kyle, D. E. Comparative pharmacokinetics and effect kinetics of orally administered artesunate in healthy volunteers and patients with uncomplicated falciparum malaria. *Am J Trop Med Hyg* **2001,** *65*, 717-721.

210. Knight, D. J.; Mamalis, P.; Peters, W. The antimalarial activity of N-benzyl-oxydihydrotriazines. III. The activity of 4,6-diamino-1,2-dihydro-2,2-dimethyl-1-(2,4,5,-trichloropropyloxy)-1,3,5-triazine hydrobromide (BRL 51084) and hydrochloride (BRL 6231). *Ann Trop Med Parasitol* **1982,** *76*, 1-7.

211. Blackie, M. A.; Yardley, V.; Chibale, K. Synthesis and evaluation of phenylequine for antimalarial activity in vitro and in vivo. *Bioorg Med Chem Lett* **2010,** *20*, 1078-1080.

212. Hrycyna, C. A.; Summers, R. L.; Lehane, A. M.; Pires, M. M.; Namanja, H.; Bohn, K.; Kuriakose, J.; Ferdig, M.; Henrich, P. P.; Fidock, D. A.; Kirk, K.; Chmielewski, J.; Martin, R. E. Quinine dimers are potent inhibitors of the Plasmodium falciparum chloroquine resistance transporter and are active against quinoline-resistant P. falciparum. *ACS Chem Biol* **2014,** *9*, 722-730.

213. Bellanca, S.; Summers, R. L.; Meyrath, M.; Dave, A.; Nash, M. N.; Dittmer, M.; Sanchez, C. P.; Stein, W. D.; Martin, R. E.; Lanzer, M. Multiple drugs compete for transport via the Plasmodium falciparum chloroquine resistance transporter at distinct but interdependent sites. *J Biol Chem* **2014,** *289*, 36336-36351.

214. Martin, R. E.; Marchetti, R. V.; Cowan, A. I.; Howitt, S. M.; Broer, S.; Kirk, K. Chloroquine transport via the malaria parasite's chloroquine resistance transporter. *Science* **2009,** *325*, 1680-1682.

215. Smith, D. A.; Obach, R. S. Metabolites and safety: What are the concerns, and how should we address them? *Chem Res Toxicol* **2006,** *19*, 1570-1579.

216. Sykes, D. A.; Parry, C.; Reilly, J.; Wright, P.; Fairhurst, R. A.; Charlton, S. J. Observed drug-receptor association rates are governed by membrane affinity: the importance of establishing "micro-pharmacokinetic/pharmacodynamic relationships" at the beta2-adrenoceptor. *Mol Pharmacol* **2014,** *85*, 608-617.

217. Taillardat-Bertschinger, A.; Perry, C. S.; Galland, A.; Prankerd, R. J.; Charman, W. N. Partitioning of halofantrine hydrochloride between water, micellar solutions, and soybean oil: Effects on its apparent ionization constant. *J Pharm Sci* **2003,** *92*, 2217-2228.

218. Raschi, E.; Ceccarini, L.; De Ponti, F.; Recanatini, M. hERG-related drug toxicity and models for predicting hERG liability and QT prolongation. *Expert Opin Drug Metab Toxicol* **2009,** *5*, 1005-1021.

219. Yu, H. B.; Zou, B. Y.; Wang, X. L.; Li, M. Investigation of miscellaneous hERG inhibition in large diverse compound collection using automated patch-clamp assay. *Acta Pharmacol Sin* **2016,** *37*, 111-123.

220. Nosten, F.; ter Kuile, F. O.; Luxemburger, C.; Woodrow, C.; Kyle, D. E.; Chongsuphajaisiddhi, T.; White, N. J. Cardiac effects of antimalarial treatment with halofantrine. *Lancet* **1993,** *341*, 1054-1056.

221. Touze, J. E.; Bernard, J.; Keundjian, A.; Imbert, P.; Viguier, A.; Chaudet, H.; Doury, J. C. Electrocardiographic changes and halofantrine plasma level during acute falciparum malaria. *Am J Trop Med Hyg* **1996,** *54*, 225-228.

222. Karbwang, J.; Milton, K. A.; Na Bangchang, K.; Ward, S. A.; Edwards, G.; Bunnag, D. Pharmacokinetics of halofantrine in Thai patients with acute uncomplicated falciparum malaria. *Br J Clin Pharmacol* **1991,** *31*, 484-487.

223. Veenendaal, J. R.; Parkinson, A. D.; Kere, N.; Rieckmann, K. H.; Edstein, M. D. Pharmacokinetics of halofantrine and n-desbutylhalofantrine in patients with falciparum malaria following a multiple dose regimen of halofantrine. *Eur J Clin Pharmacol* **1991,** *41*, 161-164.

224. Okombo, J.; Singh, K.; Mayoka, G.; Ndubi, F.; Barnard, L.; Njogu, P. M.; Njoroge, M.; Gibhard, L.; Brunschwig, C.; Vargas, M.; Keiser, J.; Egan, T. J.; Chibale, K. Antischistosomal Activity of Pyrido[1,2-a]benzimidazole Derivatives and Correlation with Inhibition of beta-Hematin Formation. *ACS Infect Dis* **2017,** *3*, 411-420.

225. Singh, K.; Okombo, J.; Brunschwig, C.; Ndubi, F.; Barnard, L.; Wilkinson, C.; Njogu, P. M.; Njoroge, M.; Laing, L.; Machado, M.; Prudencio, M.; Reader, J.; Botha, M.; Nondaba, S.; Birkholtz, L. M.; Lauterbach, S.; Churchyard, A.; Coetzer, T. L.; Burrows, J. N.; Yeates, C.; Denti, P.; Wiesner, L.; Egan, T. J.; Wittlin, S.; Chibale, K. Antimalarial Pyrido[1,2-a]benzimidazoles: Lead Optimization, Parasite Life Cycle Stage Profile, Mechanistic Evaluation, Killing Kinetics, and in Vivo Oral Efficacy in a Mouse Model. *J. Med. Chem.* **2017,** *60*, 1432-1448.

226. Sanz, L. M.; Crespo, B.; De-Cozar, C.; Ding, X. C.; Llergo, J. L.; Burrows, J. N.; Garcia-Bustos, J. F.; Gamo, F. J. P. falciparum in vitro killing rates allow to discriminate between different antimalarial mode-of-action. *PLoS One* **2012,** *7*, e30949.

227. Wicht, K. J.; Combrinck, J. M.; Smith, P. J.; Hunter, R.; Egan, T. J. Identification and SAR Evaluation of Hemozoin-inhibiting Benzamides Active Against *Plasmodium falciparum*. *J. Med. Chem.* **2016,** *59*, 6512-6530.

228. de Villiers, K. A.; Gildenhuys, J.; le Roex, T. Iron(III)Protoporphyrin IX Complexes of the Antimalarial Cinchona Alkaloids Quinine and Quinidine. *ACS Chem. Biol.* **2012,** *7*, 666-671.

229. Kitamura, A.; Higuchi, S.; Hata, M.; Kawakami, K.; Yoshida, K.; Namba, K.; Nakajima, R. Effect of beta-1,6-glucan inhibitors on the invasion process of Candida albicans: potential mechanism of their in vivo efficacy. *Antimicrob Agents Chemother* **2009,** *53*, 3963-3971.

230. Lyons, D. M.; Huttunen, K. M.; Browne, K. A.; Ciccone, A.; Trapani, J. A.; Denny, W. A.; Spicer, J. A. Inhibition of the Cellular Function of Perforin by 1-amino-2,4-dicyanopyrido[1,2-a]benzimidazoles. *Bioorg. Med. Chem.* **2011,** *19*, 4091-4100.

231. Wirth, C. C.; Glushakova, S.; Scheuermayer, M.; Repnik, U.; Garg, S.; Schaack, D.; Kachman, M. M.; Weissbach, T.; Zimmerberg, J.; Dandekar, T.; Griffiths, G.; Chitnis, C. E.; Singh, S.; Fischer, R.; Pradel, G. Perforin-like Protein PPLP2 Permeabilizes the Red Blood Cell Membrane During Egress of *Plasmodium falciparum* Gametocytes. *Cell. Microbiol.* **2014,** *16*, 709-733.

232. Khare, S.; Roach, S. L.; Barnes, S. W.; Hoepfner, D.; Walker, J. R.; Chatterjee, A. K.; Neitz, R. J.; Arkin, M. R.; McNamara, C. W.; Ballard, J.; Lai, Y.; Fu, Y.; Molteni, V.; Yeh, V.; McKerrow, J. H.; Glynne, R. J.; Supek, F. Utilizing Chemical Genomics to Identify Cytochrome b as a Novel Drug Target for Chagas Disease. *PLoS Pathog* **2015,** *11*, e1005058.

233. Chen, M. M.; Shi, L.; Sullivan, D. J., Jr. Haemoproteus and *Schistosoma* Synthesize Heme Polymers Similar to *Plasmodium* Hemozoin and Beta-hematin. *Mol. Biochem. Parasitol.* **2001,** *113*, 1-8.

234. Oliveira, M. F.; d'Avila, J. C.; Torres, C. R.; Oliveira, P. L.; Tempone, A. J.; Rumjanek, F. D.; Braga, C. M.; Silva, J. R.; Dansa-Petretski, M.; Oliveira, M. A.; de Souza, W.; Ferreira, S. T. Haemozoin in *Schistosoma mansoni*. *Mol. Biochem. Parasitol.* **2000,** *111*, 217-221.

235. de Moraes, J. Natural Products with Antischistosomal Activity. *Future Med. Chem.* **2015,** *7*, 801-820.

236. Hess, J.; Keiser, J.; Gasser, G. Toward Organometallic Antischistosomal Drug Candidates. *Future Med. Chem.* **2015,** *7*, 821-830.

237. Keiser, J.; Utzinger, J. Antimalarials in the Treatment of *Schistosomiasis*. *Curr. Pharm. Des.* **2012,** *18*, 3531-3538.

238. Xue, J.; Jiang, B.; Liu, C. S.; Sun, J.; Xiao, S. H. Comparative Observation on Inhibition of Hemozoin Formation and Their In Vitro and In Vivo Anti-schistosome Activity Displayed By 7 Antimalarial Drugs. *Zhongguo Ji Sheng Chong Xue Yu Ji Sheng Chong Bing Za Zhi.* **2013,** *31*, 161-169.

239. Manneck, T.; Keiser, J.; Muller, J. Mefloquine Interferes with Glycolysis in Schistosomula of *Schistosoma mansoni* via Inhibition of Enolase. *Parasitology* **2012,** *139*, 497-505.

240. Mattoccia, L. P.; Lelli, A.; Cioli, D. Sex and Drugs in *Schistosoma mansoni*. *J. Parasitol.* **1982,** *68*, 347-349.

241. Tan, Y.; Chen, Y.; You, Q.; Sun, H.; Li, M. Predicting the potency of hERG K(+) channel inhibition by combining 3D-QSAR pharmacophore and 2D-QSAR models. *J Mol Model* **2012,** *18*, 1023-1036.

242. Thai, K. M.; Ecker, G. F. A binary QSAR model for classification of hERG potassium channel blockers. *Bioorg Med Chem* **2008,** *16*, 4107-4119.

243. Corey, V. C.; Lukens, A. K.; Istvan, E. S.; Lee, M. C.; Franco, V.; Magistrado, P.; Coburn-Flynn, O.; Sakata-Kato, T.; Fuchs, O.; Gnadig, N. F.; Goldgof, G.; Linares, M.; Gomez-Lorenzo, M. G.; De Cozar, C.; Lafuente-Monasterio, M. J.; Prats, S.; Meister, S.;

Tanaseichuk, O.; Wree, M.; Zhou, Y.; Willis, P. A.; Gamo, F. J.; Goldberg, D. E.; Fidock, D. A.; Wirth, D. F.; Winzeler, E. A. A broad analysis of resistance development in the malaria parasite. *Nat Commun* **2016,** *7*, 11901.

244. Florens, L.; Washburn, M. P.; Raine, J. D.; Anthony, R. M.; Grainger, M.; Haynes, J. D.; Moch, J. K.; Muster, N.; Sacci, J. B.; Tabb, D. L.; Witney, A. A.; Wolters, D.; Wu, Y.; Gardner, M. J.; Holder, A. A.; Sinden, R. E.; Yates, J. R.; Carucci, D. J. A proteomic view of the Plasmodium falciparum life cycle. *Nature* **2002,** *419*, 520-526.

245. Witkowski, B.; Lelievre, J.; Barragan, M. J.; Laurent, V.; Su, X. Z.; Berry, A.; Benoit-Vical, F. Increased tolerance to artemisinin in Plasmodium falciparum is mediated by a quiescence mechanism. *Antimicrob Agents Chemother* **2010,** *54*, 1872-1877.

246. Feigon, J.; Denny, W. A.; Leupin, W.; Kearns, D. R. Interactions of antitumor drugs with natural DNA: 1H NMR study of binding mode and kinetics. *J Med Chem* **1984,** *27*, 450-465.

247. Van Miert, S.; Jonckers, T.; Cimanga, K.; Maes, L.; Maes, B.; Lemiere, G.; Dommisse, R.; Vlietinck, A.; Pieters, L. In vitro inhibition of beta-haematin formation, DNA interactions, antiplasmodial activity, and cytotoxicity of synthetic neocryptolepine derivatives. *Exp Parasitol* **2004,** *108*, 163-168.

248. Go, M. L.; Liu, M.; Wilairat, P.; Rosenthal, P. J.; Saliba, K. J.; Kirk, K. Antiplasmodial chalcones inhibit sorbitol-induced hemolysis of Plasmodium falciparum-infected erythrocytes. *Antimicrob Agents Chemother* **2004,** *48*, 3241-3245.

249. Lomenick, B.; Hao, R.; Jonai, N.; Chin, R. M.; Aghajan, M.; Warburton, S.; Wang, J.; Wu, R. P.; Gomez, F.; Loo, J. A.; Wohlschlegel, J. A.; Vondriska, T. M.; Pelletier, J.; Herschman, H. R.; Clardy, J.; Clarke, C. F.; Huang, J. Target identification using drug affinity responsive target stability (DARTS). *Proc Natl Acad Sci U S A* **2009,** *106*, 21984-21989.